

The Ventricular Fibrillation Electrocardiogram: Datamanagement, Artefact Removal, Rating, and Defibrillation

Dissertation

Zur Erlangung der Doktorwürde
an der Fakultät für Mathematik, Informatik und Physik der
Leopold-Franzens-Universität Innsbruck

eingereicht bei

Ao. Univ.-Prof. Mag. Dr. Anton Amann

vorgelegt von

Mag. rer. nat. Klaus Rheinberger

April 2006

Data on its own does not speak.

Emanuel Derman in
My Life as a Quant

Abstract

At least 225 000 people die in the United States every year from sudden cardiac arrest before they reach a hospital, and an estimated 370 000 to 750 000 patients per year have a cardiac arrest and undergo cardiopulmonary resuscitation (CPR) during hospitalisation. Almost half of all out-of-hospital cardiac arrest patients suffer from ventricular fibrillation (VF). Presently, resuscitation is guided by a standardised protocol (the international guidelines) which includes only rhythm detection for decision support. As an alternative to this approach, an extended diagnostics can be suggested, which is primarily based on the fibrillation ECG and provides information on the physiological status of the individual patient. This alternative approach promotes the development of ECG-based algorithms, resulting in parameters which reflect the myocardial metabolism of the heart and its degree of resuscitability. As an implication of this approach, the removal of artefacts resulting from CPR becomes desirable.

Hence the performance of the VF ECG parameters "mean frequency", "mean amplitude", and a linear combination of both is discussed with respect to their capability to predict the success of subsequent defibrillation attempts. The parameters yield classification accuracies of approximately 85%. Two new algorithms for CPR artefact removal are presented which are both based on state-space models and the corresponding Kalman recursions. The first algorithm models the CPR part of a corrupted ECG signal as a stochastically changing seasonal time series with an (optionally) time-dependent period. It achieves signal-to-noise ratio (SNR) improvements of approximately 3.4 dB. The second algorithm estimates the CPR part by an adaptive regression on lagged copies of some reference signal and achieves SNR improvements of approximately 5.8 dB.

The ECG parameters and artefact removal algorithms are optimised and evaluated on human and animal data which were collected at the Department of Anesthesiology and Critical Care Medicine (Innsbruck Medical University, Austria). A data management system was developed for these recordings based on open and free software.

The thesis finally contains measurement results and a corresponding analysis of the waveforms of various modern external biphasic defibrillators.

Kurzfassung

Mindestens 225 000 Menschen sterben in den USA jedes Jahr an plötzlichem Herztod bevor sie in ein Krankenhaus kommen. Geschätzte 370 000 bis 750 000 Patienten pro Jahr erleiden einen Herzstillstand und werden während der Einweisung in ein Krankenhaus einer kardiopulmonalen Reanimation (CPR) unterzogen. Fast die Hälfte aller außerklinischen Herzstillstandspatienten haben ventrikuläres Flimmern (VF). Zur Zeit wird eine Reanimation nach einem standardisierten Protokoll, den internationalen Richtlinien, durchgeführt. Diese enthalten nur die Herzrhythmuserkennung als Entscheidungshilfe. Als eine alternative Vorgehensweise könnte man sich eine erweiterte Diagnostik vorstellen, welche sich vorwiegend auf das Kammerflimmer-EKG stützt und Information über den physiologischen Zustand des individuellen Patienten liefert. Dieser alternative Ansatz verlangt nach der Entwicklung von EKG-basierten Algorithmen, die Parameter berechnen, welche den myokardialen Metabolismus des Herzens und den Grad der Wiederbelebarkeit reflektieren. Zusätzlich wird die Entfernung von Artefakten aus dem EKG, die von der CPR herrühren, notwendig.

Die VF EKG Parameter "mittlere Frequenz", "mittlere Amplitude" und eine lineare Kombination von beiden werden im Hinblick auf ihre Fähigkeit diskutiert, den Erfolg nachfolgender Defibrillationsversuche vorherzusagen. Die Parameter erreichen eine Klassifikationsgenauigkeit von etwa 85%. Zwei neue Algorithmen zur CPR-Artefaktentfernung werden vorgestellt. Beide basieren auf Zustandsraummodellen und den entsprechenden Kalman-Rekursionen. Der erste Algorithmus modelliert den CPR-Anteil eines verunreinigten EKG-Signals als eine sich stochastisch ändernde, saisonale Zeitreihe mit einer (optional) zeitabhängigen Periode und erreicht Signal-Rauschleistungs-Verhältnis (SRV) Verbesserungen von etwa 3,4 dB. Der zweite Algorithmus schätzt den CPR-Anteil mittels einer adaptiven Regression auf zeitlich verschobene Kopien eines Referenzsignals und erreicht SRV Verbesserungen von etwa 5,8 dB.

Die EKG Parameter und Artefaktentfernungsalgorithmen werden an Human- und Tierdaten optimiert und evaluiert, welche an der Klinik für Anästhesie und Allgemeine Intensivmedizin (Medizinische Universität Innsbruck, Österreich) gesammelt wurden. Ein Datenmanagementsystem, basierend auf offener und freier Software, wurde für diese Aufzeichnungen entwickelt.

Schließlich enthält die vorliegende Arbeit Messergebnisse und Auswertungsergebnisse der Entladungskurven verschiedener, externer biphasischer Defibrillatoren.

Contents

1	Introduction	1
1.1	Thesis Outline	1
1.2	Medical Background	2
1.2.1	Cardiac Arrest	2
1.2.2	The Cardiopulmonary System	2
1.2.3	Cardiopulmonary Resuscitation	3
1.2.4	International Guidelines 2000	3
1.2.5	Myocardial Metabolism, Influence of CPR	6
1.2.6	Defibrillation	6
1.3	Inferring the State of the Heart	7
1.3.1	Key Questions	7
1.3.2	Physiological Parameters	7
1.3.3	Key Problems	8
1.3.4	International Guidelines 2005	9
1.4	Further Reading	10
1.5	Paper 1	11
I	Data Management	19
2	General Approach	21
2.1	Introduction	21
2.2	Structure of Data Sets	22
2.2.1	Description of Data	22
2.2.2	Division and Structure of Data Sets	23
2.3	Demands	23
2.3.1	Annotation Files	23
2.3.2	Database	24
2.3.3	General Considerations	24
2.4	Implementation	24
2.4.1	Annotation Files	24
2.4.2	Database Design	25
2.4.3	APIs	25
2.5	Appendix	28

3	The MRL Human Study Data	33
3.1	Introduction	33
3.2	Raw Data Acquisition	34
3.2.1	Data Card Management	34
3.2.2	Management of Patient Related Data	35
3.3	Data Post-Processing	36
3.3.1	Transformation to XML-based Data Sets	36
3.3.2	Editing XML-based Data Sets and Data Analysis	37
3.4	Appendix	38
II	Mathematical Methods	45
4	Principles of Time Series	47
4.1	Modelling Time Series	47
4.1.1	Construction of the probability space, backward shift operator	48
4.1.2	Induced Structures	49
4.2	Best MSE Forecast	54
4.3	Best Linear MSE Forecast	55
4.3.1	Hilbert Space Formalism	56
4.3.2	Ordinary Least Squares, Linear Regression	58
4.3.3	Vectors of Random Variables	59
4.3.4	Iterated and Updating Projections	60
4.4	The Gaussian Case	61
5	State-Space Models and Kalman Theory	65
5.1	State-Space Models	65
5.2	The Kalman Recursions	66
5.2.1	Prediction	68
5.2.2	Filtering	72
5.2.3	Fixed-Point Smoothing	75
5.2.4	Properties of the Kalman Recursions	76
5.3	MLE and MMSE Optimisation	79
5.3.1	Maximum Likelihood Estimation	79
5.3.2	Minimum Mean Squared Error	84
III	CPR Artefact Removal	87
6	Introduction	89
6.1	Statement of the Medical Problem	89
6.2	Sources and Characteristics of CPR Artefacts	89
6.3	Overlapping of Frequencies - Why is CPR Artefact Removal Difficult?	90
6.4	More Technical Problems	91
7	Evaluation Methods and Previous Work	93
7.1	Evaluation Methods	93
7.1.1	Restored SNR	93
7.1.2	Performance of Detection and Scoring Algorithms	95

7.2	Previous Work	95
8	New Models for CPR Artefact Removal	97
8.1	The Seasonal State-Space Model	97
8.1.1	The model with Noise and Constant Period	98
8.1.2	The model with Noise and Time-Dependent Period: ATS	98
8.1.3	Calculating the Time-Dependent Period	99
8.2	Regression on Reference Signals	100
8.2.1	Reference Signals	100
8.2.2	OLS	102
8.2.3	A State-Space Model: ALR	103
9	Data, Optimisation and Evaluation Results	107
9.1	Data	107
9.1.1	Sampling and Mixing	108
9.2	Optimisation	108
9.2.1	Objective Functions: MLE, rSNR	108
9.2.2	Model Families and Search Methods	113
9.3	Evaluation	114
9.4	Results	114
9.4.1	The ATS Model	114
9.4.2	The ALR Model	118
9.5	Discussion and Future Work	123
9.5.1	Discussion of Results	123
9.5.2	Future Work	125
IV	Rating the VF ECG Signal	127
10	Published Papers	129
10.1	Overview	129
10.2	Paper 2	130
10.3	Paper 3	141
V	Defibrillator Waveform Analysis	149
11	(Un)published Papers	151
11.1	Overview	151
11.2	Paper 4	152
11.3	Paper 5	164
	List of Abbreviations	177
	Acknowledgements	178
	Curriculum Vitae	180
	List of Publications	182

Bibliography

187

Index

199

Chapter 1

Introduction

1.1 Thesis Outline

The introduction presents medical background and points out two current technical challenges in resuscitation regarding ECG signal analysis. These are the removal artefacts resulting from cardiopulmonary resuscitation (CPR) and the development of parameters derived from the ventricular fibrillation (VF) ECG signal in order to estimate the probability of success of a subsequent defibrillation attempt. The introductory chapter ends with a published review about algorithms to analyse VF signals.

Part I “Data Management” deals with the general problem of computer aided (predominantly ECG) data handling as experienced at the Department of Anaesthesiology and Critical Care Medicine (Innsbruck Medical University, Austria). An XML-based design of annotation files is presented and combined with a MySQL database and various programming interfaces. The second chapter of Part I describes the data acquisition, the data management, and the data post-processing in the study *Defibrillation in out-of-hospital cardiac arrest patients: a comparison of the mono- and biphasic defibrillation pulses of Medical Research Laboratories* as it has been developed at the Department of Anaesthesia.

Part II “Mathematical Methods” reviews in the first chapter the mathematical principles of stochastic time series and forecasting using general Hilbert space methods. The second chapter is devoted to state-space models and the corresponding Kalman recursions for prediction, filtering, and smoothing. Maximum likelihood and minimum mean squared error optimisation methods are presented and adapted to the state-space structure.

Part III “CPR Artefact Removal” first presents the underlying medical and technical problems and reviews previous work done by other research groups. Different approaches for the evaluation of CPR artefact removal algorithms are discussed. Subsequently two new algorithms based on state-space models of the CPR corrupted ECG signal are presented and then evaluated on 49 datasets which are mixtures of human artefact free VF and porcine pure CPR ECG signals.

Part IV “Rating the VF ECG signal” comprises two published papers which discuss the quality of the VF parameters “mean frequency” and “mean amplitude”, and a linear combination of both with respect to their capability to predict the success of a defibrillation attempt thereby monitoring the myocardial metabolism of the heart.

Part V ends the thesis with the measurement results and a corresponding analysis of the waveforms of various modern external biphasic defibrillators. This is done by presenting a published paper and a yet unpublished follow-up paper.

1.2 Medical Background

1.2.1 Cardiac Arrest

At least 225 000 people die in the United States every year from sudden cardiac arrest (SCA) before they reach a hospital. In addition, an estimated 370 000 to 750 000 patients per year have a cardiac arrest and undergo cardiopulmonary resuscitation during hospitalisation. Almost half of all out-of-hospital cardiac arrest patients suffer from ventricular fibrillation (VF), cf. Figure 1.1. These statistics were published in [56] in the year 2001. The frequency of cardiac death in western industrialised nations is similar to that in the United States. The incidence of cardiac death in other countries varies as a reflection of coronary artery disease prevalence in those populations. The trend towards increasing cardiac events in developing nations of the world is thought to reflect a change in dietary and lifestyle habits in these nations. In Austria the number of sudden cardiac death victims is in a range of 13 000 per year. A survival rate of 10% to 20% is reported in five European regions [73]. A meta-study analysing nearly 100 cardiac arrest studies found survival rates ranging from 1.6% to 20.7%, but with the majority below 10% [28]. For the US, a survival rate of 3% to 5% is estimated [26, 27, 99].

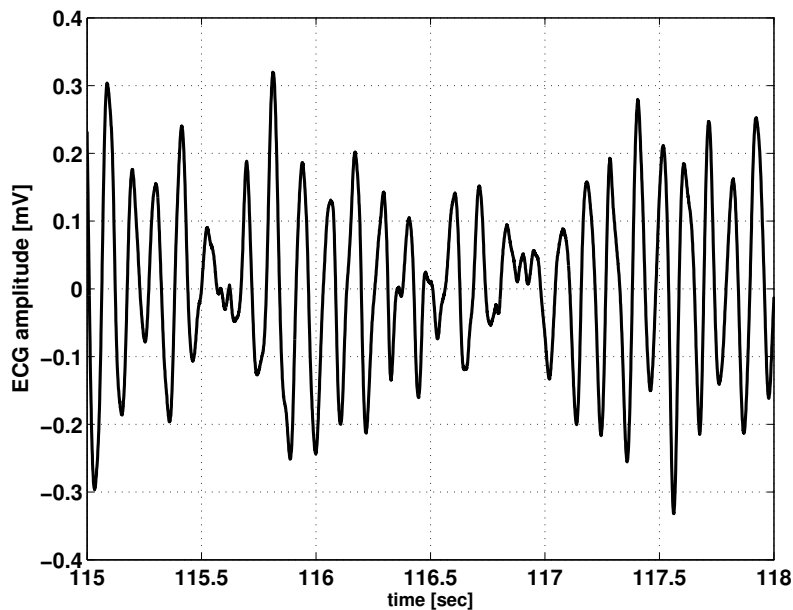


Figure 1.1: ventricular fibrillation ECG (porcine model)

1.2.2 The Cardiopulmonary System

The cardiopulmonary system establishes the exchange of oxygen and carbondioxide to the body cells. It consists of the lungs (“pulmo”) exchanging oxygen and carbondioxide to the blood and the heart (“cardio”) distributing and collecting the blood. The ECG rhythm of a healthy heart is called “normal sinus rhythm” (NSR), cf. Figure 1.2. During cardiac arrest, the heart stops pumping, and if resuscitative interventions are not begun within 5 to 7 minutes to restore normal electrical activity and circulation, there is little likelihood of successful resuscitation and functional survival [151, 95]. The most common arrhythmia

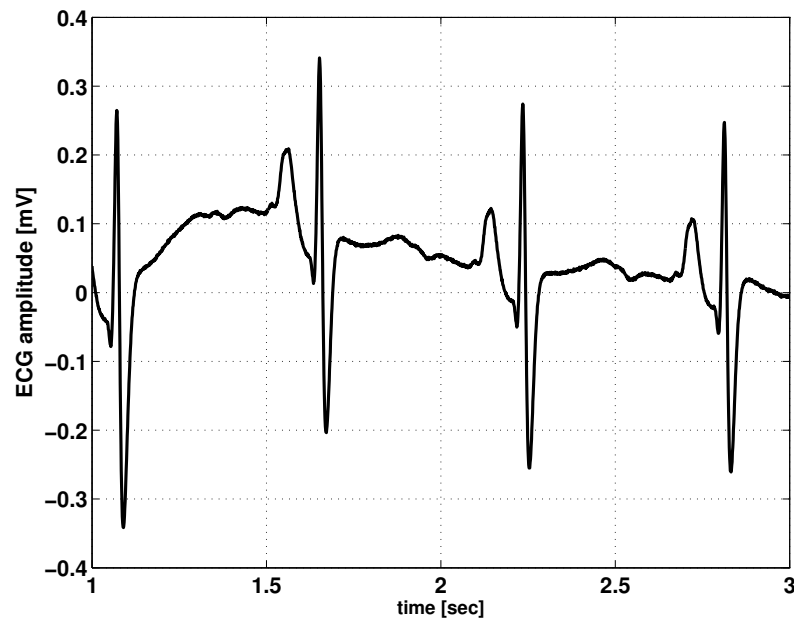


Figure 1.2: normal sinus rhythm ECG (porcine model)

causing cardiac arrest is VF, but it may also originate from ventricular and supraventricular tachycardia, asystole, pulseless electrical activity (PEA), and arrhythmias caused by sinus node failure or atrioventricular node disease [26, 122].

1.2.3 Cardiopulmonary Resuscitation

Cardiopulmonary resuscitation (CPR) consists of precordial chest compressions and ventilations. It aims to maintain artificial circulation by generation of vital organ blood flow. In cases of asystole and PEA, CPR alone can occasionally suffice to establish return of spontaneous circulation (ROSC). In case of VF, delivering an electric shock to the heart, i.e. defibrillation, is the most effective intervention [82]. International guidelines of CPR recommend the electrical defibrillation as a therapy for VF [17, 18], because besides external thoracic compressions it is the only effective intervention, which is proved to correlate with survival during CPR [16].

Laypersons are urged to perform so-called basic life support (BLS) which consists primarily in precordial chest compressions and mouth-to-mouth ventilations. Defibrillation with the use of an automated external defibrillators (cf. subsection 1.3.3) is also a BLS intervention, in most cases provided by healthcare professionals. Paramedics and emergency physicians perform advanced cardiac life support (ACLS) utilising drug administration and airway management in addition to BLS interventions.

1.2.4 International Guidelines 2000

The recommended algorithms for BLS and ACLS are presented in the international guidelines [17, 18] and give a protocol of how to treat a patient in cardiac arrest, i.e., unconscious, unresponsive, and without signs of life. Figures 1.3 and 1.4 depict roughly the chain of BLS and ACLS interventions.

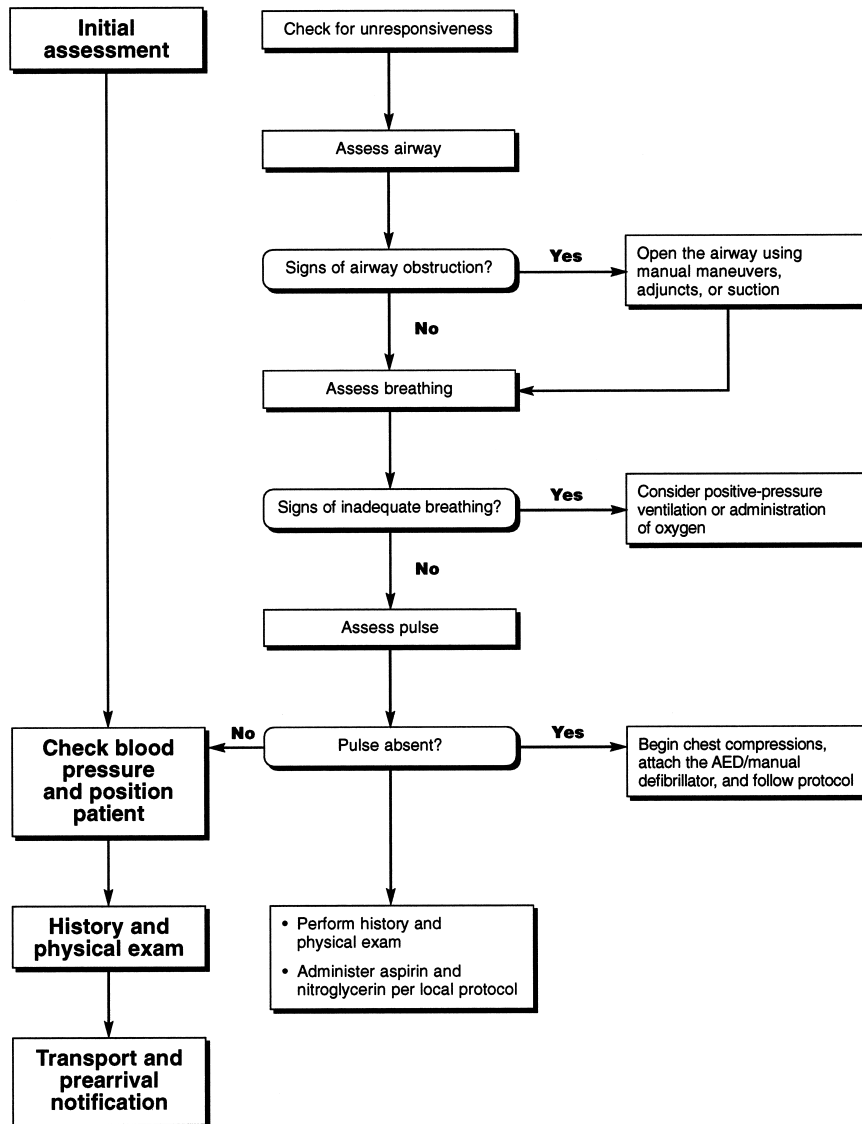


Figure 1.3: The figure reviews the BLS algorithm for ambulance providers of out-of-hospital management of patients with acute coronary syndromes. Reproduced from [17]. For a detailed description see [17, Part 3: Adult Basic Life Support. p29-71].

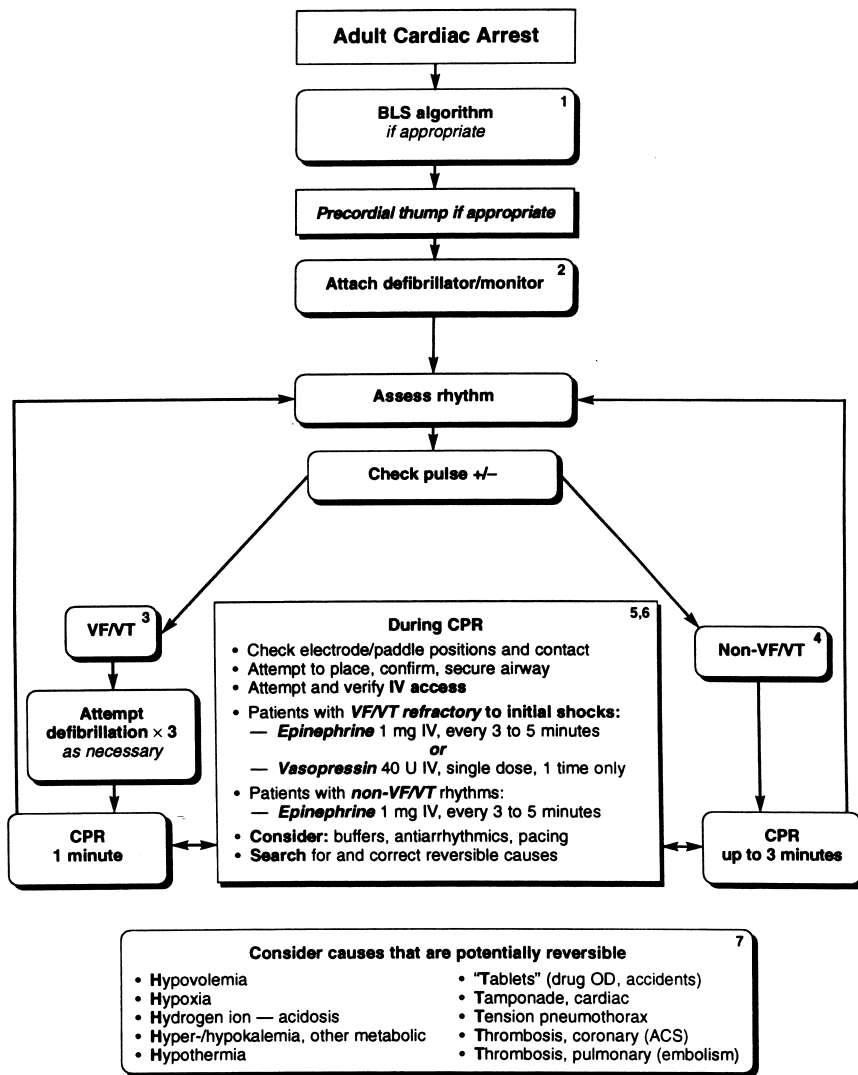


Figure 1.4: The figure reviews the Universal/International ACLS Algorithm. Reproduced from [17]. For a detailed description see [17, Part 6: Advanced Cardiovascular Life Support. p169-184-71].

1.2.5 Myocardial Metabolism, Influence of CPR

In general, the effect of any therapy in case of cardiac arrest depends on the following factors, cf. [51, p.10],

- *cardiac aetiology*: Prior heart diseases like infarction or arrhythmias influence cardiac resuscitability.
- *duration of cardiac arrest*: The energy resources of the heart are gradually emptied making resuscitation less probable.
- *bystander CPR*: precordial compressions and ventilations by lay rescuers may have a positive effect depending on the quality of CPR.

These factors have an impact on the condition of the heart, i.e., the myocardial metabolism. The myocardial metabolism comprises the physical and chemical processes making energy available to the myocardium [49]. Efficient BLS and ACLS improve the myocardial metabolism as they increase the myocardial blood flow.

In fact, several human and animal studies have shown that defibrillation can be futile and therefore harmful, if the level of myocardial metabolism is too low. However, by reestablishing a certain amount of myocardial perfusion through adequately performed CPR and possibly drug administrations, myocardial metabolism may be improved to a level, such that defibrillation can be successful. When the time between collapse and start of CPR is prolonged (> 4 min.), defibrillation of out-of-hospital patients more likely results in ROSC, if a short period (90 sec.) of chest compressions and ventilations is performed prior to defibrillation [41]. A recent out-of-hospital study in Oslo, Norway, by Wik et al. [157] showed, that patients with VF and ambulance response intervals longer than 5 minutes had better outcomes with CPR first before defibrillation was attempted. Cruz, Niemann et al. showed in animal studies, that in case of prolonged VF administration of epinephrine and 90 seconds of CPR prior to defibrillation increase the probability of ROSC significantly [42, 113, 112].

1.2.6 Defibrillation

Only if normal or supra normal coronary blood flows are established by extracorporeal circulation, spontaneous reversal of VF may be possible [59]. With this exception, defibrillation is the only option for reversing VF. If mechanical compressions are initiated within two minutes after onset of VF, the time interval for successful defibrillation is likely to be extended from three to twelve or more minutes [46]. Electrical defibrillation is intended to deliver an electrical current of sufficient intensity to depolarise ventricular myocytes, including pacemaker cells, simultaneously. Different so-called defibrillation “waveforms” [4, 5, 6] are still being discussed with respect to their efficacy and harmfulness, cf. Part V. The maximal electrical current delivered by a defibrillator may exceed 30 A [4, 5, 6], however, only approximately 4% of the current actually transverse the heart [45] depending on thoracic impedance and placement of the defibrillator’s electrodes. Cumulative unsuccessful defibrillation attempts may cause myocardial injury [161, 143]. Thus, it would be desirable to deliver an electric shock only if it is supposed to restore spontaneous circulation. A key problem is therefore whether to defibrillate or provide CPR.

1.3 Inferring the State of the Heart

Presently, resuscitation is guided by a standardised protocol, i.e., the international guidelines, which includes only rhythm detection for decision support, cf. subsection 1.2.4. An alternative to this approach would consist in an extended diagnostic procedure continuously guided by more information on the physiological state of the individual patient, cf. subsection 1.2.5, where arguments are given supporting this approach. The treatment is decided through a continuous analysis of physical measurements reflecting the myocardial metabolism of the heart and the degree of resuscitability.

1.3.1 Key Questions

The diagnostic approach should answer to the following key questions during resuscitation efforts

- Should the patient be defibrillated immediately or should CPR be started, as discussed in subsection 1.2.5?
- When is the optimal time for a defibrillation attempt?¹ This would prevent futile and harmful defibrillation attempts.
- Can the effect and quality of precordial chest compressions and ventilations be quantified and monitored? This would allow to give feedback to the rescuer on his CPR efforts, such that CPR can be optimised.
- Can the effect of drug administrations be quantified and monitored?

All key questions could be answered by continuously providing one (or more) appropriate parameters which are derived from physical measurements and reflect the actual **probability for ROSC** of a hypothetical defibrillation attempt.

1.3.2 Physiological Parameters

Different invasive and non-invasive parameters have been examined with respect to their monitoring ability of myocardial metabolism and prognostic relevance.

CPP and End-tidal CO₂

Coronary perfusion pressure (CPP), for example, correlates well during CPR with myocardial blood flow and outcome of resuscitation [86]. In animal [85] and human studies [116] it has been shown that CPP correlates with ROSC and survival. However, the measurement of this parameter is an invasive procedure since it requires placement of a central venous catheter, which is hardly practical in the out-of-hospital cardiac arrest situation.

End-tidal CO₂ varies with cardiac output [150, 66, 80, 87, 40], but has to be used with caution, because it is influenced by the general metabolic status [150, 66, 80, 87, 40], ventilation [80], the use of epinephrine [40], and time [87].

¹Here, optimal means that the probability for ROSC is maximal. Other objectives such as minimal post-resuscitation dysfunctions, early defibrillation, minimal number of defibrillation attempts could be included.

ECG

The ECG is a non-invasive and quickly available measurement giving information about the electrical activity of the heart [127]. An ECG lead measures the electrical potential difference between two points of the body. Leads I, II and III are measured over the limbs: I is from the right to the left arm, II is from the right arm to the left leg and III is from the left arm to the left leg. From this, the imaginary point V is constructed, which is located centrally in the chest above the heart. The other nine leads are derived from the potential difference between this point and the three limb leads (aVR, aVL and aVF) and the six precordial leads (V1-6). Therefore, there are twelve leads in total recording information from particular parts of the heart. The leads measure the average electrical activity generated by the summation of the action potentials of the heart at a particular moment in time.

The ECG rhythm of a normally operating heart is called “normal sinus rhythm” (NSR), cf. Figure 1.2. There exist a lot of heart rhythms deviating from NSR which are called arrhythmias [48, 131]. For a list of ECG rhythms annotated in an out-of-hospital study being carried out in Innsbruck, Austria, cf. Tables 3.1 and 3.2.

The “ventricular tachycardia” (VT) is often the initiating rhythm of cardiac arrest. In most out-of-hospital situations, however, the patient is past the initial phase of VT and is in the rhythm of VF, which is treated with defibrillation. If no CPR is given, the electrical activity of the heart disappears gradually and the final rhythm before death is termed asystole, which is a (nearly) flat line in the ECG tracing and is not treated with defibrillation. CPR and drug administration may increase circulation of blood and oxygen to the ischemic² myocardium and might result in a conversion from asystole to VF, which then can be defibrillated [102]. During asystole and VF, the heart does not contract and these rhythms are therefore pulseless. If no mechanical activity corresponds to an existing electrical activity of the myocardium, the resulting rhythm is called “electromechanical dissociation” (EMD) or “pulseless electrical activity” (PEA). This rhythm often appears in the transition from VF to asystole and is treated with medications and CPR, but does not respond to defibrillation attempts.

Different parameters derived from the VF ECG signal have been proposed for predicting the success of a defibrillation attempt thereby monitoring the myocardial metabolism of the heart. The review article of Amann et al. [11], reproduced at the end of this chapter (section 1.5), summarises the different approaches published in the literature.

1.3.3 Key Problems

In recent years, automated external defibrillators (AED) have been made available for use by the general public. These devices are commonly found in large gathering places, such as airports, casinos, and sports stadiums. An AED diagnoses the heart rhythm through the ECG lead of the adhesive pads and determines if a shock is needed. If necessary, semi-automatic AEDs prompt the user to stand clear and then push a shock button to defibrillate. Fully-automatic AEDs sound a “stand clear” alarm and then deliver the shock automatically without the user having to push the button. If a defibrillation is not appropriate, the AED prompts the user to determine the presence of pulse and start or continue CPR if indicated.

During CPR, chest compressions and ventilations cause artefacts in the ECG. In order that the rhythm detection algorithms of AEDs work properly a so-called “hands-off interval” is required, where CPR is stopped and the ECG is thus artefact-free. However, as a

²deficient blood supply

consequence of this, myocardial blood flow drops and the (probability for) success of a subsequent defibrillation attempt decreases [125, 53]. Thus, it would be desirable to remove CPR artefacts from the ECG continuously during CPR administration, cf. Part III. Thereby, continuous rhythm detection would be possible and would provide minimal “hands-off” delays before delivering the electric countershock.

Furthermore, in case of VF, CPR removal algorithms would allow for continuous monitoring of the probability for ROSC through parameters derived from the artefact-cleaned ECG signal.

An alternative approach consists in finding VF parameters and detection algorithms, which are insensitive to CPR.

1.3.4 International Guidelines 2005

Shortly before the completion of this thesis, the AHA published new guidelines³ for CPR and emergency cardiovascular care [20, 19, 72]. The following list summarises the major changes.

- Chest compressions are more important than ventilations: In the first minutes of VF SCA, ventilation does not appear to be as important as chest compressions, but it does appear to contribute to survival from prolonged and asphyxial arrest.
- High quality CPR is emphasised. Rescuers should push hard, push fast, allow full chest recoil, minimise interruptions in compressions, and defibrillate promptly when appropriate.
- There was insufficient data to recommend CPR before defibrillation for all victims of VF SCA. The data was insufficient to determine (1) whether this recommendation should be applied to in-hospital cardiac arrest, (2) the ideal duration of CPR before attempted defibrillation, or (3) the duration of VF at which rescuers should switch from defibrillation first to CPR first.
- A 1-shock strategy is recommended instead of the 3-shock strategy. Furthermore, it is recommended that rescuers resume CPR, beginning with chest compressions, immediately after attempted defibrillation. Rescuers should not interrupt chest compressions to check circulation until after about 5 cycles or approximately 2 minutes of CPR.
- Given a lack of documented effect of drug therapy in improving long-term outcome from cardiac arrest, drug administration is deemphasised and BLS is reemphasised.
- Studies have shown that a reduction in the interval between compression and shock delivery by as little as 15 seconds can increase the predicted shock success. Defibrillation manufacturers are encouraged to develop AEDs that are capable of analysing the heart rhythm during uninterrupted chest compressions.

All points in this list demonstrate that (1) parameters reflecting the actual probability of ROSC, (2) reliable detection algorithms, and (3) CPR artefact removal algorithms as described in the sections before are important issues in the improvement of current CPR techniques.

³freely available at <http://circ.ahajournals.org>

1.4 Further Reading

For an account on the history of CPR it is referred to [110].

A review about algorithms to analyse ventricular fibrillation signals is reproduced in the next section (1.5).

The doctoral thesis of Ulrich Achleitner examined different parameters derived from porcine VF ECG signals with respect to their ability to predict defibrillation outcome and their correlation with blood pressure and vasopressors administrations [3]. He also studied signals obtained from the open heart when manual CPR was replaced by a heart-lung-machine.

Trygve Eftestøl analysed in his doctoral thesis derived quantities of out-of-hospital cardiac arrest ECG signals with respect to their predictive value of defibrillation success and sketches an algorithm for CPR artefact removal [51].

Robert Tratnig examined the reliability of new and old detection algorithms for AEDs [14, 13, 144].

The effect of drug administrations such as vasopressin and epinephrine during cardiac arrest have been analysed by the research group of the Department of Anesthesiology and Critical Care Medicine at the Innsbruck Medical University, Austria [152, 7, 132, 133, 12, 105, 97].

An analysis of a selection of modern biphasic defibrillation waveforms found in commonly available defibrillators is given in [6].

1.5 Paper 1

The following review was published in *Curr Opin Crit Care* 2001 Jun;7(3):152-6, [11].

Algorithms to analyze ventricular fibrillation signals

Anton Amann, Ph.D., Klaus Rheinberger, M.Sc., Ulrich Achleitner, M.Sc.
*Department of Anesthesiology and Critical Care, Leopold-Franzens-University of
Innsbruck, Austria.*

Address for correspondence and reprints: Dr. Anton Amann, The Leopold-Franzens University of Innsbruck, Department of Anesthesiology and Critical Care, Anichstrasse 35, 6020 Innsbruck, Austria, phone: ++43 512 504 24636, fax: ++43 512 504 24683, e-mail: anton.amann@uibk.ac.at

Supported, in part, by the Austrian National Bank science projects 7280 and 7276, the Austrian Heart Foundation project 98/05, the Austrian Science Foundation P-14169-MED (all Vienna, Austria); a research grant from Bruker Medical (Ettlingen, Germany); and the Department of Anesthesiology and Critical Care, Leopold-Franzens-University of Innsbruck, Austria.

Abstract

Prediction of defibrillation success in order to avoid myocardial injury and performance feedback during cardiopulmonary resuscitation (CPR) requires algorithms to analyze ventricular fibrillation (VF) signals. In this report, we review investigations on different parameters of VF ECG signals including amplitude, frequency, bispectral analysis, amplitude spectrum area, wavelets, nonlinear dynamics, $N(\alpha)$ -histograms, and combinations of several of these parameters. To date, no satisfactory methods have been found which cope with CPR artifacts, and show adequate predictive power of successful defibrillation. Usual limitations of the studies are the small number of subjects, which preclude separation into training and test data. Since many investigations are animal studies of untreated short VF, results may be different for prolonged VF in humans. The universality of threshold values has to be examined, and promising new parameters have to be monitored over longer time periods and analyzed for effects of chest compressions, ventilation and concomitant vasopressor therapy.

Introduction

Different resuscitation strategies for prolonged VF patients are conceivable. Recent studies suggest that a brief period of myocardial perfusion before countershock with chest compressions and ventilation improves cardiac resuscitation outcome [41, 112, 42, 113]. Since cumulative defibrillation energy resulting from futile defibrillation attempts may cause myocardial injury [161], it would be important to have a noninvasive tool which permits to predict whether a shock will cause return of spontaneous circulation (ROSC), or not.

Both invasive and noninvasive parameters have been tested with regard to their capability to predict defibrillation success during cardiopulmonary resuscitation (CPR). For example, coronary perfusion pressure and myocardial blood flow during CPR have been shown in laboratory and clinical studies to be good predictors of defibrillation success. Since these monitoring techniques require intravascular and/or intracardiac catheters that are almost impossible to insert appropriately during out-of-hospital CPR, these strategies are more likely to be employed in intensive care units or CPR laboratories. In contrast, the ECG signal is a

noninvasive and readily accessible feature of ventricular fibrillation (VF) and superior, for example, to end-tidal carbon dioxide for prediction of defibrillation success [141].

Recent Results in VF Analysis

In this report, we will review the most important recent investigations on algorithms and parameters to analyze VF ECG signals, including amplitude, frequency, bispectral analysis, amplitude spectrum area, wavelets, nonlinear dynamics, $N(\alpha)$ -histograms, combinations of several of these parameters, and CPR artifact removal algorithms. Careful distinction has to be made between human and animal studies, early VF and prolonged VF, VF during CPR and untreated VF, different lengths of time windows for time course analysis, and possible different pharmacological administrations.

Amplitude

VF voltage or signal amplitude is usually defined as the maximum peak-to-trough VF amplitude in a given time window of the ECG signal [115]. Mean VF voltage is the average of VF voltage over the chosen time interval. Prolonged VF in pigs was studied by Noc et al. [115], where mean VF voltage was equivalent in predictive power with coronary perfusion pressure. In order to eliminate CPR artifacts, frequencies <4.5 Hz were excluded by a filtering procedure.

Early VF in dogs was investigated by Patwardhan et al. [117]. They compared the predictive power of (mean) VF voltage with the envelope of VF voltage which they estimated using the Hilbert transform. After 10 sec of untreated VF defibrillation, shocks were delivered. Their results suggest that both of these parameters are not robustly correlated with shock outcome for early VF.

Frequency

Various different parameters can be computed from the windowed Fourier transformation (time window length may be, e.g., 10 sec) and checked for predictive power of defibrillation outcome. Starting point for estimating median frequency, peak power frequency, edge frequency, spectral flatness measure etc. is the power spectrum defined as the square of Fourier amplitudes. Parameters computed from the power spectrum neglect phase correlations of the harmonic components of the signal.

Early VF in dogs was examined by Patwardhan et al. [118]. They used an analysis technique based on Wigner transforms to quantify time-varying dominant frequency in ECGs during trials of 10 and 30 seconds of untreated VF. Frequencies were estimated at 40 msec intervals, in comparison with 3 or 10 seconds in other work. Their results suggest that median frequency is a more robust parameter than dominant frequency.

A study by Achleitner et al. evaluated prolonged VF mean frequency and amplitude to predict defibrillation success in a porcine CPR model using repeated administration of vasopressin or epinephrine [7]. The signals were divided into consecutive 10 sec intervals, and the frequency domain was restricted to the range from 4.33 to 30 Hz in order to reduce CPR artifacts. Mean fibrillation frequency was equivalent to amplitude in predictive power, but not quite as good as coronary perfusion pressure. Interestingly, vasopressin was superior to epinephrine in maintaining these variables above a threshold necessary for successful defibrillation, which reflects itself in better defibrillation success.

A forthcoming publication by Small et al. uses two new algorithms to detect and quantify change in periodicity, reduced autoregressive modeling and near orbit analysis (Small, M., Yu, D., Harrison, R. Variation in the dominant period during ventricular fibrillation, submitted to IEEE Transactions on Biomedical Engineering). These algorithms provided results that were consistent with those obtained from Fourier methods, but were more reliable in detection of periodicities and more robust to noise.

Bispectral Analysis

Patwardhan and coworkers used the cross bispectrum to estimate the degree of phase coupling among orthogonal ECGs during early VF in dogs [119]. After 10 sec of untreated VF defibrillation, shocks were delivered. They noticed that between 200 and 1000 ms before defibrillation shock, unsuccessful defibrillation trials showed a higher mean bispectral energy than successful defibrillation trials ($p < 0.05$). The existence of overlap in range of bispectral energy between successful and unsuccessful trials suggests that this parameter is significantly correlated with shock outcome, but is not a robust predictor, i.e. does not have a high sensitivity and specificity for early VF.

Amplitude Spectrum Area

In a porcine model of cardiac arrest, Povoas et al. analyzed the VF ECG signal during CPR by estimating the amplitude spectrum area (AMSA), i.e. the area under the absolute Fourier spectrum (5 sec time windows) between 4 and 48Hz [121]. An AMSA value of 21 mVHz predicted restoration of perfusing rhythm with a positive predictive value equivalent to that of coronary perfusion pressure and a negative predictive value of 96%. AMSA, therefore, has the potential for guiding optimal timing of defibrillation.

Wavelets

Watson et al. report a new method of interrogating the surface ECG signal using techniques developed in the field of wavelet transform analysis [148]. Fourier analysis and wavelet analysis both decompose the ECG-signal with respect to basis functions. A key distinction between Fourier analysis and wavelet analysis is that a variety of wavelet basis functions are available (e.g., Daubechies wavelets, coiflets or biorthogonal wavelets). Hence, the most appropriate wavelet family may be chosen for the signal under investigation. In contrast, Fourier analysis is restricted to one basis function: the sinusoid. Applied to surface ECG signals from a porcine experimental model of prolonged VF, three dominant ridges appear in the wavelet transform surface through time showing similar time dependence as mean frequency analysis. After the onset of CPR, increases in all three bands can be observed in the scalogram.

Nonlinear dynamics

In recent publications, Small et al. present experimental evidence that the seemingly random electrical activity during VF is nonlinear in its dynamical behavior (and possibly chaotic), but cannot be modeled as a linear stochastic process [130, 167, 166, 129]. Their results demonstrate that correlation dimension estimates of VF data collected from an animal study are distinct from those expected for noise driven linear systems. Furthermore, their calculations show that VF has 80-90% low-dimensional deterministic nonlinear motion with about

5 degrees of freedom and 10-20% high-dimensional structure (either noise or chaos). They used VF ECG data within the first 3 minutes of cardiac arrest during which no clinical treatment was applied, i.e. without influence of CPR, drugs or electrical effects on the heart. No general monotonic trend of dimension change was found within this period.

Sherman, Callaway and coworkers examined the scaling exponent and the Hurst exponent for VF waveforms [36, 128]. These parameters distinguish in a robust way between early and late VF independent of the signal amplitude. The scaling exponent is a local estimate of the fractal dimension of the ECG waveform and was dependent on time-order of the data. Hurst exponents in swine VF demonstrate similar time dependence as known parameters which describe the dominant period of animal VF [33, 34, 50].

$N(\alpha)$ -Histograms

Little is known about the relation between the degree of cardiac disorganization, and the success rate of defibrillation therapy. The method of $N(\alpha)$ -histograms [10] is a strategy to estimate the degree of randomness in signals. In a forthcoming publication of prolonged VF CPR in pigs, Amann et al. compare the quotient histogramstart/histogramwidth with mean fibrillation frequency [9]. A more irregular VF ECG-signal as reflected by a higher value of histogramstart/histogramwidth was associated with significantly increased defibrillation success, whereas more regularity of ventricular fibrillation was associated with poor defibrillation success. A remarkable feature of the $N(\alpha)$ -technique is given by the fact that it does not use any filtering algorithm to eliminate the CPR artifacts.

Combination of Several Parameters

Eftestol et al. studied median frequency, peak power frequency, spectral flatness, and energy in VF ECG signals prior to 868 defibrillation shocks in 156 patients with out-of hospital cardiac arrest [52]. They generated different secondary decorrelated feature sets from the 4 original spectral features using principal component analysis. To ensure reliability, the data was split into training and test sets. Following the advice of the highest performing classifier, which corresponded to the combination of two secondary features, 328 of 781 unsuccessful shocks would have been avoided, while seven of 87 successful shocks would not have been given. According to Eftestol et al., the low specificity and positive predictive value indicates that other features should be added. However, in comparison to a similar study done by Brown et al. [32] with a smaller number of data, the study by Eftestol et al. gave poorer predictive potential.

In this context, we recall the interesting investigations of Monsieurs et al. who combined VF amplitude and the number of base-line crossings per second in human VF ECG signals into one parameter [108]. In this study, CPR was interrupted in order to avoid CPR artifacts.

CPR artifact removal algorithms

Periodic chest compressions of CPR may interfere with the ECG signal recording, affect the extracted parameters thereof, and finally, lead to incorrect prediction of countershock outcome. Though interrupting CPR in humans for a brief time period results in acquisition of reliable parameters, it shortens the period of vital myocardial perfusion [58, 108, 125]. Different attempts have been made to reduce such artifacts. Restriction to a subband of the frequency domain analysis unfortunately eliminates almost all predictive parameters for human VF-ECGs, since the fibrillation frequency of humans is lower than the fibrillation

frequency of most animals [115, 136, 138]. Using an adaptive multichannel Wiener filter, one can construct an estimate of the CPR artifact signal, which subsequently can be subtracted from the noisy human ECG signal [1]. Finally, wavelet transform techniques constitute promising methods for ECG signal filtering [148]. In contrast to these filtering techniques, $N(\alpha)$ -analysis of ECG signals as used in the forthcoming publication by Amann et al. does not use any filtering procedure to eliminate the CPR artifacts.

Discussion

(Mean) VF voltage has the disadvantage of depending on the direction of the main fibrillation vector and therefore, is subject to a great interindividual variety. Nevertheless, in many studies (mean) VF voltage has been shown to reflect vital organ blood flow, myocardial energy metabolism, defibrillation success, and time elapsed since collapse [33, 115, 136, 35, 44, 114, 149].

Median VF frequency has been shown in several clinical studies and animal experiments to be a reliable noninvasive variable which can be used to predict defibrillation success [7, 115, 141, 33, 34, 32, 108, 136, 138, 38, 103, 134, 137, 139, 140].

Pharmacologically induced changes in defibrillation success are reflected in a corresponding different time course of frequency [104]. Frequency characteristics are greatly altered by lignocaine (reducing dominant frequency through the 3 min period of analysis) and verapamil (increasing dominant frequency), but remain almost unchanged by propranolol and bretylium [39]. A study by Martin et al. showed that administration of nifedipine prior to VF maintained high (dominant) frequency in dogs over 3 min, preserving myocardial energy stores and increasing recovery chance after defibrillation [62, 104]. Therefore, in this study, the cardioprotective effect and high defibrillation success are reflected by a high (dominant) frequency.

Hence, spectral estimates such as median or dominant frequency have successfully been applied to show time-dependent trends in VF signals, correlations with different drugs, and defibrillation outcome. Unfortunately, they can not successfully be applied when CPR-related artifacts interfere with the VF-ECG. For most animal experiments, the first three overtones of CPR responsible for most of the artifacts can be eliminated by employing a lowpass filter at 4.3 Hz. For human VF-ECGs, such filtering procedures should not be applied, since the fibrillation frequencies are lower, and overlap with interference signals due to mechanical CPR.

Bispectral analysis offers the possibility of investigating phase correlations between two different leads which are neglected by standard spectral estimates. It would be interesting to compute bispectral energy for prolonged VF, and to analyze effects of chest compressions, ventilation and concomitant vasopressor therapy. Since high phase coupling indicates a higher degree of regularity of the fibrillation signal, Patwardhan's result that high phase coupling corresponds to low fibrillation success could be reformulated by stating that "the more regular a fibrillating heart behaves, the less it can successfully be defibrillated." This is an interesting new aspect in the context of parameters predicting defibrillation success, and is related to the results from $N(\alpha)$ -analysis. Namely, $N(\alpha)$ -analysis is able to extract information (e.g., on randomness of ECG-signals) from ventricular fibrillation ECG-signals (from a single lead instead from two different leads), and predict defibrillation success during CPR.

Investigations of generic character have helped to clarify the question to which extend VF is a random and/or a deterministic time series. The results of Small et al. [130, 129,

167, 166] suggest the use of nonlinear modeling techniques to characterize the dynamical behavior of VF. Parameters of such techniques have to be found which monitor the dynamic changes of the state of the heart within longer observation periods, and effects that are due to clinical treatment. The effects of chest compressions, ventilation and concomitant vasopressor therapy on the complexity of VF ECG-signal should be evaluated, and the predictive power of parameters has to be tested.

The idea of combining the aforementioned and possible new parameters to a new and better performing parameter set is interesting, and has to be pursued.

Conclusions

Usual limitations of the studies are the small number of animals or patients, which precludes separation of the group into training and test data: this means that “best-fit” threshold values are used in prediction which tend to yield artificially good sensitivity and specificity. In this case, the method needs to be applied to a new test set of data to see how much of its performance degrades. Re-exploration of data seems to be an interesting idea in this context. A database of collected human and animal ECG signals could be useful in order to re-examine different methods. We recommend data quality guidelines of 1kHz sampling rate and 12 bit amplitude resolution.

The universality of threshold values has to be examined. This means that parameters may have different threshold values for prediction of defibrillation outcome depending on pharmacologically treatment, age, body temperature, and other factors.

Implementation of the methods under discussion in out-of-hospital CPR is most likely hindered by CPR artifacts, and the technical feasibility of computing the parameter values online. For example, most processing units in common defibrillators are too slow to compute a Fourier transformation of the ECG signal within appropriate time. This could be circumvented by using the number of base-line crossings per second instead [108], or by transferring the data to a data processing center which in turn sends the parameter values back.

Recommended reading

Papers of particular interest, published within the annual period of review, have been highlighted as:

- * indicating that this paper is “of special interest”, and
 - ** indicating that this paper is “of outstanding interest”.
- ** [42] An excellent laboratory investigation which indicates that administration of epinephrine and CPR preceding countershock of prolonged (>5 min) VF significantly improves cardiac resuscitation outcome compared with immediate countershock.
- ** [113] This nice animal study shows that CPR preceding countershock of VF of 5 minute duration does not improve the response to the first shock, decrease the incidence of postshock pulseless electrical activity, or the rate of return of circulation.
- ** [115] In this excellent animal study, mean voltage of prolonged VF was equivalent in predictive power with coronary perfusion pressure. The data was divided into a derivation, and a validation group.
- ** [118] In this fine animal study of early VF, the results suggest that median frequency is a more robust parameter than dominant frequency.

- * [7] A porcine CPR model of prolonged VF which showed that vasopressin was superior to epinephrine in maintaining median frequency above a threshold value necessary for successful defibrillation.
- ** [119] An excellent animal study which uses a cross bispectrum to estimate the degree of phase coupling among orthogonal ECGs during VF in dogs. This is a promising approach, since to date only single lead ECG signals were examined, and phase correlations were neglected in spectral analysis.
- * [121] This is the first publication worldwide presenting the “amplitude spectrum area” parameter.
- ** [148] This is the first publication to date using wavelet transform techniques in order to investigate VF ECG signals.
- ** [130] Small et al. investigate the question to which extent VF is a random and/or a deterministic time series. Their impressive results suggest the use of nonlinear modeling techniques to characterize the dynamical behavior of VF.
- ** [167] Calculations in this nice animal study show that VF has 80-90% low-dimensional deterministic nonlinear motion with about 5 degrees of freedom, and 10-20% high-dimensional structure, indicating either noise or chaos.
- ** [166] In this very good animal study Yu et al. find that although there is no general trend of dimension change in deterministic dynamics, periodicity analysis reveals additional time-dependent structure in early VF.
- ** [129] When analyzing early VF in pigs, Small et al. found that data could not be adequately described by a linear stochastic model.
- ** [36] This publication presents a new measure, called the scaling exponent, describing VF waveform and distinguishing between early and late VF.
- ** [128] Using human and animal data, Sherman et al. nicely show that Hurst exponents and self-similarity dimensions are correlated with the duration of VF.
- * [10] In this investigation, the width of $N(\alpha)$ -histograms was sufficient to distinguish between a vasopressin and a placebo group during a porcine model of CPR.
- * [9] In this publication of prolonged VF CPR in pigs, Amann et al. compare the quotient histogramstart to histogramwidth with mean fibrillation frequency. A remarkable feature of the $N(\alpha)$ -technique is given by the fact that it does not use any filtering algorithm to eliminate the CPR artifacts.
- ** [52] In this impressive human study, four spectral features of ECG signals prior to 868 shocks were combined to generate different secondary decorrelated feature sets using principal component analysis. Special attention is made on separation between training and test data.
- ** [1] Using an adaptive multichannel Wiener filter, Aase et al. construct an estimate of the CPR artifact signal, which subsequently can be subtracted from the noisy human ECG signal.

Part I

Data Management

Chapter 2

General Approach

Contents

2.1	Introduction	21
2.2	Structure of Data Sets	22
2.2.1	Description of Data	22
2.2.2	Division and Structure of Data Sets	22
2.3	Demands	23
2.3.1	Annotation Files	23
2.3.2	Database	23
2.3.3	General Considerations	24
2.4	Implementation	24
2.4.1	Annotation Files	24
2.4.2	Database Design	24
2.4.3	APIs	24
2.5	Appendix	27

2.1 Introduction

Data exchange between different tools for data analysis and data manipulation is a common problem: different applications use different and often proprietary and undocumented formats for data storage.

In the last years a heap of data has been collected at the Department of Anaesthesiology and Critical Care Medicine (Innsbruck Medical University, Austria). This comprises predominantly animal data recorded during cardiac arrest experiments, so-called TOP-data. Recordings of medical parameters (ECG, EEG, CO₂, VOC,...) at humans, defibrillator waveform measurements, and foreign data not recorded at the department extend the TOP-data collection. Keeping a survey over this heterogeneous collection is getting an ever more delicate task. Furthermore, the different formats of the (annotation) data results in an abundance of programs to be written in order to process these different files. It was therefore decided to construct a common and extensible **annotation data format** which should fulfil the following demands:

- It can be "easily" processed by many different applications and programming languages (Matlab, Perl, PHP, Java, R, editors, ...).
- The annotations supply enough information for reading the corresponding (e.g. binary) measurement data file(s).
- The annotation files can be "easily" parsed in order to feed a database with (parts of) their information.

In this sense, an annotation file should serve as a mediator carrying structured information about a single data set.

Secondly, a **database** shall be designed, which supplies the following services:

- Structured organisation of the data collection: classification into studies and groups, assignment of outcomes, settings of the recording etc.
- Survey of collected data: easy browsing through the database according to different angles.
- Query the database to find data sets with given properties.

Finally, various **scripts and applications** have to be written to generate, edit and parse the annotation files, such that the different applications are able to read and write the data and interact among each other.

2.2 Structure of Data Sets

The aim of this section is to answer the question "*Which set of information entities shall be called one data set, and how shall it be structured?*". The following section exemplifies the TOP-data acquisition. However, it can be easily extended to the other data sets mentioned in the introduction.

2.2.1 Description of Data

The TOP-data collection consists of recordings which were made during animal experiments. Identically designed animal experiments belong to a determined animal *group* of at least one determined animal *study*. For one animal there are typically two or more temporally separated records, a so-called *baseline* and the *experiment* itself. The latter can be split into various parts (computer breakdown, division into smaller data files,...). Each record comprises the temporal acquisition of different parameters, so-called *channels* (various ECG leads, invasive blood pressures, blood flows, ...). The recordings originate from different medical devices: Hellige or Siemens ECG and IBP monitor, blood flow measuring devices, etc. Typically, the measurement values for one recording are stored in one *data file* (binary or ASCII). However, in the general case, more than one data acquisition devices are used to record the various parameters. This results in multiple data files for one recording episode (i.e. a *record*), which start and end at different absolute times.

Chronological Course of an Experiment:

The following diagram (Fig. 2.1) illustrates the above described chronological course of an experiment.

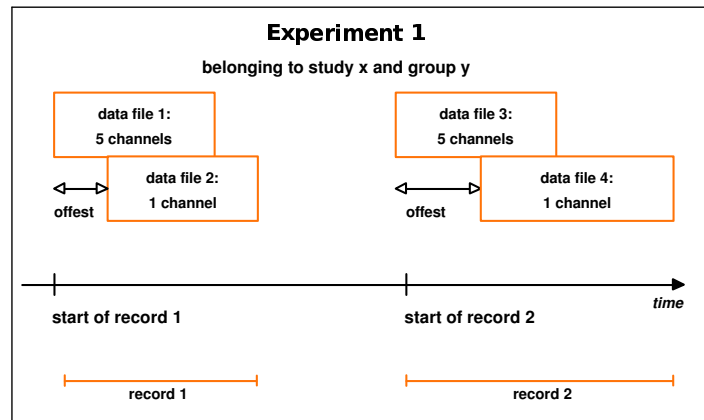


Figure 2.1: chronological course of an experiment

2.2.2 Division and Structure of Data Sets

A data collection can not only comprise data files containing the recorded measurement values, but must also include meta files - typically text files - describing and annotating the data files, i.e. the format of the data file, sampling rate, the setting of the experiment, information about the subject (animal or human) of the experiment, information about the studies and groups to which the experiment belongs, events which occurred in the course of the experiment, persons who are connected to the experiment, etc. While, in the case of the TOP-data collection, the data files have a size in the range of megabytes, annotation files are much smaller and in the range of kilobytes.

Defining a data set

An annotation file should contain all information belonging to a chosen set of data files. The annotation file together with the chosen set of data files then defines a **data set**. *We have chosen all data files of an animal experiment to be the above mentioned starting point for a data set.*

2.3 Demands

This section summarises the demands on the structure for annotation files and the characteristics of a database which shall be fed by the annotation files.

2.3.1 Annotation Files

- **Extensibility:** The information of an annotation file should be structured in a well designed way, such that this structure can also be used and extended for other data collections.

- **Accessibility:** Annotation files should be easily processable by applications (in order to read the corresponding data files correctly, fill a database by parsing all annotation files, etc.)

2.3.2 Database

- **Browse:** Applications accessing the database should provide the possibility to browse through the database, in order to get a survey of the data collection.
- **Query:** Applications accessing the database should provide the possibility to submit queries in order to find data sets with given properties.
- **Accessibility:** The database should not only be accessible from the computer where it is installed, but also from remote computers.
- **Interfaces:** Interfaces to the database should be provided for a variety of applications (Matlab, Perl, PHP/web-server, ODBC, R, MS-Excel, MS-Access, SPSS...).

2.3.3 General Considerations

- **Open Format:** Annotation files (such as data files) should be encoded in a non-proprietary way.
- **Availability:** The database software and its related applications should be free of charge.

2.4 Implementation

This section presents how we actually implemented the demands described above.

2.4.1 Annotation Files

We decided to fulfil the above mentioned demands on annotation files by using **XML files** [160]. The Extensible Markup Language (XML) is a physical data format allowing to enrich data with structure and meta-information. The *W3-consortium* [159] writes

Extensible Markup Language (XML) is a simple, very flexible text format derived from SGML (Standard Generalised Markup Language: ISO 8879). Originally designed to meet the challenges of large-scale electronic publishing, XML is also playing an increasingly important role in the exchange of a wide variety of data on the Web and elsewhere.

We already described the relations among data files and records of a data set (cf. Fig. 2.1). Besides annotating records including events, data file formats, etc., the XML file of a data set has to refer to the studies and groups it belongs to (Fig. 2.2). Finally, the XML file has to include information about the subject (animal or human) of the experiment and the persons who are connected to the experiment. The appendix (Figures 2.5 - 2.7) includes a prototype of an XML annotation file.

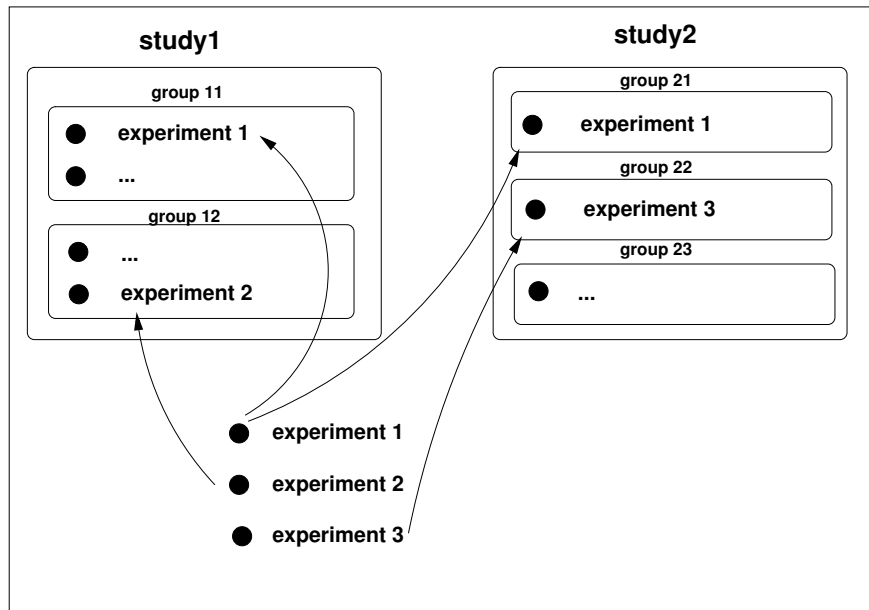


Figure 2.2: relations between studies, groups, and experiments

2.4.2 Database Design

We decided to use a *MySQL* database for implementation. The appendix (Figures 2.8 and 2.9) includes the SQL generation code for the tables included in the database, and figure 2.3 depicts the relations among these tables.

2.4.3 APIs

This subsection illustrates the APIs (Application Program Interfaces) between the XML annotation files, the database, Matlab, and an Apache webserver. Figure 2.4 shows a first overview. The XML annotation files are parsed by a **Perl** script which then inserts the database-relevant information into the **MySQL**-database. There are three **XML extra files** (*studies.xml*, *persons.xml*, *queries.xml*) which contain information about studies, persons and query templates (cf. section 2.4.3), which are not included in the XML annotation files. This information is also imported into the database by a Perl script. **Matlab** can access the database by two means: functions from the **Database Toolbox** and by launching Perl scripts from the Matlab command by using the `perl` command. The Matlab functions `xmlread` and `xmlwrite`, which use the **Java DOM** packages included in Matlab, are used to transfer the XML-structure to and from a Matlab-structure variable. The data files to which the annotation files refer are read with data file specific Matlab functions (`fread`, `textread`, etc.). **PHP** scripts can easily access the **MySQL** database by its functions and hence PHP enables the programming of dynamical web pages for browsing and querying the database. Finally, there are the cost-free software tools `mysqlcc` (MySQL Control Centre) and `phpMyAdmin`, which provide a variety of options to access the **MySQL**-database.

Query Templates

The TOP-database includes a special table called *queries*. This table lists SQL query templates which can be used by any application which can connect to the database. The tem-

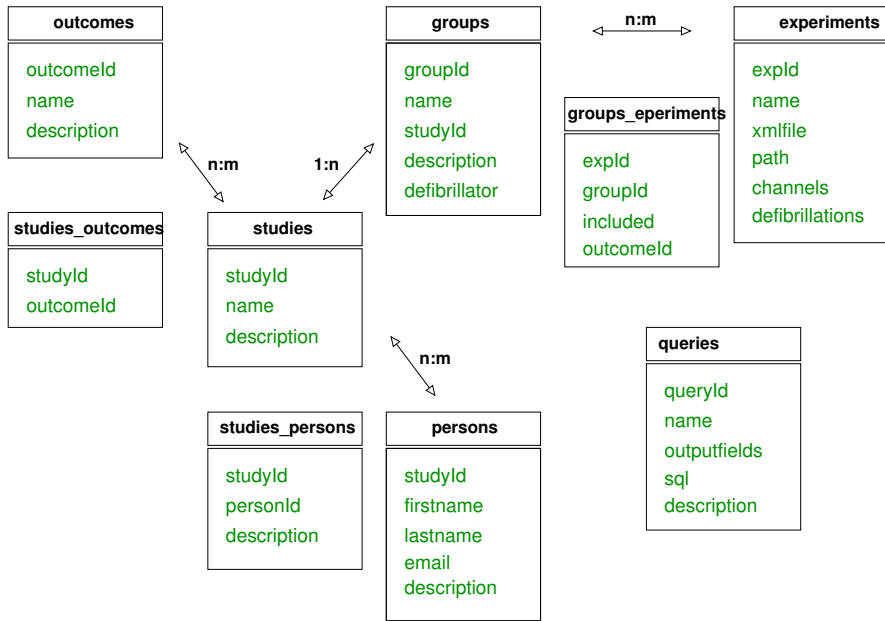


Figure 2.3: relations among tables of the TOP-database

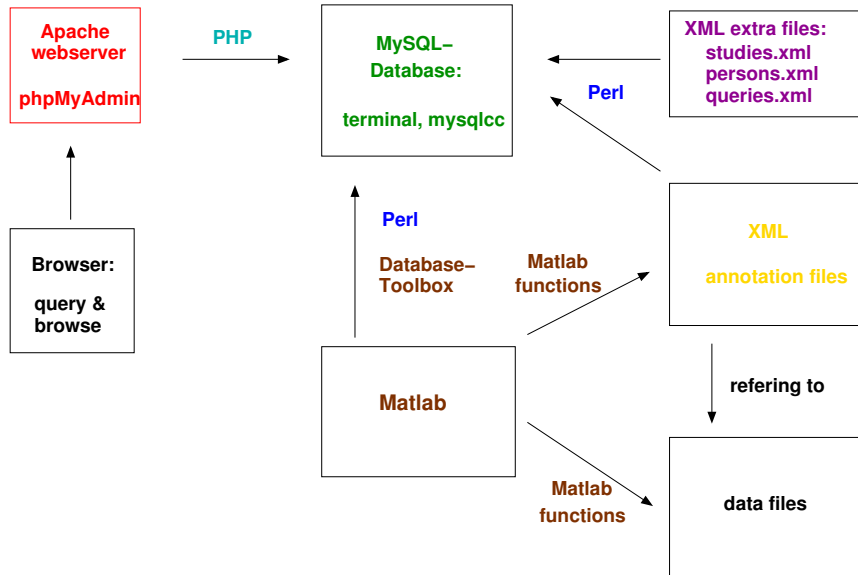


Figure 2.4: APIs

plates provide the possibility to submit queries without knowing the internal structure of the database (relations of tables, fieldnames,...).

2.5 Appendix

```

experiment_muster.xml 1
<?xml version="1.0" encoding="utf-8"?>
<!DOCTYPE experiment SYSTEM "experiments.dtd">
<experiment Id="1" Name="aprilmai_01">
  <study Id="3" Name="aprilmai" Included="yes">
    Outcome="no_ROSC" Group="combi">
    <description>animal laboratory study of V. Wenzel
      et al. which was ....</description>
    <comment></comment>
  </study>
  <study Id="5" Name="prolonged_vf" Included="no">
    Outcome="no_ROSC" Group="control">
    <description>animal laboratory study of V. Wenzel
      et al. which was ....</description>
    <comment></comment>
  </study>
  <subject Type="pig" Sex="male" Weight_kg="34">
    <description>tyrolean domestic pig</description>
    <comment>1 year old pig from Dr. Klima</comment>
  </subject>
  <record Type="experiment" Time="09:36:50.0">
    Date="1998-05-04">
    <experimenters>
      <experimenter Name="Achleitner, Ulrich">
        <comment>managed the preparation</comment>
      </experimenter>
      <experimenter Name="Rheinberger, Klaus">
        <comment>managed the experiment</comment>
      </experimenter>
    </experimenters>
    <settings>
      <setting Id="Ventilation" Value="bag with ITV"
        Unit=""/>
      <setting Id="CardiacMassage" Value="ACD masher
        (Voelckel)" Unit=""/>
    </settings>
    <comment>something was strange</comment>
    <dataFile Name="exp_ad_ad_ad_040598.bda">
      Type="transient recording" TimeOffset="0">
      <fileFormat Format="float32" Channels="4">
        SampleCount="1577984" SampleInterval="0.001"/>
      <description></description>
      <comment></comment>
      <channel Id="ekg" Unit="mV" Comment="Hellige">
        CalibOffset="0" CalibFactor="0.30769" Number="1">
        <settings>
          <setting Id="Filter" Value="on" Unit=""/>
          <setting Id="Lead" Value="I" Unit=""/>
          <setting Id="ElectrodeRedPosition"
            Value="top right" Unit=""/>
          <setting Id="ElectrodeYellowPosition"
            Value="top left" Unit=""/>
          <setting Id="ElectrodeBlackPosition"
            Value="bottom left" Unit=""/>
        </settings>
        <description>ECG of Hellige</description>
        <comment>something was strange</comment>
      </channel>
      <channel Id="art" Unit="mmHg" Comment="Hellige">
        CalibOffset="0" CalibFactor="1" Number="2">

```

Figure 2.5: page 1 of a sample XML annotation file

experiment_muster.xml	2
-----------------------	---

```

<settings>
  <setting Id="Range" Value="150" Unit="mmHg"/>
</settings>
<description/>
<comment/>
</channel>
<channel Id="zvd" Unit="mmHg" Comment="Hellige"
  CalibOffset="0" CalibFactor="1" Number="3">
  <settings>
    <setting Id="Range" Value="60" Unit="mmHg"/>
  </settings>
  <description/>
  <comment/>
</channel>
</dataFile>
<dataFile Name="co2.txt" Type="transient recording"
  TimeOffset="50">
  <fileFormat Format="ascii" Channels="2"
  SampleCount="123" Delimiter="tab" SkipRows="1"
  SkipColumns="0"/>
  <description>measurement of CO2</description>
  <comment></comment>
  <channel Id="time" Unit="sec" Comment=""
  CalibOffset="0" CalibFactor="1" Number="1"
  TimeChannel="">
  <settings/>
  <description></description>
  <comment></comment>
</channel>
<channel Id="co2" Unit="" Comment="" CalibOffset="0"
  CalibFactor="1" Number="2" TimeChannel="1">
  <settings/>
  <description>CO2 expiratory</description>
  <comment>short interruption</comment>
</channel>
</dataFile>
<dataFile Name="bild.jpg" Type="image" TimeOffset="25">
  <fileFormat Format="jpg"/>
  <description></description>
  <comment></comment>
</dataFile>
<events>
  <event Time="1425.1182" Id="Defi">
    <settings>
      <setting Id="SelectedEnergy" Value="100"
        Unit="J"/>
      <setting Id="DeliveredEnergy" Value="NaN"
        Unit="J"/>
      <setting Id="Impedance" Value="80" Unit="Ohm"/>
      <setting Id="Mode" Value="" Unit=""/>
      <setting Id="PreRhythm" Value="VF" Unit=""/>
      <setting Id="PostRhythm" Value="NSRwp" Unit=""/>
    </settings>
    <description></description>
    <comment></comment>
  </event>
  <event Time="337.2828" Id="Comment">
    <settings/>
    <description></description>
  </event>

```

Figure 2.6: page 2 of a sample XML annotation file

```
experiment_muster.xml 3
<comment>something strange happens</comment>
</event>
<event Time="527.1343" Id="DgAd">
  <settings>
    <setting Id="Access" Value="intravenous" Unit=""/>
    <setting Id="AdMode" Value="bolus" Unit=""/>
    <setting Id="Dose" Value="200" Unit="microg/kg"/>
    <setting Id="Name" Value="epi" Unit=""/>
  </settings>
  <description></description>
  <comment>foo</comment>
</event>
</events>
<calculations>
</calculations>
</record>
<record>
</record>
</experiment>
```

Figure 2.7: page 3 of a sample XML annotation file


```

top_structure.sql 1
USE top;

DROP TABLE IF EXISTS
studies, groups, experiments, outcomes, persons,
groups_experiments, studies_outcomes, studies_persons,
experiments_modified, queries;
# ----- main tables
CREATE TABLE studies (
  studyId INT NOT NULL AUTO_INCREMENT,
  name VARCHAR(60) NOT NULL UNIQUE,
  description TEXT DEFAULT NULL,
PRIMARY KEY (studyId, name)
);

CREATE TABLE groups (
  groupId INT NOT NULL AUTO_INCREMENT,
  name VARCHAR(60) NOT NULL,
  studyId INT NOT NULL,
  description TEXT DEFAULT NULL,
  defibrillator ENUM ('monophasic', 'Bruker Defigard', 'biphasic', 'Zoll M-Series')
DEFAULT NULL,
PRIMARY KEY (groupId)
);

CREATE TABLE experiments (
  expId INT NOT NULL AUTO_INCREMENT,
  name VARCHAR(60) NOT NULL UNIQUE,
  xmlfile VARCHAR(60) NOT NULL,
  path VARCHAR(60) NOT NULL,
  channels SET ('ekg', 'art', 'zvd', 'pap', 'ekg2') NOT NULL,
  defibrillations INT DEFAULT NULL,
PRIMARY KEY (expId, name)
);

CREATE TABLE outcomes (
  outcomeId INT NOT NULL AUTO_INCREMENT,
  name VARCHAR(60) NOT NULL UNIQUE,
  description TEXT DEFAULT NULL,
PRIMARY KEY (outcomeId, name)
);

CREATE TABLE persons (
  personId INT NOT NULL AUTO_INCREMENT,
  firstname VARCHAR(60) NOT NULL,
  lastname VARCHAR(60) NOT NULL,
  email VARCHAR(60) DEFAULT NULL,
  description TEXT DEFAULT NULL,
PRIMARY KEY (personId)
);

CREATE TABLE queries (
  queryId INT NOT NULL AUTO_INCREMENT,
  name VARCHAR(60) NOT NULL UNIQUE,
  inputs INT NOT NULL,
  outputs INT NOT NULL,
  sql TEXT NOT NULL,
  description TEXT DEFAULT NULL,
PRIMARY KEY (queryId)
);

```

Figure 2.8: page 1 of the SQL generation code for the TOP-database

```
top_structure.sql 2

# ----- relational tables
CREATE TABLE groups_experiments (
  expId INT NOT NULL,
  groupId INT NOT NULL,
  included ENUM ('yes', 'no', 'N/A') NOT NULL,
  outcomeId INT NOT NULL,
  PRIMARY KEY (expId, groupId, outcomeId)
);

CREATE TABLE studies_outcomes (
  studyId INT NOT NULL,
  outcomeId INT NOT NULL,
  PRIMARY KEY (studyId, outcomeId)
);

CREATE TABLE studies_persons (
  studyId INT NOT NULL,
  personId INT NOT NULL,
  description TEXT DEFAULT NULL,
  PRIMARY KEY (studyId, personId)
);

CREATE TABLE experiments_modified (
  expId INT NOT NULL,
  personId INT NOT NULL,
  time TIMESTAMP
  ,
  PRIMARY KEY (expId, personId)
);
```

Figure 2.9: page 2 of the SQL generation code for the TOP-database

Chapter 3

The MRL Human Study Data

Contents

3.1 Introduction	33
3.2 Raw Data Acquisition	34
3.2.1 Data Card Management	34
3.2.2 Management of Patient Related Data	34
3.3 Data Post-Processing	36
3.3.1 Transformation to XML-based Data Sets	36
3.3.2 Editing XML-based Data Sets and Data Analysis	37
3.4 Appendix	37

3.1 Introduction

In August 2003 Medical Research Laboratories (MRL, Buffalo Grove, Illinois, USA, meanwhile part of Welch Allyn) and the Department of Anaesthesia, Innsbruck Medical University (Austria), Division of Experimental Anaesthesia (represented by Univ.-Prof. Dr. Anton Amann and Univ.-Doz. Dr. Michael Baubin) have started the study *Defibrillation in out-of-hospital cardiac arrest patients: a comparison of the mono- and biphasic defibrillation pulses of Medical Research Laboratories*. This study comprises the comparison of MRL mono- and biphasic defibrillation pulses and the collection of ECG-data of out-of-hospital cardiac arrest patients. MRL supplied the Innsbruck emergency medical system (EMS) with 4 fully equipped "PIC" defibrillators with the possibility to record 2-3 ECG leads at 375 Hz sampling frequency. From August 19th 2003 to January 15th 2004 the two Innsbruck EMS-cars were equipped with identically looking defibrillators, one monophasic and one biphasic. Both defibrillators were used at the same escalating energy levels (200J - 300J - 360J). After January 15th 2004 only biphasic defibrillators have been used.

This chapter describes the data acquisition, the data management, and the data post-processing in the above mentioned study as it has been developed at the Department of Anaesthesia, Innsbruck Medical University, Austria. This comprises the automated transfer of the data collected by the defibrillators on an internet server, the acquisition of patient related data via a web-interface and a database on the above mentioned internet server, the transformation of the MRL proprietary data format to XML-based data sets, and custom

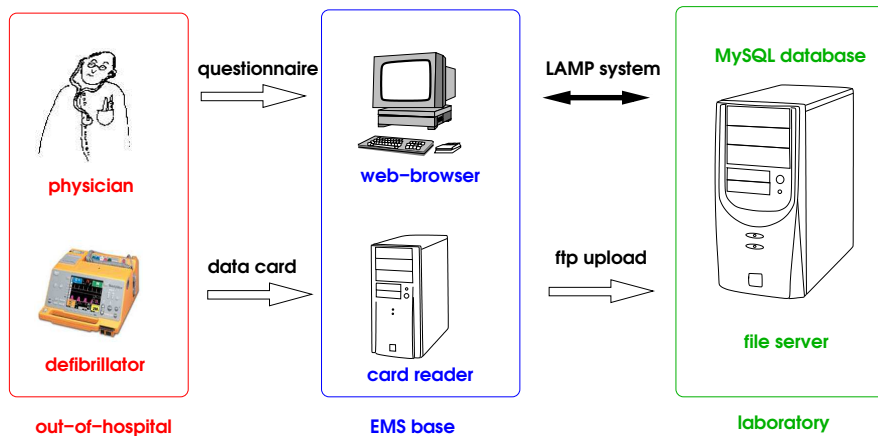


Figure 3.1: data flow of raw data acquisition

made Matlab software for editing and analysing these data sets. The intent was to provide the technical means to back up the two main aims of the study:

- The collection of patient related data of out-of-hospital cardiac arrests in order to compare the mono- and biphasic defibrillation pulses within the scope of a statistical analysis.
- The collection of annotated ECG-data of out-of-hospital cardiac arrest patients in order to analyse it with various mathematical methods in view of the predictability of defibrillation success and feedback for the advanced cardiac life support (ACLS) efforts of the physician.

3.2 Raw Data Acquisition

Figure 3.1 sketches roughly the raw data acquisition flow from the out-of-hospital setting to the EMS base and finally to the laboratory.

3.2.1 Data Card Management

The defibrillators are always loaded with data cards, which have a storage capacity of 8 MB. Thus, neither the physician nor his paramedic has to bother about inserting a data card, when they arrive at a cardiac arrest patient. Any time the defibrillator is switched on, all tracings of the defibrillator's display together with annotations are saved on the data card in terms of an *incident*. This are at most three tracings. The defibrillator has to be configured deliberately to record all tracings, as the default mode is to record only the first tracing of the display, which is always an ECG lead. After having used the defibrillator, when the physician returns to the EMS base, he plugs the data card into the card reader, no matter if he has treated a cardiac arrest patient or not. The data is read off the card and the card is cleared, now ready for new use. Custom made software on the computer, on which the card reader is installed, continuously checks the folder, where the data is transferred to by the card reader. If there is new data, an FTP upload to the server in the laboratory is launched. In this way, one can remotely keep track of new card data, and all card files (extension *.crd) are automatically collected at a central server.

3.2.2 Management of Patient Related Data

Besides uploading the annotated card data, the physician has to fill in an online questionnaire about patient related data, which is not contained on the data cards. This includes

- **administrative information:** name of the emergency physician, the emergency car, mission number, location of the emergency, start time
- **general patient data:** initials, sex, date of birth, (estimated) height, (estimated) weight
- **anamnesis:** known diseases, cerebral ability before the cardiac arrest, pregnancy, former cardiac arrests, estimated reason for actual cardiac arrest
- **CPR management:** time of cardiac arrest, CPR and defibrillation by laypersons, CPR and defibrillation by paramedics, first registered ECG rhythm
- **time course of CPR by the emergency physician:** arrival of emergency physician, intubation, intravenous access, defibrillation series (pre and post rhythm of each shock), drug administrations
- **result of reanimation efforts:** duration of spontaneous circulation, if so, together with blood pressure, heart rate, possibly more drug administrations, and admission to hospital, (technical) complications

All possible events listed in the questionnaire can be completed by a time specification. Although the annotations of the card data include the times and energies of all defibrillations, we decided to comprise defibrillations in the questionnaire, as this gives the physicians the possibility to document pre and post rhythms of the shocks, which in turn is highly useful for the data analysis. A copy of an empty questionnaire can be found in the appendix (Figures 3.3 - 3.6).

The computer at the laboratory provides a so-called *LAMP* system, i.e. a Linux operating system, an Apache web server, and a MySQL database server together with PHP (or Perl, or Python). Every emergency physician at the Department of Anaesthesia has got a username and a password to log into the PHP-webpages and insert data into a newly generated questionnaire. The physician can keep the documentation *disclosed* in order to complete it at a later login. This may happen, when the physician has to stop filling in the questionnaire because of a new emergency case, or because certain information about the patient is not available at the time. However, the documentation has to be completed sometime, and the physician can then *close* the questionnaire by clicking a certain button. However, as long as certain fields in the questionnaire are empty or not filled in correctly, the PHP page refuses the closing of the questionnaire. Blinking red buttons appear at the beginning of the incomplete or erroneous lines, cf. appendix (Figures 3.3 - 3.6).

The LAMP system also includes user administration facilities. The following different *permissions* can be granted to users:

- permission to change his own password
- permission to add new users
- permission to administrate his/her added users
- permission to add new data and edit own disclosed data

- permission to add new data and edit all disclosed data
- permission to delete disclosed data
- permission to view closed data
- permission to edit closed data

The usage of an online form with registered users as outlined above may appear like breaking a fly on the wheel, however, once constructed and at work, it provides a series of **advantages** compared to a "paper study":

- In contrast to paper forms, there are no badly readable entries.
- The physician can fill in the form from anywhere¹, all he needs is an internet browser.
- It can be clearly tracked back who generated a documentation at which time and who edited the documentation at last and at which time.
- User administration facilities are difficult to establish for "paper studies".
- The hardware costs are minimal². The software costs are zero, thanks to GNU and Linux.
- Somewhere along the way, the data of paper forms have to be typed tediously into a computer. Storing the patient related data via a PHP-form into a MySQL data base provides a good starting point for later statistical analyses with various software.
- Once a LAMP online system is constructed, a modified copy of it can easily be used contemporaneously for other studies.

It has to be noted, that the emergency physicians at the Department of Anaesthesia have to fill in a so-called *NaCaX-protocol* and a so-called *reanimation protocol* additionally to the MRL-online questionnaire. These two information sources are accessible for later corrections and comparisons.

3.3 Data Post-Processing

3.3.1 Transformation to XML-based Data Sets

The data cards of the MRL defibrillators store tracings and annotations in an MRL proprietary data format. The aim of the ECG-data acquisition is, however, to process and analyse the data by mathematical software such as Matlab, Octave, R, etc. This requires the file format of the data to be known. MRL kindly provided us with C-program code, such that software, named `mrl2bda`, could be made, which can transform a *.crd-file of the data cards into an (*.xml, *.bda) pair of files.

XML annotation files have already been discussed in chapter 2. The *.bda extension is a custom invention and is used at the Department of Anaesthesia to name a special binary file format to code transient recordings, e.g. of ECG leads, invasive blood pressures, EEG leads,

¹For security reasons, the range of IP addresses from, which the online pages are reachable, has been restricted.

²An "old" Pentium II together with an 80 GB hard disk is in use for the study in discussion.

blood flows, defibrillation pulses, etc. This binary data type stores the samples of generally multiple *channels* of transient recordings sequentially in float32 or float64 format. The channels have to be recorded at a specified common sampling rate, such that a well-defined time vector can be associated with the different channels. The same number of samples is stored for every channel. Figure 3.2 shows the structure of the *.bda file format. The

Sequence of samples in a *.bda file with 3 channels

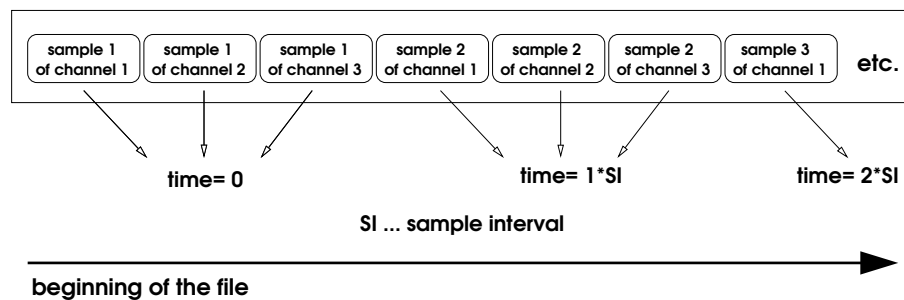


Figure 3.2: structure of the *.bda file format

sampling rate and the floating point format of a *.bda file are not coded in the file and have therefore to be annotated externally, e.g. in the XML annotation file. The *.bda file format saves disk space and the data can be quickly and easily read and written by standard C-commands, which also appear in Matlab (`fread`, `fwrite`).

Every time an MRL defibrillator equipped with a data card is switched on, a new so-called *incident* is launched on the data card. When the defibrillator is switched off again, the incident is concluded. The program `mrl2bda` now transforms every incident of a data card to an (*.xml, *.bda) pair of files. The BDA-file stores the different ECG leads and the other channels, which have been selected for display on the MRL defibrillator during the incident, as separate channels. The number of channels in the BDA-file therefore depends on how often the emergency physician or the paramedic has changed the display channels on the defibrillator.

In order to eliminate artefacts in the channels, the `mrl2bda` program replaces the neighbourhood of marginal sample values, i.e. minimal and maximal amplitudes, by NaN (not a number) values in the BDA-files.

In the general case, the defibrillator is switched on and off more than once during the course of a cardiac arrest emergency. The resultant (*.xml, *.bda) pairs of the different incidents have to be merged to one XML-based data set consisting of one XML-file and the different BDA-files. The XML-file refers to the BDA-files of the different, chronologically separated, incidents as records, cf. chapter 2.

Finally, in order to fulfil the demand, that the XML-file should contain all necessary meta data of a data set, the patient-related information collected with the PHP-online-forms has to be inserted into the XML-file. Therewith, the transformation of cardiac arrest emergencies to XML-based data sets is completed.

3.3.2 Editing XML-based Data Sets and Data Analysis

After having transformed the card data from the MRL proprietary data format to XML-based data sets with open file formats, the data is now ready to be processed by mathematical software such as Matlab, for example. A graphical user interface (GUI) called `booka` has

been programmed to view the transient recordings of the MRL defibrillator and edit events. Figures 3.7 and 3.8 in the appendix show a snapshot of the main interface and the event editing window, respectively.

The analysis of the data with various mathematical methods in view of the predictability of defibrillation success requires to know the pre and post defibrillation rhythms of the heart. Therefore, the event edit interface offers the possibility to choose from a list of ECG rhythms, which is explained in tables 3.1 and 3.2.

no information about pulse	with pulse	without pulse
VT	VTwp	VF pVT PEA
VB	VBwp	pVB A
NSR	NSRwp	pNSR
OAR	OARwp	pOAR
PM	PMwp	pPM

Table 3.1: List of ECG rhythms

A	...	asystole
VF	...	ventricular fibrillation
VT	...	ventricular tachycardia
PEA	...	pulseless electrical activity
VB	...	ventricular bradycardia
NSR	...	normal sinus rhythm (> 10 seconds)
OAR	...	other atrial rhythm
PM	...	pacemaker
Xwp	...	X with pulse
pX	...	pulseless X

Table 3.2: Legend for list of ECG rhythms

In practice, a physician - preferably the emergency physician, who recorded the data - has to go through the data set and determine all pre and post defibrillation rhythms, probably supported by the patient related data together with the *NaCaX-protocol* and the *resuscitation protocol*, cf. 3.2.2.

3.4 Appendix

Benutzer: Klaus Rheinberger

Eingabeformular zur MRL Studie der Univ. Klinik für Anästhesie, Innsbruck

Einschlusskriterium:
 außerklinischer Patient mit Kreislaufstillstand, der mit einem MRL-Defibrillator defibrilliert wurde
Ausschlusskriterien:
 es wurde **kein** MRL Defibrillator benutzt

Zeiteingaben:
 Die erste Zeiteingabe muß im Format "Jahr-Monat-Tag Stunde:Minute" erfolgen. Bei allen weiteren Zeiteingaben kann man das Datum bzw. auch die Stunde weglassen, welche dann automatisch beim "Speichern" ergänzt werden.
Speichern:
 Eingegebene Daten werden erst beim Anklicken eines "Speichern" Knopfes gespeichert. Wenn man also das Formular ohne zu Speichern verläßt, gehen neu eingegebene Daten verloren.
Fehler:
 Fehlende oder fehlerhafte Angaben werden nach dem ersten Speichern mit einem blinkenden roten Punkt markiert.

Notarzt

Rettungsmittel

Einsatznummer z.B.: 1-25-xxxxxx, wobei 25 die Nummer des Fahrzeugs und
 xxxxxx die 6-stellige von der Einsatzzentrale zugewiesene Nummer ist

Ort

Einsatzort Straße

Einsatzbeginn

Patientendaten

Name (nur Initialen)

Geschlecht männlich weiblich

Geburtsdatum

Gewicht/Größe (geschätzt) kg cm

Anamnese

bekannte Vorerkrankungen

- Z.n. ACS (akutes Coronarsyndrom = instabile AP/AMI)
- andere KHK (koronare Herzkrankheit)
- Z.n. Bypass OP
- Z.n. anderer Herzoperation
- Herzrhythmusstörungen
- Herzinsuffizienz
- Cardiomyopathien
- Vitien (Herzklappenfehler)
- Pacer (Herzschrittmacher)
- AVK (arterielle Verschlusskrankheit)
- Hypertonie (Bluthochdruck)
- Venenthrombose
- Diabetes mellitus
- Hyperlipidämie
- Adipositas
- Asthma
- COPD (chronische obstruktive pulmonale Erkrankung)
- Lungenerkrankung
- Niereninsuffizienz
- Dialysepatient
- Leberzirrhose
- C₂-Abusus (AlkoholiKER)

Figure 3.3: page 1 of the MRL online questionnaire

Nikotin-Abusus
 i.V. Drogen-Abusus

zerebrale Leistungsfähigkeit vor dem Kreislaufstillstand **vor** gut mittel schlecht Koma

gut: Bei Bewußtsein, aufmerksam, arbeitsfähig. Der Patient ist in der Lage ein normales Leben zu führen. Eventuell milde neurologische und psychologische Defizite (milde Dysphasie, nicht störende Hemiparese).
mittel: Bei Bewußtsein. Der Patient ist in der Lage Teilzeitarbeit in einer geschützten Werkstätte zu verrichten und kann einfache Dinge des täglichen Lebens bewältigen (kann sich selbst anziehen, Mahlzeiten zubereiten, öffentliche Verkehrsmittel benutzen).
schlecht: Bei Bewußtsein. Der Patient ist wegen seiner eingeschränkten Hirnfunktion von der Hilfe anderer abhängig. Kognitionsfähigkeit zumindest eingeschränkt.
Koma: Nicht bei Bewußtsein. Keine Wahrnehmung der Umgebung. Keine verbale oder psychologische Interaktion mit der Umwelt möglich.

schwanger nein ja unbekannt
früherer Kreislaufstillstand nein ja unbekannt (wenn ja, dann bitte wann 'Jahr' oder 'Jahr-Monat' oder 'Jahr-Monat-Tag')

vermutete Ursache des aktuellen Kreislaufstillstandes unbekannt
kardial bedingter Kreislaufstillstand:
 Herzinfarkt
 primäre Rhythmusstörung
 Myokarditis
nicht kardial bedingter Kreislaufstillstand:
 Lungenembolie
 Intoxikation
 primäres zerebrales Ereignis
 Kreislaufstillstand nach Trauma (inkl. Erhängen,...)
 hämorrhagischer Schock
 Asphyxie (Ertrinken,...)

CPR Management

Uhrzeit (Minuten' oder 'Stunden:Minuten' oder 'jjjj-mm-dd hh:mm')

Zeitpunkt des Kreislaufstillstandes ziemlich genau eher ungenau

Reanimationsmaßnahmen durch Laien

CPR durch Laien
 Defibrillation durch Laien (PAD): Anzahl Schocks
 keine Laien-Defibrillation
 Fred Easy
 Lifepak CR+
 MRL Lifequest
 Laerdal FR
Defipulsform:
 monophasisch biphasisch unbekannt

Reanimationsmaßnahmen durch geschultes nicht ärztliches Rettungs- oder Pflegepersonal

CPR durch geschultes Rettungs- oder Pflegepersonal
 Frühdefibrillation: Anzahl Schocks
 keine Frühdefibrillation
 Fred
 Lifepak 12
 Lifepak 500
 MRL Lifequest
 Forerunner FR1
 Forerunner FR2
Defipulsform:
 monophasisch biphasisch unbekannt

Definitionen:
Spontankreislauf: elektrische Aktivität mit Auswurf und Puls.
defibrillationswürdige Rhythmen:
pVT: pulslose ventrikuläre Tachykardie, regelmäßiger EKG-Rhythmus konstanter Amplitude mit QRS-Verbreiterung > 0.12 sec und

Figure 3.4: page 2 of the MRL online questionnaire

Frequenz > 100/min, jedoch ohne Puls.
VF/kaFl: ventrikuläres Flimmern / Kammerflimmern, in Frequenz und Amplitude unkoordiniertes EKG ohne effiziente Ventrikelkontraktion.
nicht defibrillationswürdige Rhythmen:
PEA/EMD: pulslose elektrische Aktivität / elektromechanische Entkopplung, jede Form elektrischer Aktivität außer VF/pVT, die zwar mit einer elektrischen Depolarisation einhergeht, welche einen Auswurf erwarten ließe, aber ohne darauffolgende Ventrikelkontraktion und damit ohne Auswurf.
Asystolie: Elektrischer Herzstillstand, keine ventrikuläre Erregung, z.B. O-Linie, dying heart, reine Vorhoferregung.

erstes registriertes EKG Speichern Speichern und Beenden Abbrechen

Spontankreislauf pVT VF PEA/EMD Asystolie

Notärztliches Ereignisprotokoll (mit MRL Defibrillator)

Uhrzeit (hh:mm) zeitlicher Ablauf muß nicht in dieser Reihenfolge sein

Eintreffen des Notarztes

Intubation

Intravenöser Zugang

1. Defibrillationsserie Speichern Speichern und Beenden Abbrechen

Ausgangsrhythmus pVT VF unbekannt

EKG nach 1. Schock Spontankreislauf pVT VF PEA/EMD Asystolie kein Schock

EKG nach 2. Schock Spontankreislauf pVT VF PEA/EMD Asystolie kein Schock

EKG nach 3. Schock Spontankreislauf pVT VF PEA/EMD Asystolie kein Schock

Medikamentengabe Speichern Speichern und Beenden Abbrechen

Adrenalin mg

Pitressin Einheiten

Atropin mg

Sedacorone mg

Lidocain mg

Mg⁺⁺ g

NaHCO₃ ml

Ergebnis Speichern Speichern und Beenden Abbrechen

Spontankreislauf

keiner min

Dauer min

bis Klinikaufnahme

Blutdruck mmHg stabil instabil

Herzfrequenz min⁻¹

weitere Medikamentengaben


Figure 3.5: page 3 of the MRL online questionnaire

<input type="text"/>	<input checked="" type="checkbox"/> Klinikaufnahme <input type="checkbox"/> MZA Schockraum <input type="checkbox"/> Unfall Schockraum <input type="checkbox"/> Hall Schockraum <input type="checkbox"/> Abbruch der Reanimation / Todesfeststellung
----------------------	---

weiteres

Komplikationen	<input type="checkbox"/> Aspiration <input type="checkbox"/> Thoraxinstabilität sonstige
Technische Probleme	

<input type="button" value="Speichern"/>	<input type="button" value="Speichern und Beenden"/>	<input type="button" value="Abbrechen"/>
--	--	--



[Tier-OP Datenbank](#)
[MRL Studie \(Hilfe\)](#)
[Administration](#)
[Logout](#)
© 2003 Peter Hamm, Univ. Klinik für Anästhesie, Innsbruck

Figure 3.6: page 4 of the MRL online questionnaire

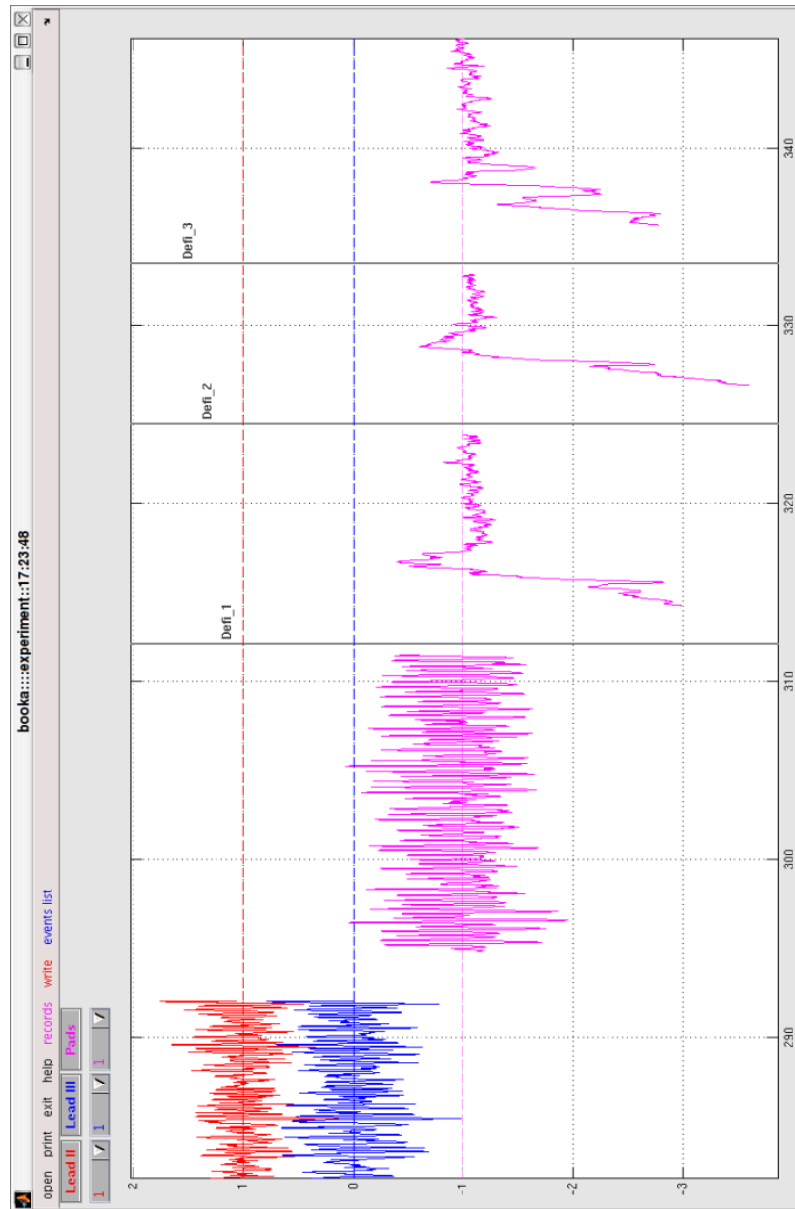


Figure 3.7: Matlab GUI for viewing channels of XML-based data sets

Parameter	Value	Unit
SelectedEnergy	200	J
DeliveredEnergy	191	J
Impedance	102	Ohm
Current	170	A
Mode	biphasic, MRL-PIC	
PreRhythm		
PostRhythm		

Buttons: Cancel (red), Set it! (green)

Figure 3.8: editing events of XML-based data sets

Part II

Mathematical Methods

Chapter 4

Principles of Time Series

Contents

4.1	Modelling Time Series	47
4.1.1	Construction of the probability space, backward shift operator	48
4.1.2	Induced Structures	49
4.2	Best MSE Forecast	54
4.3	Best Linear MSE Forecast	55
4.3.1	Hilbert Space Formalism	55
4.3.2	Ordinary Least Squares, Linear Regression	58
4.3.3	Vectors of Random Variables	59
4.3.4	Iterated and Updating Projections	60
4.4	The Gaussian Case	60

4.1 Modelling Time Series

This section handles with the mathematical modelling of data generated in a measurement process. The distinction between the values (i.e. recorded numbers) of observations and the mathematical structure modelling the realisation of these values is strongly emphasised. Much of the material covered here (and a lot more) can be found in [31, 30, 100].

Definition 4.1 (Time Series (TS)) *A time series is a function $x : T \rightarrow \mathbb{R}$ which assigns an observation or data value $x(t)$ to a specified time $t \in T$, when the observation was recorded. If $T \subseteq \mathbb{R}$ is a discrete set, e.g., $T = \mathbb{Z}$, the observations are denoted x_t and the time series is called a discrete time series. If T is a continuous set, e.g. $T = [0, 1] \subseteq \mathbb{R}$, the observations are denoted $x(t)$ and the time series is called a continuous time series.*

We will restrict ourselves to discrete time series subsequently, because all data we are dealing with was recorded at discrete times.

The notion *time series* describes the data values or samples collected during a certain measurement process. In order to build a mathematical model for the process itself, generating the data, one has to allow for the *possibly unpredictable* nature of (future) observations. The common way of handling this task is to assume that each observation x_t is a realised value of a certain *random variable* X_t . This results in the following definition.

Definition 4.2 (Stochastic Process) A stochastic process X is a family of random variables $\{X_t, t \in T\}$ defined on a common probability space $\{\Omega, \mathbb{F}, P\}$.

This means that for every $t \in T$ there is a random variable X_t , i.e. a function

$$\begin{aligned} X_t : \Omega &\rightarrow \mathbb{R} \\ \omega &\mapsto X_t(\omega). \end{aligned}$$

Such a random variable X_t models all possible observations x_t , which could be recorded at time t . Vice versa, if the observation x_t is a realisation of the random variable X_t , there exists an $\omega \in \Omega$ such that $x_t = X_t(\omega)$. This can be clarified more by defining functions

$$\begin{aligned} X(\omega) : T &\rightarrow \mathbb{R} \\ t &\mapsto X_t(\omega), \end{aligned}$$

for every $\omega \in \Omega$. Such a function is called a *realisation* or *sample-path* of the stochastic process X . A time series x is generated by a stochastic process X , if there exists a realisation $X(\omega)$, i.e. an $\omega \in \Omega$, such that

$$x = X(\omega).$$

Remark 4.1 The distinction between a time series and its generating stochastic process is often silently blurred or even ignored, and one uses the notion time series for both mathematical structures.

4.1.1 Construction of the probability space, backward shift operator

To get an impression of the space Ω , we construct it explicitly by defining $\Omega := \mathbb{R}^T$, i.e., $\Omega = \{x : T \rightarrow \mathbb{R}\}$, which is the set of all sample-paths corresponding to the chosen time-set T .

Using this definition and restricting ourselves to the case that $T = \mathbb{Z}$, the random variables $\{X_t, t \in \mathbb{Z}\}$ and the *backward shift operator* B can be nicely defined. For every $t \in \mathbb{Z}$ define X_t by

$$\begin{aligned} X_t : \mathbb{R}^{\mathbb{Z}} &\rightarrow \mathbb{R} \\ x &\mapsto X_t(x) := x(t). \end{aligned}$$

The random variable X_t is therefore the evaluation function with argument t , or the projection onto the t -th component of x . Now define on \mathbb{Z} the backward translation

$$\begin{aligned} b : \mathbb{Z} &\rightarrow \mathbb{Z} \\ t &\mapsto b(t) := t - 1. \end{aligned}$$

This induces a pullback operation b^* on $\mathbb{R}^{\mathbb{Z}}$

$$\begin{aligned} b^* : \mathbb{R}^{\mathbb{Z}} &\rightarrow \mathbb{R}^{\mathbb{Z}} \\ t &\mapsto b^*(x) := x \circ b. \end{aligned}$$

We define the *backward shift operator* B on the family of random variables $\{X_t, t \in \mathbb{Z}\}$ by

$$\begin{aligned} B : \{X_t, t \in \mathbb{Z}\} &\rightarrow \{X_t, t \in \mathbb{Z}\} \\ X_t &\mapsto B(X_t) := X_t \circ b^* = X_{t-1} \end{aligned}$$

4.1.2 Induced Structures

Given a probability space $\{\Omega, \mathbb{F}, P\}$, a random variable $X : \Omega \rightarrow \mathbb{R}$ induces a probability measure P^* on \mathbb{R} . For a (measurable) subset $A \subseteq \mathbb{R}$ define

$$P^*(A) := P(X^{-1}(A)).$$

The *probability distribution function* $F_X : \mathbb{R} \rightarrow [0, 1]$ of P^* is defined as

$$F_X(x) := P^*((-\infty, x)).$$

The *probability density function* $f_X : \mathbb{R} \rightarrow \mathbb{R}$ is the first (generalised) derivative of F_X . It follows that

$$F_X(a) = \int_{-\infty}^a f_X(x) dx$$

and

$$\int_{-\infty}^{\infty} f_X(x) dx = 1.$$

The *expectation* $E(X)$ or *mean* μ of a random variable $X : \Omega \rightarrow \mathbb{R}$ is defined as

$$E(X) := \int_{\mathbb{R}} x f_X(x) dx. \quad (4.1)$$

A function $g : \mathbb{R} \rightarrow \mathbb{R}$ can be used to generate a new random variable $g(X) := g \circ X$ from X . The following proposition asserts how random variables of this kind can be handled, cf. [24, 25].

Proposition 4.1 *The expectation $E(g(X))$ of $g(X)$ can be computed using the probability density function f_X of X :*

$$E(g(X)) = \int_{\mathbb{R}} g(x) f_X(x) dx.$$

Proof.

Substituting with respect to g one can write

$$E(g(X)) = \int_{\mathbb{R}} y f_{g(X)}(y) dy = \int_{\mathbb{R}} g(x) f_{g(X)}(g(x)) |g'(x)| dx.$$

On the other hand $(f_{g(X)} \circ g) \cdot |g'|$ is the probability density function f_X of X , because for all $A \subseteq \mathbb{R}$ it holds that

$$\int_A f_X(x) dx = \int_{g(A)} f_{g(X)}(y) dy,$$

and according to the same substitution as above the right-hand side of the last equation equals

$$\int_A f_{g(X)}(g(x)) |g'(x)| dx.$$

□

Corollary 4.1 *The expectation operator E is linear, i.e. for random variables X and Y and numbers a and $b \in \mathbb{R}$ it holds that*

$$E(aX + bY) = aE(X) + bE(Y).$$

The variance $\text{Var}(X)$ of a random variable X is defined as

$$\text{Var}(X) := \mathbb{E}([X - \mathbb{E}(X)]^2) = \int_{\mathbb{R}} (x - \mathbb{E}(X))^2 f_X(x) dx,$$

and because of Corollary 4.1 we have

$$\begin{aligned} \text{Var}(X) &= \mathbb{E}(X^2) - \mathbb{E}(X)^2 \\ \text{Var}(a + bX) &= b^2 \text{Var}(X) \quad \forall a, b \in \mathbb{R}. \end{aligned}$$

Let's consider two random variables X and Y defined on a common probability space $\{\Omega, \mathbb{F}, P\}$. Just as in the case of only one random variable, now the pair $(X, Y) : \Omega \rightarrow \mathbb{R}^2$ induces a probability measure on \mathbb{R}^2 . The induced probability density function $f_{X,Y} : \mathbb{R}^2 \rightarrow \mathbb{R}$ is called the *joint distribution function*. The probability density function f_X of X can be reconstructed from the joint distribution function $f_{X,Y}$ via the so-called *marginal density function* :

$$f_X(x) = \int_{\mathbb{R}} f_{X,Y}(x, y) dy.$$

The marginal density function for Y is defined analogously. The *conditional density function* of Y given $X = x$ is the probability density function $f_{Y|X}(\cdot|x)$ on \mathbb{R} defined as

$$f_{Y|X}(y|x) := \begin{cases} \frac{f_{X,Y}(x,y)}{f_X(x)} & \text{if } f_X(x) > 0 \\ 0 & \text{otherwise} \end{cases}$$

Figure 4.1 shows in an example that the conditional density function of Y given $X = 2$ equals the intersecting line of the joint distribution function at $x = 2$ but normalised to yield unit area under the distribution. The definition of the conditional density function implies the *Bayes' theorem* for density functions

$$f_{X,Y}(x, y) = f_{Y|X}(y|x) f_X(x).$$

The *conditional expectation of Y given $X = x$* , denoted as $\mathbb{E}(Y|X = x)$, is the mean of the conditional density function of Y given $X = x$, i.e.,

$$\mathbb{E}(Y|X = x) := \int_{\mathbb{R}} y f_{Y|X}(y|x) dy.$$

Figure 4.2 shows as a contour plot the joint distribution function and the conditional expectation of Y given $X = x$ as a function of x . Not specifying a certain value for X yields the notion of the *conditional expectation of Y given X* , denoted as $\mathbb{E}(Y|X)$. It is defined as a random variable in terms of X , which his means that $\mathbb{E}(Y|X)$ is a function $g \circ X$ of X , mostly denoted $g(X)$:

$$\begin{aligned} g \circ X : \Omega &\rightarrow \mathbb{R} \rightarrow \mathbb{R} \\ \omega &\mapsto X(\omega) =: x \mapsto g(x) := \mathbb{E}(Y|X = x) \end{aligned}$$

Remark 4.2 Note that $\mathbb{E}(Y|X = x)$, the conditional expectation of Y given $X = x$, is a number, while $\mathbb{E}(Y|X)$, conditional expectation of Y given X , is a random variable.

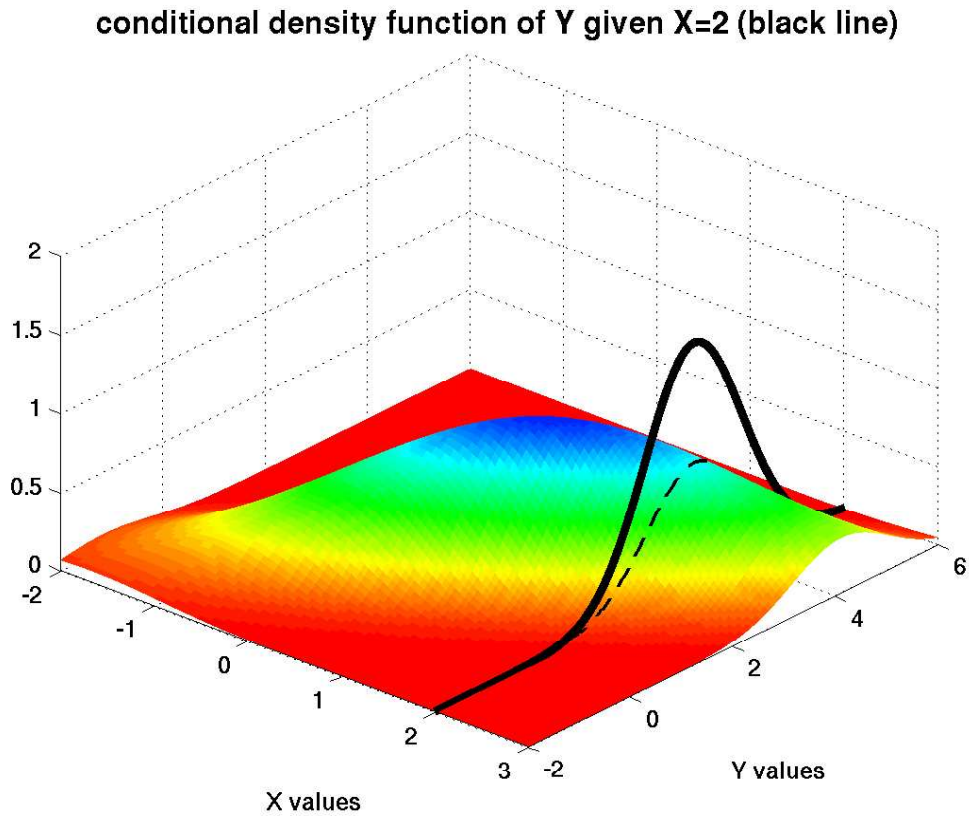


Figure 4.1: Surface plot of an exemplary Gaussian joint distribution function $f_{X,Y}$ and the attendant conditional density function $f_{Y|X}(y|x)$ for $x = 2$.

Corollary 4.2 (law of iterated expectations) *The expectation of the conditional expectation of Y given X is equal to the expectation of Y, i.e.,*

$$E(E(Y|X)) = E(Y).$$

Proof.

$$\begin{aligned} E(E(Y|X)) &= \int_{\mathbb{R}} \int_{\mathbb{R}} y f_{Y|X}(y|x) dy f_X(x) dx \\ &= \int_{\mathbb{R}} \int_{\mathbb{R}} y f_{X,Y}(x,y) dx dy \\ &= \int_{\mathbb{R}} y f_Y(y) dy \\ &= E(Y), \end{aligned}$$

where Bayes' theorem was used for the second equality and the definition of marginal distribution was used for the third equality. □

Two random variables X and Y (defined on the same probability space) are *independent*, if their joint distribution function factorises to the product of their marginal density functions:

$$f_{X,Y}(x,y) = f_X \cdot f_Y(y).$$

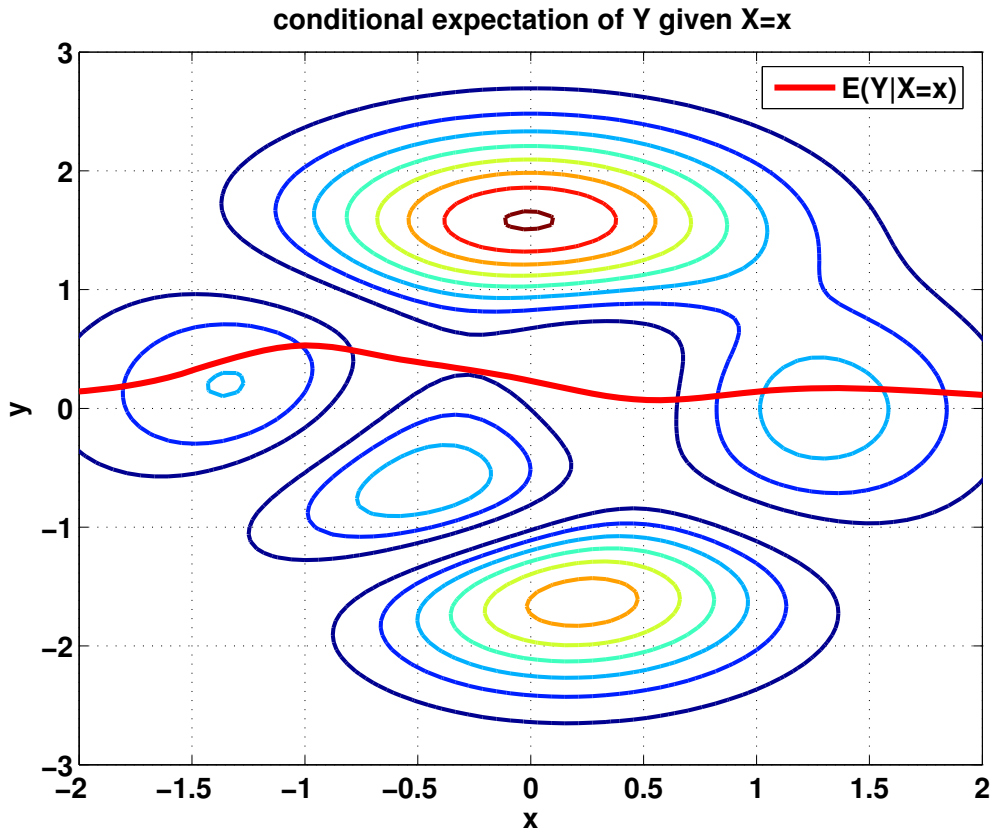


Figure 4.2: Contour plot of an exemplary non-Gaussian joint distribution function $f_{X,Y}$ and appendant conditional expectation $E(Y|X = x)$ as a function of x .

In this case the conditional density function of Y given $X = x$ equals the marginal density function of Y for all values of x :

$$f_{Y|X}(y|x) = f_Y(y).$$

Example 4.1 (IID) A stochastic process X is called independent identically distributed noise (IID), denoted $X \sim \text{IID}$, if all random variables X_t induce the same probability measure on \mathbb{R} and are pairwise independent.

Example 4.2 (Random Walk) Assume $\{X_t, t \in \mathbb{N}\}$ is IID with zero-mean, i.e., for all $t \in \mathbb{N}$ we have $E(X_t) = 0$.¹ Then the stochastic process $\{S_t, t \in \mathbb{N}\}$, defined by

$$S_t := \sum_{k=1}^t X_k$$

is called random walk. If the X_t have a symmetric probability density function, then the corresponding random walk is called symmetric.

For two random variables X and Y (defined on the same probability space) the *covariance* is defined as

$$\text{Cov}(X, Y) := E([X - E(X)][Y - E(Y)]).$$

¹The set of natural numbers \mathbb{N} is defined to be $\{1, 2, 3, \dots\}$.

Because of the linearity of the expectation operator E , we have the identity

$$\text{Cov}(X, Y) = E(XY) - E(X)E(Y).$$

This means, if at least one of the random variables is zero-mean, the covariance equals the expectation of their product. Furthermore, $\text{Cov}(X, Y) = \text{Cov}(Y, X)$.

Corollary 4.3 *For two random variables X and Y (defined on the same probability space) and numbers a and $b \in \mathbb{R}$ we have*

$$\text{Var}(aX + bY) = a^2\text{Var}(X) + 2ab\text{Cov}(X, Y) + b^2\text{Var}(Y).$$

Proof.

Straight forward, cf. for example [68, p.744].

□

Suppose we have two *vectors of random variables*² $\vec{X} : \Omega \rightarrow \mathbb{R}^v$ and $\vec{Y} : \Omega \rightarrow \mathbb{R}^w$ with, in general, different dimensions v and w . The expectation operator E and the covariance operator Cov can be generalised to vectors and matrices of random variables by element-wise application, such that with

$$\vec{\mu}_X := E(\vec{X}) \in \mathbb{R}^v \quad \text{and} \quad \vec{\mu}_Y := E(\vec{Y}) \in \mathbb{R}^w$$

we can define the *covariance matrix* of \vec{X} and \vec{Y} as

$$\begin{aligned} \text{Cov}(\vec{X}, \vec{Y}) &:= E([\vec{X} - \vec{\mu}_X][\vec{Y} - \vec{\mu}_Y]^T) \\ &= E(\vec{X}\vec{Y}^T) - \vec{\mu}_X\vec{\mu}_Y^T, \end{aligned}$$

where A^T denotes the transpose of a matrix or vector A .

Corollary 4.4 *The affine transform $\vec{Y} := \vec{a} + B\vec{X}$ of a vector \vec{X} of random variables has expectation*

$$E(\vec{Y}) = \vec{a} + BE(\vec{X})$$

and covariance matrix

$$\text{Cov}(\vec{Y}, \vec{Y}) = B\text{Cov}(\vec{X}, \vec{X})B^T$$

The *correlation* of two random variables X and Y (defined on the same probability space) is defined as

$$\text{Corr}(X, Y) := \frac{\text{Cov}(X, Y)}{\sqrt{\text{Var}(X)}\sqrt{\text{Var}(Y)}}.$$

X and Y are *uncorrelated* if $\text{Corr}(X, Y) = 0$, which is equivalent to $\text{Cov}(X, Y) = 0$.

Example 4.3 (WN) *A stochastic process X is called white noise (WN), denoted*

$$X \sim \text{WN}(\mu, \sigma^2),$$

if all random variables X_t have mean μ , variance σ^2 and are pairwise uncorrelated.

Corollary 4.5 *If two random variables X and Y are independent, then they are also uncorrelated. The converse is not true in general.*

²Vectors are used as column-vectors unless stated differently.

Proof.

The first statement follows from

$$\int_{\mathbb{R}} \int_{\mathbb{R}} xy f_{X,Y}(x,y) dx dy = \int_{\mathbb{R}} \int_{\mathbb{R}} xy f_X(x) f_Y(y) dx dy = E(X)E(Y).$$

A counter example for the second statement is given in [31, p. 42 Problem 1.8].

□

Thus IID is uncorrelated, but WN is in general not independent.

4.2 Best MSE Forecast

The aim of this section is to elaborate a first notion of *forecast* in terms of a stochastic process modelling a time series. A basic and simple setting is the example of only two random variables $\{X_1, X_2\}$ making up a stochastic process X . The problem of forecasting X_2 by X_1 is to find a random variable \hat{X}_2 which approximates or forecasts X_2 "optimally by taking X_1 into account". To evaluate the quality of a forecast, one usually specifies a so-called *loss function*, which is a summary of how concerned one is, if the forecast is off by a particular amount. The optimisation problem is then to find a forecast \hat{X}_2 , which minimises the value of the loss function. We will use the following loss function

Definition 4.3 (mean squared error MSE) *The mean squared error (MSE) of a random variable \hat{X} forecasting X is defined as*

$$\text{MSE}(X, \hat{X}) := E([X - \hat{X}]^2)$$

We first need the following lemma before we can prove the main result of Theorem 4.1.

Lemma 4.1 (best constant MSE forecast) *The best constant MSE forecast of a random variable X is $E(X)$, i.e., with respect to a given random variable X the minimum MSE element in the set $\{c : \Omega \rightarrow \mathbb{R} : c(\omega) = c \in \mathbb{R}\}$ of constant random variables is $E(X)$.*

Proof.

In order to minimise

$$E([X - c]^2) = \int_{\mathbb{R}} (x - c)^2 f_X(x) dx$$

differentiate with respect to c and set the first derivative to zero:

$$-2 \int_{\mathbb{R}} (x - c) f_X(x) dx = 0$$

$$c = \int_{\mathbb{R}} x f_X(x) dx = E(X)$$

□

Theorem 4.1 (best MSE forecast) *The best MSE forecast of a random variable X_2 in terms of a random variable X_1 is the conditional expectation $E(X_2|X_1)$, i.e., in the set of functions $g(X_1)$ the minimum MSE element is $E(X_2|X_1)$.*

Proof.

$$\begin{aligned} \mathbb{E}([X_2 - g(X_1)]^2) &= \int_{\mathbb{R}} \int_{\mathbb{R}} (x_2 - g(x_1))^2 f_{X_1, X_2}(x_1, x_2) dx_2 dx_1 \\ &= \int_{\mathbb{R}} \left(\int_{\mathbb{R}} (x_2 - g(x_1))^2 f_{X_2|X_1}(x_2|x_1) dx_2 \right) f_{X_1}(x_1) dx_1 \end{aligned}$$

The MSE can be minimised by choosing for every x_1 an optimal number $g(x_1) \in \mathbb{R}$, which minimises the inner integral of the last expression. This is however accomplished by the mean of $f_{X_2|X_1}$, as was shown in Lemma 4.1.

$$g(x_1) = \int_{\mathbb{R}} x_2 f_{X_2|X_1}(x_2|x_1) dx_2 = \mathbb{E}(X_2|X_1 = x_1),$$

which proves the theorem. □

The result of Theorem 4.1 can be easily generalised to the problem of forecasting a random variable X_{n+1} in terms of a vector $\vec{X} = (X_1, \dots, X_n)^T$ of random variables, i.e., finding a function $g : \mathbb{R}^n \rightarrow \mathbb{R}$ having minimum MSE when combined with \vec{X} to give the predictor $g(\vec{X}) = g(X_1, \dots, X_n)$:

$$\begin{aligned} f_{\vec{X}}(\vec{x}) &= \int_{\mathbb{R}} f_{\vec{X}, X_{n+1}}(\vec{x}, x_{n+1}) dx_{n+1} \\ f_{X_{n+1}|\vec{X}}(x_{n+1}|\vec{x}) &:= \begin{cases} \frac{f_{\vec{X}, X_{n+1}}(\vec{x}, x_{n+1})}{f_{\vec{X}}(\vec{x})} & \text{if } f_{\vec{X}}(\vec{x}) > 0 \\ 0 & \text{otherwise} \end{cases} \\ \mathbb{E}(X_{n+1}|\vec{X} = \vec{x}) &:= \int_{\mathbb{R}} x_{n+1} f_{X_{n+1}|\vec{X}}(x_{n+1}|\vec{x}) dx_{n+1} =: g(\vec{x}) \\ \mathbb{E}(X_{n+1}|\vec{X}) &:= g(\vec{X}) \end{aligned}$$

$\mathbb{E}(X_{n+1}|\vec{X})$ is the minimum MSE (scalar) random variable with respect to X_{n+1} and \vec{X} . Thus, the conditional expectation solves the minimisation problem

$$\operatorname{argmin}_{\{g: \mathbb{R}^n \rightarrow \mathbb{R}\}} \mathbb{E}([X_{n+1} - g(\vec{X})]^2).$$

4.3 Best Linear MSE Forecast

As is shown in Fig. 4.2 the conditional expectation $\mathbb{E}(Y|X)$ is in general a non-linear function of X and difficult to compute. We will thus work with a linear forecasting theory. The aim is therefore to determine the best MSE-forecast \hat{X}_{n+1} of X_{n+1} in terms of $\vec{X} = (X_1, \dots, X_n)^T$ by means of a linear combination

$$\hat{X}_{n+1} = \alpha_1 X_n + \alpha_2 X_{n-1} + \dots + \alpha_n X_1.$$

The problem of the best linear MSE-forecast can be reformulated and solved in terms of an orthogonal projection in the linear space of random variables with finite second order moment. Strictly mathematically speaking, we will work within the structure of a Hilbert space.

4.3.1 Hilbert Space Formalism

General Theory

For a thorough presentation of the mathematical theory of Hilbert spaces it is referred to [67]. A Hilbert space \mathbb{H} is an inner product space, which is complete, i.e., every Cauchy sequence converges in the induced norm of the inner product space to some element of \mathbb{H} . An inner product space \mathbb{H} is a vector space equipped with a sesqui-linear³ map $\langle \cdot, \cdot \rangle : \mathbb{H} \times \mathbb{H} \rightarrow \mathbb{C}$, called inner product, fulfilling the following properties

- (1) $\langle x, y \rangle = \langle y, x \rangle^*$ the conjugate complex of $\langle x, y \rangle$
- (2) $\langle \cdot, \cdot \rangle$ is positive definite, i.e.,
 $\langle x, x \rangle \geq 0 \forall x \in \mathbb{H}$ and
 $\langle x, x \rangle = 0 \Leftrightarrow x = 0$

The induced norm of a Hilbert space is defined as

$$\|x\| = \sqrt{\langle x, x \rangle},$$

and has the following properties

$$\begin{aligned} |\langle x, y \rangle| &\leq \|x\| \cdot \|y\| && \text{(Cauchy-Schwarz inequality)} \\ \|x + y\| &\leq \|x\| + \|y\| && \text{(triangle inequality)} \\ \|x + y\|^2 + \|x - y\|^2 &= 2\|x\|^2 + 2\|y\|^2 && \text{(parallelogram law)} \end{aligned}$$

Example 4.4 *The vector spaces \mathbb{R}^n and \mathbb{C}^n , equipped with the inner product*

$$\langle x, y \rangle := \sum_{k=1}^n x_k^* \cdot y_k$$

are finite real, respectively complex, Hilbert spaces.

Hilbert Space of Random Variables

Given a probability space $\{\Omega, \mathbb{F}, P\}$ we construct the induced Hilbert space $L^2(\Omega, \mathbb{F}, P)$ of random variables. First we define the set \mathcal{C} of random variables having finite second order moment.

$$\mathcal{C} := \{X : \rightarrow \mathbb{R} \mid E(X^2) < \infty\}.$$

Remember, the expectation operator E is the integral

$$E(X) = \int_{\mathbb{R}} x f_X(x) dx,$$

cf. equation (4.1). It can be shown, that map

$$\langle X, Y \rangle := E(XY)$$

is an inner product⁴ on \mathcal{C} and thus makes \mathcal{C} into a Hilbert Space, which we denote as $L^2(\Omega, \mathbb{F}, P)$.

³sesqui-linear means linear in one component and anti-linear in the other.

⁴In order to guarantee the positive definiteness of the inner product, one has to build equivalence classes \bar{X} of random variables by $X \sim X' \Leftrightarrow P(X - X' = 0) = P((X - X')^{-1}(0)) = 1$. For the sake of simplicity, we will identify a random variable X with its equivalence classes \bar{X} .

Remark 4.3 Applying the Cauchy-Schwarz inequality for $X, Y \in L^2(\Omega, \mathbb{F}, P)$ to their detrended random variables $\tilde{X} := X - E(X)$ and $\tilde{Y} := Y - E(Y)$ shows, that

$$\begin{aligned} 1 &\geq \frac{|\langle \tilde{X}, \tilde{Y} \rangle|}{\|\tilde{X}\| \cdot \|\tilde{Y}\|} = \frac{|E(\tilde{X}\tilde{Y})|}{\sqrt{E(\tilde{X}\tilde{X})} \cdot \sqrt{E(\tilde{Y}\tilde{Y})}} = \\ &= \left| \frac{\text{Cov}(X, Y)}{\sqrt{\text{Var}(X)\text{Var}(Y)}} \right| = |\text{Corr}(X, Y)|. \end{aligned}$$

This means that the correlation of two random variables is always between -1 and 1 .

Orthogonal Projection in a Hilbert space

The so-called "Projection Theorem" (Theorem 4.2) gives the solution to the problem of finding the best linear approximation of a vector y in terms of vectors $x_k, k = 1, \dots, n$ in a given Hilbert space. By the best linear approximation a vector \hat{y} is meant, which is a linear combination

$$\hat{y} = \sum_{k=1}^n \alpha_k x_k, \quad \alpha_k \in \mathbb{R}, \text{ respectively } \mathbb{C}$$

such that

$$\|y - \hat{y}\|^2$$

is minimised. In the case of $L^2(\Omega, \mathbb{F}, P)$ this refers to the best linear MSE-forecast of a random variable Y in terms of n other random variables $X_k, k = 1, \dots, n$.

Theorem 4.2 (Projection Theorem) *The best linear approximation \hat{y} of a vector y in terms of vectors $x_k, k = 1, \dots, n$ in a Hilbert space \mathbb{H} is unique and given by the orthogonal projection $P_M(y)$ of y onto the linear span $M := [x_1, \dots, x_n]_{\mathbb{R}}$ of the vectors $x_k, k = 1, \dots, n$, i.e., there exists a unique vector $\hat{y} \in M$, such that*

$$\|y - \hat{y}\| = \min_{x \in M} \|y - x\|$$

and this vector is uniquely identified by the property

$$y - \hat{y} \perp M$$

which means that $\langle y - \hat{y}, x \rangle = 0, \forall x \in M$.

Proof. A proof can be found for example in [30, p.51] and [100, p.51].

□

Figure 4.3 depicts the orthogonal projection of a vector $y \in \mathbb{R}^3$ onto the plane spanned by two vectors $x_1, x_2 \in \mathbb{R}^3$.

Proposition 4.2 *The orthogonal projection $P_M : \mathbb{H} \rightarrow M$ in a Hilbert space \mathbb{H} onto the linear span $M := [x_1, \dots, x_n]_{\mathbb{R}}$ of vectors $x_k \in \mathbb{H}, k = 1, \dots, n$ has the following properties*

1. P_M is linear.
2. $\|y\|^2 = \|P_M(y)\|^2 + \|(1 - P_M)(y)\|^2$ (Pythagoras)
3. $y \in M \Leftrightarrow P_M(y) = y$

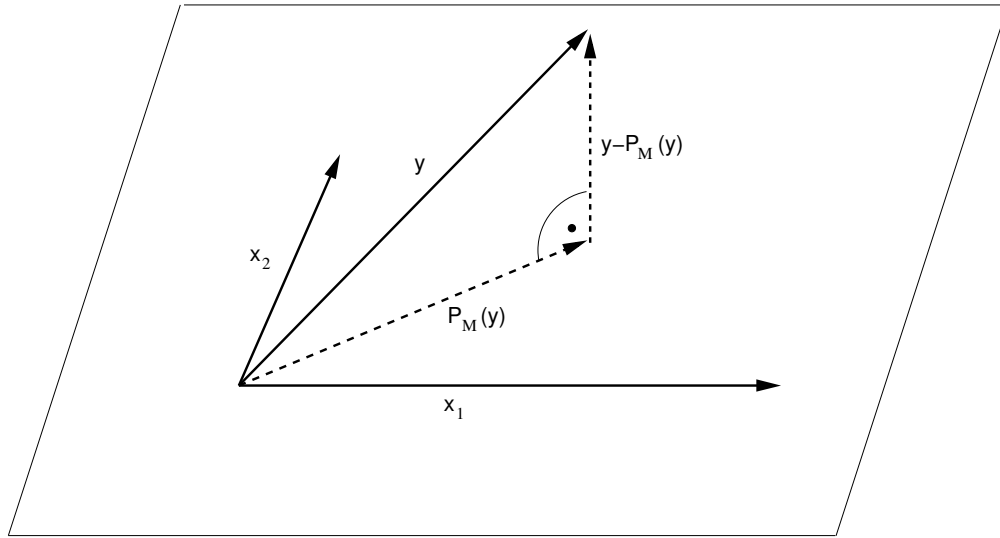


Figure 4.3: Orthogonal projection of a vector $y \in \mathbb{R}^3$ onto the plane spanned by two vectors $x_1, x_2 \in \mathbb{R}^3$.

$$4. y \in M^\perp \Leftrightarrow P_M(y) = 0$$

$$5. M_1 \subseteq M_2 \Leftrightarrow P_{M_1} P_{M_2} = P_{M_1}$$

Remark 4.4 In the case of the Hilbert space $L^2(\Omega, \mathbb{F}, P)$ the n equations

$$\langle y - \hat{y}, x_k \rangle = 0, k = 1, \dots, n$$

are called "prediction equations" and are often described by saying, that the prediction error $y - \hat{y}$ is uncorrelated⁵ with the predictors x_k .

Remark 4.5 The coefficients α_k in the expression

$$\hat{y} = P_M(y) = \sum_{k=1}^n \alpha_k x_k, \quad \alpha_k \in \mathbb{R}, \text{ respectively } \mathbb{C}$$

are not necessarily unique, however $\hat{y} = P_M(y)$ is unique.

4.3.2 Ordinary Least Squares, Linear Regression

The ordinary least squares approximation of a vector $y \in \mathbb{R}^n$ in terms vectors $x_k \in \mathbb{R}^n, k = 1, \dots, m$ constitutes, according to the projection theorem, the same problem as finding the orthogonal projection of y onto the linear span $M := [x_1, \dots, x_m]_{\mathbb{R}}$. This is the same as solving the overdetermined system of linear equations

$$y \sim [x_1, \dots, x_m] \beta$$

by finding a vector $\beta_0 \in \mathbb{R}^m$, such that

$$\|y - [x_1, \dots, x_m] \beta_0\| = \min_{\beta \in \mathbb{R}^m},$$

⁵Using the word "uncorrelated" is only correct, when a constant random variable is included in the set of predictors $x_k, \forall k = 1, \dots, n$

where $\|\cdot\|$ is the induced norm of the standard inner product in \mathbb{R}^n . Finally, the linear regression of n observations $y^l, l = 1, \dots, n$ on n observations of m different regressors $x_k^l, l = 1, \dots, n, k = 1, \dots, m$ is the problem of finding coefficients $\beta^k \in \mathbb{R}, k = 1, \dots, m$ such that

$$\sum_{l=1}^n (y^l - \sum_{k=1}^m \beta^k x_k^l)^2$$

is minimal.⁶ The last expression can be written in matrix form as

$$\|y - X\beta\|^2,$$

where $\|\cdot\|$ is again the induced norm of the standard inner product in \mathbb{R}^n . All in all, we see that all problem sets (ordinary least squares, overdetermined system of linear equations, and linear regression) are solved using the method of orthogonal projection in \mathbb{R}^n , which is best presented in matrix notation. The projection

$$P_M(y) = [x_1, \dots, x_m]\beta = X\beta$$

is the unique vector fulfilling

$$\langle y - X\beta, x_k \rangle = 0, \forall k = 1, \dots, m,$$

which is the same as

$$\langle x_k, X\beta \rangle = \langle x_k, y \rangle, \forall k = 1, \dots, m.$$

These m equations can be written as rows of the following matrix equation

$$X^T X \beta = X^T y.$$

If the $m \times m$ matrix $X^T X$ is invertible, the vector of coefficients β is unique and can be computed as

$$\beta = (X^T X)^{-1} X^T y. \quad (4.2)$$

Otherwise, β is not unique, and a solution can be computed in the same way by using a generalised inverse of $X^T X$ in place of $(X^T X)^{-1}$. The projection $X\beta$, however, is still unique.

4.3.3 Vectors of Random Variables

The previous section dealt with the application of the projection theorem to vectors in the Hilbert space \mathbb{R}^n . In this section we consider $\mathbb{H} = L^2(\Omega, \mathbb{F}, P)$ as Hilbert space and develop the formulas for the projection of w random variables, subsumed under a w -dimensional vector \vec{Y} , onto the linear span of v random variables, subsumed under a v -dimensional vector \vec{X} . By

$$P(\vec{Y}|\vec{X}) \text{ or short } \hat{Y}$$

we denote the w -dimensional vector containing the w best linear MSE predictors of the w random variables in \vec{Y} in terms of the v random variables in \vec{X} . $P(\vec{Y}|\vec{X})$ must have the form

$$P(\vec{Y}|\vec{X}) = M\vec{X},$$

⁶Usually a constant regressor of 1s is added in order to include a possible offset in the observations y^l . This means the insertion of a column of 1s in the matrix X .

where M is a $w \times v$ matrix, and must fulfil

$$\begin{aligned}\langle \vec{Y} - \hat{\vec{Y}}, \vec{X}^T \rangle &= 0 \\ \langle \vec{Y}, \vec{X}^T \rangle &= \langle \hat{\vec{Y}}, \vec{X}^T \rangle = M \langle \vec{X}, \vec{X}^T \rangle.\end{aligned}$$

Thus, if $\langle \vec{X}, \vec{X}^T \rangle = E(\vec{X}\vec{X}^T)$ is invertible, there is a unique solution for M , namely

$$M = \langle \vec{Y}, \vec{X}^T \rangle \langle \vec{X}, \vec{X}^T \rangle^{-1} = E(\vec{Y}\vec{X}^T)E(\vec{X}\vec{X}^T)^{-1}.$$

If $E(\vec{X}\vec{X}^T)$ is not invertible, there is no unique solution for M , but still a unique solution for $\hat{\vec{Y}} = P(\vec{Y}|\vec{X})$. It can be constructed by choosing any generalised inverse⁷ of $E(\vec{X}\vec{X}^T)$ in place of $E(\vec{X}\vec{X}^T)^{-1}$.

4.3.4 Iterated and Updating Projections

The so-called "law of iterated projections" says that projecting the projection of a vector y onto the linear span of the vectors x_1, x_2 onto the vector x_1 leads to the same result as projecting y onto x_1 only, or more concisely

$$P(P(y|x_1, x_2)|x_1) = P(y|x_1).$$

This is just a special case of one of the properties of orthogonal projections mentioned earlier in Proposition 4.2:

$$M_1 \subseteq M_2 \Leftrightarrow P_{M_1}P_{M_2} = P_{M_1}.$$

The so-called "law of updating a projection" says how a projection changes when a vector is added to the linear span of vectors to be projected on.

Theorem 4.3 (law of updating a projection) *The orthogonal projection onto the linear span of the vectors $x_1, \dots, x_{n+1} \in \mathbb{H}$ can be decomposed by use of the so-called innovation*

$$i_{n+1} := x_{n+1} - P(x_{n+1}|x_1, \dots, x_n)$$

into

$$P(\cdot|x_1, \dots, x_{n+1}) = P(\cdot|x_1, \dots, x_n) + P(\cdot|i_{n+1})$$

Proof.

Lets denote $[x_1, \dots, x_{n+1}]_{\mathbb{R}}$ by M , $[x_1, \dots, x_n]_{\mathbb{R}}$ by M_1 and $[i_{n+1}]_{\mathbb{R}}$ by M_2 . From

$$i_{n+1} = (1 - P_{M_1})(x_{n+1})$$

it follows that

$$i_{n+1} \perp M_1 \quad \text{i.e.} \quad M_2 \perp M_1.$$

Additionally, M_1 and i_{n+1} span the the whole space M , i.e.,

$$M = M_1 \oplus M_2.$$

From standard Hilbert space theory it follows that the projection onto M can be decomposed into the sum of the projections onto the orthogonal subspaces M_1 and M_2 , cf. Figure 4.4

$$P_M = P_{M_1} + P_{M_2}$$

□

⁷A generalised inverse of a matrix A is a matrix A^- such that $AA^-A = A$. Every matrix has at least one, cf. [37, 100].

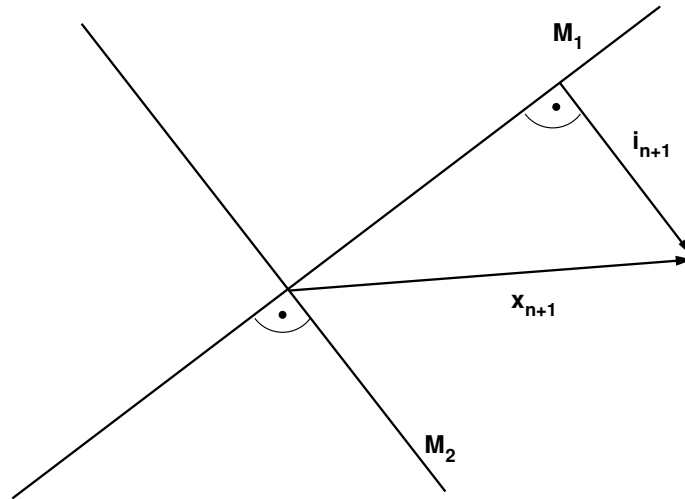


Figure 4.4: Law of updating a projection.

4.4 The Gaussian Case

The optimal MSE-forecast of a random variable X_2 in terms of a random variable X_1 is the conditional expectation $E(X_2|X_1)$, whereas the best linear MSE-forecast is given by the orthogonal projection $P(X_2|X_1)$ having at least the same mean squared error.

$$\text{MSE}\{P(X_2|X_1)\} \geq \text{MSE}\{E(X_2|X_1)\}$$

There exists an important class of random variables, for which the above inequality is an equality, or more precisely, for which $P(X_2|X_1) = E(X_2|X_1)$. This is the class of Gaussian random variables.

Definition 4.4 (Gaussian Random Variables) A random variable X is a Gaussian random variable, denoted by $X \sim N(\mu, \sigma^2)$, if its probability density function is given by

$$f_X(x) = \frac{1}{\sigma\sqrt{2\pi}} \exp\left(-\frac{(x-\mu)^2}{2\sigma^2}\right),$$

for $\mu, \sigma \in \mathbb{R}$ and $\sigma > 0$. A vector of random variables $\vec{X} = (X_1, \dots, X_n)^T$ is called multivariate Gaussian or jointly Gaussian, denoted by $\vec{X} \sim N(\vec{\mu}, \Omega)$, if its joint distribution function is given by

$$f_{\vec{X}}(\vec{x}) = (2\pi)^{-\frac{n}{2}} \det(\Omega)^{-\frac{1}{2}} \exp\left(-\frac{1}{2}(\vec{x}-\vec{\mu})^T \Omega^{-1}(\vec{x}-\vec{\mu})\right),$$

for $\vec{\mu} \in \mathbb{R}^n$ and $\Omega \in \mathbb{R}^{n,n}$ symmetric and positive semi-definite.

Corollary 4.6 The following properties follow easily from the definition.

1. The mean (vector) and the variance (variance-covariance matrix) is given by

$$\begin{aligned} E(X) &= \mu, \\ E(\vec{X}) &= \vec{\mu} \\ \text{Var}(X) &= \sigma^2 \\ \text{Cov}(\vec{X}, \vec{X}) &= \Omega \end{aligned}$$

The last equation shows that Ω has to be symmetric and positive semi-definite.

2. (Multivariate) Gaussian random variables are completely determined by their mean $\boldsymbol{\mu}$ (mean vector $\vec{\boldsymbol{\mu}}$) and variance $\boldsymbol{\sigma}^2$ (variance-covariance matrix $\boldsymbol{\Omega}$).
3. If $\vec{X} \sim N(\vec{\boldsymbol{\mu}}, \boldsymbol{\Omega})$ then for any $H \in \mathbb{R}^{n,n}$ and any $\vec{a} \in \mathbb{R}^n$ we have that

$$H\vec{X} + \vec{a} \sim N(H\vec{\boldsymbol{\mu}} + \vec{a}, H^T\boldsymbol{\Omega}H)$$

4. The random variables of a multivariate Gaussian are pairwise uncorrelated, if and only if $\boldsymbol{\Omega}$ is diagonal. In this case, the joint distribution function factorises and the random variables are thus independent. The converse is not true.

Theorem 4.4 If $\vec{X} = (X_1, \dots, X_{n+1})^T$ is a multivariate Gaussian vector of random variables, then the best linear MSE-forecast $P(X_n|X_n, \dots, X_1, X_0)$ including a constant random variable, e.g. $X_0 = 1$, is the best MSE-forecast and thus equals the conditional expectation $E(X_n|X_n, \dots, X_1)$, i.e.

$$P(X_n|X_n, \dots, X_1, X_0) = E(X_n|X_n, \dots, X_1).$$

Proof.

We sketch the proof only for the bivariate case. The general case is handled e.g. in [68, p.100ff.]. For two jointly Gaussian random variables

$$(X_1, X_2) \sim N((\boldsymbol{\mu}_1, \boldsymbol{\mu}_2)^T, \boldsymbol{\Omega})$$

with

$$\boldsymbol{\Omega} = \begin{pmatrix} \boldsymbol{\omega}_{11} & \boldsymbol{\omega}_{12} \\ \boldsymbol{\omega}_{21} & \boldsymbol{\omega}_{22} \end{pmatrix}$$

the conditional density function can be computed as

$$f_{X_2|X_1}(x_2, x_1) = \frac{1}{\sqrt{2\pi H}} \exp\left(-\frac{(x_2 - m(x_1))^2}{2H}\right)$$

with

$$H := \boldsymbol{\omega}_{22} - \frac{\boldsymbol{\omega}_{21}\boldsymbol{\omega}_{12}}{\boldsymbol{\omega}_{11}} \quad \text{and} \quad m(x_1) := \boldsymbol{\mu}_2 + \frac{\boldsymbol{\omega}_{21}}{\boldsymbol{\omega}_{11}}(x_1 - \boldsymbol{\mu}_1)$$

This is a univariate Gaussian probability density distribution centred at $m(x_1)$. The conditional expectation

$$E(X_2|X_1 = x_1) = \int_{\mathbb{R}} x_2 f_{X_2|X_1}(x_2, x_1) dx_2 = m(x_1)$$

is thus given by

$$E(X_2|X_1) = \boldsymbol{\mu}_2 + \frac{\boldsymbol{\omega}_{21}}{\boldsymbol{\omega}_{11}}(X_1 - \boldsymbol{\mu}_1),$$

which is linear in X_1 and $X_0 := 1$.

□

Figure 4.5 shows as a contour plot of the joint distribution function of two jointly Gaussian random variables X and Y , some conditional density functions of Y on X and the conditional expectation of Y given $X = x$ as a function of x .

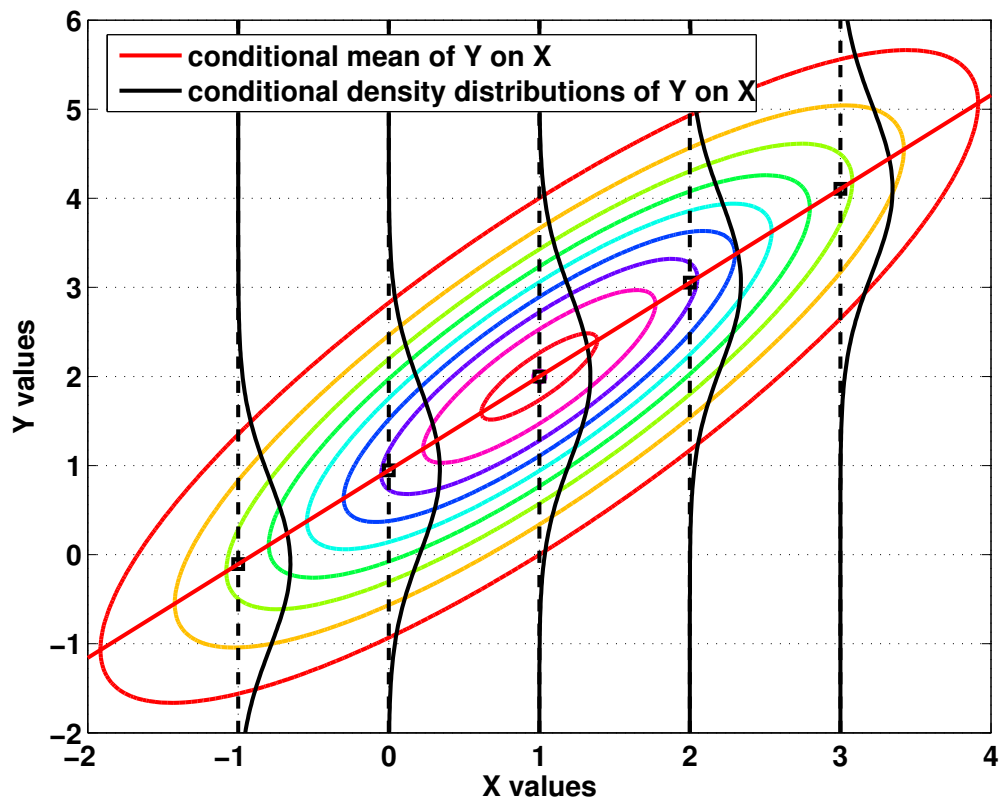


Figure 4.5: Contour plot of an exemplary Gaussian joint distribution function $f_{X,Y}$ together with some conditional density functions $f_{Y|X}(\cdot|x)$, and the conditional expectation $E(Y|X = x)$ as a function of x .

Chapter 5

State-Space Models and Kalman Theory

Contents

5.1 State-Space Models	65
5.2 The Kalman Recursions	66
5.2.1 Prediction	68
5.2.2 Filtering	73
5.2.3 Fixed-Point Smoothing	74
5.2.4 Properties of the Kalman Recursions	76
5.3 MLE and MMSE Optimisation	78
5.3.1 Maximum Likelihood Estimation	79
5.3.2 Minimum Mean Squared Error	83

A very rich class of time series models, including ARIMA and classical decomposition models with random variations, can be formulated by state-space models. The Kalman recursions allow a unified approach to prediction and estimation for all processes that can be given a state-space formulation.

The subsequent presentation follows [31, 30]. More on state-space models and Kalman theory can be found for example in [65, 68, 71, 98].

5.1 State-Space Models

Definition 5.1 (state-space model) *A state-space model for a (possibly multivariate) time series $\{Y_t\}, t \in \mathbb{N}$ consists in the specification of two equations. The observation equation*

$$Y_t = G_t X_t + W_t, \quad t \in \mathbb{N}$$

expresses for every time $t \in \mathbb{N}$ the w -dimensional random variable Y_t , called observation or measurement, as a linear function of the v -dimensional random variable X_t , called state, plus a measurement noise term W_t , where

$$\{W_t\} \sim WN(0, \{R_t\})$$

and $\{G_t\}$ is a sequence of $w \times v$ matrices. The notation $\{W_t\} \sim \text{WN}(0, \{R_t\})$ indicates that the sequence of random vectors $\{W_t\}$ has mean zero and covariance matrix $E(W_t W_s') = R_t \delta_{t,s}$. The second equation

$$X_{t+1} = F_t X_t + V_t, \quad t \in \mathbb{N}$$

is called the state equation, and determines the state X_{t+1} at time $t + 1$ in terms of the previous state X_t and a noise term V_t , where

$$\{V_t\} \sim \text{WN}(0, \{Q_t\})$$

and $\{F_t\}$ is a sequence of $v \times v$ matrices. The noise sequences $\{W_t\}$ and $\{V_t\}$ are uncorrelated, i.e., $E(W_t V_s') = 0$ for all s and $t \in \mathbb{N}$. It is finally assumed that the initial state X_1 is uncorrelated with all noise terms of $\{W_t\}$ and $\{V_t\}$.

Remark 5.1 Different generalisations of the above definition exist. The noise terms $\{W_t\}$ and $\{V_t\}$ can be allowed to correlate, and in control theory an additional term $H_t u_t$ is added in the state equation.

Remark 5.2 In many cases the matrices F_t, G_t, Q_t and R_t are time-independent, in which case the subscript is suppressed.

Corollary 5.1 It follows from the definition that X_t and Y_t are linear functions

$$\begin{aligned} X_t &= l_t(X_1, V_1, \dots, V_{t-1}) \\ Y_t &= m_t(X_1, V_1, \dots, V_{t-1}, W_t) \end{aligned}$$

of the initial state and noise terms up to $t - 1$ and t , respectively.

Corollary 5.2 From 5.1 and the assumptions on the noise terms, it follows that

$$E(V_t X_s') = 0, \quad E(V_t Y_s') = 0, \quad E(W_t X_s') = 0 \quad \forall 1 \leq s \leq t$$

and

$$E(W_t Y_s') = 0 \quad \forall 1 \leq s < t.$$

Remark 5.3 Neither $\{X_t\}$ nor $\{Y_t\}$ are necessarily stationary¹.

Remark 5.4 If the sequence $\{X_1, V_1, V_2, \dots\}$ is independent, then $\{X_t\}$ has the Markov property, i.e., the distribution of X_{t+1} given X_t, \dots, X_1 is the same as the distribution of X_{t+1} given X_t . This property is possessed by many physical systems, provided that one includes sufficiently many components in X_t .

5.2 The Kalman Recursions

For a given state-space model the Kalman recursions solve the problem of finding the minimum MSE linear predictors of the state X_t in terms of the observations Y_1, Y_2, \dots and a random vector Y_0 which is orthogonal to all V_t and $W_t \forall t \geq 1$. In many cases Y_0 is chosen to be the constant random vector $(1, \dots, 1)^T$.

Estimation of X_t in terms of

¹For the definition of stationarity cf. e.g. [31]

- $Y_0, Y_1, Y_2, \dots, Y_{t-1}$ defines the *prediction* problem,
- $Y_0, Y_1, Y_2, \dots, Y_t$ defines the *filtering* problem,
- $Y_0, Y_1, Y_2, \dots, Y_n$ ($n > t$) defines the *fixed-point smoothing* problem.

Each of these problems can be solved recursively using the appropriate Kalman recursions. For a state-vector $X = (X^1, X^2, \dots, X^v)^T$ we introduce the following notation

$$P_t(X) := \begin{pmatrix} P_t(X^1) \\ \vdots \\ P_t(X^v) \end{pmatrix},$$

where

$$P_t(X^k) := P(X^k | Y_0, Y_1, \dots, Y_t)$$

is the best, i.e. the minimum MSE, linear predictor of X^k in terms of all components of Y_0, Y_1, \dots, Y_t . This means, $P_t(X)$ is the unique vector of random variables of the form

$$P_t(X) = A_0 Y_0 + \dots + A_t Y_t$$

with $A_i \in \mathbb{R}^{v,w}$, such that

$$[X - P_t(X)] \perp Y_s, \quad \forall s = 0, \dots, t. \quad (5.1)$$

In other words, each component of $P_t(X)$ is the unique orthogonal projection of the respective component of X onto the linear span generated by all components of

$$Y_0, Y_1, \dots, Y_t.$$

The operator P_t is linear, i.e., for a matrix A and a vector V of appropriate dimensions

$$P_t(AX) = AP_t(X)$$

and

$$P_t(X + V) = P_t(X) + P_t(V).$$

Remark 5.5 *If all components of X, Y_1, \dots, Y_t are jointly normally distributed and $Y_0 = (1, \dots, 1)^T$, then*

$$P_t(X) = E(X | Y_1, \dots, Y_t),$$

as was demonstrated in Theorem 4.4

Remark 5.6 *For a v -dimensional state-vector X and a w -dimensional observation Y , the orthogonal projection $P(X|Y)$ is of the form*

$$P(X|Y) = MY,$$

where $M \in \mathbb{R}^{v,w}$ is given by

$$M = E(XY^T) [E(Y Y^T)]^{-1},$$

cf. subsection 4.3.3. If $E(Y Y^T)$ is not invertible, it can be replaced by any generalised inverse of $E(Y Y^T)$.

The three types of estimation problems mentioned above can now be formulated by the determination of three projectors

- *prediction* problem: determine $P_{t-1}(X_t)$
- *filtering* problem: determine $P_t(X_t)$
- *fixed-point smoothing* problem: determine $P_n(X_t)$, ($n > t$)

The following three theorems solve each of these problems recursively and are thus known as the Kalman recursions.

5.2.1 Prediction

Theorem 5.1 (Kalman Prediction) *The 1-step predictors $\hat{X}_t := P_{t-1}(X_t)$ and their error covariance matrices $\Omega_t := E[(X_t - \hat{X}_t)(X_t - \hat{X}_t)^T]$ are determined by (a) the initial conditions*

$$\begin{aligned}\hat{X}_1 &= P(X_1|Y_0), \text{ and} \\ \Omega_1 &= E[(X_1 - \hat{X}_1)(X_1 - \hat{X}_1)^T]\end{aligned}$$

(b) and the recursions for $t = 1, 2, \dots$

$$\hat{X}_{t+1} = F_t \hat{X}_t + \Theta_t \Delta_t^{-1} (Y_t - G_t \hat{X}_t) \quad (5.2)$$

$$\Omega_{t+1} = F_t \Omega_t F_t^T + Q_t - \Theta_t \Delta_t^{-1} \Theta_t^T, \text{ where} \quad (5.3)$$

$$\Delta_t := G_t \Omega_t G_t^T + R_t \quad (5.4)$$

$$\Theta_t := F_t \Omega_t G_t^T \quad (5.5)$$

and Δ_t^{-1} is any generalised inverse of Δ_t

Remark 5.7 *The recursions for Ω_t , Δ_t and Θ_t are independent of the observations Y_t .*

Remark 5.8 *The matrices*

$$K_t := \Omega_t G_t^T (G_t \Omega_t G_t^T + R_t)^{-1}$$

(or sometimes $F_t K_t$) are called the Kalman gain matrices. They reflect the impact of new observation data on the predictor \hat{X}_{t+1} .

Proof of Theorem 5.1.

We define the sequence of **innovations** $\{I_t\}$ by

$$\begin{aligned}I_0 &:= Y_0, \text{ and} \\ I_t &:= Y_t - P_{t-1}(Y_t) \quad \forall t = 1, 2, \dots\end{aligned}$$

Note that the innovations I_t for $t = 1, 2, \dots$ can be written as

$$I_t = Y_t - G_t \hat{X}_t = G_t (X_t - \hat{X}_t) + W_t$$

because P_{t-1} is linear and W_t is orthogonal to the linear span onto which the operator P_{t-1} projects. Furthermore, $\{I_t\}$ is an orthogonal sequence which results from the fact that the

innovations are prediction errors, cf. equation (5.1). From the "law of updating a projection" (Theorem 4.3) it follows that

$$P_t(\cdot) = P_{t-1}(\cdot) + P(\cdot|I_t)$$

Applying $P_t(\cdot)$ on X_{t+1} and using the last equation yields

$$\begin{aligned} P_t(X_{t+1}) &= P_{t-1}(X_{t+1}) + P(X_{t+1}|I_t) \\ \hat{X}_{t+1} &= P_{t-1}(F_t X_t + V_t) + M I_t \\ &= F_t \hat{X}_t + M I_t, \end{aligned}$$

where the linearity of P_{t-1} was used and the fact that V_t is orthogonal to the linear span onto which the operator P_{t-1} projects. The matrix M can be computed according to Remark 5.6 as

$$M = E(X_{t+1} I_t^T) E(I_t I_t^T)^{-1}$$

We define Δ_t as the covariance matrix of the innovation at time t

$$\begin{aligned} \Delta_t &:= E(I_t I_t^T) \\ &= E\{[G_t(X_t - \hat{X}_t) + W_t][G_t(X_t - \hat{X}_t) + W_t]^T\} \\ &= G_t E[(X_t - \hat{X}_t)(X_t - \hat{X}_t)^T] G_t^T + R_t \\ &= G_t \Omega_t G_t^T + R_t, \end{aligned}$$

where the linearity of the expectation operator E and the orthogonality of $(X_t - \hat{X}_t)$ with W_t was used. We define Θ_t as the matrix of scalar products of the components of the state at time $t + 1$ with the components of the innovation at time t .

$$\begin{aligned} \Theta_t &:= E(X_{t+1} I_t^T) \\ &= E\{[F_t X_t + V_t][G_t(X_t - \hat{X}_t) + W_t]^T\} \\ &= F_t E[X_t(X_t - \hat{X}_t)^T] G_t^T, \end{aligned}$$

where it was used that $W_t \perp V_t$, $W_t \perp X_t$, and $V_t \perp (X_t - \hat{X}_t)$. The predictor \hat{X}_t is orthogonal to the prediction error $X_t - \hat{X}_t$, i.e.,

$$E[\hat{X}_t(X_t - \hat{X}_t)^T] = 0,$$

and thus

$$E[X_t(X_t - \hat{X}_t)^T] = E[(X_t - \hat{X}_t)(X_t - \hat{X}_t)^T]$$

Using this we can write

$$\Theta_t = F_t E[(X_t - \hat{X}_t)(X_t - \hat{X}_t)^T] G_t^T = F_t \Omega_t G_t^T.$$

This completes the proof of equation (5.2). To prove the recursions for Ω_t we compute

$$\begin{aligned} \Omega_{t+1} &= E[(X_{t+1} - \hat{X}_{t+1})(X_{t+1} - \hat{X}_{t+1})^T] \\ &= E(X_{t+1} X_{t+1}^T) - E(X_{t+1} \hat{X}_{t+1}^T) - E(\hat{X}_{t+1} X_{t+1}^T) + E(\hat{X}_{t+1} \hat{X}_{t+1}^T) \end{aligned}$$

However,

$$\begin{aligned} E(X_{t+1} \hat{X}_{t+1}^T) &= E[(X_{t+1} - \hat{X}_{t+1} + \hat{X}_{t+1}) \hat{X}_{t+1}^T] = E(\hat{X}_{t+1} \hat{X}_{t+1}^T), \text{ and} \\ E(\hat{X}_{t+1} X_{t+1}^T) &= E[\hat{X}_{t+1} (\hat{X}_{t+1} - \hat{X}_{t+1} + X_{t+1})^T] = E(\hat{X}_{t+1} \hat{X}_{t+1}^T), \end{aligned}$$

because predictor \hat{X}_{t+1} is orthogonal to the prediction error $X_{t+1} - \hat{X}_{t+1}$, i.e.,

$$E[\hat{X}_{t+1}(X_{t+1} - \hat{X}_{t+1})^T] = 0.$$

Thus, the expansion for Ω_{t+1} can be further simplified to

$$\Omega_{t+1} = E(X_{t+1}X_{t+1}^T) - E(\hat{X}_{t+1}\hat{X}_{t+1}^T) \quad (5.6)$$

And using the recursions

$$\begin{aligned} X_{t+1} &= F_t X_t + V_t, \text{ and} \\ \hat{X}_{t+1} &= F_t \hat{X}_t + \Theta_t \Delta_t^{-1} (Y_t - G_t \hat{X}_t), \end{aligned}$$

we get

$$\begin{aligned} \Omega_{t+1} &= F_t E(X_t X_t^T) F_t^T + Q_t - F_t E(\hat{X}_t \hat{X}_t^T) F_t^T - \\ &\quad - \Theta_t \Delta_t^{-1} E(I_t I_t^T) \Delta_t^{-T} \Theta_t^T \\ &= F_t [E(X_t X_t^T) - E(\hat{X}_t \hat{X}_t^T)] F_t^T + Q_t - \Theta_t \Delta_t^{-1} \Theta_t^T, \end{aligned}$$

where we used the definition $\Delta_t = E(I_t I_t^T)$ and the fact $\Delta_t = \Delta_t^T$. Finally, we apply equation (5.6) with time t , we get

$$\Omega_{t+1} = F_t \Omega_t F_t^T + Q_t - \Theta_t \Delta_t^{-1} \Theta_t^T,$$

which completes the proof. □

An Example - Estimation of Position from Acceleration

As a first and simple example for an application of state-space models and Kalman recursions let's assume to have recordings $\{y_t\}$ of acceleration measurements. These could originate, for example, from a compression acceleration measurement during CPR application. Without any further assumptions, the problem of finding the position of a device corresponding to its acceleration is only solvable when the initial position and the initial velocity (or equivalent information) are known. We will circumvent this problem by assuming that the position is located near the coordinate origin and that positions and velocities are damped by a factor $0 < \gamma < 1$. More accurately, the state space model is defined in the following way. A state

$$X_t = \begin{pmatrix} X_t^q \\ X_t^v \\ X_t^a \\ 1 \end{pmatrix}$$

at time t consists of a position component X_t^q , a velocity component X_t^v , an acceleration component X_t^a , and the constant number 1. The state transition matrix at time t is defined by

$$F_t = \Gamma \begin{pmatrix} 1 & dt & 0 & 0 \\ 0 & 1 & dt & 0 \\ 0 & 0 & 0 & y_{t+1} \\ 0 & 0 & 0 & 1 \end{pmatrix},$$

where dt is the sampling time and

$$\Gamma = \begin{pmatrix} \gamma & 0 & 0 & 0 \\ 0 & \gamma & 0 & 0 \\ 0 & 0 & 1 & 0 \\ 0 & 0 & 0 & 1 \end{pmatrix}.$$

Note, that the state transition matrix F_t contains the observed acceleration y_{t+1} . In general, this value is not observed until time $t + 1$ and is thus not available for an on-line computation of the predicted state \hat{X}_{t+1} at time t . We assume, however, that all computations are made a posteriori or with an appropriate time delay.

Finally, the observation projection matrix G_t fetches the acceleration component X_t^a from the state and is thus given by

$$G_t = (0 \ 0 \ 1 \ 0).$$

We simulate the series $\{y_t\}$ of observed accelerations by a deterministic signal, which is zero or rectangular, plus a white noise term $\text{WN}(0, \sigma_w^2)$ with $\sigma_w = 0.1$. The sampling time dt is chosen to be 0.1 seconds and the damping parameter γ is set to 0.99. The noise covariance matrix Q of the state equation is set zero and initial values for position and velocity are set to $X_0^q = 2$ and $X_0^v = -1$, respectively. Figures 5.1 and 5.2 show the simulation data for zero and rectangular acceleration over $N = 700$ sample points. By means of the Kalman

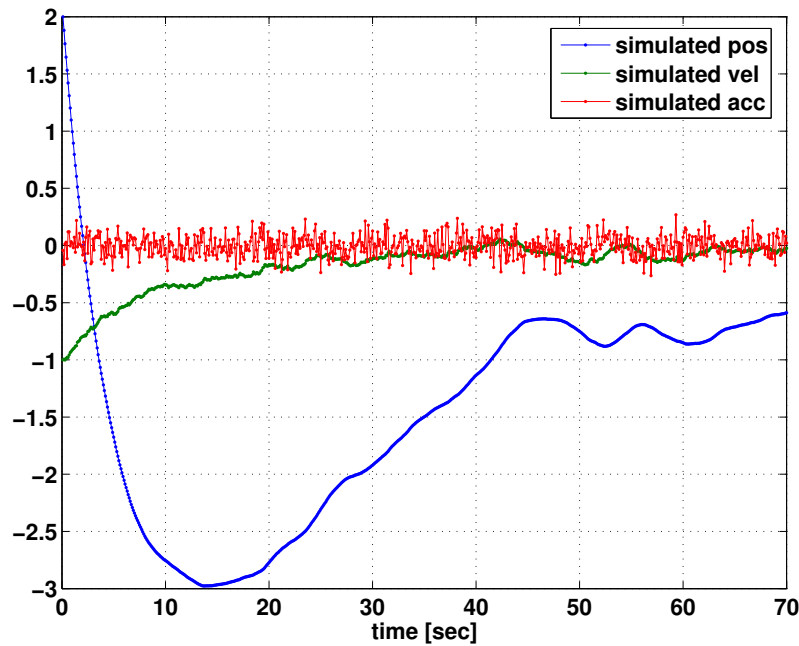


Figure 5.1: Simulated data for the estimation of position from zero acceleration.

prediction recursions estimates of the unknown states, i.e. the position and the velocity can be computed from the observed acceleration. Figures 5.3 and 5.4 show the estimates for zero and rectangular acceleration and compare them to the simulated signals. Normal random values with standard deviation $\sigma_e = 4$ were chosen for the position and the velocity component of the initial state, the initial acceleration component were set to the initially

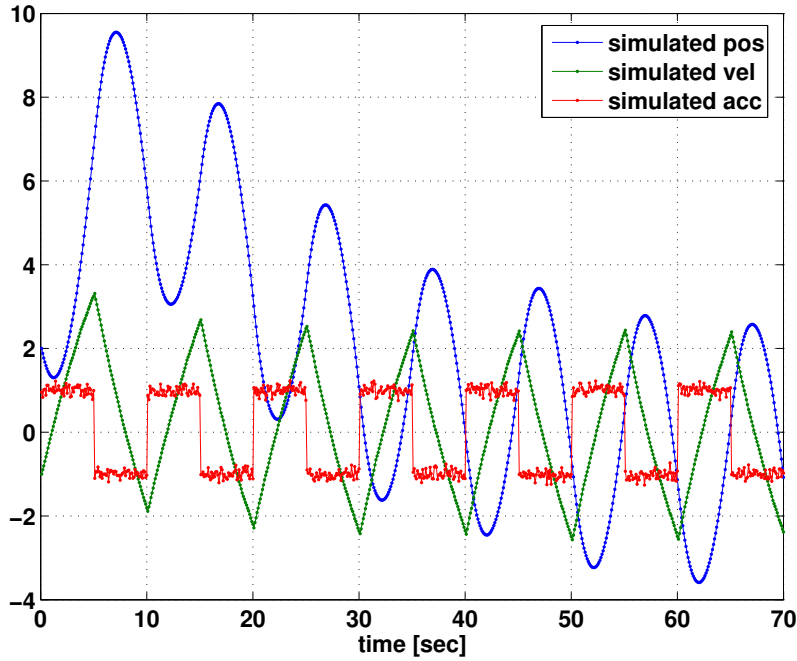


Figure 5.2: Simulated data for the estimation of position from rectangular acceleration.

observed acceleration value. The initial error covariance matrix Ω_1 was set to

$$\Omega_1 = \begin{pmatrix} \sigma_e^2 & 0 & 0 & 0 \\ 0 & \sigma_e^2 & 0 & 0 \\ 0 & 0 & 0 & 0 \\ 0 & 0 & 0 & 0 \end{pmatrix}.$$

If no Γ matrix had been used, or equivalently $\gamma = 1$, the estimated position would not have converged to the simulated position. The smaller γ is chosen the faster the estimates converge to the simulated signals. However, choosing for example $\gamma = 0.75$ the damping of the position and the velocity variable is that strong, such that they can not be interpreted any more as the integrals of the observed acceleration.

5.2.2 Filtering

Theorem 5.2 (Kalman Filtering) *The filtered estimates $X_{t|t} := P_t(X_t)$ and their error covariance matrices $\Omega_{t|t} := E[(X_t - X_{t|t})(X_t - X_{t|t})^T]$ are determined by the recursions*

$$X_{t|t} = \hat{X}_t + \Omega_t G_t^T \Delta_t^{-1} (Y_t - G_t \hat{X}_t) \quad (5.7)$$

$$\Omega_{t|t} = \Omega_t - \Omega_t G_t^T \Delta_t^{-1} G_t \Omega_t^T \quad (5.8)$$

Remark 5.9 *The estimate $X_{t|t} = P_t(X_t)$ is often called the "a posteriori estimate" of X_t , because it estimates X_t by means of all measurements up to and including Y_t . The estimate $\hat{X}_t = P_{t-1}(X_t)$ is often called the "a priori estimate" of X_t , because it estimates X_t before including the measurement Y_t .*

Remark 5.10 *Rewriting equations (5.2) and (5.3) from the Kalman prediction Theorem 5.1*

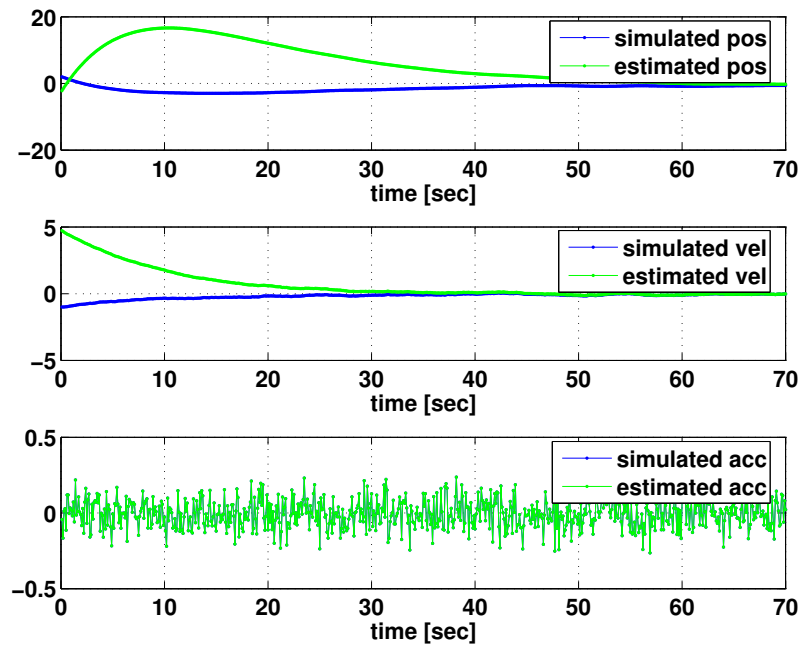


Figure 5.3: Estimates for zero acceleration.

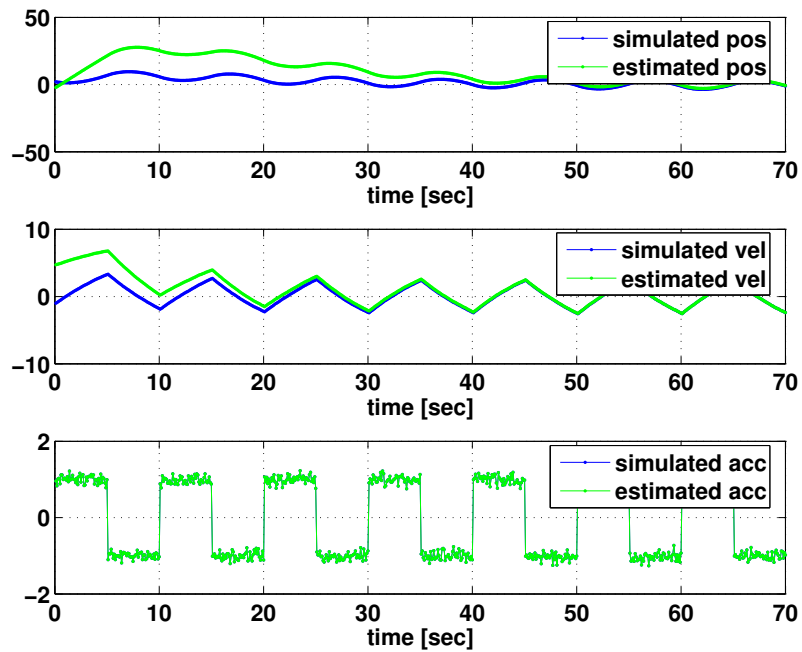


Figure 5.4: Estimates for rectangular acceleration.

we get

$$\begin{aligned}\hat{X}_{t+1} &= F_t \{ \hat{X}_t + \Omega_t G_t^T \Delta_t^{-1} (Y_t - G_t \hat{X}_t) \} \\ &= F_t X_{t|t}, \text{ and} \\ \Omega_{t+1} &= F_t (\Omega_t - \Omega_t G_t^T \Delta_t^{-1} G_t \Omega_t) F_t^T + Q_t \\ &= F_t \Omega_{t|t} F_t^T + Q_t.\end{aligned}$$

Thus, the a priori estimate at time $t + 1$ is the a posteriori estimate at time t multiplied by the state-transition matrix F_t . Likewise, the error covariance matrix of the a priori estimate at time $t + 1$ can be computed from the error covariance matrix of the a posteriori estimate at time t by multiplication of the state-transition matrix F_t from both sides and addition of the state-noise covariance matrix Q_t .

Proof of Theorem 5.2.

From the "law of updating a projection" (Theorem 4.3) it follows that

$$\begin{aligned}P_t(X_t) &= P_{t-1}(X_t) + P(X_t|I_t), \text{ or} \\ X_{t|t} &= \hat{X}_t + P(X_t|I_t), \text{ where} \\ P(X_t|I_t) &= M I_t = M(Y_t - G_t \hat{X}_t), \text{ and} \\ M &= E(X_t I_t^T) E(I_t I_t^T)^{-1} \\ &= E\{X_t [G_t(X_t - \hat{X}_t) + W_t]^T\} \Delta_t^{-1} \\ &= E[X_t(X_t - \hat{X}_t)^T] G_t^T \Delta_t^{-1} \\ &= E[(X_t - \hat{X}_t)(X_t - \hat{X}_t)^T] G_t^T \Delta_t^{-1} \\ &= \Omega_t G_t^T \Delta_t^{-1},\end{aligned}$$

which proves equation (5.7). To prove equation (5.8) we write using the "law of updating a projection"

$$\begin{aligned}X_t - P_{t-1}(X_t) &= X_t - P_t(X_t) + P_t(X_t) - P_{t-1}(X_t) \\ X_t - P_{t-1}(X_t) &= X_t - P_t(X_t) + M I_t \\ X_t - \hat{X}_t &= X_t - X_{t|t} + M I_t\end{aligned}$$

The filter error $X_t - X_{t|t}$ is orthogonal on the linear span of Y_0, Y_1, \dots, Y_t in which the innovation I_t lies. Thus we have

$$\begin{aligned}E[(X_t - \hat{X}_t)(X_t - \hat{X}_t)^T] &= E[(X_t - X_{t|t})(X_t - X_{t|t})^T] + E[M I_t (M I_t)^T] \\ \Omega_t &= \Omega_{t|t} + M E(I_t I_t^T) M^T \\ \Omega_t &= \Omega_{t|t} + \Omega_t G_t^T \Delta_t^{-1} \Delta_t \Delta_t^{-1} G_t \Omega_t^T \\ \Omega_t &= \Omega_{t|t} + \Omega_t G_t^T \Delta_t^{-1} G_t \Omega_t^T,\end{aligned}$$

which proves equation (5.8) and completes the proof of Theorem 5.2.

□

5.2.3 Fixed-Point Smoothing

Theorem 5.3 (Kalman Fixed-Point Smoothing) For $n \geq t$ and fixed t , the fixed-point smoothed estimates $X_{t|n} := P_n(X_t)$ and error covariance matrices

$$\Omega_{t|n} := E[(X_t - X_{t|n})(X_t - X_{t|n})^T]$$

are determined by the following recursions for $n = t, t+1, \dots$

$$X_{t|n} = X_{t|n-1} + \Omega_{t,n} G_n^T \Delta_n^{-1} (Y_n - G_n \hat{X}_n), \quad (5.9)$$

$$\Omega_{t,n+1} = \Omega_{t,n} (F_n - \Theta_n \Delta_n^{-1} G_n)^T, \quad (5.10)$$

$$\Omega_{t|n} = \Omega_{t|n-1} - \Omega_{t,n} G_n^T \Delta_n^{-1} G_n \Omega_{t,n}^T \quad (5.11)$$

with $\Omega_{t,n} := E[(X_t - \hat{X}_t)(X_n - \hat{X}_n)^T]$ and with initial conditions

$$\begin{aligned} X_{t|t-1} &= \hat{X}_t, \text{ and} \\ \Omega_{t,t} &= \Omega_{t|t-1} = \Omega_t \end{aligned}$$

Proof of Theorem 5.3.

Again we use the "law of updating a projection" (Theorem 4.3) and write

$$\begin{aligned} P_n(X_t) &= P_{n-1}(X_t) + P(X_t|I_n), \text{ or} \\ X_{t|n} &= X_{t|n-1} + CI_n, \text{ with} \\ C &= E(X_t I_n^T) E(I_n I_n^T)^{-1} \\ &= E[X_t [G_n(X_n - \hat{X}_n) + W_n]^T] \Delta_n^{-1} \\ &= E[X_t (X_n - \hat{X}_n)] G_n^T \Delta_n^{-1} \\ &= E[(X_t - \hat{X}_t)(X_n - \hat{X}_n)] G_n^T \Delta_n^{-1} \\ &= \Omega_{t,n} G_n^T \Delta_n^{-1} \end{aligned}$$

which proves equation (5.9). In the penultimate step it was used that the predictor \hat{X}_t lies in the linear span of observations up to and including Y_{t-1} and thus is orthogonal to the prediction error $X_n - \hat{X}_n$ which is orthogonal to the linear span of observations up to and including Y_{n-1} , where $n \geq t$.

To prove equation (5.10) we write

$$\begin{aligned} \Omega_{t,n+1} &= E[(X_t - \hat{X}_t)(X_{n+1} - \hat{X}_{n+1})^T], \text{ and} \\ X_{n+1} - \hat{X}_{n+1} &= F_n X_n + V_n - \{F_n \hat{X}_n + \Theta_n \Delta_n^{-1} [G_n(X_n - \hat{X}_n) + W_n]\} \end{aligned}$$

The noise terms V_n and W_n are both orthogonal to $X_t - \hat{X}_t$ and therefore

$$\begin{aligned} \Omega_{t,n+1} &= E\{(X_t - \hat{X}_t)[(F_n - \Theta_n \Delta_n^{-1} G_n)(X_n - \hat{X}_n)]^T\} \\ &= E[(X_t - \hat{X}_t)(X_n - \hat{X}_n)]^T (F_n - \Theta_n \Delta_n^{-1} G_n)^T \\ &= \Omega_{t,n} (F_n - \Theta_n \Delta_n^{-1} G_n)^T, \end{aligned}$$

which proves equation (5.10).

Finally, to prove equation (5.11) we write using the "law of updating a projection"

$$\begin{aligned} X_t - P_n(X_t) &= X_t - P_{n-1}(X_t) + P_{n-1}(X_t) - P_n(X_t) \\ X_t - X_{t|n} &= X_t - X_{t|n-1} - CI_n, \text{ or} \\ X_t - X_{t|n-1} &= X_t - X_{t|n} + CI_n \end{aligned}$$

The fixed-point smoothing error $X_t - X_{t|n}$ is orthogonal on the linear span of the observations Y_0, Y_1, \dots, Y_n in which the innovation I_n lies. Thus we have

$$\begin{aligned} E[(X_t - X_{t|n-1})(X_t - X_{t|n-1})^T] &= E[(X_t - X_{t|n})(X_t - X_{t|n})^T] + C\Delta_n C^T \\ \Omega_{t|n-1} &= \Omega_{t|n} + C\Delta_n C^T, \text{ or} \\ \Omega_{t|n} &= \Omega_{t|n-1} - C\Delta_n C^T \\ &= \Omega_{t|n-1} - \Omega_{t,n} G_n^T \Delta_n^{-1} \Delta_n \Delta_n^{-t} G_n \Omega_{t,n}^T \\ &= \Omega_{t|n-1} - \Omega_{t,n} G_n^T \Delta_n^{-1} G_n \Omega_{t,n}^T, \end{aligned}$$

which proves equation (5.11) and completes the proof of Theorem 5.3. □

5.2.4 Properties of the Kalman Recursions

For the estimation of state-space models, cf. section 5.3, a proposition is presented, which compares the evolution of the Kalman recursions of a state space model with different noise terms and initial conditions. More precisely, for given structural matrices $\{F_t\}$ and $\{G_t\}$, and **univariate** observations $\{Y_t\}$ let the state space model \mathbb{M} be completed by the covariance matrix Q for the state-noise, the covariance matrix $R = \sigma_w^2 \neq 0$ for the observation-noise, the initial error covariance matrix Ω_1 and the initial state $\hat{X}_1 = \mu \in \mathbb{R}^v$. The corresponding **normalised state-space model** \mathbb{M}^* is then given by completing $\{F_t\}$, $\{G_t\}$ and $\{Y_t\}$ with the covariance matrices and initial conditions

$$\begin{aligned} Q^* &:= \frac{Q}{\sigma_w^2}, & R^* &:= \frac{R}{\sigma_w^2} = 1, \\ \Omega_1^* &:= \frac{\Omega_1}{\sigma_w^2}, & \hat{X}_1^* &= 0. \end{aligned}$$

Then the following proposition holds

Proposition 5.1 *The Kalman prediction and fixed-point smoothing recursions for the models \mathbb{M} and \mathbb{M}^* yield for all $t = 1, 2, 3, \dots$ and $n = t, t+1, t+2, \dots$*

$$\Omega_t^* = \frac{\Omega_t}{\sigma_w^2}, \tag{5.12}$$

$$\Delta_t^* = \frac{\Delta_t}{\sigma_w^2}, \tag{5.13}$$

$$\Theta_t^* = \frac{\Theta_t}{\sigma_w^2}, \tag{5.14}$$

$$\hat{X}_t = \hat{X}_t^* + C_t \mu, \text{ with} \tag{5.15}$$

$$C_1 = 1, \text{ and } C_{t+1} = (F_t - \Theta_t \Delta_t^{-1} G_t) C_t, \tag{5.16}$$

$$\Omega_{t|n}^* = \frac{\Omega_{t|n}}{\sigma_w^2}, \tag{5.17}$$

$$X_{t|n} = X_{t|n}^* + D_{t|n} \mu, \text{ with} \tag{5.18}$$

$$D_{t|t} = (1 - \Omega_{t,t} G_t^T \Delta_t^{-1} G_t) C_t, \text{ and} \tag{5.19}$$

$$D_{t|n+1} = D_{t|n} - \Omega_{t,n+1} G_{n+1}^T \Delta_{n+1}^{-1} G_{n+1} C_{n+1} \tag{5.20}$$

Remark 5.11 Note that the computation of the matrices C_t and $D_{t|t}$ can be made in the model \mathbb{M} or in the model \mathbb{M}^* , i.e.,

$$C_t = C_t^* \quad \text{and} \quad D_{t|t} = D_{t|t}^*.$$

The case of Kalman filtering is covered by the statements of Proposition 5.1 for fixed-point smoothing when n is set to t .

Proof of Proposition 5.1.

We prove all statements by induction.

For $t = 1$ we have $\Omega_1^* = \Omega_1 / \sigma_w^2$ by definition and from equation (5.4) that

$$\Delta_1^* = G_1 \Omega_1^* G_1^T + R^* = \frac{1}{\sigma_w^2} (G_1 \Omega_1 G_1^T + R) = \frac{\Delta_1}{\sigma_w^2}$$

and from equation (5.5) that

$$\Theta_1^* = F_1 \Omega_1^* G_1^T = \frac{1}{\sigma_w^2} F_1 \Omega_1 G_1^T = \frac{\Theta_1}{\sigma_w^2}.$$

Now the induction step for Ω_t^* , Δ_t^* and Θ_t^* from $t \rightarrow t + 1$. From equation (5.3) we conclude that

$$\begin{aligned} \Omega_{t+1}^* &= F_t \Omega_t^* F_t^T + Q^* - \Theta_t^* \Delta_t^{*-1} \Theta_t^{*T} \\ &= F_t \frac{\Omega_t}{\sigma_w^2} F_t^T + \frac{Q}{\sigma_w^2} - \frac{\Theta_t}{\sigma_w^2} \left(\frac{\Delta_t}{\sigma_w^2} \right)^{-1} \frac{\Theta_t^T}{\sigma_w^2} \\ &= \frac{1}{\sigma_w^2} (F_t \Omega_t F_t^T + Q - \Theta_t \Delta_t^{-1} \Theta_t^T) \\ &= \frac{\Omega_{t+1}}{\sigma_w^2} \end{aligned}$$

Analogously, we get

$$\begin{aligned} \Delta_{t+1}^* &= G_{t+1} \Omega_{t+1}^* G_{t+1}^T + R^* \\ &= G_{t+1} \frac{\Omega_{t+1}}{\sigma_w^2} G_{t+1}^T + \frac{R}{\sigma_w^2} \\ &= \frac{1}{\sigma_w^2} (G_{t+1} \Omega_{t+1} G_{t+1}^T + R) \\ &= \frac{\Delta_{t+1}}{\sigma_w^2} \\ \Theta_{t+1}^* &= F_{t+1} \Omega_{t+1}^* G_{t+1}^T \\ &= F_{t+1} \frac{\Omega_{t+1}}{\sigma_w^2} G_{t+1}^T \\ &= \frac{\Theta_{t+1}}{\sigma_w^2} \end{aligned}$$

Again, for $t = 1$ we have

$$\begin{aligned} \hat{X}_1 &= \hat{X}_1^* + C_1 \mu \\ \mu &= 0 + C_1 \mu, \end{aligned}$$

if $C_1 = 1$. The induction step $t \rightarrow t + 1$:

$$\begin{aligned}\hat{X}_{t+1}^* &= F_t \hat{X}_t^* + \Theta_t^* \Delta_t^{*-1} (Y_t - G_t \hat{X}_t^*) \\ &= F_t \hat{X}_t + \Theta_t \Delta_t^{-1} (Y_t - G_t \hat{X}_t) \\ &\quad - (F_t - \Theta_t \Delta_t^{-1} G_t) C_t \mu \\ &= \hat{X}_{t+1} - (F_t - \Theta_t \Delta_t^{-1} G_t) C_t \mu,\end{aligned}$$

from which it follows that $C_{t+1} = (F_t - \Theta_t \Delta_t^{-1} G_t) C_t$. In order to prove the relations for the fixed-point smoothing recursions, we first prove by induction over $n = t, t + 1, t + 2, \dots$ that $\Omega_{t,n}$ and $\Omega_{t,n}^*$ are proportional, too.

Induction start $n = t$:

$$\Omega_{t,t} = \Omega_t = \sigma_w^2 \Omega_t^* = \sigma_w^2 \Omega_{t,t}^*$$

Induction step $n \rightarrow n + 1$:

$$\begin{aligned}\Omega_{t,n+1} &= \Omega_{t,n} (F_n - \Theta_n \Delta_n^{-1} G_n)^T \\ &= \sigma_w^2 \Omega_{t,n}^* (F_n - \Theta_n^* \Delta_n^{*-1} G_n)^T \\ &= \sigma_w^2 \Omega_{t,n+1}^*\end{aligned}$$

Then we conclude by induction over $n = t - 1, t, t + 1, \dots$ that $\Omega_{t,n}$ and $\Omega_{t,n}^*$ are proportional.

Induction start $n = t - 1$:

$$\Omega_{t|t-1} = \Omega_t = \sigma_w^2 \Omega_t^* = \sigma_w^2 \Omega_{t|t-1}^*$$

Induction step $n \rightarrow n + 1$:

$$\begin{aligned}\Omega_{t|n+1} &= \Omega_{t|n} - \Omega_{t,n+1} G_{n+1}^T \Delta_{n+1}^{-1} G_{n+1} \Omega_{t,n+1}^T \\ &= \sigma_w^2 \Omega_{t|n}^* - \sigma_w^2 \Omega_{t,n+1}^* G_{n+1}^T \Delta_{n+1}^{*-1} G_{n+1} \Omega_{t,n+1}^{*T} \\ &= \sigma_w^2 \Omega_{t|n+1}^*\end{aligned}$$

Finally, we prove the statements for $X_{t|n}$ and $X_{t|n}^*$ by induction over $n = t, t + 1, \dots$

Induction start $n = t$:

$$\begin{aligned}X_{t|t} &= \hat{X}_t + \Omega_{t,t} G_t^T \Delta_t^{-1} (Y_t - G_t \hat{X}_t) \\ &= \hat{X}_t^* + \Omega_{t,t} G_t^T \Delta_t^{-1} (Y_t - G_t \hat{X}_t^*) \\ &\quad + C_t \mu - \Omega_{t,t} G_t^T \Delta_t^{-1} G_t C_t \mu \\ &= X_{t|t}^* + (1 - \Omega_{t,t} G_t^T \Delta_t^{-1} G_t) C_t \mu,\end{aligned}$$

from which we conclude $D_{t|t} = (1 - \Omega_{t,t} G_t^T \Delta_t^{-1} G_t) C_t$.

Induction step $n \rightarrow n + 1$:

$$\begin{aligned}X_{t|n+1} &= X_{t|n} + \Omega_{t,n+1} G_{n+1}^T \Delta_{n+1}^{-1} (Y_{n+1} - G_{n+1} \hat{X}_{n+1}) \\ &= X_{t|n}^* + \Omega_{t,n+1} G_{n+1}^T \Delta_{n+1}^{-1} (Y_{n+1} - G_{n+1} \hat{X}_{n+1}^*) \\ &\quad + D_{t|n} \mu - \Omega_{t,n+1} G_{n+1}^T \Delta_{n+1}^{-1} G_{n+1} C_{n+1} \mu \\ &= X_{t|n+1}^* + (D_{t|n} - \Omega_{t,n+1} G_{n+1}^T \Delta_{n+1}^{-1} G_{n+1} C_{n+1}) \mu,\end{aligned}$$

from which it follows, that $D_{t|n+1} = D_{t|n} - \Omega_{t,n+1} G_{n+1}^T \Delta_{n+1}^{-1} G_{n+1} C_{n+1}$. This completes the proof of Proposition 5.1.

□

Remark 5.12 *The recursions for the normalised state-space could also be started with a non-zero initial state $\hat{X}_1^* = \mu^*$. The statements of Proposition 5.1 still hold when μ is replaced by $\mu - \mu^*$ in equations (5.15) and (5.18).*

5.3 MLE and MMSE Optimisation

In this section two different methods are presented which allow the selection of a distinct state-space model from a set of models by analysing realisations $\{y_t\}$ of a time series $\{Y_t\}$ of observations. The first method, called **Maximum Likelihood Estimation** and abbreviated **MLE**, selects the model, for which the given data $\{y_t\}$ has a maximal value of the probability density function corresponding to the model. The other method, called **Minimum Mean Squared Error** and abbreviated **MMSE**, selects the model with minimal mean squared difference between realisations $\{y_t\}$ of $\{Y_t\}$ or $\{x_t\}$ of $\{X_t\}$ and the corresponding estimates $\{\hat{y}_t\}$ or $\{\hat{x}_t\}$, which could be predicted, filtered or fixed-point smoothed estimates.

5.3.1 Maximum Likelihood Estimation

Definition 5.2 (Likelihood) *For a univariate, but not necessarily stationary, Gaussian time series $\{Y_t\}_{t=1,\dots,n}$ with mean zero and autocovariance function*

$$\varkappa(i, j) = (\Gamma_n)_{i,j} = \text{Cov}(Y_i, Y_j)$$

the likelihood L is the random variable defined by

$$L := (2\pi)^{-n/2} [\det(\Gamma_n)]^{-1/2} \exp \left\{ -\frac{1}{2} \vec{Y}_n^T \Gamma_n^{-1} \vec{Y}_n \right\},$$

where $\vec{Y}_n := (Y_1, \dots, Y_n)^T$ and Γ_n is assumed to be non-singular.

The definition of the likelihood uses the probability density function

$$\begin{aligned} f_{\vec{Y}_n} : \mathbb{R}^n &\rightarrow \mathbb{R} \\ (y_1, \dots, y_n) &\mapsto f_{\vec{Y}_n}(y_1, \dots, y_n) \end{aligned}$$

of the n jointly Gaussian random variables $\{Y_t\}_{t=1,\dots,n}$, cf. definition 4.4, and replaces the real variables (y_1, \dots, y_n) by the corresponding random variables

$$\begin{aligned} Y_t : \Omega &\rightarrow \mathbb{R} \\ \omega &\mapsto Y_t(\omega) = y_t. \end{aligned}$$

In [31, p.158ff.] it is derived that the likelihood L can be represented by means of the one-step predictors \hat{Y}_t as

$$\begin{aligned} L &= (2\pi)^{-n/2} \left(\prod_{t=1}^n \Delta_t \right)^{-1/2} \exp \left\{ -\frac{1}{2} \sum_{t=1}^n \frac{(Y_t - \hat{Y}_t)^2}{\Delta_t} \right\}, \text{ with} \\ \Delta_t &:= \text{E}[(Y_t - \hat{Y}_t)^2]. \end{aligned}$$

For a set of univariate state-space models, which is completely parametrised by a vector $\vartheta \in \Theta \subseteq \mathbb{R}^m$, the maximum likelihood estimate (MLE) of ϑ is found by maximising the likelihood of each model with respect to the given observation data $\{y_t\}$, i.e., by finding the value of ϑ , which maximises the function

$$l: \Theta \rightarrow \mathbb{R}$$

$$\vartheta \mapsto l(\vartheta) = (2\pi)^{-n/2} \left(\prod_{t=1}^n \Delta_t \right)^{-1/2} \exp \left\{ -\frac{1}{2} \sum_{t=1}^n \frac{(y_t - \hat{y}_t)^2}{\Delta_t} \right\},$$

where the $\hat{y}_t = \hat{Y}_t(\omega)$ are the realisations of the predictor random variables \hat{Y}_t just as the $y_t = Y_t(\omega)$ are the realisations of the random variables Y_t . The predicted values \hat{y}_t are computed for example by means of the Kalman prediction recursions using $Y_0 := 1$. It can be shown, cf. [30, p.483], that for multivariate state-space models with a w -dimensional observation space the likelihood can be written analogously as

$$L = (2\pi)^{-nw/2} \left(\prod_{t=1}^n \det(\Delta_t) \right)^{-1/2} \exp \left\{ -\frac{1}{2} \sum_{t=1}^n I_t^T \Delta_t^{-1} I_t \right\}, \quad (5.21)$$

where

$$I_t = Y_t - \hat{Y}_t, \text{ and}$$

$$\Delta_t = E(I_t I_t^T),$$

are both found for example from the Kalman prediction recursions with $Y_0 := 1$. Thus, the numerical value of $l(\vartheta)$ for each Kalman model identified by ϑ can be computed by means of the Kalman prediction recursions.

Remark 5.13 *The method of maximum likelihood estimation is widely used in time series analysis even if the time series $\{Y_t\}_{t=1, \dots, n}$ is not Gaussian.*

Direct maximisation of $l(\vartheta)$ is numerically slow, if the dimension of the state-space or the dimension of the parameter-space Θ is large. The following paragraph gives a technique to reduce the parameter dimension $\dim(\Theta)$ of the maximisation problem $l: \Theta \rightarrow \mathbb{R}$ for a special class of model families.

MLE for Structural State-Space Models

Let $\{Y_t\}_{t=1, \dots, n}$ be a univariate time series of the form

$$X_{t+1} = F_t X_t + V_t, \quad V_t \sim WN(0, Q)$$

$$Y_t = G_t X_t + W_t, \quad W_t \sim WN(0, \sigma_w^2),$$

where $t = 1, 2, \dots$ and $\{F_t\}$ and $\{G_t\}$ are assumed to be known. The covariance matrices Q and σ_w^2 are assumed not to be known. Models of this type are called "structural state-space models".

We set $Y_0 = 1$ in order to include constant terms in the prediction. Lets assume, that the initial state is the unknown but constant random variable $X_1 = \mu \in \mathbb{R}^v$. It follows that

$$\hat{X}_1 = P(X_1 | Y_0) = P(\mu | 1) = \mu$$

and

$$\Omega_1 = E[(X_1 - \hat{X}_1)(X_1 - \hat{X}_1)^T] = 0.$$

We thus consider the family of state-space models parametrised by

$$\mu \in \mathbb{R}^v, Q \in \text{Sym}(\mathbb{R}^{v,v}) \text{ and } \sigma_w^2 \in \mathbb{R}_+,$$

which results in a parameter set Θ of dimension

$$\dim(\Theta) = \frac{v(v+1)}{2} + v + 1 = \frac{v(v+3)}{2} + 1.$$

We will show, that the maximisation problem for the likelihood function

$$l(\vartheta) = l(\mu, Q, \sigma_w^2)$$

can be reduced to the problem of minimising the so-called "reduced likelihood"

$$\tilde{l}(Q^*) = -\frac{2}{n} \ln \left[l(\hat{\mu}(Q^*), \hat{\sigma}_w^2(Q^*)Q^*, \hat{\sigma}_w^2(Q^*)) \right] + C, C \in \mathbb{R},$$

which reduces the dimension of the parameter set to

$$\dim(\Theta^*) = \frac{v(v+1)}{2}.$$

In place of the family $\{\mathbb{M}_{\vartheta}\}_{\vartheta \in \Theta}$ we consider the family of normalised state space models

$$\{\mathbb{M}_{\vartheta^*}\}_{\vartheta^* \in \Theta^*},$$

cf. subsection 5.2.4. The quadratic form in the likelihood function $l(\vartheta)$ of equation (5.21) with $w = 1$ (univariate) can be rewritten as

$$\begin{aligned} S(\mu, Q, \sigma_w^2) &:= \sum_{t=1}^n I_t^T \Delta_t^{-1} I_t \\ &= \sum_{t=1}^n \frac{(Y_t - \hat{Y}_t)^2}{\Delta_t} \\ &= \sum_{t=1}^n \frac{(Y_t - G_t \hat{X}_t^* - G_t C_t \mu)^2}{\sigma_w^2 \Delta_t^*} \\ &=: \frac{1}{\sigma_w^2} S^*(\mu, Q^*) \end{aligned}$$

The likelihood of equation (5.21) with $w = 1$ can be rewritten as

$$\begin{aligned} L(\mu, Q, \sigma_w^2) &= (2\pi)^{-n/2} \left(\prod_{t=1}^n \Delta_t \right)^{-1/2} \exp \left\{ -\frac{1}{2} \sum_{t=1}^n I_t^T \Delta_t^{-1} I_t \right\} \\ &= (2\pi)^{-n/2} \left(\prod_{t=1}^n \sigma_w^2 \Delta_t^* \right)^{-1/2} \exp \left\{ -\frac{1}{2\sigma_w^2} S^*(\mu, Q^*) \right\} \\ &=: L^*(\mu, Q^*, \sigma_w^2) \end{aligned}$$

Computing $-2\ln [L^*(\mu, Q^*, \sigma_w^2)]$ gives

$$\begin{aligned} -2\ln [L^*(\mu, Q^*, \sigma_w^2)] &= n\ln(2\pi) + n\ln(\sigma_w^2) + \sum_{t=1}^n \ln(\Delta_t^*) + \frac{1}{\sigma_w^2} S^*(\mu, Q^*) \\ &= n\ln(2\pi) + n\ln(\sigma_w^2) + \sum_{t=1}^n \ln(\Delta_t^*) + \\ &\quad + \frac{1}{\sigma_w^2} \sum_{t=1}^n \frac{(Y_t - G_t \hat{X}_t^* - G_t C_t \mu)^2}{\Delta_t^*}. \end{aligned}$$

Maximising

$$l(\vartheta) = l(\mu, Q, \sigma_w^2) = [L(\mu, Q, \sigma_w^2)](\omega) = [L^*(\mu, Q^*, \sigma_w^2)](\omega)$$

corresponds to minimising $\{-2\ln [L^*(\mu, Q^*, \sigma_w^2)]\}(\omega)$. However, for fixed Q^* the latter can be minimised analytically. First, minimisation with respect to the variable μ presents an OLS problem with the quadratic form

$$[S^*(\mu, Q^*)](\omega) = \sum_{t=1}^n \frac{(y_t - G_t \hat{x}_t^* - G_t C_t \mu)^2}{\Delta_t^*},$$

where the $\{\hat{x}_t^*\}$ are the values of the predicted states of the normalised model with respect to the given data $\{y_t\}$. Comparing with subsection 4.3.2, we identify the corresponding overdetermined system of linear equations

$$\frac{y_t - G_t \hat{x}_t^*}{\sqrt{\Delta_t^*}} \sim \frac{G_t C_t}{\sqrt{\Delta_t^*}} \mu, \quad \forall t = 1, 2, \dots, n$$

The OLS solution is given by applying equation (4.2) with

$$\begin{aligned} X &= \begin{pmatrix} \frac{G_1 C_1}{\sqrt{\Delta_1^*}} \\ \vdots \\ \frac{G_n C_n}{\sqrt{\Delta_n^*}} \end{pmatrix} \text{ and} \\ y &= \begin{pmatrix} \frac{y_1 - G_1 \hat{x}_1^*}{\sqrt{\Delta_1^*}} \\ \vdots \\ \frac{y_n - G_n \hat{x}_n^*}{\sqrt{\Delta_n^*}} \end{pmatrix}. \end{aligned}$$

The optimal initial state for fixed Q^* is therefore

$$\mu(Q^*) = \left[\frac{\sum_{t=1}^n C_t^T G_t^T G_t C_t}{\Delta_t^*} \right]^{-1} \sum_{t=1}^n \frac{C_t^T G_t^T (y_t - G_t \hat{x}_t^*)}{\Delta_t^*}.$$

Minimisation with respect to the variable σ_w^2 can be done by setting the partial derivative zero.

$$\frac{\partial}{\partial \sigma_w^2} \{-2\ln [L^*(\mu, Q^*, \sigma_w^2)](\omega)\} = \frac{n}{\sigma_w^2} - \frac{S^*(\mu, Q^*)}{(\sigma_w^2)^2} = 0,$$

which is solved for

$$\sigma_w^2(Q^*) = \frac{S^*(\mu, Q^*)}{n}.$$

Thus, for fixed Q^* the minimal value of $\{-2 \ln [L^*(\mu, Q^*, \sigma_w^2)]\}(\omega)$ is achieved when

$$\begin{aligned}\mu &= \hat{\mu}(Q^*) = \left[\frac{\sum_{t=1}^n C_t^T G_t^T G_t C_t}{\Delta_t^*} \right]^{-1} \sum_{t=1}^n \frac{C_t^T G_t^T (y_t - G_t \hat{x}_t^*)}{\Delta_t^*}, \text{ and} \\ \sigma_w^2 &= \hat{\sigma}_w^2(Q^*) = \frac{S^*(\hat{\mu}(Q^*), Q^*)}{n} = \sum_{t=1}^n \frac{(Y_t - G_t \hat{X}_t^* - G_t C_t \hat{\mu}(Q^*))^2}{\Delta_t^*}.\end{aligned}$$

Substituting these optimal values into

$$-2 \ln [L^*(\mu, Q^*, \sigma_w^2)](\omega) = -2 \ln [l(\mu, \sigma_w^2 Q^*, \sigma_w^2)]$$

gives

$$\begin{aligned}-2 \ln [l(\hat{\mu}(Q^*), \hat{\sigma}_w^2(Q^*) Q^*, \hat{\sigma}_w^2(Q^*))] &= \\ n \ln(2\pi) + n \ln(\hat{\sigma}_w^2(Q^*)) + \sum_{t=1}^n \ln(\Delta_t^*) + \frac{1}{\hat{\sigma}_w^2(Q^*)} S^*(\hat{\mu}(Q^*), Q^*) &= \\ n \ln(2\pi) + n \ln(\hat{\sigma}_w^2(Q^*)) + \sum_{t=1}^n \ln(\Delta_t^*) + n.\end{aligned}$$

Dividing by n and neglecting constants we get the so-called "reduced likelihood"

$$\begin{aligned}\tilde{l}(Q^*) &:= \ln(\hat{\sigma}_w^2(Q^*)) + \frac{1}{n} \sum_{t=1}^n \ln(\Delta_t^*) \\ &= \ln \left[\frac{1}{n} \sum_{t=1}^n \frac{(Y_t - G_t \hat{X}_t^* - G_t C_t \hat{\mu}(Q^*))^2}{\Delta_t^*} \right] + \frac{1}{n} \sum_{t=1}^n \ln(\Delta_t^*).\end{aligned}$$

We summarise our results in the following proposition.

Proposition 5.2 *For a family $\{\mathbb{M}_\vartheta\}_{\vartheta \in \Theta}$ of univariate structural state-space models with $\vartheta = (\mu, Q, \sigma_w^2)$ as defined above and observation data $\{y_t\}_{t=1, \dots, n}$, the MLE can be computed by minimising the corresponding reduced likelihood $\tilde{l}(Q^*)$. The latter can be computed by applying the Kalman **prediction** recursions for the family of normalised state-space models $\{\mathbb{M}_{\vartheta^*}\}_{\vartheta^* \in \Theta^*}$. Let \hat{Q}^* be the minimiser of $\tilde{l}(Q^*)$. Then, the MLE $\hat{\vartheta} = (\hat{\mu}, \hat{Q}, \hat{\sigma}_w^2)$ is given by*

$$\begin{aligned}\hat{\mu} &= \hat{\mu}(Q^*) = \left[\frac{\sum_{t=1}^n C_t^T G_t^T G_t C_t}{\Delta_t^*} \right]^{-1} \sum_{t=1}^n \frac{C_t^T G_t^T (y_t - G_t \hat{x}_t^*)}{\Delta_t^*}, \\ \hat{\sigma}_w^2 &= \hat{\sigma}_w^2(Q^*) = \sum_{t=1}^n \frac{(Y_t - G_t \hat{X}_t^* - G_t C_t \hat{\mu}(Q^*))^2}{\Delta_t^*}, \text{ and} \\ \hat{Q} &= \hat{\sigma}_w^2(Q^*) Q^*.\end{aligned}$$

Remark 5.14 *Proposition 5.2 still holds when the normalised state-space models are initialised with a non-zero state $\hat{X}_1^* = \mu^*$, cf. Remark 5.12. Then, the expression for $\hat{\mu}$ in Proposition 5.2 is the MLE of the difference $\hat{\mu} - \mu^*$.*

5.3.2 Minimum Mean Squared Error

Definition 5.3 (Mean Squared Error (MSE)) For a family $\{\mathbb{M}_\vartheta\}_{\vartheta \in \Theta}$ of state-space models with observation data $\{y_t\}_{t=1, \dots, n}$ and estimates $\{\tilde{y}_t\}_{t=1, \dots, n}$ the mean squared error (MSE) for each model M_ϑ is defined by

$$m(\vartheta) = \frac{1}{n} \sum_{t=1}^n \|y_t - \tilde{y}_t\|^2,$$

where $\|\cdot\|$ is the Euclidean norm in the observation-space \mathbb{R}^w . The $\tilde{y}_t := G_t \tilde{x}_t$ could result from predicted, filtered or fixed-point smoothed state-estimates \tilde{x}_t resulting from the corresponding Kalman recursions when applied to the data $\{y_t\}$. Analogously, if realisations of the states $\{x_t\}_{t=1, \dots, n}$ are known, the MSE in the state-space can be computed for each model M_ϑ by

$$m(\vartheta) = \frac{1}{n} \sum_{t=1}^n \|x_t - \tilde{x}_t\|^2,$$

where in this case $\|\cdot\|$ is the Euclidean norm in the state-space \mathbb{R}^v and the \tilde{x}_t are predicted, filtered or fixed-point smoothed state-estimates.

A model $M_{\hat{\vartheta}}$ in $\{\mathbb{M}_\vartheta\}_{\vartheta \in \Theta}$ is called minimum mean squared error (MMSE) estimate, if it has minimal MSE $m(\hat{\vartheta})$ with respect to all other models in $\{\mathbb{M}_\vartheta\}_{\vartheta \in \Theta}$.

Let's assume we have a family $\{\mathbb{M}_\vartheta\}_{\vartheta \in \Theta}$ of structural state-space models with

$$\vartheta = (\mu, Q, \sigma_w^2),$$

cf. subsection 5.3.1, and estimates $\{\tilde{y}_t = G_t \tilde{x}_t\}_{t=1, \dots, n}$. Consider the corresponding family of normalised state space models $\{\mathbb{M}_{\vartheta^*}\}_{\vartheta^* \in \Theta^*}$, cf. subsection 5.2.4. The quadratic form

$$m(\mu, Q, \sigma_w^2) = \frac{1}{n} \sum_{t=1}^n \|y_t - \tilde{y}_t\|^2,$$

can be rewritten as

$$\begin{aligned} m(\mu, Q, \sigma_w^2) &= \frac{1}{n} \sum_{t=1}^n \|y_t - G_t \tilde{x}_t\|^2 \\ &= \frac{1}{n} \sum_{t=1}^n \|y_t - G_t \tilde{x}_t^* - G_t L_t \mu\|^2 \\ &=: m^*(\mu, Q^*), \end{aligned} \tag{5.22}$$

where the matrices L_t are the respective matrices from Proposition 5.1, equations (5.15) and (5.18), depending on the chosen type of Kalman recursions (predictor, filter or fixed-point smoother). Minimisation with respect to the variable μ presents an OLS problem. The OLS solution is given by applying equation (4.2) with

$$\begin{aligned} X &= \begin{pmatrix} G_1 L_1 \\ \vdots \\ G_n L_n \end{pmatrix} \text{ and} \\ y &= \begin{pmatrix} y_1 - G_1 \tilde{x}_1^* \\ \vdots \\ y_n - G_n \tilde{x}_n^* \end{pmatrix}. \end{aligned}$$

The optimal initial state for fixed Q^* is therefore

$$\mu(Q^*) = \left[\sum_{t=1}^n L_t^T G_t^T G_t L_t \right]^{-1} \sum_{t=1}^n L_t^T G_t^T (y_t - G_t \tilde{x}_t^*). \quad (5.23)$$

Corollary 5.3 *Equations (5.22) and (5.23) show, that the MMSE estimate depends only on the ratio $Q^* = \frac{Q}{\sigma_w^2}$. The MMSE estimate therefore is not unique.*

Analogous results hold for the MSE estimation in state-space.

$$\begin{aligned} m(\mu, Q, \sigma_w^2) &= \frac{1}{n} \sum_{t=1}^n \|x_t - \tilde{x}_t\|^2 \\ &= \frac{1}{n} \sum_{t=1}^n \|x_t - \tilde{x}_t^* - L_t \mu\|^2 \\ &=: m^*(\mu, Q^*), \end{aligned}$$

and thus

$$\mu(Q^*) = \left[\sum_{t=1}^n L_t^T L_t \right]^{-1} \sum_{t=1}^n L_t^T (x_t - \tilde{x}_t^*).$$

Remark 5.15 *Note, that, in general, the observation estimates defined as $\tilde{y}_t := G_t \tilde{x}_t$ are not the corresponding estimates of y_t . Only in the case of the Kalman prediction recursions we have*

$$\begin{aligned} P(Y_t | Y_0, \dots, Y_{t-1}) &= P(G_t X_t + W_t | Y_0, \dots, Y_{t-1}) \\ &= G_t P(X_t | Y_0, \dots, Y_{t-1}) + P(W_t | Y_0, \dots, Y_{t-1}) \\ &= G_t P(X_t | Y_0, \dots, Y_{t-1}) + 0 \end{aligned}$$

For the fixed-point smoother recursions, including the filter recursions, we have for $n \geq t$

$$P(Y_t | Y_0, \dots, Y_n) = Y_t,$$

and on the other hand

$$\begin{aligned} P(Y_t | Y_0, \dots, Y_n) &= P(G_t X_t + W_t | Y_0, \dots, Y_n) \\ &= G_t P(X_t | Y_0, \dots, Y_n) + P(W_t | Y_0, \dots, Y_n), \end{aligned}$$

where $P(W_t | Y_0, \dots, Y_n) \neq 0$ unless $W_t = 0$.

Remark 5.16 *In some situations, it may be desirable to minimise the MSE of $\tilde{y}_t := G_t \tilde{x}_t$ not with respect to the noisy observations $y_t = G_t x_t + w_t$ but to the “pure” observations $G_t x_t$, in case the latter are available.*

Part III

CPR Artefact Removal

Chapter 6

Introduction

Contents

6.1	Statement of the Medical Problem	87
6.2	Sources and Characteristics of CPR Artefacts	87
6.3	Overlapping of Frequencies - Why is CPR Artefact Removal Difficult?	88
6.4	More Technical Problems	89

6.1 Statement of the Medical Problem

During CPR chest compressions and ventilations cause artefacts in the ECG. Fig. 6.1 shows the introduction of artefacts in a VF ECG signal during the onset of CPR in a porcine model. In order that the rhythm detection algorithms of AEDs work properly, the international guidelines [17] prescribe a so-called “hands-off interval” for the time of analysis. During this period CPR is stopped and the ECG signal is thus artefact free. However, as a consequence of this, myocardial blood flow drops and both the success of a subsequent defibrillation attempt [125] and the probability of success [54, 53] decrease. Thus, it would be desirable to remove CPR artefacts from the ECG signal continuously during CPR. Thereby, continuous rhythm detection would be possible and would provide minimal “hands-off” delay before the delivery of an electric countershock. Furthermore, in the case of VF, CPR removal algorithms would allow for continuous monitoring of the myocardial metabolism of the heart through parameters derived from the artefact cleaned ECG signal, cf. subsection 1.3.1.

CPR artefact removal is thus a crucial step towards diagnostic based defibrillation and has the potential of dramatically improving the survival rate of cardiac arrest patients.

6.2 Sources and Characteristics of CPR Artefacts

Langhelle et al. [94] propose a CPR artefact component model consisting of four sources.

G1: Signal components originating from the heart due to mechanical stimulation of the heart itself.

G2: Signal components generated by mechanical stimulation of thoracic muscles.

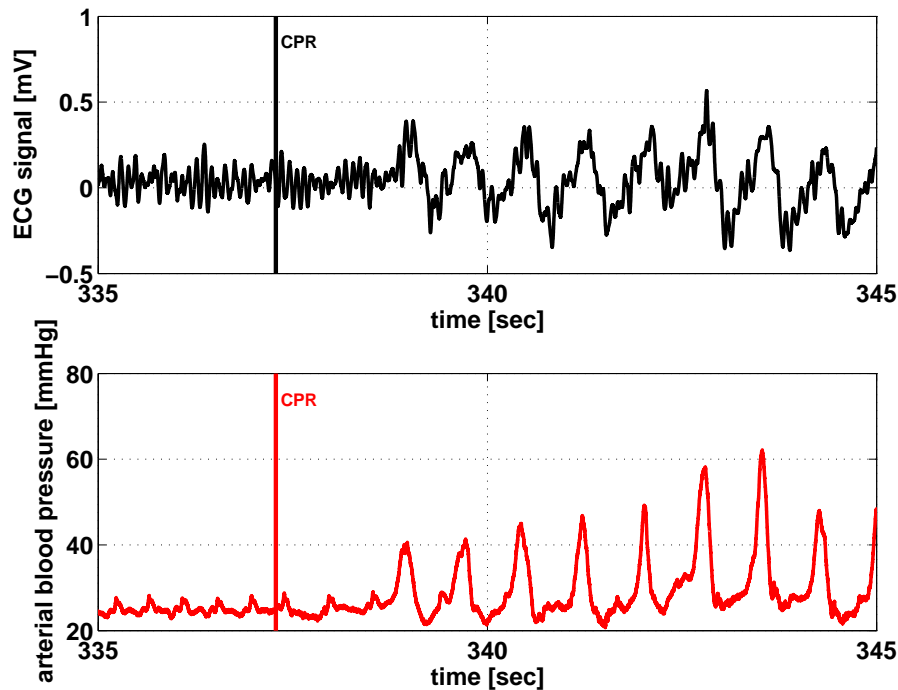


Figure 6.1: Onset of CPR in a porcine model recorded in the ventricular fibrillation ECG signal (upper figure) and in the arterial blood pressure signal (lower figure)

G3: Signal components originating from the electrodes and caused by electrode tapping or dragging.

G4: Signal components caused by static electricity and the following charge equalising currents between the ECG amplifier and the patient.

Some of the listed artefacts can be reduced by measurement methodology [94], and some by filtering methodology. Furthermore, the magnitude of CPR artefacts in the ECG signal depends on the present ECG rhythm (VF, asystole, NSR, etc) and can be different for different recording devices.

For our purposes, we expect that the CPR artefacts are primarily composed of G1 and G2. In addition, we hypothesise that the G1 and G2 components are

- periodic signals with slowly changing period and shape, and
- correlated to signals reflecting the chest compression magnitude (compression depth and acceleration, thorax impedance, arterial blood pressure, etc.), cf. [94, 78] and Fig. 6.1.

6.3 Overlapping of Frequencies - Why is CPR Artefact Removal Difficult?

Many artefact removal problems in signal analysis can be handled by appropriate band-pass filters. A necessary prerequisite is that the artefacts and the artefact-free part of the signal are separated in the frequency domain. In the case of porcine VF ECG signals this is true

(Fig. 6.2), and thus a simple high-pass filter can be applied to remove CPR artefacts from the corrupted ECG signal to a satisfactory extent [138, 12]. However, the human heart

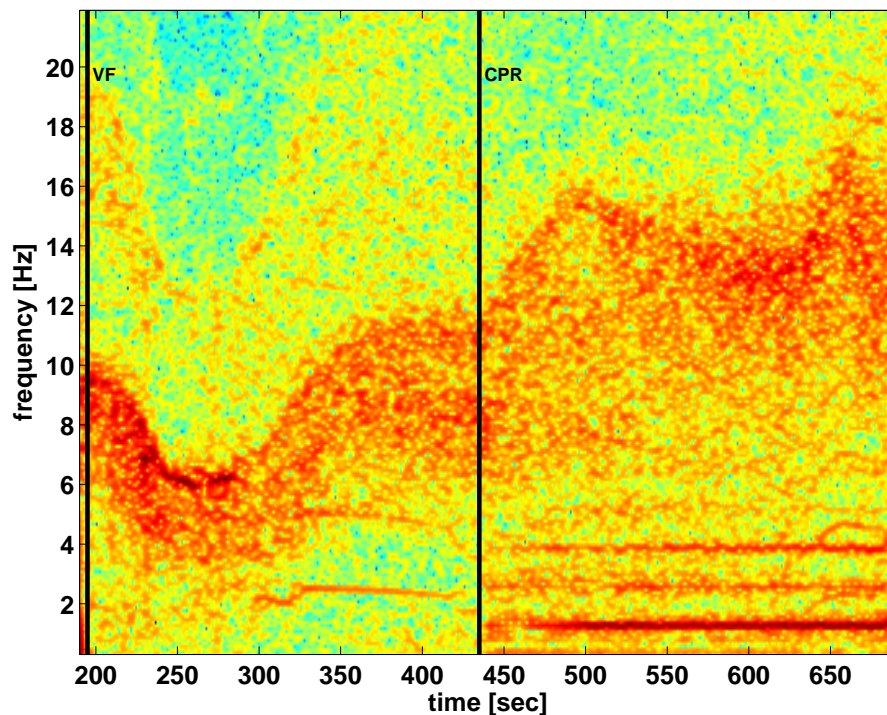


Figure 6.2: Spectrogram transition from pure VF to VF with CPR artefacts in a porcine ECG signal: The dominating VF frequencies do not overlap with the dominating frequencies of the CPR artefacts.

fibrillates at frequencies that overlap with the characteristic frequencies of CPR artefacts [136] (Fig. 6.3), which are determined by the chest compression rate. This is one of the reasons why CPR artefact removal presents a delicate signal processing problem.

6.4 More Technical Problems

Besides the overlapping of signal and noise frequencies, there are some more technical problems, which have to be addressed by a CPR artefact removal algorithm.

- In real life situations, the rates and amplitudes of chest compressions and ventilations are not constant over time.
- The CPR ECG artefacts are in general not sinusoidal and thus can contain various (high) frequencies.
- The shape of the CPR ECG artefacts can change in the course of time.
- The coupling to the chest compressions and thus the amplitude of the CPR ECG artefacts can change in the course of time.

These items suggest that sophisticated **adaptive** removal algorithms are needed.

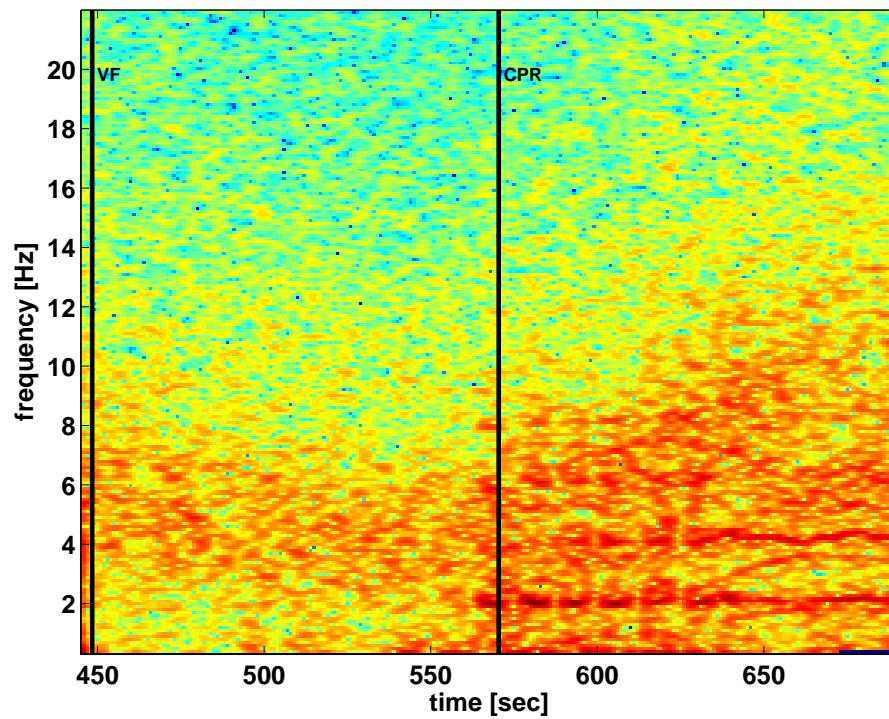


Figure 6.3: Spectrogram transition from pure VF to VF with CPR artefacts in a human ECG signal: The dominating VF frequencies overlap with the dominating frequencies of the CPR artefacts.

Chapter 7

Evaluation Methods and Previous Work

Contents

7.1 Evaluation Methods	91
7.1.1 Restored SNR	91
7.1.2 Performance of Detection and Scoring Algorithms	92
7.2 Previous Work	93

7.1 Evaluation Methods

This section deals with methods to quantify and evaluate the performance of a CPR removal algorithm. Besides visual inspection in time-domain and in time-frequency domain (using the spectrogram), there are two evaluation methods by which one can quantify the algorithm performance:

- the restored signal-to-noise ratio (rSNR), and
- the performance of detection and scoring algorithms.

7.1.1 Restored SNR

An asystole ECG signal a_t containing CPR artefacts (the *noise*), and an artefact free ECG signal x_t (the *signal*) are normalised to unit variance. Both signals are then added with a specific signal-to-noise ratio (SNR), more precisely, the sum y_t is constructed as

$$y_t = x_t + \alpha \cdot a_t,$$

where $\alpha > 0$ is chosen such that the SNR of the mixture

$$SNR_{mix} = 10 \cdot \log_{10} \left(\frac{Var(x)}{Var(\alpha \cdot a)} \right) = -20 \cdot \log_{10}(\alpha)$$

has a specific fixed value. The scaling factor α has to be chosen as

$$\alpha = \frac{1}{\sqrt{10^{SNR_{mix}/10}}}.$$

A CPR removal algorithm separates the mixed signal y_t into an estimate \hat{x}_t of the normalised artefact free ECG signal and into an estimate of the \hat{a}_t of the normalised CPR artefacts:

$$y_t = \hat{x}_t + \hat{a}_t.$$

Note that in general $\text{Var}(\hat{x}_t) \neq 1$ and $\text{Var}(\hat{a}_t) \neq \alpha^2$. Figure 7.1 shows a diagram of the mixing and separation of signal and noise. The estimation error e_t is defined as

$$e_t = x_t - \hat{x}_t = \hat{a}_t - \alpha \cdot a_t$$

Finally, the rSNR of the separation is defined by [94, 124]

$$SNR_{restored} := 10 \cdot \log_{10} \left(\frac{\text{Var}(x)}{\text{Var}(e)} \right) = -10 \cdot \log_{10} (\text{Var}(e)).$$

It reflects the mean squared error of the reconstruction.

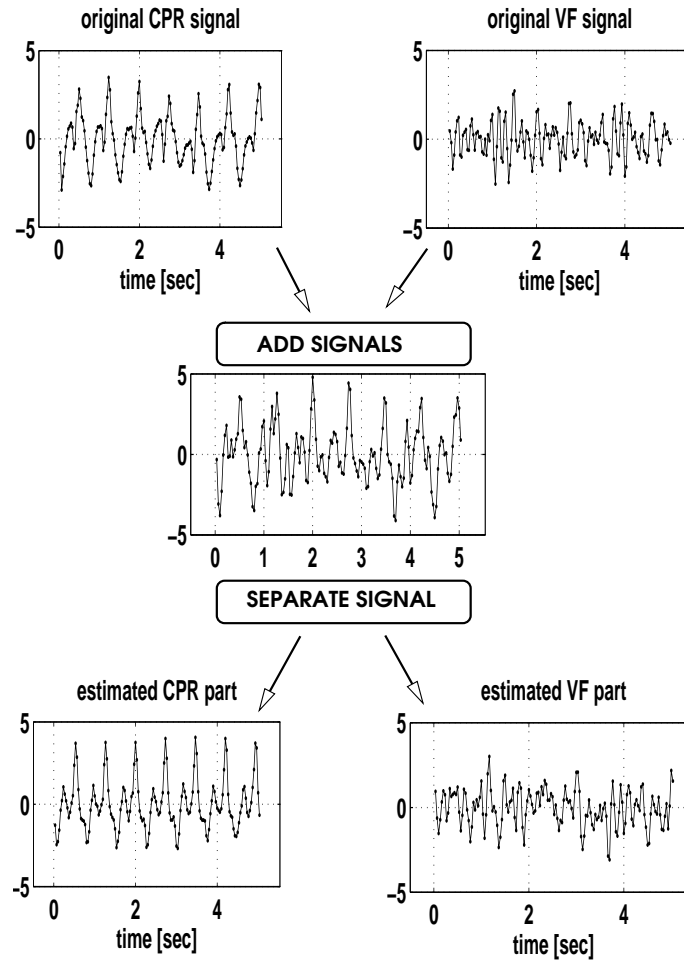


Figure 7.1: *Evaluation Method 1 (depicted for VF)*: The restored signal-to-noise ratio [94, 124] reflects the mean squared error when estimating the CPR part of the mixed signal. Other artefact free ECG rhythms besides VF can be used analogously.

7.1.2 Performance of Detection and Scoring Algorithms

A more pragmatic evaluation consists in the comparison of the values of one or more typical ECG parameters. These can be computed e.g. for an artefact free ECG signal and an adjacent artefact removed signal, cf. Fig. 7.2 and [55], but also for an artefact free ECG signal and the estimated VF part after additive mixing with a CPR signal, c.f. 7.1.1. In the

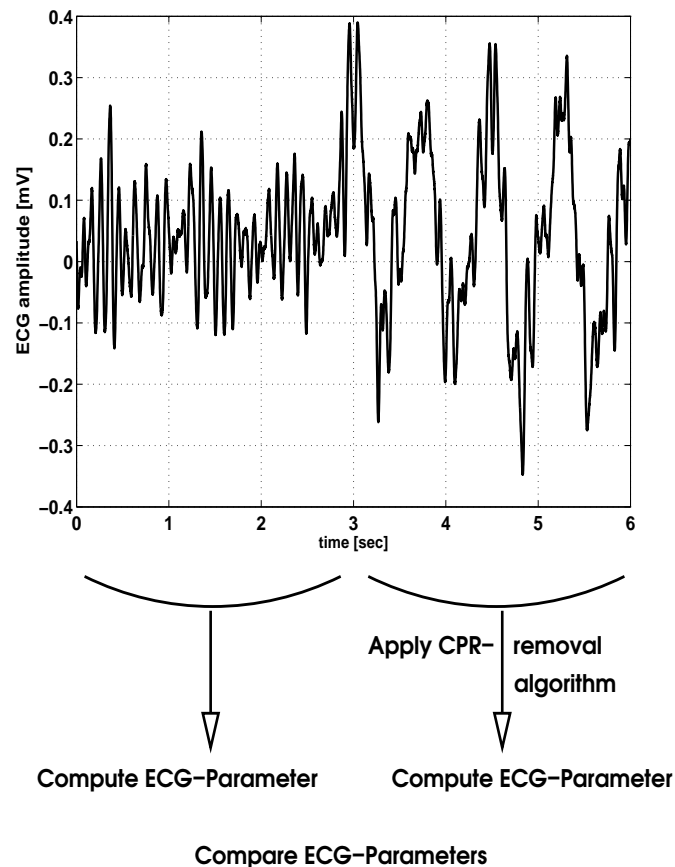


Figure 7.2: *Evaluation Method 2 (depicted for VF)*: For an ECG signal with an artefact free and a CPR contaminated part, the values of different typical ECG parameters computed for the artefact free part and the artefact removed part can be compared.

former case of adjacent signal segments, the value of the ECG parameter should not differ significantly, if one had applied a perfect artefact removal algorithm. Thus, the smaller the difference of the ECG parameter, the better the performance of the artefact removal algorithm. Possible ECG parameters are the decision of shock advice algorithms [55] and VF parameters reflecting the probability of success of a hypothetical defibrillation [11, 12].

7.2 Previous Work

In animal models a simple band-pass filter was used to remove CPR artefacts from the VF ECG signal [138, 12]. This works well for the porcine model, however, the human VF frequencies overlap with the CPR introduced frequencies and can thus not be separated by means of a band-pass filter [136]. More sophisticated mathematical methods have to be

used. In contrast to the large amount of literature about algorithms to detect and analyse VF signals [14, 11], there are surprisingly only few and recent publications addressing the problem of removing CPR artefacts:

- Ruiz et al. [124] use Kalman filters assuming that the CPR artefact as well as the VF signal can be modelled by sinusoidal functions of known angular frequencies. After adding human asystole ECGs containing CPR artefacts to human artefact free VF signals they evaluated the performance of their filtering algorithm by computing the rSNR of the separated signals with respect to the original signals, cf. Fig. 7.1.
Criticism: We consider Kalman filters as a valuable technique for CPR removal, however, their state space model should be modified to allow for more general CPR and VF forms as observed in real life situations.
- Klotz et al. [89, 88] propose a methodology based on time-frequency methods and local coherent line removal.
Criticism: They evaluated their algorithms so far only with porcine animal data by visual inspection of the spectrogram.
- The Norwegian research group of Eftestol, Husoy et al. [94, 78, 55] apply an adaptive filtering approach using additional reference signals (thoracic impedance, compression depth, etc.), which correlate with the CPR artefact signal. They added animal asystole ECGs containing CPR artefacts to human artefact free ECG signals and computed the rSNR, cf. Fig. 7.1 and [78]. In a subsequent analysis, the performance of a shock advice algorithm before and after artefact removal was used for evaluation, cf. Fig. 7.2 and [55].
Criticism: They observed large and spiky ECG artefacts without a similar shape in the reference channels. These artefacts could thus not be reconstructed by a regression on the reference channels.

Chapter 8

New Models for CPR Artefact Removal

Contents

8.1	The Seasonal State-Space Model	95
8.1.1	The model with Noise and Constant Period	96
8.1.2	The model with Noise and Time-Dependent Period: ATS	96
8.1.3	Calculating the Time-Dependent Period	97
8.2	Regression on Reference Signals	98
8.2.1	Reference Signals	98
8.2.2	OLS	99
8.2.3	A State-Space Model: ALR	100

We propose Kalman state-space methods [15, 65, 71] (cf. chapter 5) for CPR artefact removal, because:

- The Kalman recursions provide a numerically fast and adaptive way to compute estimates of the CPR part of the CPR corrupted signal.
- The underlying state space models include all classical time series models, can be combined in a straightforward way, and allow for integration of reference signals (thoracic impedance, compression depth, etc.).
- There exist established optimisation techniques for the estimation of model parameters.

8.1 The Seasonal State-Space Model

This model is motivated by the idea that CPR artefacts form a roughly periodical signal, whereas the VF ECG signal is not periodical, or at least at a much higher rate. However, during uniformly applied CPR the artefact signal can unpredictably, but slowly change its shape and period in the course of time.

The so-called "seasonal" state-space model [31, p.266f] allows for the modelling of a periodical signal with an arbitrary and stochastically changing shape and admits to handle a time-dependent period. This is appropriate for estimating the CPR part of a corrupted signal,

as its shape and period typically change over time. The artefact free signal is estimated as the observation error. More sophisticated models could include for example an auto-regressive model for the artefact free signal.

8.1.1 The model with Noise and Constant Period

The seasonal state-space model with noise and constant period $d > 0$ is presented in [31, p.266f]. For a strictly seasonal (i.e. no noise) time series $\{Y_t\}$ with constant period d and period mean zero it holds that

$$\begin{aligned} Y_{t+d} &= Y_t, \forall t \text{ and} \\ \sum_{s=t-d+2}^{t+1} Y_s &= 0, \forall t. \end{aligned}$$

Such a time series is governed by the recursions

$$Y_{t+1} = -Y_t - \dots - Y_{t-d+2}. \quad (8.1)$$

In order to allow for random variations from strict periodicity, one introduces a white noise term $\{S_t\}$ with mean zero in equation (8.1).

$$Y_{t+1} = -Y_t - \dots - Y_{t-d+2} + S_t. \quad (8.2)$$

By this generalisation the time series $\{Y_t\}$ is now allowed to change the shape of its periodic signal (Y_t, \dots, Y_{t+d-1}), but not the period d itself! Equation (8.2) represents an auto-regressive time series and can be easily transformed into a state-space model, cf. [31, p.266f].

8.1.2 The model with Noise and Time-Dependent Period: ATS

Here, we generalise the above model to a state-space model - called ATS (Adaptive Time-dependent Seasonal) - with noise and time-dependent period $d(t) > 0, \forall t = 1, 2, \dots, T$. Let $D := \max\{d(t), t = 1, 2, \dots, T\}$ be the maximum period during the times $t = 1, 2, \dots, T$, and let the observations be denoted by the random variables $Y_t, t = -D + 3, \dots, 0, 1, 2, \dots, T$.¹ Strict time-dependent periodicity of $\{Y_t\}$ can be expressed by

$$Y_{t+1} = -Y_t - \dots - Y_{t-d(t)+2}. \quad (8.3)$$

Again, to allow for random variations from strict time-dependent periodicity, one introduces a white noise term $\{S_t\}$ in equation (8.3) with mean zero, which leads to

$$Y_{t+1} = -Y_t - \dots - Y_{t-d(t)+2} + S_t. \quad (8.4)$$

A corresponding $D - 1$ -dimensional state space model including the possibility to handle observation noise can be defined analogously to [31, p.266f]. The states $\{X_t\}$ are formed by the vectors

$$X_t := \begin{pmatrix} Y_t \\ Y_{t-1} \\ \vdots \\ Y_{t-D+2} \end{pmatrix}$$

¹Similar to the model with constant period, we require observations to be known for the times $t = -D + 3, \dots, 0$.

The observations $\{Y_t\}$ are recovered from the states by the observation equation

$$Y_t = G_t X_t + W_t = \begin{pmatrix} 1 & 0 & \dots & 0 \end{pmatrix} X_t + W_t,$$

where W_t is a possibly non-zero observation noise. Finally, the state equation is given by

$$X_{t+1} = F_t X_t + V_t,$$

with

$$V_t = \begin{pmatrix} S_t \\ 0 \\ \vdots \\ 0 \end{pmatrix}$$

and

$$F_t = \begin{pmatrix} & f_t & & & \\ 1 & 0 & \dots & 0 & 0 \\ 0 & 1 & \dots & 0 & 0 \\ \vdots & \vdots & \ddots & \vdots & \vdots \\ 0 & 0 & \dots & 1 & 0 \end{pmatrix},$$

where for every t the row vector f_t has length $D - 1$ and entries defined by

$$f_t(k) := \begin{cases} -1 & \text{if } k \leq d(t) - 1 \\ 0 & \text{otherwise.} \end{cases}$$

To estimate the artefact and the artefact free parts of a CPR corrupted ECG signal one assumes non-zero observation noise W_t which models the artefact removed ECG signal.

8.1.3 Calculating the Time-Dependent Period

The estimation of the (usually time-dependent) CPR-period of a CPR corrupted ECG signal can be accomplished by means of the (windowed) sample autocorrelation function.

For a weakly stationary time series² $\{X_t\}$ the autocorrelation function (ACF) is defined for every $h \in \mathbb{Z}$ as

$$\rho(h) := \frac{\text{Cov}(X_t, X_{t+h})}{\text{Var}(X_t)}$$

and is independent of t . For n realisations, i.e., observed data $\{x_1, \dots, x_n\}$ of the time series $\{X_t\}$ the sample ACF $\hat{\rho}$ is an estimate of ρ . It is computed using the sample autocovariance function (sample ACVF) $\hat{\gamma}$ defined as

$$\hat{\gamma}(h) := \frac{1}{n} \sum_{t=1}^{n-|h|} (x_{t+|h|} - \bar{x})(x_t - \bar{x}), \quad n > h > -n$$

$$\hat{\rho}(h) := \frac{\hat{\gamma}(h)}{\hat{\gamma}(0)}$$

Now, the maximum sample ACF value in a specified range of lags $h \in \mathbb{Z}$ can be used as an estimate of the period of a time series. If CPR reference signals (cf. subsection 8.2.1) are available, such as the chest compression force or depth, then such signals are preferable

²For the definition of stationarity cf. e.g. [31]

to the CPR corrupted ECG signal for period estimation, because they usually contain no (or less) noise. Figures 8.1 and 8.2 show the sample ACF and its maximum value in a specified range for an arterial blood pressure signal during CPR and for a VF ECG signal during CPR, respectively. The arterial blood pressure signal would be a good CPR reference signal, but is not available in practice.

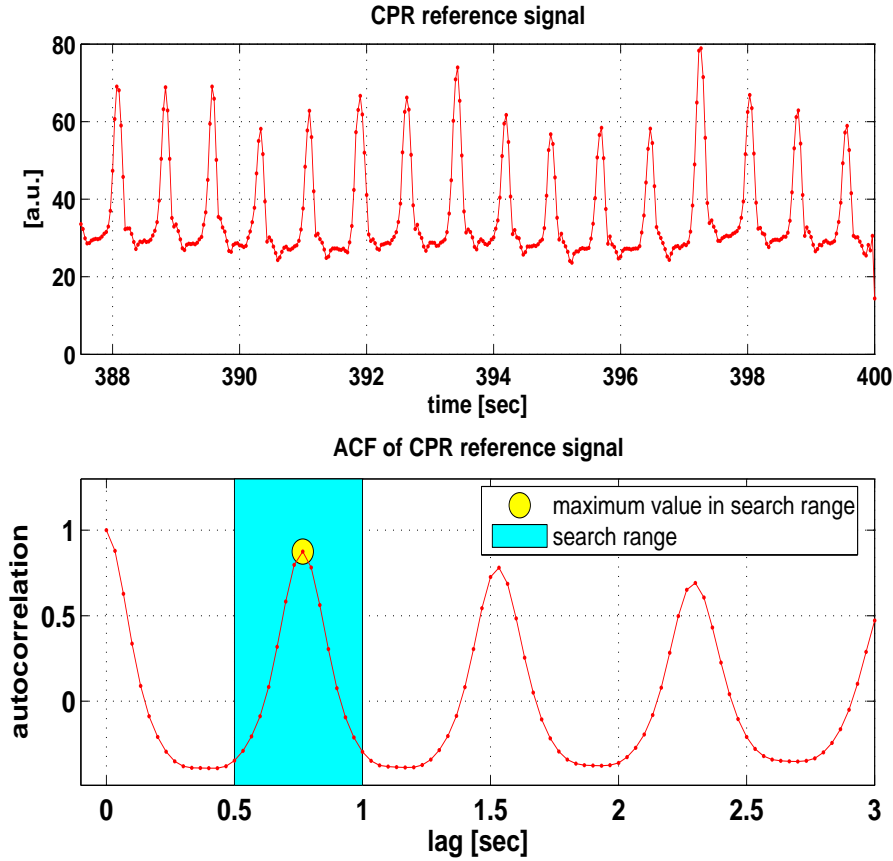


Figure 8.1: ACF of an arterial blood pressure signal during CPR at a sampling frequency of 30 Hz.

The windowed sample ACF estimates the current ACF (and thus the current period) of a time-dependent periodic signal by means of the sample ACF in a symmetric time window around each time point. Figures 8.3 and 8.4 show the windowed sample ACF and its maximum values in a specified range for an arterial blood pressure signal during CPR and for a VF ECG signal during CPR, respectively.

8.2 Regression on Reference Signals

Regression on reference signals can be used to estimate the CPR part of a corrupted ECG signal. The artifact free signal is estimated as the regression error.

8.2.1 Reference Signals

Reference signals are signals which correlate with the artefacts [55, 78, 94, 1] and have already been mentioned in the context of CPR period estimation, cf. subsection 8.1.3.

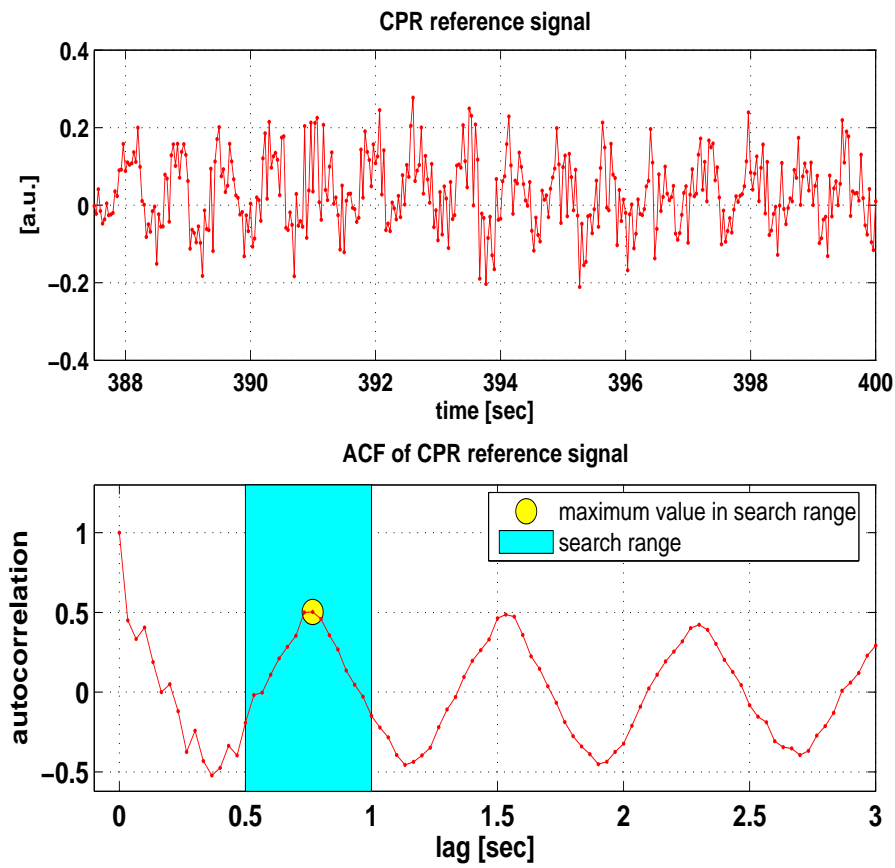


Figure 8.2: ACF of a VF ECG signal during CPR at a sampling frequency of 30 Hz.

Various reference signals conceivable:

- Chest Compression Force, Acceleration, and Depth: see also subsection 5.2.1
- Thorax Impedance: used as a reference signal for ventilation (and compression) induced artefacts.
- ECG common: used as a reference signal for static electricity type artefact components.
- Logical signals: indicate the beginning of each chest compression and can be used together with the compression acceleration signal to estimate the compression depth [78, 2].
- Blood Pressures: would be a good CPR reference signals, but are invasive parameters and thus not available in out-of-hospital practice. However, in animal models, blood pressures are often recorded.

Lagging of Reference Signals In many cases it is appropriate to not only regress on one reference signal, which was recorded synchronously with the CPR corrupted ECG signal, but also to regress on lagged copies of the reference signal. In this case, the OLS regression can be viewed as finding a minimum least squares filter.

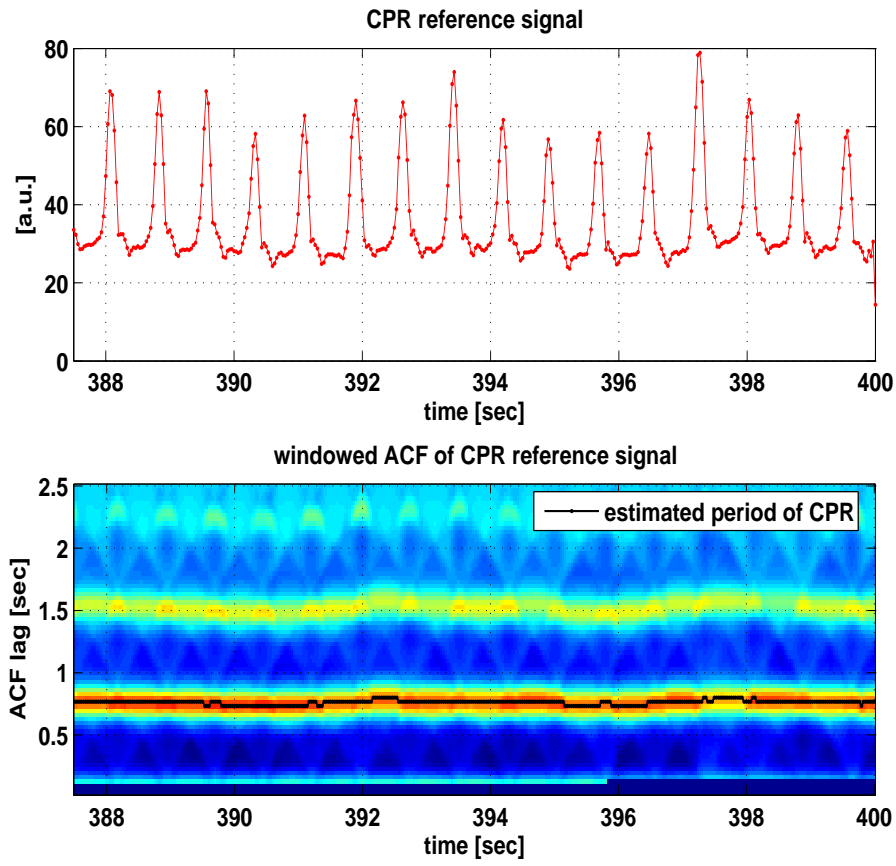


Figure 8.3: Windowed ACF of an arterial blood pressure signal during CPR at a sampling frequency of 30 Hz.

8.2.2 OLS

Probably the easiest regression model consists in OLS, cf. subsection 4.3.2. Let

$$\{y_t\}_{t=1,\dots,T}$$

denote observations of a CPR corrupted ECG signal and

$$\{R_{t,k}\}_{t=1,\dots,T}^{k=1,\dots,m}$$

the matrix of m reference signals at the same sampling time points. Either one subtracts the means of all signals, or, in order to estimate the mean of y one includes an additional constant reference signal consisting of 1s. Anyway, OLS corresponds to finding a column vector $\hat{\beta} \in \mathbb{R}^m$, such that

$$\|y - R\hat{\beta}\|$$

is minimal for all $\beta \in \mathbb{R}^m$ in the Euclidean norm. The OLS estimate

$$\hat{y} := R\hat{\beta}$$

is an estimate the CPR part of a corrupted ECG signal, whereas the regression errors, or residuals

$$e := y - \hat{y}$$

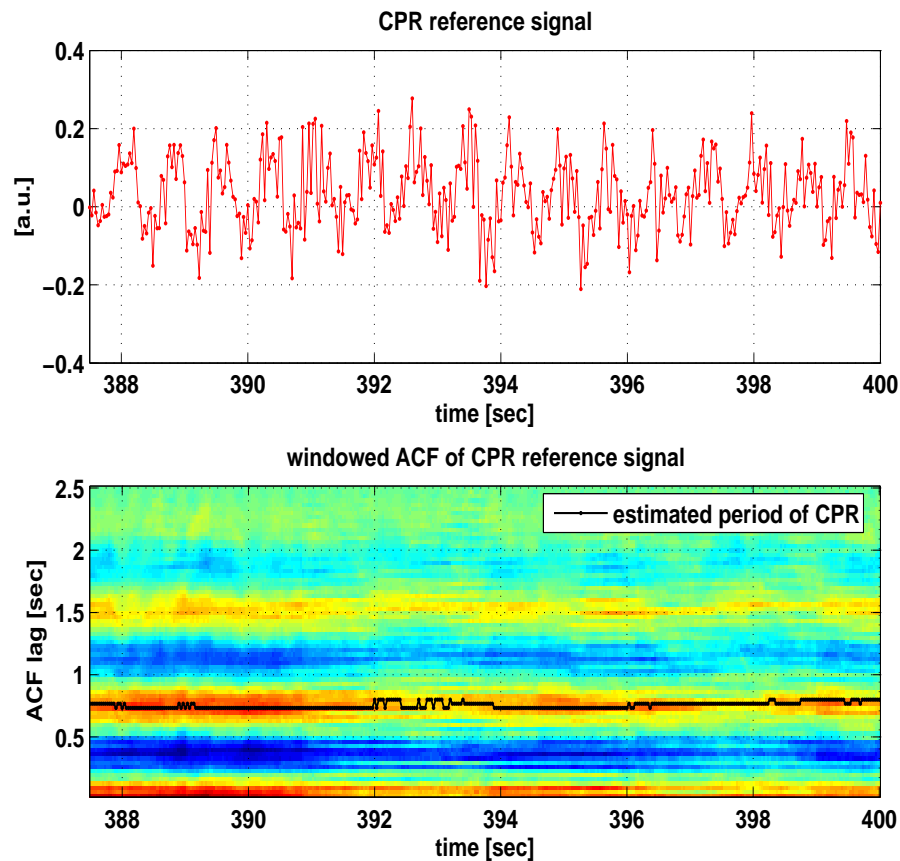


Figure 8.4: Windowed ACF of a VF ECG signal during CPR at a sampling frequency of 30 Hz.

form an estimate of the artifact removed ECG signal.

Figures 8.5 and 8.6 show the result of a OLS regression on various lagged copies of the arterial blood pressure signal in a porcine model of CPR. Negative (shift towards the past) and positive lags (shift towards the future) are used. In both directions the OLS regression coefficients are non-zero. Thus also future parts of the reference signal are useful for estimating the CPR artefact part of a corrupted signal. This fact is not a hindrance for practical on-line implication as it leads only to a short time delay.

8.2.3 A State-Space Model: ALR

As pointed out at the end of the introduction (p. 91), the coupling to the chest compressions and the shape of the CPR ECG artefacts can change in the course of time. An adaptive regression model could handle these features. We propose a state-space regression model - called ALR (Adaptive Lagged Regression) - whose states are time-varying regression coefficients, cf. [21]. This is generalisation of the OLS model having constant coefficients. Let

$$\{y_t\}_{t=1,\dots,T}$$

denote observations of a CPR corrupted ECG signal and

$$\{R_{t,k}\}_{t=1,\dots,T}^{k=1,\dots,m}$$

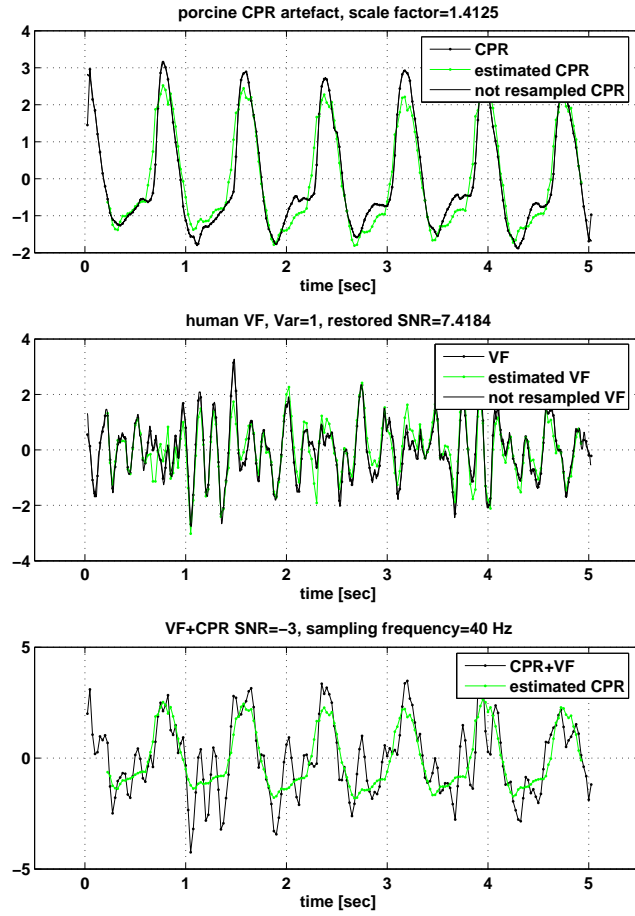


Figure 8.5: OLS regression of a CPR corrupted VF ECG signal on lagged copies of the arterial blood pressure signal in a porcine model of CPR. The regression coefficients are plotted in Figure 8.6.

the matrix of m (lagged copies of) reference signals at the same sampling time points. The observation equation reads

$$Y_t = G_t X_t + W_t, \text{ where}$$

$$G_t = (R_{t,1}, \dots, R_{t,m}), \text{ and}$$

W_t is a possibly non-zero observation noise, which models the artifact removed ECG signal. The state equation is given by

$$X_{t+1} = F_t X_t + V_t,$$

with

$$F_t = \begin{pmatrix} 1 & 0 & \dots & 0 \\ 0 & 1 & \dots & 0 \\ \vdots & \vdots & \ddots & \vdots \\ 0 & 0 & \dots & 1 \end{pmatrix} =: 1_m.$$

The state transition matrices F_t are thus just the $m \times m$ identity matrix 1_m . The state noise vector V_t is assumed to have a covariance matrix $Q = \sigma_v^2 1_m$. The case $\sigma_v = 0$ reproduces the OLS model, where the regression coefficients do not change in the course of time. A

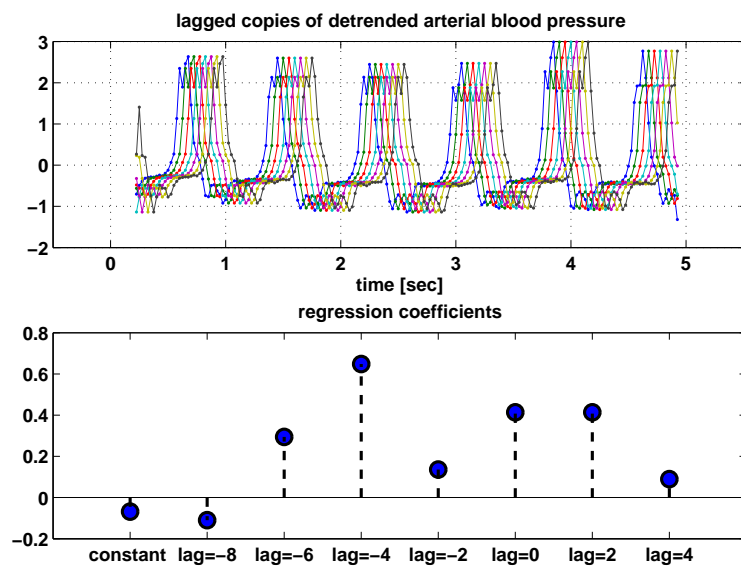


Figure 8.6: OLS regression coefficients corresponding to Figure 8.5. A lag of, for example, -8 means that the original reference signal is shifted 8 samples towards the past, in other words, the reference signal values of 8 samples ahead are used.

state noise covariance matrix $Q \neq 0$ allows for a dynamic evolution of the states, or, in other words, for adaptive regression coefficients.

Chapter 9

Data, Optimisation and Evaluation Results

Contents

9.1 Data	105
9.1.1 Sampling and Mixing	106
9.2 Optimisation	106
9.2.1 Objective Functions: MLE, rSNR	106
9.2.2 Model Families and Search Methods	106
9.3 Evaluation	111
9.4 Results	112
9.4.1 The ATS Model	112
9.4.2 The ALR Model	116
9.5 Discussion and Future Work	122
9.5.1 Discussion of Results	122
9.5.2 Future Work	123

This chapter deals with a small evaluation of the above proposed two new Kalman models ATS and ALR for CPR artefact removal. We apply the models to an additive mixture of porcine asystole ECG signals during CPR and human VF ECG signals. Optimal models are found by MLE and MMSE optimisation, cf. section 5.3, using either a linear grid search or reduced methods, c.f. proposition 5.2 and subsection 5.3.2. We evaluate the rSNR and compare the mean frequency of the original VF signal to the mean frequency of the estimated VF signal after CPR artefact removal.

9.1 Data

In order to keep the computation time for the different models, optimisation procedures, search methods etc “acceptable”, only seven porcine asystole ECG signals during CPR were mixed with seven human VF ECG signals resulting in 49 mixed signals. The MMSE optimisation computes the MSE of the current estimation by knowledge of the true CPR artefact signal (or VF signal). This is obviously not known in practice. Therefore, optimisation and evaluation have to be divided into learning and testing data sets, i.e. the optimal values for the noise variances in the state-space models are estimated on the basis of a 7×7

learning data set, and the mean variances are then evaluated on a disjoint 7×7 testing data set.

All CPR artefact recordings include arterial blood pressure signals, lagged copies of which were used as reference signals in the Kalman regression model, c.f. subsection 8.2.3. Figures 9.1, 9.2, 9.3, and 9.4 show the learning and testing data sets of CPR and VF signals used.

9.1.1 Sampling and Mixing

The human artefact free VF signals are originally sampled at 375 Hz, whereas the porcine CPR artefact signals and their reference signals are originally sampled at 1000 Hz. For the purpose of CPR artefact removal by means of our models, it suffices to work at a sampling frequency of approx. 20-50 Hz, which usually covers the frequencies contained in the CPR artefact signal. This is because our models estimate the CPR artefact signal and handle the VF part as residuals. Therefore, the following procedure can be applied:

1. Down-sample the CPR and VF signals from their original sampling frequencies to a sampling frequency $f \in [20, 50]$, which results in the two signals VF_f and CPR_f .
2. Normalise VF_f and CPR_f and scale CPR_f such that a desired SNR_{mix} is accomplished, c.f. subsection 7.1.1.
3. Estimate the CPR part of the mixture by means of the chosen model and the chosen optimisation procedure resulting in the signal CPR_f^{est} .
4. Under the assumption that all frequencies of the CPR artefact signal are contained in $[0, f/2]$, the restored SNR can be computed at the sampling frequency f by calculating the difference between the scaled true CPR signal and its estimate from the model, c.f. subsection 7.1.1.
5. In order to get an estimate of the VF part including as much frequencies as possible, one up-samples CPR_f^{est} to the original VF sampling frequency (375 Hz for our data), and subtracts it from the CPR+VF mixture at this sampling frequency.

9.2 Optimisation

This section deals with the methods to select an optimal model from a given family of models.

9.2.1 Objective Functions: MLE, rSNR

For both the ATS and the ALR model we will apply MLE as well as maximise the rSNR. MLE was presented in subsection 5.3.1 and amounts to applying the Kalman predictor recursions to the different models in the family. Maximising the rSNR is equivalent to minimising the MSE, c.f. 7.1.1. The estimated observations can result from predicted, filtered or fixed-point smoothed state-estimates. As already pointed out, computing the MSE requires knowing the true CPR artefact signal. Therefore, in the case of rSNR maximisation, optimisation and evaluation have to be divided into learning and testing data sets.

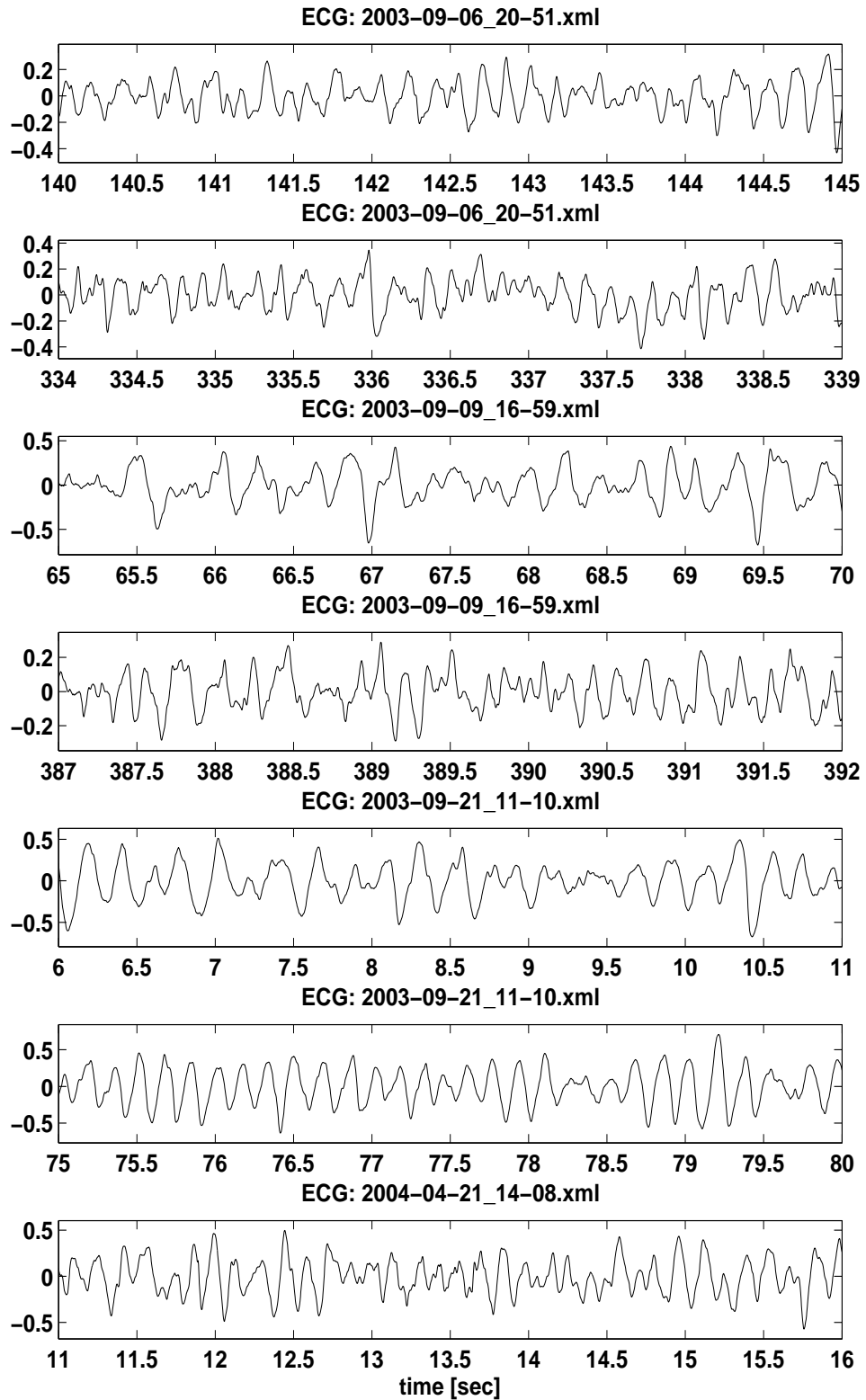


Figure 9.1: Artefact free VF signals of the learning data set.

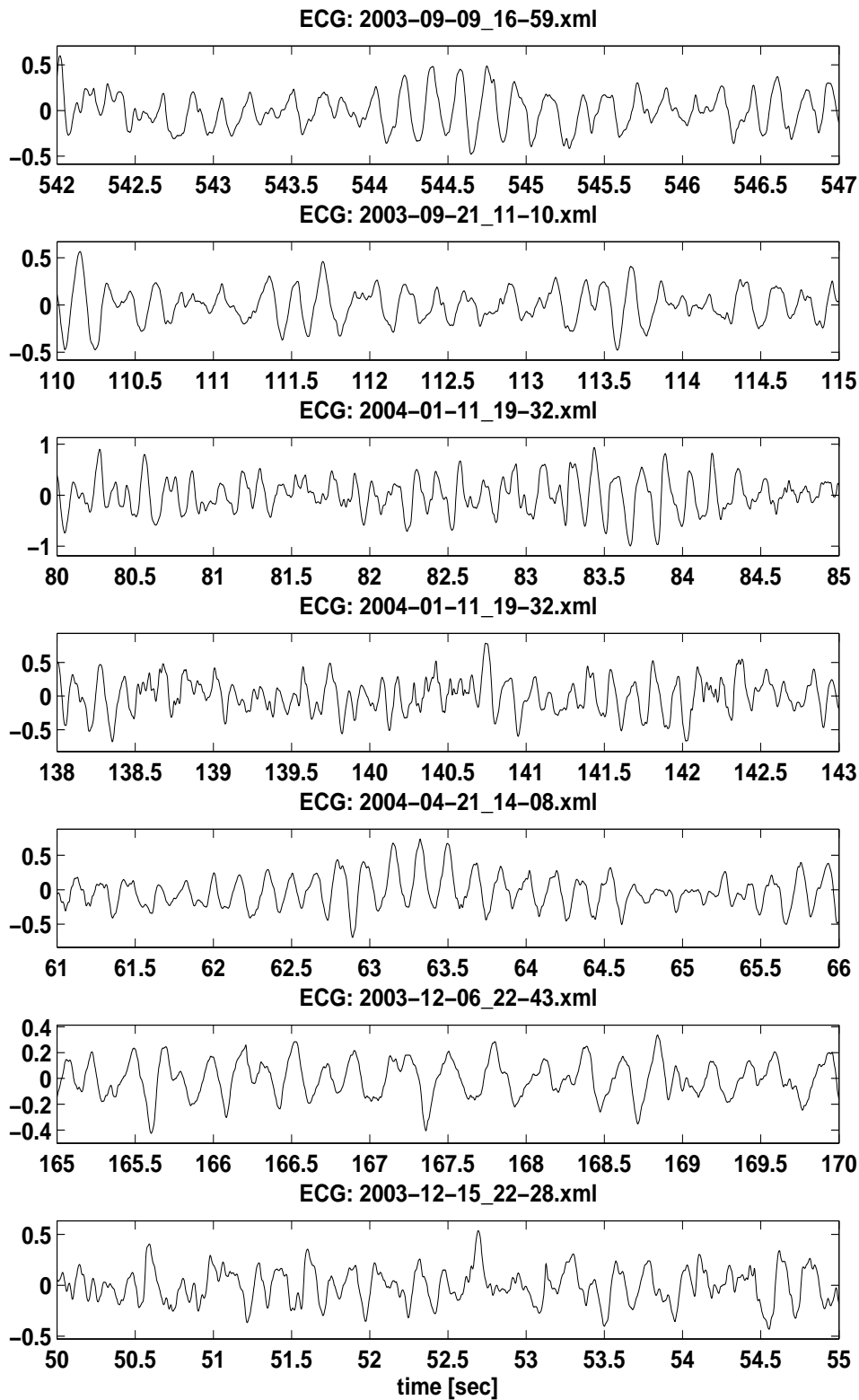


Figure 9.2: Artefact free VF signals of the testing data set.

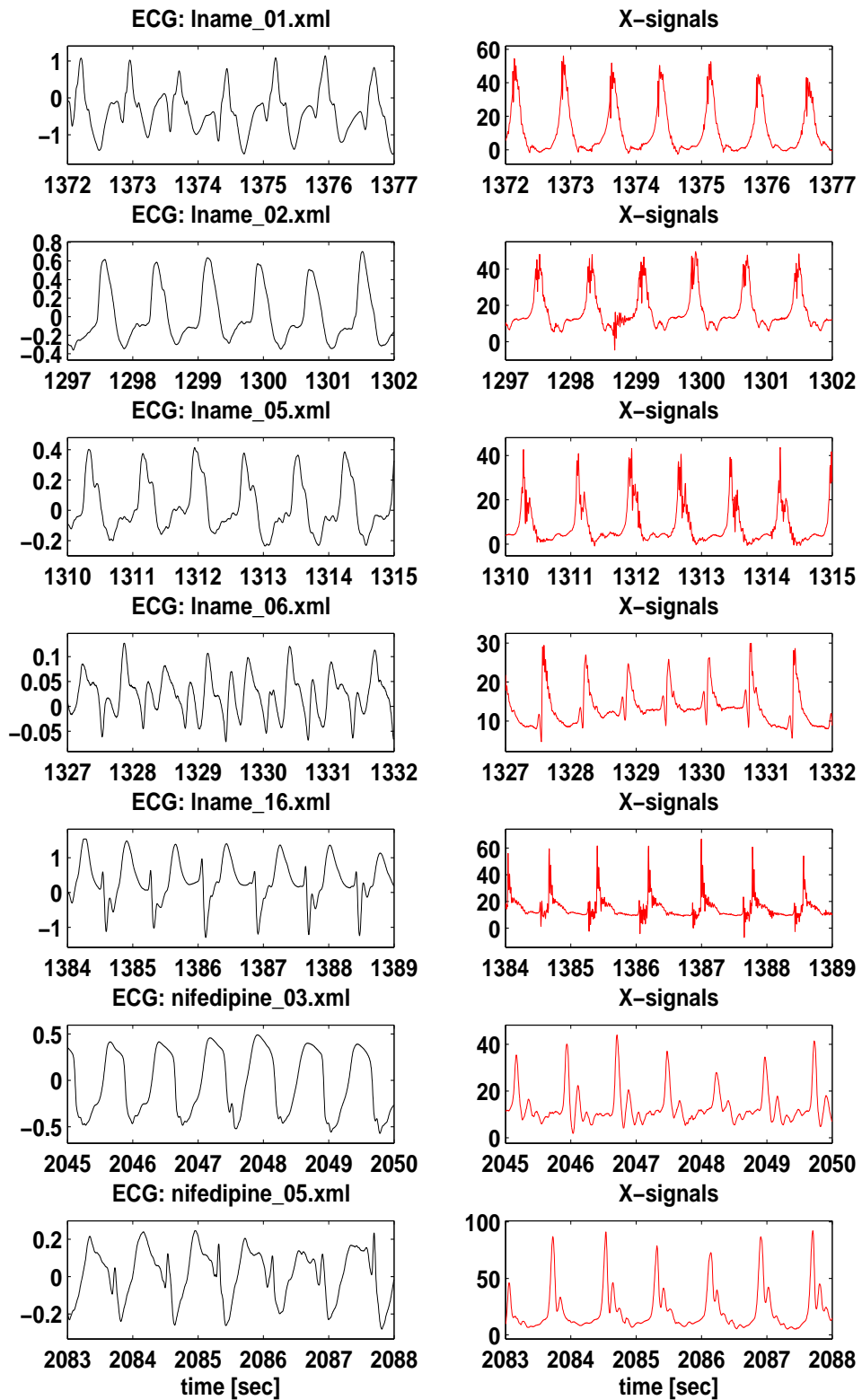


Figure 9.3: CPR artefact signals of the learning data set.

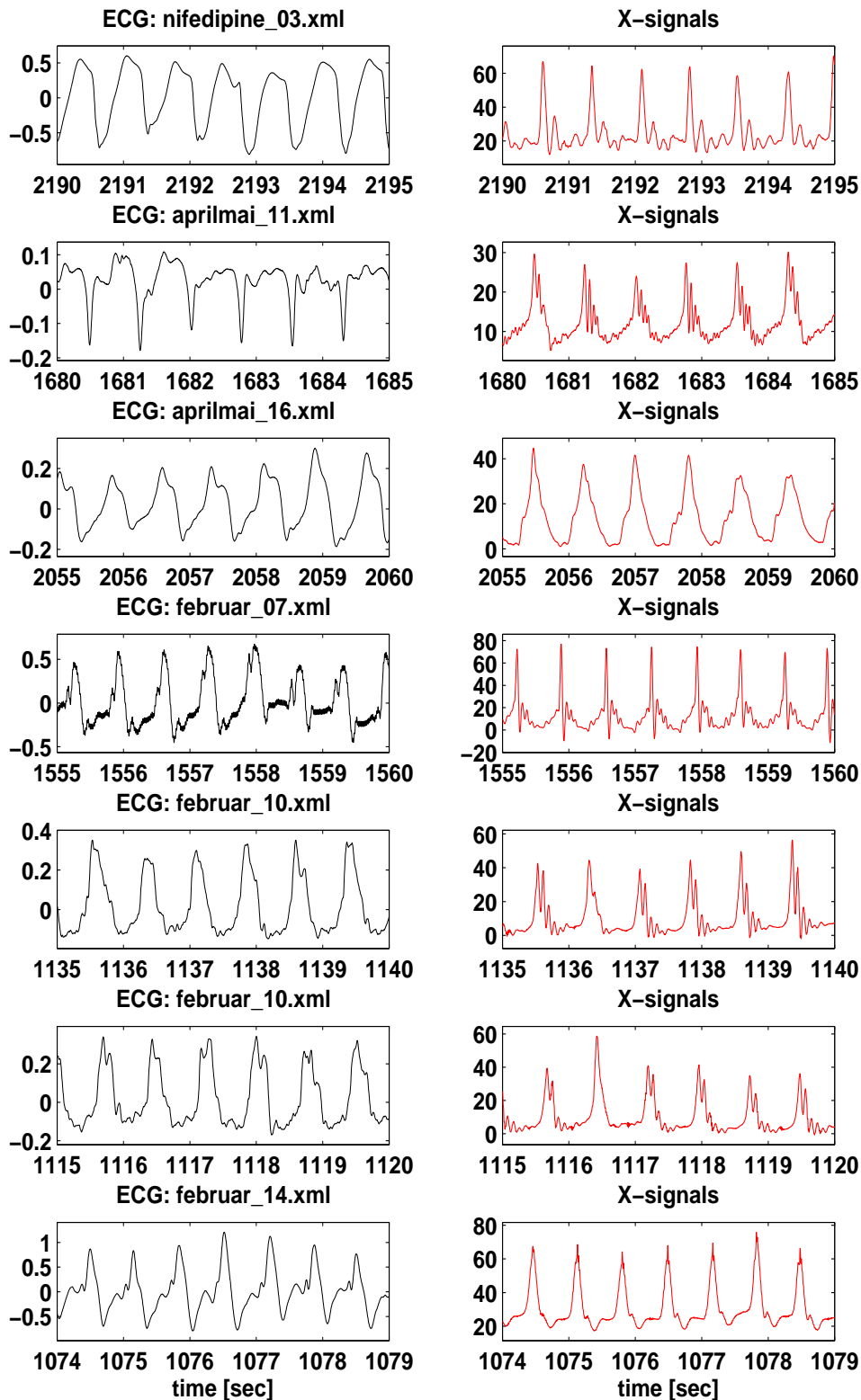


Figure 9.4: CPR artefact signals of the testing data set.

9.2.2 Model Families and Search Methods

Both the ATS and the ALR model are structural state-space models where the transition and observation matrices are known, c.f. 5.3.1. Thus, an ATS or ALR model is determined by giving

- the variance σ_v^2 of the state noise, remember $Q = \sigma_v^2 1_m$ for the ALR model, and $Q = \sigma_v^2(1, 0, \dots, 0)^T$ for the ATS model.
- the variance σ_w^2 of the observation noise,
- the initial state predictor \hat{X}_1 , and
- the initial error covariance matrix Ω_1 .

One-Point Model Families The easiest case is a model family consisting of only one model. For our purposes we prescribe the variances σ_v^2 and σ_w^2 , whereas - to keep the number of parameters to be optimised small - the initial state predictor \hat{X}_1 and the initial error covariance matrix Ω_1 are determined depending on the chosen model as follows.

For the ATS model the initial state predictor \hat{X}_1 is estimated as the periodic mean of the observations, i.e. for an estimated period of say d samples the observation signal is divided into adjacent segments of d samples and the periodic mean is computed as the mean vector of the segments. The initial error covariance matrix Ω_1 is set to zero.

For the ALR model the initial state predictor \hat{X}_1 is estimated by means of OLS regression using the Matlab command `regress`. The initial error covariance matrix Ω_1 is then estimated via the 95% confidence intervals (a, b) of the OLS regression coefficients which are also returned by `regress`: For each regression coefficient the variance of a normal fit of its distribution is computed from the 95% confidence intervals as $[(b - a)/(2 \cdot 1.96)]^2$. The diagonal matrix with these entries for each regression coefficient is then used as initial error covariance matrix.

The time, which the Kalman recursions potentially need to tune in, can be excluded from the maximum likelihood or MSE evaluation of the model.

Grid Search A linear grid search in the 2-dimensional space of state and observation noise variances is accomplished by prescribing two variance vectors

$$\Sigma_v^2 = (\sigma_v^2(1), \dots, \sigma_v^2(n)) \quad \text{and} \quad \Sigma_w^2 = (\sigma_w^2(1), \dots, \sigma_w^2(m)).$$

Each combination of variances then defines a model, where the initial state predictor \hat{X}_1 and the initial error covariance matrix Ω_1 are determined as in the preceding paragraph. From the $n \times m$ models in the family the one with the maximum likelihood or the minimum MSE is chosen as optimal.

Reduced Methods Reduced methods were presented in proposition 5.2 and subsection 5.3.2. They come with two main advantages compared to the grid search:

- The number of searched parameters is reduced.
- The initial state predictor \hat{X}_1 and the initial error covariance matrix Ω_1 need not be prescribed by some self-made rules as described in the preceding paragraphs. The initial state predictor is estimated optimally, and Ω_1 is set to zero.

9.3 Evaluation

After having found the optimal model out of a given model family and according to some search method the model can be evaluated in different directions.

MLE has the advantage that the true CPR artefact signal need not be known for optimisation. The unknown model parameters are found for each signal using only this signal, i.e, the corrupted ECG signal and, in the case of the ALR model, the reference signal. MLE individually finds the optimal model parameters, no splitting into learning and testing data sets is needed. Therefore the optimal model can be evaluated on each signal of the data set on which the optimisation was processed.

As already pointed out, in the case of MSE optimisation the true CPR signal has to be known and thus evaluation has to be performed on an extra data set, which is disjoint from the learning data set on which optimisation was performed. The optimal values for the noise variances in the state-space models are found from the learning data set, and the mean variances are then used for evaluation on a disjoint testing data set.

In general, all three types of Kalman recursions (prediction, filtering, and fixed-point smoothing) can be applied in the evaluation. Furthermore, the time, which the Kalman recursions potentially need to tune in, can be excluded from the evaluation. Finally, we will quantify the quality of our removal algorithms by the restored SNR and by comparing the mean frequency of the original VF signal to the mean frequency of the estimated VF signal after CPR artefact removal, c.f. section 7.1.

9.4 Results

In order not to overcrowd this section we compute the results for the different models and optimisation methods only using the reduced methods omitting the grid search.

9.4.1 The ATS Model

As the signal segments being investigated are very short (5 seconds length) a constant period was estimated for each ATS model (Fig. 9.5).

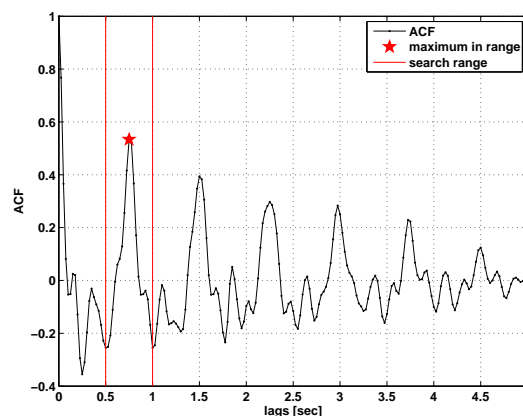


Figure 9.5: Estimation of the constant period of the signal segment by searching the maximum of the ACF in a specified range, shown for an example dataset.

In the following, typical optimisation and evaluation results in the case of MLE are

given exemplarily for one of the totally 49 data sets. The original artefact free VF ECG signal and the original CPR artefact signal were detrended¹, normalised, and resampled to 40 Hz, and the SNR was chosen to be -3 dB. The optimal MLE model was evaluated using the Kalman predictor.

Fig. 9.6 depicts the estimation of the CPR part of the mixed signal and its separation into estimated VF and CPR signals. All signals in Fig. 9.6 are plotted at the model frequency of 40 Hz. The rSNR at this sampling frequency is 4.03 dB. The estimated optimal state-

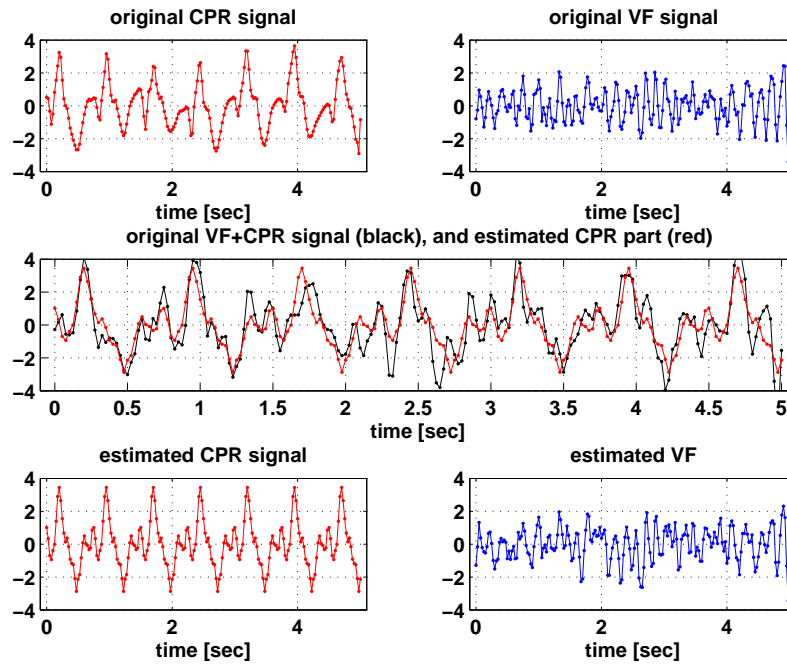


Figure 9.6: Original and estimated signals at the model frequency of 40 Hz, shown for an example dataset.

space variance σ_v^2 of the example dataset is zero. Thus the Kalman gain is constantly zero. The estimated optimal observation-noise variance σ_w^2 is 1.03. Fig. 9.7 shows the original and the estimated signals at after resampling to 375 Hz. The rSNR at this sampling frequency is 4.12 dB. Fig. 9.8 gives a closer look to the differences due to the different sampling frequencies. FS denotes sampling frequency. Fig. 9.9 depicts the powerspectra of the original and estimated CPR and VF signals after resampling to 375 Hz.

MLE optimisation

Now we give the results for all 49 datasets. The original artefact free VF ECG signals and the original CPR artefact signals were detrended, normalised, and resampled to 20, 30, and 40 Hz, and the SNR was chosen to be -5, 0, and 5 dB. The optimal MLE models were evaluated using the Kalman predictor. Table 9.1 shows the results.

¹using the Matlab command `detrend`

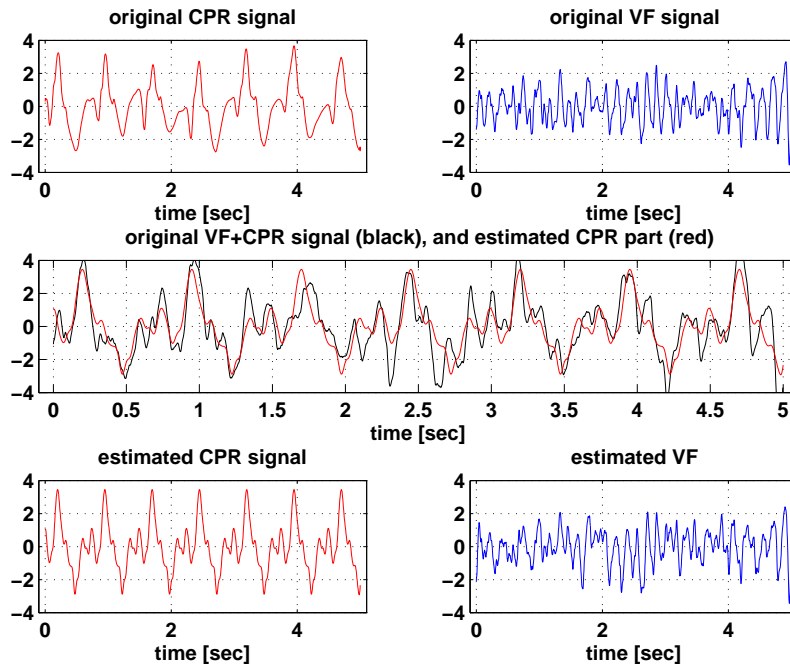


Figure 9.7: Original and the estimated signals at after resampling to 375 Hz.

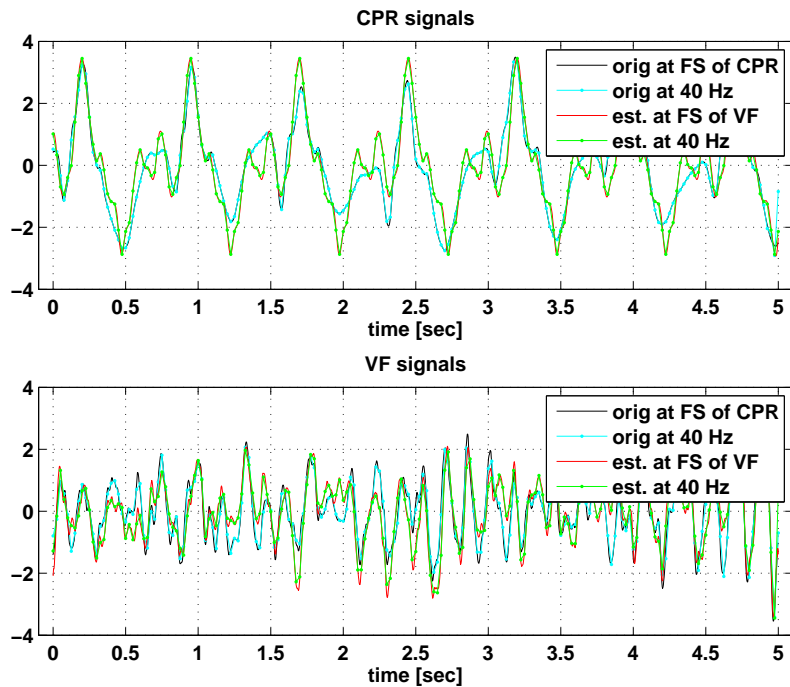


Figure 9.8: Comparison of the original and estimated CPR and VF signals at the different sampling frequencies.

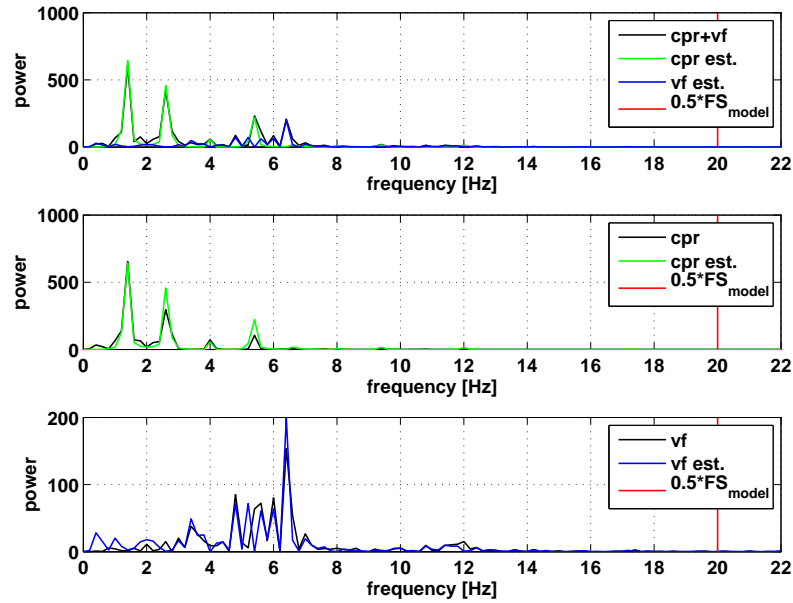


Figure 9.9: Powerspectra of the original and estimated CPR and VF signals after resampling to 375 Hz. FS_{model} denotes the sampling frequency used for the Kalman model.

FS= 20	SNR=-5	SNR=0	SNR=5
$\hat{\sigma}_v^2$	0.05±0.31	0.02±0.12	0.01±0.04
$\hat{\sigma}_w^2$	1.46±0.53	1.17±0.28	0.99±0.15
rSNR	1.81±3.17	3.58±2.93	4.88±2.26
$\Delta(\text{MF})$	0.93±0.76	0.76±0.64	0.54±0.39

FS= 30	SNR=-5	SNR=0	SNR=5
$\hat{\sigma}_v^2$	0.00±0.00	0.00±0.00	0.00±0.00
$\hat{\sigma}_w^2$	1.46±0.42	1.15±0.22	0.96±0.14
rSNR	1.83±2.36	3.35±2.20	4.40±1.57
$\Delta(\text{MF})$	0.92±0.72	0.79±0.61	0.53±0.43

FS= 40	SNR=-5	SNR=0	SNR=5
$\hat{\sigma}_v^2$	0.00±0.00	0.00±0.00	0.00±0.00
$\hat{\sigma}_w^2$	1.47±0.43	1.12±0.23	0.98±0.14
rSNR	1.71±2.29	3.34±2.00	4.58±1.60
$\Delta(\text{MF})$	1.00±0.66	0.74±0.55	0.58±0.42

Table 9.1: Results of the MLE optimisation for the ATS model. FS denotes the model sampling frequency, and $\Delta(\text{MF})$ denotes the difference of the mean frequency of the original VF signal and the mean frequency of the estimated VF signal after CPR artefact removal. All values are given as mean \pm standard deviation.

FS= 20	SNR=-5	SNR=0	SNR=5
$\hat{\sigma}_v^2$	0.08±0.55	0.00±0.00	0.00±0.00
$\hat{\sigma}_w^2$	1.00±0.00	1.00±0.00	1.00±0.00
rSNR	1.84±3.15	3.70±2.86	5.06±2.55
$\Delta(\text{MF})$	0.93±0.75	0.75±0.61	0.53±0.40

FS= 30	SNR=-5	SNR=0	SNR=5
$\hat{\sigma}_v^2$	0.00±0.00	0.00±0.00	0.00±0.00
$\hat{\sigma}_w^2$	1.00±0.00	1.00±0.00	1.00±0.00
rSNR	1.83±2.36	3.35±2.21	4.41±1.58
$\Delta(\text{MF})$	0.92±0.72	0.80±0.61	0.53±0.43

FS= 40	SNR=-5	SNR=0	SNR=5
$\hat{\sigma}_v^2$	0.00±0.00	0.00±0.00	0.00±0.01
$\hat{\sigma}_w^2$	1.00±0.00	1.00±0.00	1.00±0.00
rSNR	1.71±2.29	3.34±2.00	4.59±1.60
$\Delta(\text{MF})$	1.00±0.66	0.75±0.55	0.60±0.41

Table 9.2: Results of the MSE learning optimisation for the ATS model. FS denotes the model sampling frequency, and $\Delta(\text{MF})$ denotes the difference of the mean frequency of the original VF signal and the mean frequency of the estimated VF signal after CPR artefact removal. All values are given as mean \pm standard deviation.

MSE optimisation

Learning The same 49 datasets as for MLE optimisation were used as learning datasets. The observation noise variance σ_w^2 was always set equal to 1, because the MSE depends only on the ratio of the variances $Q^* = \frac{Q}{\sigma_w^2}$, cf. Corollary 5.3 and Proposition 5.1. The Kalman predictor recursions were chosen both for optimising and for evaluating. Table 9.2 shows the results of the learning procedure.

Testing The mean optimal values of the noise variances found from the learning data set for each sampling frequency were used for evaluation on disjoint 49 testing datasets. The mean variances were $\sigma_v^2 = 0.027$ for FS= 20 Hz, $\sigma_v^2 = 0.001$ for FS= 30 Hz, and $\sigma_v^2 = 0.001$ for FS= 40 Hz. Testing with fixed variances corresponds to a one-point model family, cf. subsection 9.2.2. The Kalman predictor recursions were chosen for evaluating, and the first second was excluded from the evaluation of the model. The initial state predictor and the initial error covariance matrix were set as described in subsection 9.2.2. Table 9.3 shows the results of the testing procedure.

9.4.2 The ALR Model

In the following, typical optimisation and evaluation results in the case of MLE are given exemplarily for one of the totally 49 data sets. The original artefact free VF ECG signal and the original CPR artefact signal were detrended, normalised, and resampled to 30 Hz, and the SNR was chosen to be -3 dB. The optimal MLE model was evaluated using the Kalman predictor. The copies of the reference signal were lagged by -0.25 seconds up to 0.10 seconds with a stepsize of 0.05 seconds, cf. Fig. 9.14.

FS= 20	SNR=-5	SNR=0	SNR=5
$\hat{\sigma}_v^2$	0.03±0.00	0.03±0.00	0.03±0.00
$\hat{\sigma}_w^2$	1.00±0.00	1.00±0.00	1.00±0.00
rSNR	0.65±1.77	2.54±1.73	3.99±1.66
$\Delta(\text{MF})$	1.68±0.83	1.03±0.73	0.62±0.47

FS= 30	SNR=-5	SNR=0	SNR=5
$\hat{\sigma}_v^2$	0.00±0.00	0.00±0.00	0.00±0.00
$\hat{\sigma}_w^2$	1.00±0.00	1.00±0.00	1.00±0.00
rSNR	1.16±2.05	2.70±1.91	4.25±1.46
$\Delta(\text{MF})$	0.96±0.94	0.93±0.72	0.52±0.46

FS= 40	SNR=-5	SNR=0	SNR=5
$\hat{\sigma}_v^2$	0.00±0.00	0.00±0.00	0.00±0.00
$\hat{\sigma}_w^2$	1.00±0.00	1.00±0.00	1.00±0.00
rSNR	0.96±2.12	2.87±1.96	4.31±1.55
$\Delta(\text{MF})$	0.74±1.03	0.72±0.86	0.48±0.52

Table 9.3: Results using testing data after MSE learning optimisation for the ATS model. FS denotes the model sampling frequency, and $\Delta(\text{MF})$ denotes the difference of the mean frequency of the original VF signal and the mean frequency of the estimated VF signal after CPR artefact removal. All values are given as mean \pm standard deviation.

Fig. 9.10 depicts the estimation of the CPR part of the mixed signal and its separation into estimated VF and CPR signals. All signals in Fig. 9.10 are plotted at the model frequency of 30 Hz. The rSNR at this sampling frequency is 3.73 dB. The estimated optimal state-space variance $\hat{\sigma}_v^2$ of the example dataset is zero. Thus the Kalman gain is constantly zero. The estimated optimal observation-noise variance $\hat{\sigma}_w^2$ is 1.34. Fig. 9.11 shows the original and the estimated signals at after resampling to 375 Hz. The rSNR at this sampling frequency is 3.76 dB. Fig. 9.12 gives a closer look to the differences due to the different sampling frequencies. FS denotes sampling frequency. Fig. 9.13 depicts the powerspectra of the original and estimated CPR and VF signals after resampling to 375 Hz. Fig. 9.14 shows the original mixed signal and its CPR part estimation, lagged copies of the reference signal and the time course of the regression coefficients, i.e. the states, all at 30 Hz.

MLE optimisation

Now we give the results for all 49 datasets. The original artefact free VF ECG signals and the original CPR artefact signals were detrended, normalised, and resampled to 20, 30, and 40 Hz, and the SNR was chosen to be -5, 0, and 5 dB. The optimal MLE models were evaluated using the Kalman predictor. Table 9.4 shows the results.

MSE optimisation

Learning The same 49 datasets as for MLE optimisation were used as learning datasets. The observation noise variance σ_w^2 was always set equal to 1, because the MSE depends only on the ratio of the variances $Q^* = \frac{Q}{\sigma_w^2}$, cf. Corollary 5.3 and Proposition 5.1. The

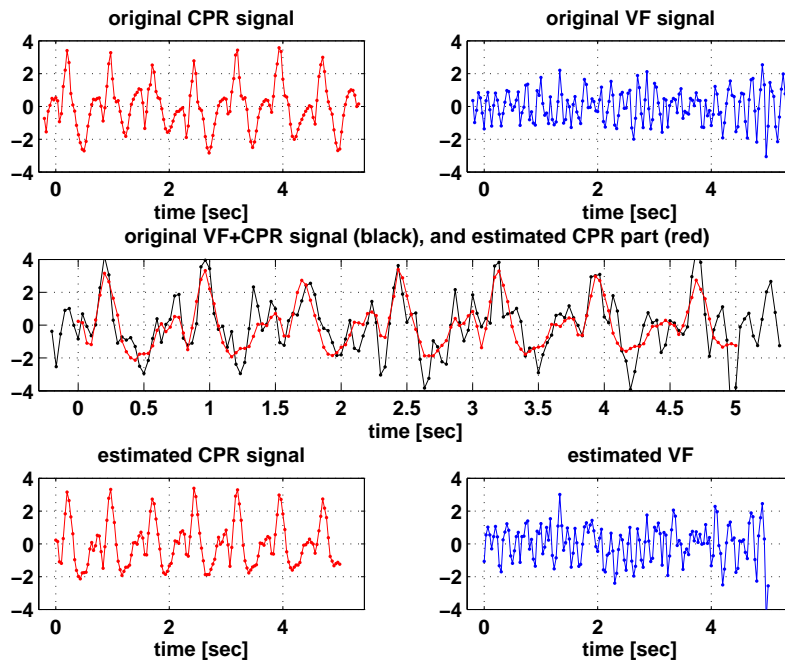


Figure 9.10: Original and estimated signals at the model frequency of 30 Hz, shown for an example dataset.

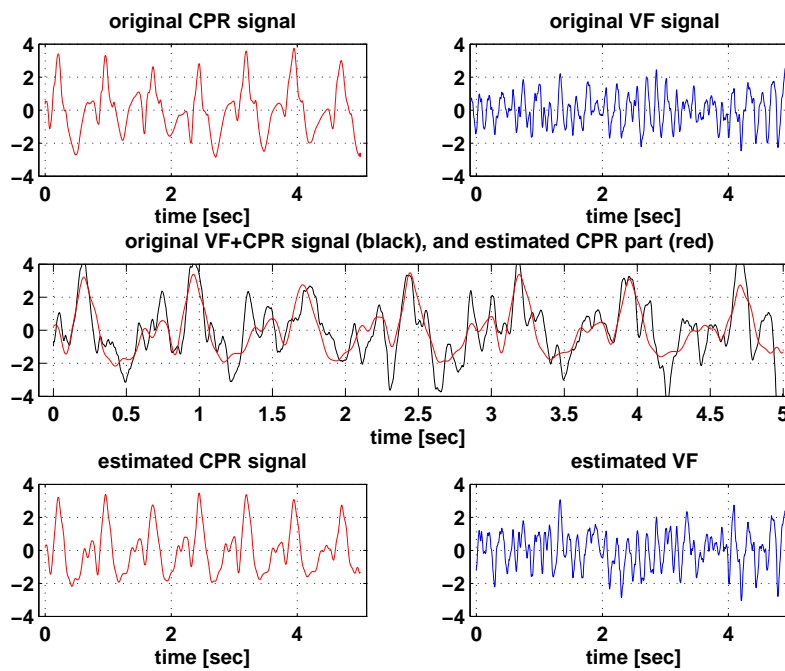


Figure 9.11: Original and the estimated signals after resampling to 375 Hz.

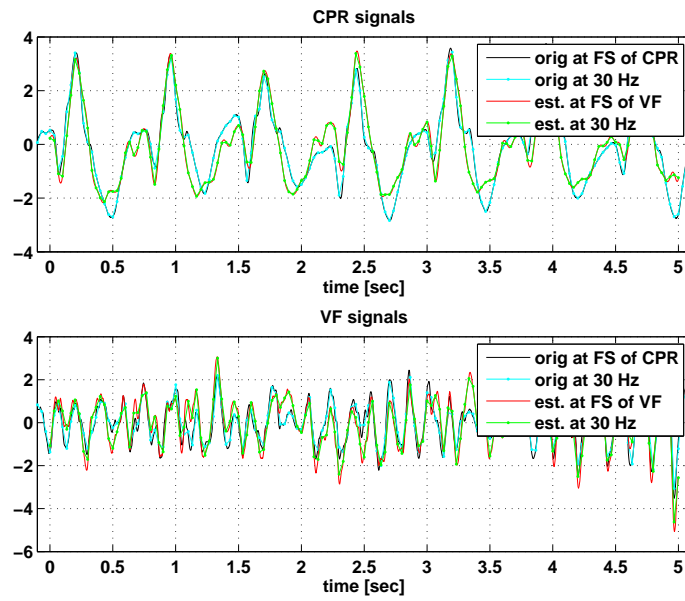


Figure 9.12: Comparison of the original and estimated CPR and VF signals at the different sampling frequencies.

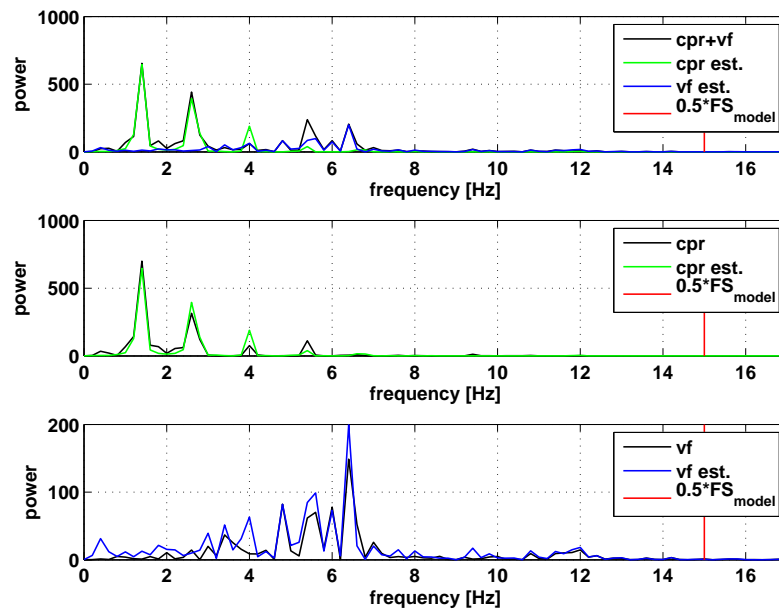


Figure 9.13: Powerspectra of the original and estimated CPR and VF signals after resampling to 375 Hz. FS_{model} denotes the sampling frequency used for the Kalman model.

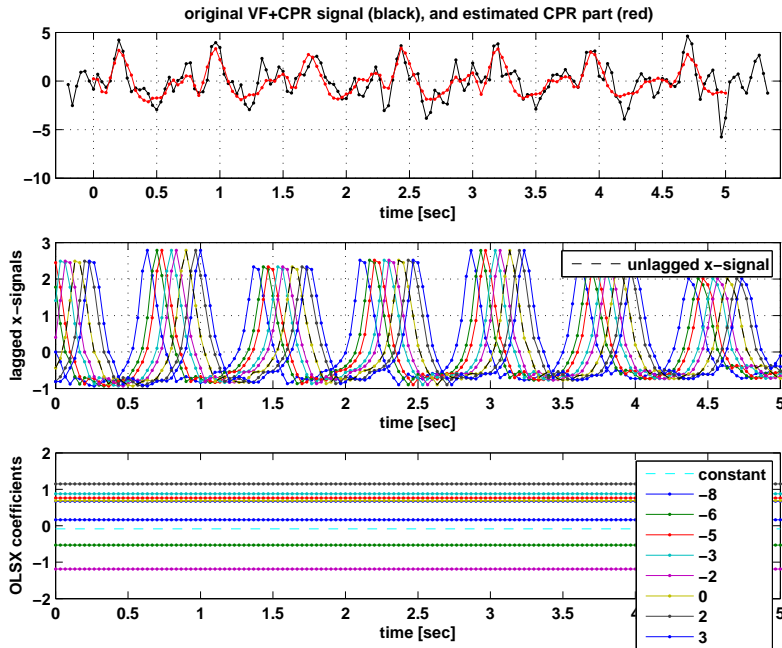


Figure 9.14: The figure shows the original mixed signal and its CPR part estimation, lagged copies of the reference signal and the time course of the regression coefficients, i.e. the states, all at 30 Hz.

FS= 20	SNR=-5	SNR=0	SNR=5
$\hat{\sigma}_v^2$	0.00±0.00	0.00±0.00	0.00±0.00
$\hat{\sigma}_w^2$	1.60±0.49	1.13±0.17	0.98±0.08
rSNR	2.00±3.02	6.11±2.70	9.24±2.41
$\Delta(\text{MF})$	0.84±0.56	0.37±0.35	0.12±0.19

FS= 30	SNR=-5	SNR=0	SNR=5
$\hat{\sigma}_v^2$	0.01±0.03	0.01±0.02	0.00±0.02
$\hat{\sigma}_w^2$	1.47±0.68	1.05±0.36	0.93±0.25
rSNR	1.22±3.18	5.21±3.62	8.55±3.85
$\Delta(\text{MF})$	0.55±1.00	0.19±0.65	0.01±0.44

FS= 40	SNR=-5	SNR=0	SNR=5
$\hat{\sigma}_v^2$	0.05±0.05	0.03±0.03	0.02±0.03
$\hat{\sigma}_w^2$	0.80±1.01	0.70±0.61	0.61±0.49
rSNR	1.35±3.30	2.16±4.57	4.52±5.76
$\Delta(\text{MF})$	1.32±2.13	1.03±1.86	1.14±1.69

Table 9.4: Results of the MLE optimisation for the ALR model. FS denotes the model sampling frequency, and $\Delta(\text{MF})$ denotes the difference of the mean frequency of the original VF signal and the mean frequency of the estimated VF signal after CPR artefact removal. All values are given as mean \pm standard deviation.

FS= 20	SNR=-5	SNR=0	SNR=5
$\hat{\sigma}_v^2$	0.00±0.00	0.00±0.00	0.00±0.00
$\hat{\sigma}_w^2$	1.00±0.00	1.00±0.00	1.00±0.00
rSNR	2.00±3.02	6.11±2.71	9.26±2.42
$\Delta(\text{MF})$	0.84±0.56	0.38±0.35	0.13±0.19

FS= 30	SNR=-5	SNR=0	SNR=5
$\hat{\sigma}_v^2$	0.00±0.00	0.00±0.00	0.00±0.00
$\hat{\sigma}_w^2$	1.00±0.00	1.00±0.00	1.00±0.00
rSNR	1.92±2.71	6.14±2.51	9.46±2.33
$\Delta(\text{MF})$	0.77±0.57	0.34±0.34	0.09±0.18

FS= 40	SNR=-5	SNR=0	SNR=5
$\hat{\sigma}_v^2$	2.82±19.71	0.00±0.00	0.00±0.00
$\hat{\sigma}_w^2$	1.00±0.00	1.00±0.00	1.00±0.00
rSNR	1.84±3.10	6.16±2.72	9.48±2.43
$\Delta(\text{MF})$	0.68±0.72	0.31±0.31	0.08±0.16

Table 9.5: Results of the MSE learning optimisation for the ALR model. FS denotes the model sampling frequency, and $\Delta(\text{MF})$ denotes the difference of the mean frequency of the original VF signal and the mean frequency of the estimated VF signal after CPR artefact removal. All values are given as mean \pm standard deviation.

Kalman predictor recursions were chosen both for optimising and for evaluating. Table 9.5 shows the results of the learning procedure.

Testing The mean optimal values of the noise variances found from the learning data set for each sampling frequency were used for evaluation on disjoint 49 testing datasets. The mean variances were $\sigma_v^2 = 0.000$ for FS= 20 Hz, $\sigma_v^2 = 0.000$ for FS= 30 Hz, and $\sigma_v^2 = 0.938$ for FS= 40 Hz. Testing with fixed variances corresponds to a one-point model family, cf. subsection 9.2.2. The Kalman predictor recursions were chosen for evaluating, and the first second was excluded from the evaluation of the model. The initial state predictor and the initial error covariance matrix were set as described in subsection 9.2.2. Table 9.6 shows the results of the testing procedure.

9.5 Discussion and Future Work

9.5.1 Discussion of Results

Comparison of Results

Let's first discuss the ATS and ALR model results on its own and then compare them.

ATS models: The estimated state-space variance σ_v^2 of the MLE ATS models decreases with increasing SNR for FS=20Hz. It is neglectable for the remaining FS values. The estimated observation-space variance σ_w^2 is comparable for the different FS values and clearly

FS= 20	SNR=-5	SNR=0	SNR=5
$\hat{\sigma}_v^2$	0.00±0.00	0.00±0.00	0.00±0.00
$\hat{\sigma}_w^2$	1.00±0.00	1.00±0.00	1.00±0.00
rSNR	1.91±1.50	5.63±1.33	8.13±1.41
$\Delta(\text{MF})$	0.96±0.50	0.45±0.29	0.21±0.16

FS= 30	SNR=-5	SNR=0	SNR=5
$\hat{\sigma}_v^2$	0.00±0.00	0.00±0.00	0.00±0.00
$\hat{\sigma}_w^2$	1.00±0.00	1.00±0.00	1.00±0.00
rSNR	1.45±1.89	5.46±1.57	8.42±1.39
$\Delta(\text{MF})$	0.48±0.56	0.19±0.29	0.05±0.16

FS= 40	SNR=-5	SNR=0	SNR=5
$\hat{\sigma}_v^2$	0.94±0.00	0.94±0.00	0.94±0.00
$\hat{\sigma}_w^2$	1.00±0.00	1.00±0.00	1.00±0.00
rSNR	3.56±1.64	2.85±1.23	2.58±1.11
$\Delta(\text{MF})$	2.89±0.96	2.89±0.82	2.88±0.76

Table 9.6: Results using testing data after MSE learning optimisation for the ALR model. FS denotes the model sampling frequency, and $\Delta(\text{MF})$ denotes the difference of the mean frequency of the original VF signal and the mean frequency of the estimated VF signal after CPR artefact removal. All values are given as mean \pm standard deviation.

decreases with increasing SNR. The rSNR and $\Delta(\text{MF})$ are clearly better for increasing SNR, however, they are quite independent of the selected FS.

The estimated state-space variances $\hat{\sigma}_v^2$ of the “learning” MSE ATS models are almost always neglectable. This is promising in order to choose their mean values for testing purposes. Note, that the observation noise variance $\hat{\sigma}_w^2$ – without loss of generality – is always set to 1, because the MSE depends only on the ratio of the variances $Q^* = \frac{Q}{\sigma_w^2}$, cf. Corollary 5.3 and Proposition 5.1. Both rSNR and $\Delta(\text{MF})$ values of the “learning” set are comparable with the MLE results. This is surprising, because MLE does not know the true CPR signal in contrast to MSE optimisation.

The rSNR values of the “testing” ATS models are explicitly worse compared to the “learning” results. This may be because of the different data sets. However, the initial state is estimated during testing via a periodic mean vector, cf. 9.2.2, and this initial state is not altered much over time because of the very small or zero state-space variances $\hat{\sigma}_v^2$. Maybe a slightly bigger state-space variances $\hat{\sigma}_v^2$ would yield better results.

ALR models: The estimated state-space variance $\hat{\sigma}_v^2$ of the MLE ALR models increases with increasing FS and clearly decreases with increasing SNR. The estimated observation-space variance $\hat{\sigma}_w^2$ decreases with increasing FS and clearly decreases with increasing SNR. These results suggest the interpretation that the MLE ALR models adopt the states more for increasing FS. This could be an explanation of the fact that the rSNR decreases with increasing FS. The $\Delta(\text{MF})$ values are surprisingly best for FS=30Hz.

With the exception of FS=40Hz and SNR=-5, the estimated state-space variances $\hat{\sigma}_v^2$ is neglectable for the “learning” MSE ALR models. The rSNR is comparable to the MLE values at FS=20Hz, however, it does not substantially change for greater FS values. The

$\Delta(\text{MF})$ values are better for increasing SNR and FS values.

The rSNR values of the “testing” ALR models are worse compared to the “learning” results with the exception of FS=40Hz and SNR=-5. The $\Delta(\text{MF})$ values are similar or worse compared to the MLE results. They are best for FS=30Hz. The high mean σ_v^2 value taken from the “learning” set for FS=40Hz produces bad rSNR values in the “testing” sets. This suggests the interpretation that an ALR model with a too high σ_v^2 value adopts its states too much, such that too much of the CPR corrupted signal is “explained” as CPR.

Comparison of models: In the case of MLE, the rSNR values at FS=20Hz are much better for the ALR model compared to the ATS model. Likewise, at FS=20Hz and 30Hz the ALR $\Delta(\text{MF})$ values are better. Thus, at small sampling rates the ALR models clearly outperform the ATS models, whereas at the high sampling rate FS=40Hz the ALR models loose performance, while the ATS models stay at their low performance.

In the case of MSE optimisation, the rSNR of the testing dataset is always better for the ALR models. The $\Delta(\text{MF})$ values of the ATS models are only better at FS=40Hz.

The general predominance of the ALR model over the ATS model is presumably due to the extra information in the ALR model which enters through the lagged reference signals.

Comparison of Estimation Methods and General Considerations

In the majority of cases, the MLE optimisation method gives better rSNR and $\Delta(\text{MF})$ values than the “testing” models after MSE “learning”.

At higher sampling rates especially the ALR models tend to loose performance. A plausible explanation could be the following: Both, the ATS and the ALR models model the VF part of a CPR corrupted signal as observation noise. The optimisation procedures MLE and MMSE search for model parameters for which the model explains as much as possible as projected states, i.e. CPR, minimising thereby the observation noise. For too high sampling rates, this adoption is too high.

Practical Implications and Discussion

In practice, the model variances σ_v^2 and σ_w^2 may vary during the course of time. In order to incorporate this, one could divide a long ECG record into time segments and apply e.g. MLE to every segment individually.

In view of the particular practical purpose of CPR artefact removal, the question has to be answered, which parameter should be optimised: the rSNR (which amounts to minimising the MSE), the likelihood, $\Delta(\text{MF})$, or even one or both model variances σ_v^2 and σ_w^2 .

In the investigations presented here, the copies of the reference signal were lagged by some predefined time values, namely from -0.25 seconds up to 0.10 seconds with a stepsize of 0.05 seconds, cf. Fig. 9.14. This choice was not justified by some optimisation procedure.

9.5.2 Future Work

A lot more analysis could be made in some future work.

- Long time evaluations together with spectrogram evaluations could be made.
- The performance of detection and scoring algorithms could be investigated, cf. subsection 7.1.2.

- The two proposed algorithms could be optimised and evaluated on the basis of more datasets.
- The two proposed algorithms could be compared to existing algorithms on the basis of common datasets, cf. section 7.2.
- The two proposed algorithms are state-space models and could thus be combined [31, p.267].
- The choice of time lags in the ALR model could be optimised.
- The estimated CPR parts could be smoothed by some standard filtering procedure in order to exclude too high frequencies.
- The VF part of a CPR corrupted signal could be modelled differently than by white noise, e.g. by some AR process.

Part IV

Rating the VF ECG Signal

Chapter 10

Published Papers

Contents

10.1 Overview	127
10.2 Paper 2	128
10.3 Paper 3	138

10.1 Overview

It was already pointed out in the introduction (cf. subsection 1.3.1) that all key questions of a diagnostic approach to defibrillation as presented there could be answered by continuously providing one (or more) appropriate parameters which are derived from physical measurements and reflect the actual probability for ROSC of a hypothetical defibrillation attempt. The following two publications present the performance and problems of different ECG parameters for that purpose.

10.2 Paper 2

The following paper was published in *Anesth Analg* 2002 ;95:716-23, [12].

Prediction of Defibrillation Outcome Employing a New Combination of Mean Frequency and Amplitude in Porcine Models of Cardiac Arrest

Anton Amann, PhD, Klaus Rheinberger, MSc, Ulrich Achleitner, MSc, Anette C. Krismer, Werner Lingnau, MD, Karl H. Lindner, MD, and Volker Wenzel, MD

Department of Anesthesiology and Critical Care Medicine, Leopold-Franzens-University Innsbruck, Innsbruck, Austria

Supported in part by the Austrian National Bank science projects 7280 and 7276, the Austrian Heart Foundation project 98/05, and the Austrian Science Foundation P-14169-MED, all of Vienna, Austria; a research grant from Bruker Medical, Ettlingen, Germany; departmental funds; and a Science Foundation grant of the University of Innsbruck, Austria.

Presented in part at the Austrian Society of Anesthesiology, Resuscitation and Intensive Care Medicine Congress, Vienna, Austria, September, 2001, and the 23rd annual meeting of the European Academy of Anesthesiology, Graz, Austria, August, 2001.

Accepted for publication May 22, 2002.

Address correspondence and reprint requests to Dr. Anton Amann, Leopold-Franzens-University Innsbruck, Department of Anesthesiology and Critical Care, Anichstrasse 35, 6020 Innsbruck, Austria. Address e-mail to anton.amann@uibk.ac.at.

Alternate address: Dr. Anton Amann, Swiss Federal Institute of Technology, E23.2, ETH-Hoenggerberg, CH-8093 Zurich, Switzerland.

Abstract

We estimated the predictive power with respect to defibrillation outcome of ventricular fibrillation (VF) mean frequency (FREQ), mean peak-to-trough amplitude (AMPL), and their combination. We examined VF electrocardiogram signals of 64 pigs from 4 different cardiac arrest models with different durations of untreated VF, different durations of cardiopulmonary resuscitation, and use of different drugs (epinephrine, vasopressin, N-nitro-L-arginine methyl ester, or saline placebo). The frequency domain was restricted to the range from 4.33 to 30 Hz. In the 10-s epoch between 20 and 10 s before the first defibrillation shock, FREQ and AMPL were estimated. We introduced the survival index (SI; $0.68 \text{ Hz}^{-1} \cdot \text{FREQ} + 12.69 \text{ mV}^{-1} \cdot \text{AMPL}$) by use of multiple logistic regression.

Kruskal-Wallis nonparametric one-way analysis was used to analyze the different porcine models for significant difference. The variables FREQ, AMPL, and SI were compared with defibrillation outcome by means of univariate logistic regression and receiver operating characteristic curves. SI increased predictive power compared with AMPL or FREQ alone, resulting in 89% sensitivity and 86% specificity. The probabilities of predicting defibrillation outcome for FREQ, AMPL, and SI were 0.85, 0.89 and 0.90, respectively. FREQ, AMPL, and SI values were not sensitive in regard to the four different cardiac arrest models but were significantly different for vasopressin and epinephrine animals.

Introduction

During cardiopulmonary resuscitation (CPR), the international guidelines recommend defibrillation 1 to 3 min after drug administration [17]. Unfortunately, this strategy does not

address individual response to CPR efforts, rendering defibrillation attempts in many cases a matter of chance. Thus, a lucky shock may convert ventricular fibrillation (VF) into return of spontaneous circulation (ROSC) with subsequent long-term survival, whereas less fortunate defibrillation attempts may simply cause massive thermal injury to the heart [161, 143], which may cause fatal cardiac failure after ROSC in the intensive care unit. To improve defibrillation success, algorithms to analyze VF wave forms during CPR have been developed. However, VF analysis is usually based on only one variable derived from the electrocardiogram (ECG) signal of the fibrillating heart. It has been demonstrated in clinical and animal studies that the amplitude and frequency of the ECG signal during VF were good predictors of defibrillation outcome [11].

When the predictive power of VF variables and threshold values for outcome prediction are compared, careful distinction has to be made between human and animal studies, short versus prolonged duration of untreated VF, VF during CPR and untreated VF, drug effects, and different VF analysis strategies. It is surprising that few attempts have been made to combine VF analysis variables to improve the prediction of defibrillation success. Although predictive power in regard to defibrillation success has been improved by combining median and dominant frequency [32], combining amplitude and the number of baseline crossings per second [108], combining mean amplitude and dominant frequency [115], and combining four spectral features [52], both sensitivity (Se) and specificity (Sp) remained disappointingly low. Moreover, because human VF wave forms are more difficult to analyze than those of animals in VF because of a larger effect of chest compression-related artifacts, it seems obvious that a new VF analysis strategy needs to be extremely good to successfully extrapolate laboratory experience into clinical practice.

In this study, we retrospectively examined VF data from 64 pigs undergoing CPR. Furthermore, we introduced a combination of mean peak-to-trough amplitude (AMPL) and mean frequency (FREQ), denominated as survival index (SI). Our hypothesis was that SI is a more effective predictor of defibrillation outcome than AMPL or FREQ.

Methods

This project was approved by the Austrian Federal Animal Investigational Committee, and the animals were managed in accordance with American Physiological Society and institutional guidelines. This study was performed according to Utstein-style guidelines [79] on healthy, 12- to 16-wk-old swine (Tyrolean domestic pigs) of either sex weighing 30 to 40 kg. The animals were fasted overnight but had free access to water. The pigs were premedicated with azaperone (neuroleptic drug; 4 mg/kg IM) and atropine (0.1 mg/kg IM) 1 h before surgery, and anesthesia was induced with thiopental (7 to 15 mg/kg IV). After intubation during spontaneous respiration, the pigs were ventilated with a volume-controlled ventilator (EV-A; Draeger, Lübeck, Germany) with 100% oxygen at 20 breaths/min and with a tidal volume adjusted to maintain normocapnia. Anesthesia was maintained with propofol (6 to 8 mg · kg⁻¹ · h⁻¹) and a single dose of piritramide (30 mg). We achieved muscle paralysis with 8 mg of pancuronium after intubation and subsequently with repeated doses of 8 mg of pancuronium as needed. Lactated Ringer's solution (6 mL · kg⁻¹ · h⁻¹) and a 3% gelatin solution (4 mL · kg⁻¹ · h⁻¹) was administered in the preparation phase before the induction of cardiac arrest and in the postresuscitation phase. A standard lead III ECG was used to monitor cardiac rhythm; depth of anesthesia was judged according to blood pressure, heart rate, and electroencephalography (Neurotrac; Engström, Munich, Germany). If cardiovascular variables or electroencephalography indicated a reduced depth

of anesthesia, we increased the propofol dose, and additional piritramide was given. Body temperature was maintained with a heating blanket between 38.0°C and 39.0°C.

A 7F catheter was advanced into the descending aorta via femoral cutdown for measurement of arterial blood pressure. Another 7F catheter was placed into the right atrium via femoral cutdown for drug administration. Blood pressures were measured with salinefilled catheters attached to pressure transducers (model 1290A; Hewlett-Packard, Böblingen, Germany), which were calibrated to atmospheric pressure at the level of the right atrium.

The data of four different, but similar, partly previously published models of cardiac arrest [91, 92, 153, 154], including 64 pigs, were analyzed retrospectively (Fig. 10.1, Table 10.1). In one model, after 4 min of cardiac arrest, followed by 3 min of basic life

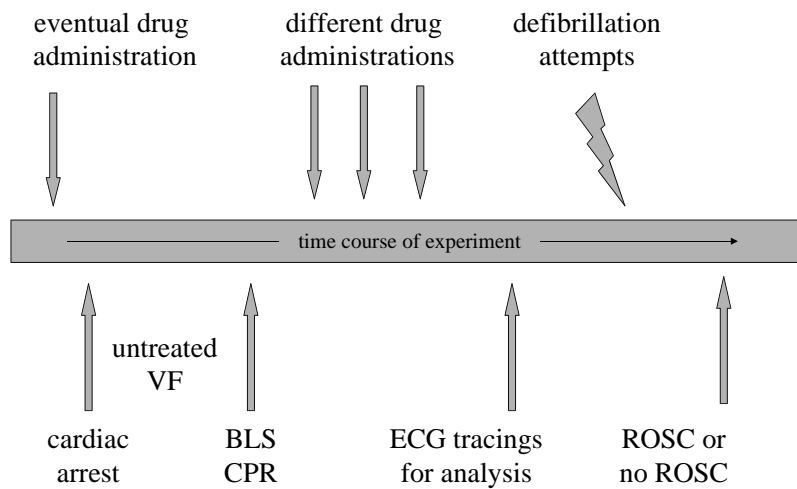


Figure 10.1: Common time course of the experimental protocols. VF = ventricular fibrillation; BLS = CPR basic life support cardiopulmonary resuscitation; ROSC = return of spontaneous circulation; ECG = electrocardiogram.

Table 10.1: Different Models of Cardiac Arrest

Model	Duration of cardiac arrest (min)	Duration of basic life support (min)	Partly epidural anesthesia	Delay to defibrillation (minutes after cardiac arrest)	No. ROSC/ total no. animals
1	4	3	No	22	16/25
2	4	3	No	22	4/11
3	1	3	Yes	19	14/23
4	7	3	No	25	2/5

ROSC = return of spontaneous circulation

support (BLS) CPR, 16 animals were randomly assigned to receive every 5 min either vasopressin (0.4, 0.4, and 0.8 U/kg; n = 11) or epinephrine (45, 45, and 200 µg/kg; n = 5). Another nine animals were randomly allocated after 4 min of cardiac arrest, followed by 8 min of BLS CPR, to receive every 5 min either vasopressin (0.4 and 0.8 U/kg; n = 5) or

epinephrine (45 and 200 $\mu\text{g}/\text{kg}$; $n = 4$). Defibrillation was attempted after 22 min of cardiac arrest [153, 154].

In Model 2, BLS CPR was started after 4 min of cardiac arrest, and 11 animals were randomly assigned to receive N -nitro-L-arginine methyl ester (25 mg/kg; $n = 6$) or saline placebo ($n = 5$) after 3 and 13 min of BLS CPR, respectively. Defibrillation was attempted after 22 min of cardiac arrest [92].

In Model 3, 30 min before the induction of cardiac arrest, 12 pigs received epidural anesthesia with bupivacaine; another 11 pigs received only a saline administration epidurally. After 1 min of cardiac arrest, followed by 3 min of BLS CPR, epidural animals randomly received every 5 min either epinephrine (45, 45, and 200 $\mu\text{g}/\text{kg}$; $n = 6$) or vasopressin (0.4, 0.4, and 0.8 U/kg; $n = 6$); likewise, control animals received every 5 min either epinephrine (45, 45, and 200 $\mu\text{g}/\text{kg}$; $n = 6$) or vasopressin (0.4, 0.4, and 0.8 U/kg; $n = 5$). Defibrillation was attempted after 19 min of cardiac arrest [91].

In Model 4, after 7 min of cardiac arrest, followed by 3 min of BLS CPR, five animals were randomly assigned to receive every 5 min either vasopressin (0.4, 0.4, and 0.8 U/kg; $n = 2$) or epinephrine (45, 45, and 200 $\mu\text{g}/\text{kg}$; $n = 3$). Defibrillation was attempted after 25 min of cardiac arrest.

Fifteen minutes before cardiac arrest, 5000 U of heparin was administered IV to prevent intracardiac clot formation, a single dose of 15 mg of piritramide and 8 mg of pancuronium was given, and hemodynamic variables, as well as blood gases, were measured. A 50-Hz, 60-V alternating current was then applied via two subcutaneous needle electrodes to induce VF. Cardiopulmonary arrest was defined as the point at which the aortic pressure decreased profoundly to hydrostatic pressure and the ECG showed VF; ventilation was stopped at that point. Closed-chest CPR was performed manually, and mechanical ventilation was resumed with the same setting as before the induction of cardiac arrest. Chest compression was always performed by the same investigator at a rate of 80/min, guided by acoustical audio tones. This investigator was blinded to hemodynamic and end-tidal carbon dioxide monitor tracings.

All drugs were diluted to 10 mL with normal saline and subsequently injected into the right atrium, which was followed by a 20-mL saline flush (investigators were blinded to the drugs). Up to three countershocks were administered with an energy of 3, 4, and 6 J/kg, respectively. If asystole or pulseless electrical activity was present after defibrillation, the experiment was terminated. ROSC was defined as an unassisted pulse with a systolic arterial blood pressure of ≥ 80 mm Hg, lasting for at least 5 min. After finishing the experimental protocol, the animals were killed and necropsied to verify correct positioning of the catheters and injuries to the rib cage.

The VF ECG signal was monitored continuously and recorded on hard disk by a personal computer-based data acquisition system (Dewetron, Graz, Austria; DASYLab GmbH, Mönchengladbach, Germany; and Datalogger, custom-made software). Digitization was performed at a sampling rate of 1000 Hz and with an amplitude resolution of 12 bits (4096 equal steps between minimal and maximal amplitude). The recorded ECG signals were analyzed with the mathematical software package Matlab (The MathWorks Inc., Natick, MA). Computation of the areas under receiver operating characteristic (ROC) curves and P values of their statistical comparison was performed with the software package GraphROC for Windows (Version 2.0). The signals were divided into consecutive 10-s epochs, and each epoch was transformed into the frequency domain by Fourier transformation. For signal analysis, the frequency domain was restricted to the range from 4.33 to 30 Hz, as previously described [138]. In the 10-s epoch between 20 and 10 s before the first defibrillation

shock, *FREQ* and *AMPL* were estimated. In addition, we introduced the *SI* by defining

$$SI = 0.68 \text{ Hz}^{-1} \cdot \text{FREQ} + 12.69 \text{ mV}^{-1} \cdot \text{AMPL}$$

This corresponds to the introduction of a new coordinate axis in the *FREQ-AMPL* plane by means of linear transformation. The coefficients 0.68, SE 0.29 and 12.69, and SE 4.25 were derived from multiple logistic regression by using maximum likelihood estimation with respect to *FREQ* and *AMPL* (explanatory variables) and defibrillation outcome, i.e., ROSC or no ROSC after a maximum of three defibrillation attempts (response variable) [76].

For the four different models of cardiac arrest, a Kruskal-Wallis nonparametric one-way analysis of variance was performed to look for possible significant differences of *FREQ*, *AMPL*, or *SI*. For the 24 animals receiving epinephrine and the 29 animals receiving vasopressin, a Kruskal-Wallis nonparametric one-way analysis of variance was performed to look for possible significant differences of *FREQ*, *AMPL*, or *SI*.

The data of VF (*FREQ*, *AMPL*, or *SI*) of the 10-s epoch between 20 and 10 s before the first defibrillation shock were labeled with 1 in case of ROSC or 0 in case of no ROSC after a maximum of three defibrillation attempts. Threshold values for *AMPL*, *FREQ*, and *SI* were computed by fitting the labeled data, by using maximum likelihood estimation, to the logistic distribution.

$$P(\text{data}) = \frac{1}{1 + \exp[-s \cdot (\text{data} - m)]},$$

where P is the probability of successful defibrillation [76]. Variables to be fitted were m , by definition the threshold value of *data*, i.e., the value of data associated with a 50% probability of successful defibrillation, and s , the steepness of the logistic distribution. Estimates of the SEs for m and s , and the normalized SEs of m , i.e., divided by the respective m , were computed for all variables.

Accuracy (*Ac*), *Se*, *Sp*, positive predictive value (*PPV*), and negative predictive value (*NPV*) were computed corresponding to selected data and estimated threshold value. ROC curves were computed for *FREQ*, *AMPL*, and *SI* to determine their value as predictors of successful defibrillation. These curves plot the true-positive rate (*Se*) versus the false-positive rate ($1 - \text{Sp}$) for different threshold values of the respective variable. The area under the ROC curve represents the probability to which the variable can be used to predict defibrillation outcome. In fact, both the area under the ROC curve and the Wilcoxon statistic measure the probability that in a randomly drawn (ROSC or no ROSC) pair the perceived variable values will allow them to be correctly identified [69]. For the paired testing of the significance of the difference of areas under two ROC curves, the method of Hanley and McNeil [70] was used. The P value for comparing the area under the ROC curve of *FREQ* versus *AMPL* was a two-tailed significance, whereas the P values for *SI* versus *AMPL* and *SI* versus *FREQ* were one-tailed significances. Optimal threshold values were computed by maximizing the sum of *Se* and *Sp*.

Results

The four different models of cardiac arrest did not show significantly different *FREQ*, *AMPL*, or *SI* values ($P > 0.5$). Figure 10.2 shows the data distribution of the four models in the *FREQ-AMPL* plane.

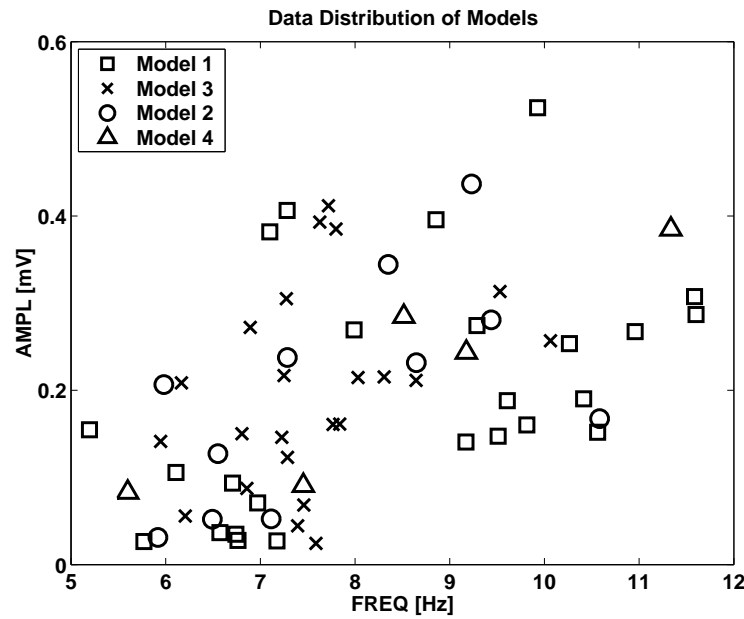


Figure 10.2: Data distribution for the four models of cardiac arrest in the mean frequency (FREQ)/mean peak-to-trough amplitude (AMPL) plane.

The 24 animals receiving epinephrine and the 29 animals receiving vasopressin showed significantly different FREQ, AMPL, and SI values ($P < 0.0001$). Figure 10.3 shows the data distribution of epinephrine and vasopressin animals in the FREQ-AMPL plane.

Figure 10.4 shows the distribution of all ROSC and no-ROSC data in the FREQ-AMPL plane. FREQ was capable of predicting defibrillation outcome well for values >8.10 Hz (upper threshold) or values <6.80 Hz (lower threshold). AMPL was capable of predicting defibrillation outcome well for values >0.24 mV (upper threshold) or values <0.13 mV (lower threshold). Between these upper and lower thresholds, FREQ and AMPL were poorly predictive. Figure 10.5 shows the distribution of ROSC and noROSC data, the logistic regression line, and threshold (P_{50}), P_5 , and P_{95} for FREQ, AMPL, and SI, respectively. Table 10.2 shows the estimates for the logistic regression fitting variables m and s together with their SEs; normalized SEs of threshold values; and Ac, Se, Sp, PPV, and NPV regarding FREQ, AMPL, and SI. All values for Ac, Se, Sp, PPV, and NPV of SI were superior to FREQ or AMPL, resulting in 89% Se and 86% Sp. The predictive power of AMPL is comparable to that of FREQ, but the normalized SE of the AMPL threshold is greater compared with FREQ or SI. The ROC curves (Fig. 10.6) have been plotted by computing Se and Sp of predicting ROSC/no ROSC with different thresholds for FREQ, AMPL, and SI. The probabilities of predicting defibrillation outcome, i.e., the area under the ROC curve, for FREQ, AMPL, and SI were 0.85 SE 0.05, 0.89 SE 0.05 and 0.90 SE 0.04, respectively. The two-tailed P value for comparison of the areas under the ROC curve for AMPL versus FREQ was 0.51. The one-tailed P values for SI versus FREQ and SI versus AMPL were 0.09 and 0.33, respectively. Optimal thresholds corresponding to ROC curve analysis for FREQ, AMPL, and SI were 7.59 Hz, 0.13 mV, and 6.84, respectively.

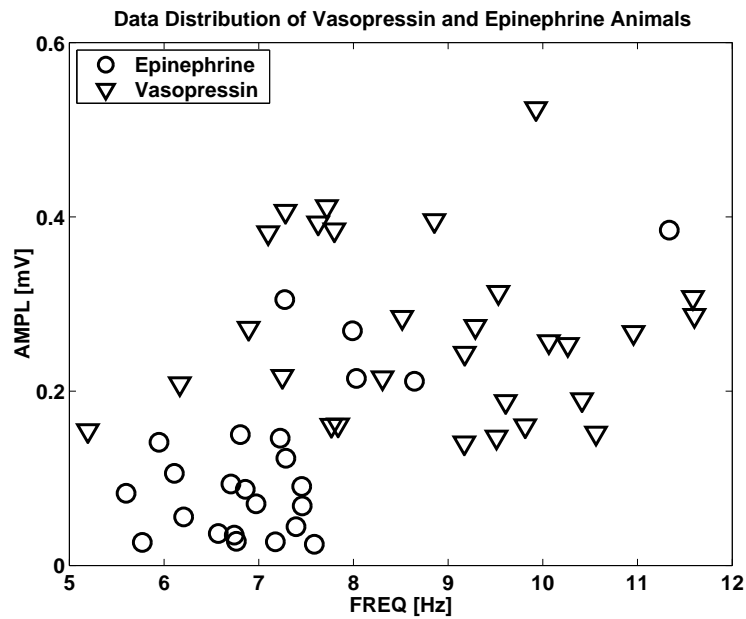


Figure 10.3: Data distribution of epinephrine and vasopressin animals in the mean frequency (FREQ)/mean peak-to-trough amplitude (AMPL) plane.

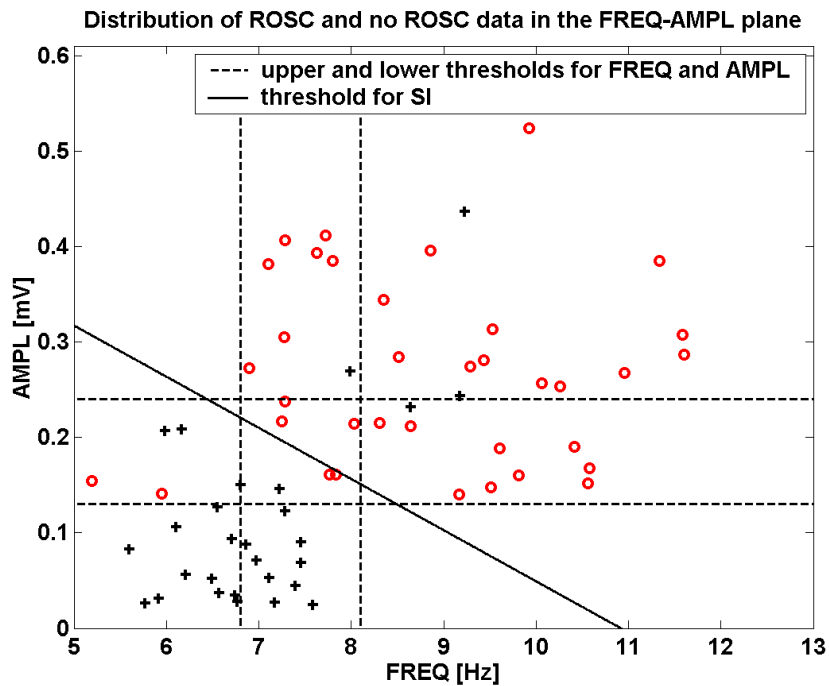


Figure 10.4: Distribution of return of spontaneous circulation (ROSC; o) and no-ROSC (+) data sets in the mean frequency (FREQ)/mean peak-to-trough amplitude (AMPL) plane. Dashed lines are upper and lower thresholds for AMPL and FREQ, respectively. FREQ is capable of predicting defibrillation outcome well for values >8.10 Hz (upper threshold) or values <6.80 Hz (lower threshold). AMPL is capable of predicting defibrillation outcome well for values >0.24 mV (upper threshold) or values <0.13 mV (lower threshold). The solid line is the threshold for the survival index (SI) estimated by logistic regression.

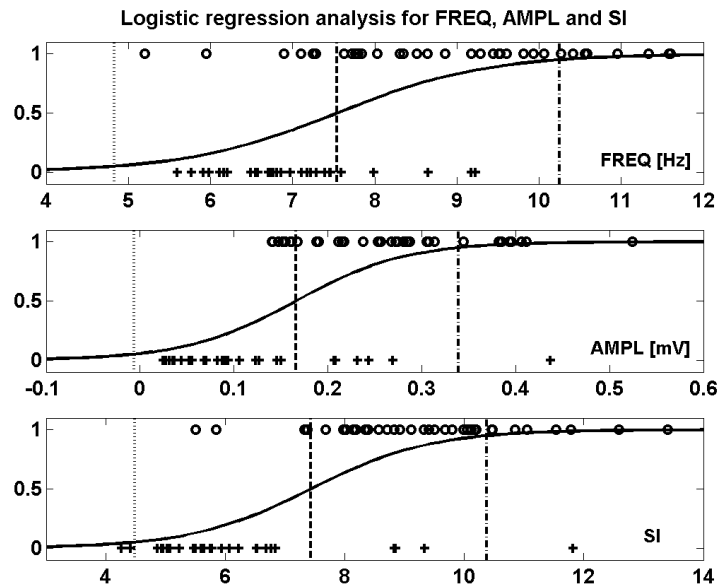


Figure 10.5: Distribution of return of spontaneous circulation (ROSC; o) and no-ROSC (+) data for mean frequency (FREQ), mean peak-to-trough amplitude (AMPL), and survival index (SI). For every ventricular fibrillation variable, the logistic regression (solid line), threshold (P₅₀; dashed line), P₅ (dotted line), and P₉₅ (dot and dash line) are displayed.

Table 10.2: Results of Logistic Regression Analysis

VF Variable	Ac(%)	Se(%)	Sp(%)	PPV(%)	NPV(%)
FREQ	80	78	82	85	74
AMPL	78	78	79	82	73
SI	88	89	86	89	86

VF Variable	Threshold (m±SE)	Steepness (s±SE)	Normalized SE of threshold: SE/m
FREQ	7.54±0.28 Hz	1.09±0.29 Hz ⁻¹	0.04
AMPL	0.17±0.02 mV	17.04±4.20 mV ⁻¹	0.12
SI	7.43±0.36	1.00±0.22	0.05

Ac = accuracy; Se = sensitivity; Sp = specificity; PPV = positive predictive value
 NPV = negative predictive value; FREQ = mean frequency
 AMPL = peak-to-trough amplitude; SI = survival index; VF= ventricular fibrillation.

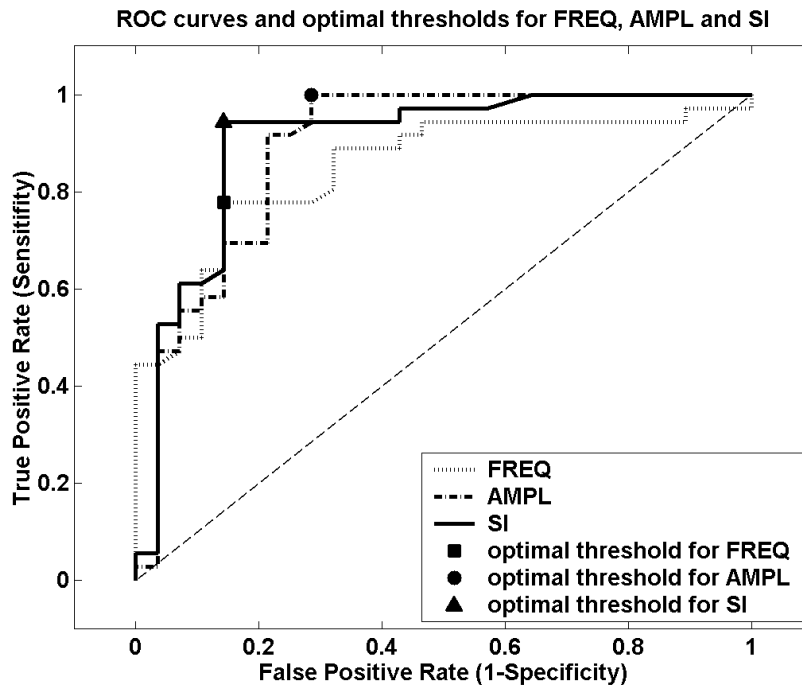


Figure 10.6: Receiver operating characteristic (ROC) curves and corresponding optimal thresholds for mean frequency (FREQ), mean peak-to-trough amplitude (AMPL), and survival index (SI).

Discussion

This analysis of different animal studies shows that FREQ, AMPL, and SI values, computed shortly before the first defibrillation shock, were not significantly different in regard to the four different cardiac arrest models. This legitimates the pooling of the data.

Many human and animal studies have shown that FREQ and AMPL are reliable variables for the prediction of defibrillation outcome [11]. In comparison with AMPL, FREQ is independent of electrode contact quality, which makes FREQ more practicable and predictive in humans. In this study, FREQ and AMPL were both capable of predicting defibrillation outcome. Unfortunately, there is a range of FREQ and AMPL between an upper and a lower threshold where prediction of ROSC or no ROSC is poor because of an overlap of ROSC and no-ROSC data.

To improve this dilemma of a foggy prediction in some circumstances, we introduce the SI, which corresponds to a new coordinate axis in the FREQ-AMPL plane by means of linear transformation. By using multiple logistic regression analysis, we identified the relevant coefficients of FREQ and AMPL in predicting defibrillation outcome, resulting in the definition of SI. Univariate logistic regression and ROC curve analysis showed that SI had a robust threshold value and predicted defibrillation outcome with better probabilities compared with FREQ or AMPL alone.

There are more sophisticated (e.g., nonlinear) methods of combining FREQ and AMPL to a new VF variable, which would probably perform better than SI. However, this would likely lead to over-fitting of the 64 data points.

The P_5 value of logistic regression for AMPL is negative (Fig. 10.5). This reflects a

limitation of logistic regression when it is applied to data for which only positive values make sense. A way out would be to work with the logarithm of AMPL values. However, for the sake of mathematical comprehensibility, we accepted this inconsistency.

In this study, we chose the P_{50} value of logistic linear regression as the definition of threshold value for a VF variable. One could also choose a different P value. ROC curve analysis rendered slightly different optimal threshold values. Ultimately, an optimal threshold value has to be defined according to clinical relevance.

Further analysis has to be performed to investigate whether CPR itself or additional drug administration changes the pattern of VF by means of increased SI and a better probability of ROSC. In fact, *FREQ* and *AMPL* served as noninvasive markers to monitor continuing CPR efforts and were sensitive to the administration of vasopressin and epinephrine [7, 8]. In this study, which analyzes *FREQ*, *AMPL*, and *SI* values shortly before the first defibrillation shock, we showed that animals receiving vasopressin showed significantly higher *FREQ*, *AMPL*, and *SI* values than animals receiving epinephrine.

There are a number of studies that combine various variables of VF rather than comparing these variables. For example, Brown and Dzwonczyk [32] retrospectively analyzed 55 VF patients out of hospital, and they found that the combination of median and dominant frequency improved predictive power when compared with the analysis of median frequency alone. This group reported a *Sp* of 47% when the threshold value was set to yield a sensitivity of 100%. Furthermore, Monsieurs et al. [108] combined amplitude and the number of baseline crossings per second in human VF into a survival index. With this index, 79% of the survivors and 70% of the nonsurvivors could be classified correctly; adding age increased the correct classification of survivors to 86% and to 73% for the nonsurvivors. In a laboratory study, Noc et al. [115] divided animals into a derivation and a validation group. When mean amplitude and dominant frequency were combined, predictability was improved compared with single use. In the validation group, defibrillation attempts were uniformly unsuccessful if the combination of mean amplitude and dominant frequency did not exceed the threshold values obtained in the derivation study. In the most recent investigation, Eftestol et al. [52] predicted defibrillation outcome by combining four spectral features in VF ECG signals before 868 defibrillation attempts in 156 patients with out-of-hospital cardiac arrest. They split the data into training and test sets and used classifier generalization techniques to increase the degree of expected reliability. Different secondary decorrelated feature sets were generated from the four original features by using principal component analysis. Following the advice of the highest performing classifier, which corresponded to the combination of 2 secondary features, 328 (42%) of 781 unsuccessful shocks would have been avoided, whereas 7 (8%) of 87 successful shocks would not have been given. Although it seems obvious that combining VF variables improves predictability of successful defibrillation, it seems obvious as well that this approach still has significant limitations. For example, it has to be noted that a 47% *Sp*, as observed in Brown and Dzwonczyk's study [32], is as good as flipping a coin; furthermore, if 8% of successful shocks are withheld, as in the report of Eftestol et al. [52], efficiency of this strategy is dissatisfying. Eftestol et al. recognized this problem as well and suggested that the low *Sp* and *PPV* indicate that other features should be added; this may be extremely important in humans undergoing CPR, because VF analysis in this setting is especially prone to chest compression-related artifacts. In this context, the method of $N(\alpha)$ -histograms [9], which does not use any filtering algorithm to eliminate the CPR artifacts, and other nonlinear VF variables, as recently discussed in Amann et al. [11], could prove useful.

In conclusion, *FREQ*, *AMPL*, and *SI* values were not sensitive in regard to the four dif-

ferent cardiac arrest models but were significantly different for vasopressin and epinephrine animals. Further, we showed that a combination of *FREQ* and *AMPL* with a new predictive variable, *SI*, leads to a better forecast of successful defibrillation compared with either *FREQ* and *AMPL* alone.

10.3 Paper 3

The following paper was published in *Anesth Analg* 2003 ;97:226-30, [132].

The Effects of Nifedipine on Ventricular Fibrillation Mean Frequency in a Porcine Model of Prolonged Cardiopulmonary Resuscitation

Karl H. Stadlbauer, MD, Klaus Rheinberger, MSc, Volker Wenzel, MD, Claus Raedler, Anette C. Krismer, MD, Hans-Ulrich Strohmenger, MD, Sven Augenstein, MD, Horst G. Wagner-Berger, MD, Wolfgang G. Voelckel, MD, Karl H. Lindner, MD, and Anton Amann, PhD

Department of Anesthesiology and Critical Care Medicine, Leopold-Franzens-University, Innsbruck, Austria

Supported by the Austrian National Bank, Vienna, Austria; the Austrian Heart Foundation Project 98/05, Vienna, Austria; a dean's grant for medical school graduates of the Leopold-Franzens University, Innsbruck, Austria; the Department of Anesthesiology and Critical Care Medicine, Leopold-Franzens-University, Innsbruck, Austria; and Austrian Science Foundation Grant P14169MED, Vienna, Austria.

No author has a conflict of interest with regard to drugs or devices discussed in this article.

Accepted for publication January 23, 2003.

Address correspondence and reprint requests to Karl H. Lindner, MD, Leopold-Franzens-University, Department of Anesthesiology and Critical Care Medicine, Anichstrasse 35, 6020 Innsbruck, Austria. Address e-mail to karl-heinz.stadlbauer@uibk.ac.at

Abstract

We assessed the effects of a calcium channel blocker versus saline placebo on ventricular fibrillation mean frequency and hemodynamic variables during prolonged cardiopulmonary resuscitation (CPR). Before cardiac arrest, 10 animals were randomly assigned to receive either nifedipine (0.64 mg/kg; n = 5) or saline placebo (n = 5) over 10 min. Immediately after drug administration, ventricular fibrillation was induced. After 4 min of cardiac arrest and 18 min of basic life support CPR, defibrillation was attempted. Ninety seconds after the induction of cardiac arrest, ventricular fibrillation mean frequency was significantly ($P < 0.01$) increased in nifedipine versus placebo pigs (mean \pm SD: 12.4 ± 2.1 Hz versus 8 ± 0.7 Hz). From 2 to 18.5 min after the induction of cardiac arrest, no differences in ventricular fibrillation mean frequency were detected between groups. Before defibrillation, ventricular fibrillation mean frequency was significantly ($P < 0.05$) increased in nifedipine versus placebo animals (9.7 ± 1.2 Hz versus 7.1 ± 1.3 Hz). Coronary perfusion pressure was significantly lower in the nifedipine than in the placebo group from the induction of ventricular fibrillation to 11.5 min of cardiac arrest; no animal had a return of spontaneous circulation after defibrillation. In conclusion, nifedipine, but not saline placebo, prevented a rapid decrease of ventricular fibrillation mean frequency after the induction of cardiac arrest and maintained ventricular fibrillation mean frequency at ~ 10 Hz during prolonged CPR; this was nevertheless associated with no defibrillation success.

Introduction

Intracellular Ca^{2+} increases promptly with the induction of ventricular fibrillation [90]. This increase in intracellular Ca^{2+} is several times more than the peak systolic intracellular

Ca^{2+} content during normal sinus rhythm and has important metabolic and mechanical consequences. For example, a large concentration of intracellular Ca^{2+} increases activation of enzymes that actively transport Ca^{2+} into the sarcoplasmic reticulum and mitochondria [109, 123, 75], resulting in a significant intracellular energy deficit. Accordingly, calcium channel blockers may preserve metabolic machinery and reduce the production of cerebral catabolites, resulting in prolonged cell viability during global ischemia [145].

Although a randomized clinical trial using a calcium channel blocker in comatose survivors of cardiac arrest did not reveal beneficial effects of this drug with regard to neurologic outcome during a 6-mo followup, it is possible that the treatment effect was simply too small to be detectable in a clinical trial of only 520 cardiac arrest patients [29]. Also, the calcium channel blocker was given after the return of spontaneous circulation, which may have limited the protective effects on the cerebrum. Thus, if calcium overloading is prevented early, beneficial effects may be more likely; further, if the goal of the treatment strategy is not an extremely difficult target, such as preventing postcardiac arrest brain damage, but a relatively simple one, such as protecting the fibrillating myocardium, the success of a given study may be more likely. In fact, Martin et al. [104] showed that a calcium channel blocker, but not saline placebo, maintained high ventricular fibrillation mean frequency in a cardiac arrest model and facilitated defibrillation. However, they observed this phenomenon only during the first 90 s of cardiac arrest, which may not be applicable to cardiopulmonary resuscitation (CPR) in humans, in whom basic and advanced cardiac life support are mostly initiated after approximately 5 min or even longer [74]. Thus, it is unknown whether the underlying beneficial Ca^{2+} antagonist effect occurring 90 s after collapse may be present later as well. More knowledge about this physiology may improve the prediction of countershock success. Accordingly, the purpose of this study was to assess the effects of a calcium channel blocker versus saline placebo on ventricular fibrillation mean frequency and coronary perfusion pressure during prolonged CPR.

Methods

This project was approved by the Austrian Federal Animal Investigational Committee, and the animals were managed in accordance with the American Physiological Society institutional guidelines and the Position of the American Heart Association on Research Animal Use, as adopted on November 11, 1984. Animal care and use were performed by qualified individuals who were supervised by veterinarians, and all facilities and transportation complied with current legal requirements and guidelines. Anesthesia was used in all surgical interventions, all unnecessary suffering was avoided, and research was terminated if unnecessary pain or fear resulted. Our animal facilities meet the standards of the American Association for Accreditation of Laboratory Animal Care. This study was performed according to Utstein-style guidelines [79] with 10 healthy, 12- to 16-wk-old swine weighing 30 to 40 kg. The animals were fasted overnight but had free access to water. The pigs were premedicated with azaperone (4 mg/kg IM) and atropine (0.1 mg/kg IM) 1 h before surgery, and anesthesia was induced with propofol (12 mg/kg IV). After intubation during spontaneous respiration, the pigs were ventilated with a volume-controlled ventilator (EV-A; Draeger, Lübeck, Germany) with 35% oxygen at 20 breaths/min and with a tidal volume adjusted to maintain normocapnia. Anesthesia was maintained with propofol ($6-8 \text{ mg} \cdot \text{kg}^{-1} \cdot \text{h}^{-1}$) and a single injection of piritramide (30 mg) [155]. Muscle paralysis was achieved with $0.2 \text{ mg} \cdot \text{kg}^{-1} \cdot \text{h}^{-1}$ of pancuronium after intubation. Ringer's solution ($6 \text{ mL} \cdot \text{kg}^{-1} \cdot \text{h}^{-1}$) and a 3% gelatin solution ($4 \text{ mL} \cdot \text{kg}^{-1} \cdot \text{h}^{-1}$) were administered in the preparation phase.

A standard Lead III electrocardiogram (ECG) was used to monitor cardiac rhythm; depth of anesthesia was judged according to blood pressure, heart rate, and electroencephalography (Engström, Munich, Germany). If cardiovascular variables or electroencephalography indicated a reduced depth of anesthesia, additional propofol and piritramide were given. Body temperature was maintained between 38.0°C (100.4°F) and 39.0°C (102.2°F). A 7F catheter was advanced into the descending aorta via femoral cutdown for withdrawal of arterial blood samples and measurement of arterial blood pressure.

A 7.5F pulmonary artery catheter was placed via cutdown into the neck for measurement of right atrial and pulmonary artery pressure. Blood pressure was measured with a saline-filled catheter attached to a pressure transducer (Model 1290A; Hewlett-Packard, Böblingen, Germany) that was calibrated to atmospheric pressure at the level of the right atrium.

The ventricular fibrillation ECG signal (standard Lead III) and pressure tracings were monitored continuously and recorded on hard disk by a computerbased data acquisition system (Port 2000; Dewetron, Graz, Austria; and Datalogger [custom-made software]). Digitization was performed at a sampling rate of 1000 Hz and with an amplitude resolution of 12 bits (4096 equal steps between minimal and maximal amplitude). The recorded ECG signals were analyzed by using the mathematical software package Matlab (Math Works Inc., Natick, MA). The signals were divided into consecutive 10-s epochs; each epoch was transformed into the frequency domain by Fourier transformation. To filter out CPR-related artifacts, the frequency domain was restricted to the range from 4.33 to 30 Hz, as previously described [138]. Mean fibrillation frequency for the 10-s epoch after 1.5, 7, 12, 18.5, and 22 min after the induction of cardiac arrest was calculated from the restricted spectrum. The mean ventricular fibrillation peak-to-trough amplitude (difference between a peak and the next trough of the ECG signal) was calculated at the same time segments as mean fibrillation frequency.

Fifteen minutes before cardiac arrest, 5000 U of heparin was administered IV to prevent intracardiac clot formation, and single doses of piritramide 0.8 mg/kg and pancuronium 0.2 mg/kg were given. Subsequently, 10 animals were randomly assigned to receive either nifedipine (0.64 mg/kg; $n = 5$) [104] or saline placebo ($n = 5$) over 10 min (investigators were blinded to the drugs). Immediately after drug administration, ventricular fibrillation was induced with a 50-Hz alternating current applied via two subcutaneous needles, and ventilation was stopped. After 4 min of untreated ventricular fibrillation, closed-chest standard CPR was performed, and ventilation was resumed with the same ventilator setting as before the induction of cardiac arrest. Chest compressions were always performed by the same investigator at a rate of 100/min, guided by acoustical audiotones. This investigator was blinded to hemodynamic monitor tracings. Hemodynamic variables were measured before the induction of cardiac arrest, as well as 1.5, 4.5, 8, 9.5, 13, 14.5, and 18 min after initiation of CPR. After 22 min of cardiac arrest, including 18 min of standard CPR, we attempted to restore spontaneous circulation with up to 5 countershocks (monophasic wave forms) with an energy of 3, 4, and 6 J/kg, respectively. If asystole or pulseless electrical activity was present after defibrillation, the experiment was terminated. Return of spontaneous circulation was defined as an unassisted pulse with a systolic arterial pressure of more than 80 mm Hg for longer than 5 min. After the experimental protocol was finished, the animals were killed with an overdose of potassium chloride and fentanyl; all pigs were necropsied to check correct positioning of the catheters and damage to the rib cage and internal organs.

Values are expressed as mean \pm SD. The comparability of weight and baseline data was verified by using the unpaired Student's *t*-test for continuous variables. To identify statis-

tically significant differences of mean frequency, mean amplitude, and coronary perfusion pressure between groups, one-way analysis of variance was used, followed by a nonparametric Wilcoxon's ranked sum test; all P values were corrected with the Bonferroni method for multiple comparisons, and values of $P < 0.05$ were considered significant. The association between coronary perfusion pressure and ventricular fibrillation mean frequency was examined with linear regression analyses.

Results

After the induction of cardiac arrest, the ventricular fibrillation mean frequency was higher in the nifedipine group than in the saline solution placebo group for approximately 2 min. From 2 to 18.5 min after the induction of cardiac arrest, including 14.5 min of CPR, no differences in ventricular fibrillation mean frequency could be detected. From 18.5 to 22 min of cardiac arrest, the ventricular fibrillation mean frequency of the placebo group deteriorated, and the mean frequency in the nifedipine group remained higher (Fig. 10.7). Ninety

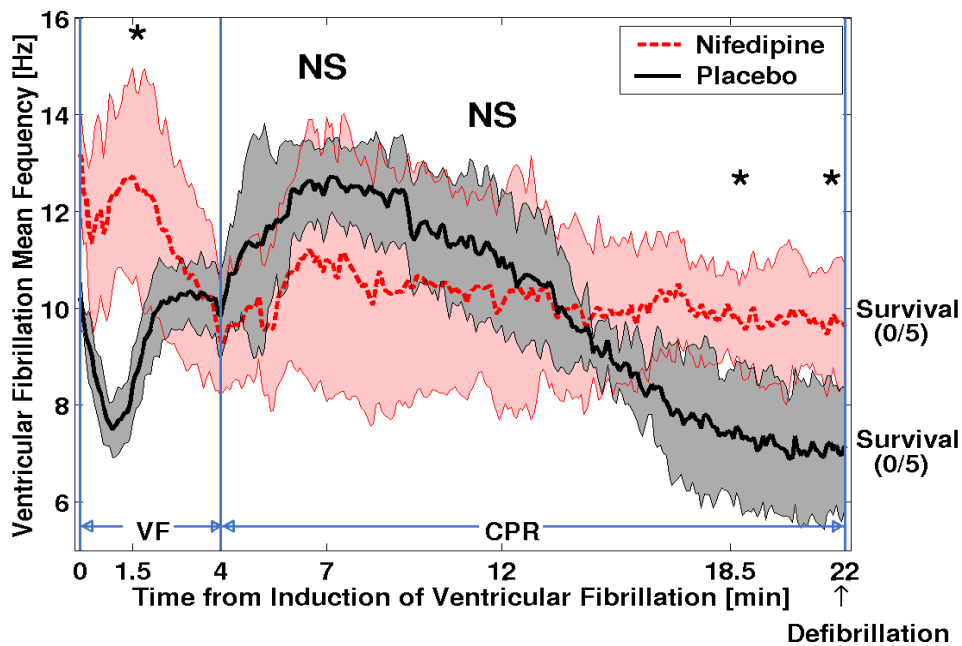


Figure 10.7: Mean \pm SD ventricular fibrillation mean frequency in the nifedipine and placebo groups during untreated cardiac arrest and basic life support cardiopulmonary resuscitation (CPR). NS = not significant for nifedipine versus placebo; VF ventricular fibrillation. * $P < 0.01$.

seconds after the induction of cardiac arrest, the ventricular fibrillation mean frequency was 12.4 ± 2.1 Hz in the nifedipine group versus 8.0 ± 0.7 Hz in the placebo group ($P < 0.01$) and 9.7 ± 1.2 Hz versus 7.1 ± 1.3 Hz shortly before defibrillation ($P < 0.05$), respectively. There were no significant differences in mean ventricular fibrillation peak-trough amplitude before defibrillation. Coronary perfusion pressure was lower in the nifedipine than in the

placebo group from the induction of ventricular fibrillation to 11.5 min of cardiac arrest. From 11.5 to 22 min of cardiac arrest, coronary perfusion pressure in both groups was low and comparable (Fig. 10.8). There was a correlation index of $r = 0.99$ in the placebo group

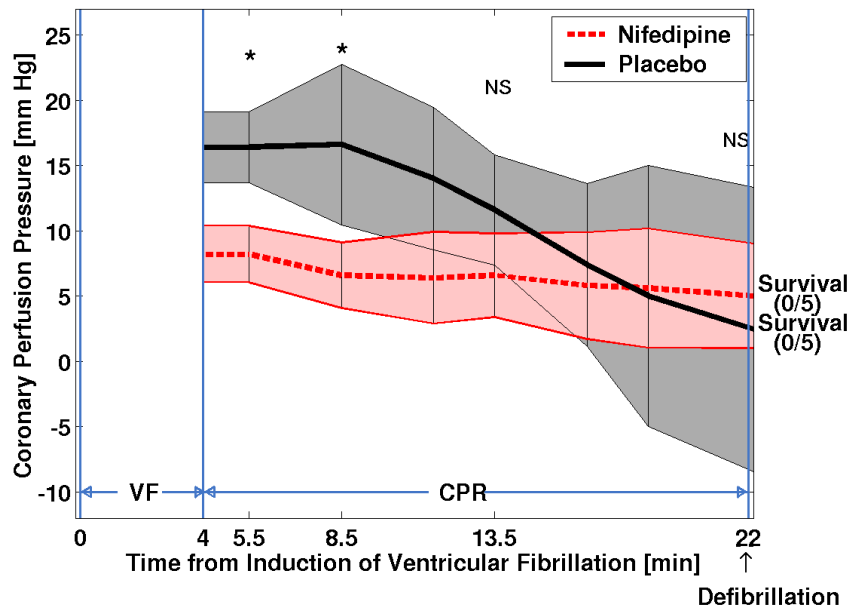


Figure 10.8: Mean \pm SD coronary perfusion pressure of the nifedipine group versus the saline placebo group during cardiac arrest. NS not significant for nifedipine versus placebo; VF = ventricular fibrillation; CPR = cardiopulmonary resuscitation. * $P < 0.01$.

versus $r = 0.15$ in the nifedipine group between coronary perfusion pressure and ventricular fibrillation mean frequency. No animal had a return of spontaneous circulation after defibrillation; necropsy revealed proper instrumentation in all animals.

Discussion

Nifedipine, but not saline placebo, prevented a rapid decrease of ventricular fibrillation mean frequency immediately after the induction of cardiac arrest and maintained the ventricular fibrillation mean frequency at ~ 10 Hz during prolonged CPR. However, the significantly increased frequency values in the nifedipine group were not associated with increased defibrillation success.

Our observation is in full agreement, with respect to time course of ventricular fibrillation mean frequency, with an earlier study by Martin et al. [104], who also injected nifedipine during spontaneous circulation and then measured ventricular fibrillation mean frequency during CPR. Although Martin et al.'s results with regard to ventricular fibrillation mean frequency in the first 2 minutes were almost identical to those of our study, we continued the experiment for another 2 minutes of untreated ventricular fibrillation and, subsequently, 18 minutes of basic life support CPR. In Martin et al.'s study, nifedipine seemed

to have a beneficial effect on the fibrillating myocardium by maintaining the ventricular fibrillation mean frequency on a high level and by prolonging the duration to convert ventricular fibrillation into a spontaneous rhythm, and not pulseless electrical activity, from ~ 60 to ~ 90 seconds. This experience is in agreement with both laboratory and clinical data, wherein high ventricular fibrillation mean frequencies correlated with high return of spontaneous circulation rates [7, 135].

In previous studies, ventricular fibrillation mean frequency has been shown to correlate positively with coronary perfusion pressure [115]. Interestingly, we observed a high mean frequency of ~ 9 to ~ 11 Hz during CPR in all nifedipine pigs, but coronary perfusion pressure was comparably low, at ~ 6 mm Hg. Accordingly, the correlation index between ventricular fibrillation mean frequency and coronary perfusion pressure was approximately -0.15 throughout the CPR interval, whereas this value was at an established level of 0.99 in the saline placebo pigs. We deliberately did not attempt to defibrillate the animals until 22 minutes into the experiment to measure ventricular fibrillation mean frequency. Because of the prolonged interval of low coronary perfusion pressure, which may be at least partly due to the antihypertensive effects of calcium channel blockade, it is not surprising that no animal could be converted from ventricular fibrillation to return of spontaneous circulation.

In a previous study, a ventricular fibrillation mean frequency >8.4 Hz predicted successful defibrillation with a sensitivity of 100% and a specificity of 80% [7]. Conversely, although four of five nifedipine-treated animals had a ventricular fibrillation mean frequency >8.4 Hz, none was successfully defibrillated. Without doubt, the negative correlation between ventricular fibrillation mean frequency and coronary perfusion pressure and, therefore, the insufficient predictability of defibrillation success with ventricular fibrillation analysis in this experiment were due to the administration of nifedipine. However, it is unlikely that a calcium channel blocker such as nifedipine is a significant source of false-positive ventricular fibrillation mean frequency values during CPR in humans. Nevertheless, the results of our experiment document that the present approach to analyzing ventricular fibrillation signals may be insufficient to adequately predict successful defibrillation. For example, analysis of ventricular fibrillation mean frequency in one clinical study achieved a sensitivity of only 73% and a specificity of only 67% [135], indicating that the move to $>95\%$ predictability of successful defibrillation may require more information than ventricular fibrillation analysis is capable of providing. Mean peak-to-trough amplitude would be a good predictive variable in our experiment; however, ventricular fibrillation amplitude depends on the direction of the main fibrillation vector, and, therefore, there is great individual variety. Other strategies to solve this dilemma may be to use alternative methods of ventricular fibrillation analysis, such as $N(\alpha)$ histograms [9], or other nonlinear modeling techniques [128, 130]. Furthermore, combined use of ventricular fibrillation variables leads to an improved forecast of defibrillation outcome, as we have shown in a previous study [12]. For example, by using this new combination of mean frequency and amplitude (survival index) [12], the specificity for prediction of successful defibrillation would be improved in this example from 20% to 60% . However, both laboratory and clinical investigations would have to confirm the possible value of these strategies.

There are several limitations to this study. First, the absolute values of ventricular fibrillation mean frequency differ significantly between animals and humans [103]. Also, we used young, healthy pigs that were free of atherosclerotic disease. Because of design limitations, we administered no vasopressor, which may have biased the results of ventricular fibrillation mean frequency analysis. Also, it is not possible to administer a calcium channel blocker before cardiac arrest. In conclusion, nifedipine, but not saline placebo, prevented

a rapid decrease of ventricular fibrillation mean frequency after the induction of cardiac arrest and maintained ventricular fibrillation mean frequency at ~ 10 Hz during prolonged CPR; this was nevertheless associated with no defibrillation success, which suggests that ventricular fibrillation-derived variables predicting defibrillation success are dependent on the study conditions.

Part V

Defibrillator Waveform Analysis

Chapter 11

(Un)published Papers

Contents

11.1 Overview	147
11.2 Paper 4	148
11.3 Paper 5	160

11.1 Overview

International guidelines of CPR recommend electrical defibrillation as a therapy for VF [17, 18], because besides external thoracic compressions it is the only effective intervention, which is proved to correlate with survival during CPR [16]. The time course of the electrical current or voltage delivered by a defibrillator is called “waveform”. Different defibrillation “waveforms” of the various manufacturers are still being discussed with respect to their efficacy and harmfulness. All internal defibrillators and increasingly more external defibrillators use biphasic waveforms. The following two papers present and discuss many of the biphasic waveforms implemented in external defibrillators available on the market at present.

11.2 Paper 4

The following paper was published in *Resuscitation* 2001 ;50(1):61-70, [6].

Waveform Analysis of Biphasic External Defibrillators

Ulrich Achleitner, Klaus Rheinberger, Bernhard Further, Anton Amann¹, Michael Baubin²

Department of Anaesthesiology and Critical Care, University of Innsbruck, Anichstrasse
35, 6020 Innsbruck, Austria

Received 30 October 2000; received in revised form 27 December 2000; accepted 10 January 2001

Abstract

Background and Objective: All internal defibrillators and some external defibrillators use biphasic waveforms. The study analysed the discharged waveform pulses of two manual and two semi-automated biphasic external defibrillators. *Methods and Results:* The defibrillators were discharged into resistive loads of 25, 50 and 100 Ω simulating the patient's transthoracic impedance. The tested biphasic defibrillators differed in initial current as well as initial voltage, varying from 10.9 to 73.3 A and from 482.8 to 2140.0 V, respectively. The energies of the manual defibrillators set at 100, 150 and 200 J deviated by up to + 19.1 or - 28.9% from the selected energy. Impedance-normalised delivered energy varied from 1.0 to 12.5 J/ Ω . Delivered energy, shock duration and charge flow were examined with respect to the total pulse, its splitting into positive and negative phases and their impedance dependence. For three defibrillators pulse duration increased with the resistive load, whereas one defibrillator always required 9.9 ms. All tested defibrillators showed a higher charge flow in the positive phase. Defibrillator capacitance varied between approximately 200 and 100 mF and internal resistance varied from 2.0 to 7.6 V. Defibrillator waveform tilt ranged from -13.1 to 61.4%. *Conclusions:* The tested defibrillators showed remarkable differences in their waveform design and their varying dependence on transthoracic impedance. **Keywords:**

Automated external defibrillator (AED); Cardiac arrest; Defibrillation; Emergency medical services; Manual defibrillator; Transthoracic impedance

Introduction

Ventricular fibrillation is the principal cause of sudden cardiac arrest. The most effective treatment for ventricular fibrillation is electrical defibrillation [18]. Besides performing defibrillation at the earliest possible time, the waveform may also be crucial for success. Presently the majority of external defibrillators use monophasic waveforms. In contrast to external defibrillators, state-of-the-art internal defibrillators use biphasic truncated exponential waveforms [126] which have proved superior to monophasic waveforms [43, 57]. Positive evidence for safety and clinical effectiveness of biphasic truncated exponential waveforms for internal and external use was ascertained by the AHA ECC committee [18, 43].

Clinical studies [22, 23, 47, 64, 106, 107, 120, 156], reports [158] and animal experiments [63, 96, 143, 147, 163] have shown at least equality between biphasic and monophasic

¹Tel.: + 43-512-504 24636; fax: + 43-512-504 24683

²Corresponding author. Tel.: + 43-512-504 22400; fax: +43-512-504 22450.

E-mail addresses: anton.amann@uibk.ac.at (A. Amann), michael.baubin@uibk.ac.at (M. Baubin).

waveforms for transthoracic defibrillation and transthoracic cardioversion. Biphasic waveforms offer the benefit of a lower defibrillation threshold; the risk of heart damage from excessive pulse energy is thus lowered and the chance for successful defibrillation increases.

Using different waveforms and variable energy levels defibrillator manufacturers offer various types of external defibrillators. This holds both for monophasic [4, 5] and biphasic waveforms. The aim of the present laboratory study was to determine the energy content of the discharge in comparison to the selected energy and to ascertain the actual discharge waveform described by different characteristic parameters.

The discharged pulse energy and waveform of two manually biphasic external defibrillators (MCED) and two semi-automated biphasic external defibrillators (SAED) was analysed.

Materials and methods

Two MCED, the Medtronic Physio-Control LIFEPAK 12 (LIFEPAK 12) and the Zoll M-Series Biphasic (M-Series), and two SAED, the Laerdal Heartstart ForeRunner (ForeRunner) and the Survivalink FirstSave STAR (FirstSave), were tested. The MRL defibrillator was not available to the authors.

The MCED provide a variety of shock energies from 2 to 360 J. The appropriate energy is selected before defibrillation. The SAED, as first-responder devices, do not allow manual selection of energy.

Pulse generation

According to the manufacturer's manuals, three of the four tested defibrillators, LIFEPAK 12, ForeRunner and FirstSave, use a truncated exponentially decaying waveform (Fig. 11.1), both for the positive and negative part of the biphasic waveform. These defibrillators store their electrical energy in a capacitor which is charged to a certain voltage level according to the required energy. Discharging a charged capacitor into a resistor results in an exponential decay of the shock waveform. To achieve a biphasic truncated exponentially decaying waveform, the current of the capacitor discharge is switched off automatically after a certain time (time of phase reversal). Then the current is reversed in polarity and switched on again for a certain negative shock period.

In contrast, the M-Series defibrillator employs a serrated positive waveform phase and an exponentially decaying negative waveform phase (Fig. 11.1). The serrated positive component is brought about by adjusting the defibrillator's internal resistance during the first waveform phase.

The capacitor, the internal resistance, the waveformtruncating and phase-reversing timing circuit and the patient's transthoracic impedance constitute the discharge circuit of the four tested defibrillators. By changing the patient's transthoracic impedance the characteristics of the discharge circuit can be altered. Consequently, the patient's transthoracic impedance determines the waveform of the shock and thus its energy, initial voltage, pulse duration and time of phase reversal.

In order to detect the patient's transthoracic impedance the defibrillators may use manufacturer-dependent integrated measuring devices (patents: US 5645571, US 6047212, US 5230336, US 5431687, US 5800462, US 5904706, US 5111813, EP 315368, EP 457604; [83]).

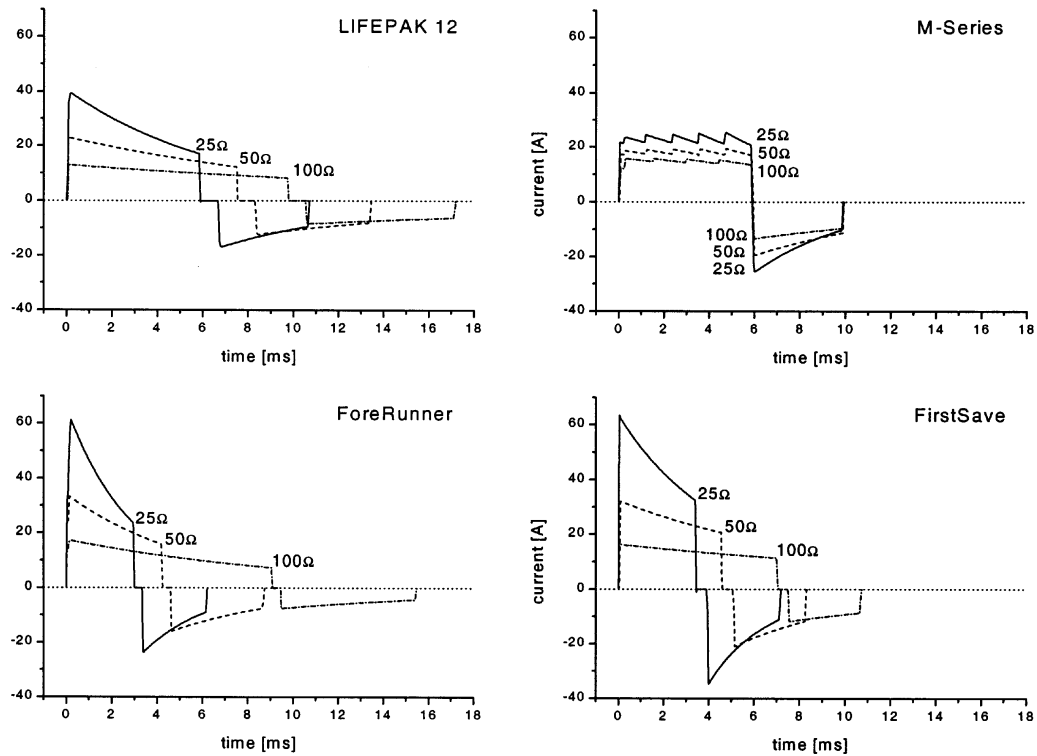


Figure 11.1: Different biphasic defibrillation waveforms for resistive loads of 25, 50 and 100 Ω . An energy of 150 J was selected for the Medtronic Physio-Control LIFEPAK 12 and the Zoll M-Series Biphasic. The Laerdal Heartstart ForeRunner automatically delivers an energy of approximately 150 J for any test resistor. For the Survivalink FirstSave STAR the second shock after turning on the defibrillator was chosen, delivering mean energies of 219.3 J (25 Ω), 194.2 J (50 Ω) and 165.0 J (100 Ω). The Medtronic Physio-Control LIFEPAK 12, the Laerdal Heartstart ForeRunner and the Survivalink FirstSave STAR show a biphasic truncated exponential waveform. The Zoll M-Series Biphasic shows a biphasic truncated exponential waveform with serrated positive waveform phase.

Waveform measurement

The defibrillators were discharged into resistive loads of 25, 50 and 100 Ω simulating the patient's individual transthoracic impedance, as described recently for monophasic defibrillators [4, 5]. The various loads were achieved by combining two resistors, a 1 Ω resistor and an adjustable 1100 Ω resistor, in a series configuration providing voltage proportioning. The voltage across the 1 Ω resistor was connected to a PC-based measurement system (Dewetron, Graz, Austria). The waveform was digitised and stored at a sampling rate of 20 kHz and 16 bit amplitude resolution. Pulse amplitude resolution was better than 0.6 V or 6 mA for 100 Ω (12 mA for 50 Ω and 24 mA for 25 Ω).

The two MCED LIFEPAK 12 and M-Series were charged to selected energies of 100, 150 and 200 J and discharged into the different resistive loads. The two first responder devices ForeRunner and FirstSave did not allow manual selection of energy.

Regular calibration guaranteed reliability and accuracy of the test resistors. Each test was performed at least three times.

Data analysis

The recorded waveforms were analysed using mathematical software (MatLab 5.3, The Mathworks Inc, Natick, MA).

The waveform energy content, impedance-normalised delivered energy, initial voltage and initial current, waveform duration, charge flow as well as the tilt were calculated. The impedance-normalised delivered energy is defined as the waveform energy content, i.e. the total delivered energy, divided by the test resistance. The charge flow Q of a current pulse $I(t)$ is the integral

$$Q = \int I(t) dt$$

over the time of the shock. The tilt of a defibrillator's pulse is defined as

$$(A - D)/A,$$

where A is the initial voltage (of the positive shock) and D is the absolute value of the initial voltage of the negative shock. The initial voltage of the positive and negative pulse is defined as the maximum voltage within the first millisecond of the positive and negative pulse, respectively. The initial current was computed by dividing the initial voltage by the test resistance, i.e. by applying Ohm's law.

The energy discharged during the positive and the negative phase and their ratio to the total discharged energy, the duration of the positive and the negative phase and their ratio to the total duration, and the charge flow of the positive and the negative phase and their ratio to the sum of both absolute values were computed. The absolute values are given as mean \pm S.D.

Finally, the capacitor capacitance of three defibrillators was computed by fitting the exponential decay of the negative pulse for different resistive loads. A charged capacitor discharges into a series configuration of an internal resistor and a test resistor according to

$$U(t) = U(0)e^{-t/\tau},$$

where $U(t)$ is the voltage across the test resistor t seconds after the beginning of the discharge process. The time constant τ depends on the capacitor capacitance C , the internal resistance R_i and the test resistance R via

$$\tau = C(R_i + R).$$

Fitting the exponential decay of the negative pulse yields the time constant τ . Assuming the internal resistance R_i (and the capacitance C) to be constant for two different test resistances R_1 and R_2 , one can extract the capacitance C and the internal resistance R_i from the two time constants τ_1 and τ_2 , corresponding to R_1 and R_2 , respectively:

$$C = (\tau_2 - \tau_1)/(R_2 - R_1) \quad (11.1)$$

and

$$R_i = \tau_1/C - R_1 = \tau_2/C - R_2. \quad (11.2)$$

For the LIFEPAK 12, the ForeRunner and the FirstSave calculations (11.1) and (11.2) were made for all three combinations of the resistive loads 25, 50 and 100 Ω . Results are given as mean \pm S.D. of these three values. The M-Series defibrillator changes its internal resistance and therefore does not conform to the above requirements.

Results

The typical discharge waveforms at 25, 50 and 100 Ω are represented graphically in Figs. 11.1 and 11.2. The characteristic parameters describing the discharge waveforms are shown

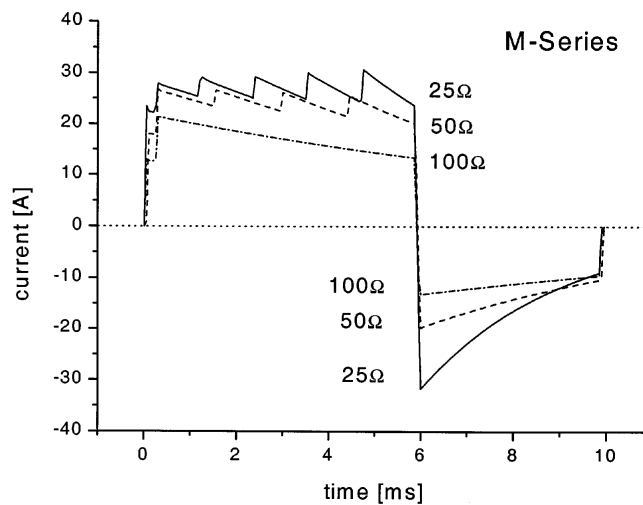


Figure 11.2: Defibrillation waveforms for the Zoll M-Series Biphasic defibrillator for test resistive loads of 25, 50 and 100 Ω and a selected energy of 200 J. In contrast to all other configurations, the M-Series does not show the typical serrated positive waveform at an energy/impedance configuration of 200 J and 100 Ω , using a truncated exponential waveform instead.

in Tables 1 - 6. In Tables 1 - 5 the values depend on the various resistive loads and the energy selected for the MCED. For the ForeRunner the values depend only on the various resistive loads. For the FirstSave the values additionally depend on the number of shocks already discharged after turning on the defibrillator. The values in Table 6 were computed by combining the fitted time constants for different combinations of two resistive loads using Eqs. (11.1) and (11.2). The values therefore depend on the selected energy regarding the MCED and the number of shocks already discharged for the FirstSave.

Discharge waveform (Figs. 1 and 2)

The LIFEPAK 12, the ForeRunner and the FirstSave use a biphasic truncated exponential waveform (Fig. 1). The M-Series uses a biphasic truncated exponential waveform with serrated positive waveform phase in all but one energy-impedance configurations (Fig. 1); at a configuration of 100 Ω and 200 J the M-Series has an anomaly using a truncated exponential waveform without the typical serrated positive waveform (Fig. 2).

Discharge energy (Table 1)

Generally, the MCED did not deliver the precise amount of energy that had been selected. The delivered energies deviated from the selected energy by up to + 19.1 or -28.9%. The LIFEPAK 12 always delivered less energy than selected, the M-Series less or more depending on the resistive load. The energy delivered by both MCED increased with increasing resistive load. The energy delivered by the FirstSave decreased with increasing resistive load and depended on the number of shocks discharged after turning on the defibrillator. The ForeRunner automatically delivered an energy of approximately 150 J for any test resistor.

In case of the MCED impedance-normalised delivered energy decreased with increasing resistive load and increased with increasing selected energy as expected. Maximum and minimum values were achieved by the LIFEPAK 12 defibrillator at 7.8 and 1.0 J/ Ω , respectively. For the SAED impedance-normalised delivered energy decreased with increasing resistive load. The maximum value was achieved by the FirstSave (12.5 J/ Ω) and the minimum value by the ForeRunner defibrillator (1.5 J/ Ω).

In general, more than 70% of the delivered energy was delivered in the first phase of the shock. The LIFEPAK 12 shows energy splitting into approximately 88% for the positive part and 12% for the negative part at 25 and 50 Ω and into 76 and 24% at 100 Ω independent of the selected energy. The ForeRunner shows energy splitting into approximately 88 and 12%. The two remaining defibrillators show a variety of groupings in the energy splitting.

Initial voltage (Table 2a)

For all tested defibrillators initial voltage increased with the selected energy or the number of shocks and with the resistive load. The values of the MCED showed a wide range, whereas the values of the SAED showed a narrow range. Maximum and minimum values were achieved by the M-Series defibrillator at 2140.0 and 482.8 V, respectively.

Initial current (Table 2b)

For all tested defibrillators initial current increased with the selected energy or the number of shocks but decreased with the resistive load. The MCED values showed a narrow range, whereas the SAED values showed a wide range. The maximum value was achieved by the FirstSave (73.3 A) and the minimum value by the LIFEPAK 12 defibrillator (10.9 A).

Pulse duration (Table 3)

Generally, total pulse duration was independent of the selected energy or the number of shocks. For all but the M-Series defibrillator total pulse duration increased with the resistive load. The M-Series pulse always required 9.9 ms.

Table 1

Mean ratio of the energies of the positive and negative waveform phase together with the absolute values, the total delivered energy (TDE) and the impedance-normalized delivered energy (INDE)^a

Selected energy (J) ^b	Test resistive load					
	25 Ω		50 Ω		100 Ω	
	Positive	Negative	Positive	Negative	Positive	Negative
<i>Medtronic Physio-Control LIFEPAK 12</i>						
100	88 (83.9 ± 0.0)	12 (11.8 ± 0.0)	82 (80.2 ± 0.2)	18 (17.5 ± 0.0)	76 (75.2 ± 0.0)	24 (23.4 ± 0.0)
	TDE: 95.8 ± 0.0	INDE: 3.8 ± 0.0	TDE: 97.8 ± 0.2	INDE: 2.0 ± 0.0	TDE: 98.7 ± 0.0	INDE: 1.0 ± 0.0
150	87 (109.9 ± 0.8)	13 (16.6 ± 0.2)	82 (112.0 ± 0.5)	18 (25.3 ± 0.2)	76 (107.5 ± 0.3)	24 (34.6 ± 0.3)
	TDE: 126.6 ± 0.8	INDE: 5.1 ± 0.0	TDE: 137.5 ± 0.6	INDE: 2.7 ± 0.0	TDE: 142.2 ± 0.6	INDE: 1.4 ± 0.0
200	88 (169.7 ± 1.0)	12 (24.1 ± 0.2)	82 (161.5 ± 0.3)	18 (35.3 ± 0.1)	76 (149.9 ± 0.1)	24 (47.2 ± 0.0)
	TDE: 194 ± 1.2	INDE: 7.8 ± 0.0	TDE: 197.1 ± 0.1	INDE: 3.9 ± 0.0	TDE: 197.7 ± 0.1	INDE: 2.0 ± 0.0
<i>Zoll M-Series Biphasic</i>						
100	72 (50.7 ± 0.1)	28 (20.1 ± 0.1)	68 (63.4 ± 0.2)	32 (30.4 ± 0.1)	71 (84.1 ± 0.3)	29 (34.3 ± 0.1)
	TDE: 71.1 ± 0.1	INDE: 2.8 ± 0.0	TDE: 94.3 ± 0.2	INDE: 1.9 ± 0.0	TDE: 119.1 ± 0.5	INDE: 1.2 ± 0.0
150	71 (76.0 ± 0.1)	29 (30.2 ± 0.1)	67 (94.9 ± 0.1)	33 (45.6 ± 0.1)	71 (125.0 ± 0.5)	29 (51.2 ± 0.2)
	TDE: 106.8 ± 0.2	INDE: 4.3 ± 0.0	TDE: 141.3 ± 0.1	INDE: 2.8 ± 0.0	TDE: 177.5 ± 0.5	INDE: 1.8 ± 0.0
200	74 (105.1 ± 0.6)	26 (36.7 ± 0.3)	79 (164.1 ± 0.3)	21 (43.2 ± 0.1)	77 (169.4 ± 0.6)	23 (50.1 ± 0.2)
	TDE: 142.3 ± 0.7	INDE: 5.7 ± 0.0	TDE: 208.0 ± 0.2	INDE: 4.2 ± 0.0	TDE: 220.8 ± 0.7	INDE: 2.2 ± 0.0
Shock ^b						
<i>Laerdal Heartstart ForeRunner</i>						
–	88 (124.4 ± 0.6)	12 (17.4 ± 0.0)	82 (119.3 ± 0.6)	18 (26.6 ± 0.0)	87 (129.8 ± 0.3)	13 (19.8 ± 0.1)
	TDE: 142.2 ± 0.9	INDE: 5.7 ± 0.0	TDE: 146.2 ± 0.9	INDE: 2.9 ± 0.0	TDE: 149.6 ± 0.3	INDE: 1.5 ± 0.0
<i>Survivalink FirstSave STAR</i>						
First shock	82 (183.2 ± 8.0)	18 (40.2 ± 0.6)	79 (155.8 ± 2.7)	21 (42.1 ± 0.7)	81 (141.1 ± 5.4)	19 (33.6 ± 0.2)
	TDE: 223.6 ± 8.4	INDE: 8.9 ± 0.3	TDE: 198.8 ± 3.5	INDE: 4.0 ± 0.1	TDE: 174.9 ± 5.7	INDE: 1.7 ± 0.1
Second shock	83 (182.2 ± 2.3)	17 (36.4 ± 0.5)	79 (152.4 ± 0.6)	21 (41.1 ± 0.6)	80 (131.8 ± 0.9)	20 (32.7 ± 0.4)
	TDE: 219.3 ± 2.3	INDE: 8.8 ± 0.1	TDE: 194.2 ± 1.6	INDE: 3.9 ± 0.0	TDE: 165.0 ± 1.1	INDE: 1.7 ± 0.0
Following	83 (258.7 ± 3.4)	17 (52.8 ± 0.3)	79 (218.7 ± 2.6)	21 (59.0 ± 0.6)	80 (187.9 ± 1.8)	20 (46.3 ± 0.4)
	TDE: 311.6 ± 3.5	INDE: 12.5 ± 0.1	TDE: 278.1 ± 3.1	INDE: 5.6 ± 0.1	TDE: 235.0 ± 2.3	INDE: 2.4 ± 0.0

^a The absolute values are given as mean ± S.D.

^b Mean ratio of the energies of the positive and negative waveform phase, absolute values, TDE and INDE [% (J), J, J,Ω]

The LIFEPAK 12 and the M-Series showed a constant duration splitting of 5638 and 6040%, respectively. Duration splitting depended on the resistive load for the SAED. In general, the first positive pulse was longer than the second negative pulse.

Charge flow (Table 4)

For the MCED total charge flow increased with the selected energy and decreased with the resistive load. No rule could be determined for the SAED. Overall, the total charge flow is positive, i.e. the first phase carries more charge than the second phase of the shock. None of the tested defibrillators therefore showed a balanced charge flow. The maximum value was achieved by the LIFEPAK 12 (129.0 mC) and the minimum value by the M-Series defibrillator (33.4 mC).

Splitting of the charge flow into the first and second phases occurred independently of the selected energy for the LIFEPAK 12 and independently of the number of shocks for the FirstSave and showed different groupings for both defibrillators. Generally, more than 64% of the charge was delivered in the first phase.

Tilt (Table 5)

Roughly speaking, the tilt did not depend on the selected energy or the number of shocks and varied from 61.4% for the ForeRunner to -13.1% for the M-Series defibrillator. The tilt of the LIFEPAK 12 and the FirstSave decreased with the resistive load, whereas the tilt of the M-Series increased with the resistive load.

Table 2
Initial voltage (a) and current (b) given as mean \pm S.D.

	Test resistive load		
	25 Ω	50 Ω	100 Ω
(a) Selected energy (J)	Initial voltage (V)		
<i>Medtronic Physio-Control LIFEPAK 12</i>			
100	877.8 \pm 0.8	978.0 \pm 0.2	1086.0 \pm 0.3
150	981.4 \pm 1.0	1139.0 \pm 3.2	1293.0 \pm 3.8
200	1246.0 \pm 6.3	1383.0 \pm 0.7	1536.0 \pm 0.6
<i>Zoll M-Series Biphasic</i>			
100	482.8 \pm 1.5	759.3 \pm 1.3	1290.0 \pm 3.8
150	588.7 \pm 0.6	928.4 \pm 0.6	1572.0 \pm 4.3
200	706.7 \pm 7.9	1329.0 \pm 9.2	2140.0 \pm 11.6
Shock	Initial voltage (V)		
<i>Laerdal Heartstart ForeRunner</i>			
–	1535.0 \pm 10.7	1657.0 \pm 8.5	1712.0 \pm 6.0
<i>Survivalink FirstSave STAR</i>			
First shock	1570.0 \pm 36.0	1597.0 \pm 10.3	1616.0 \pm 23.4
Second shock	1573.0 \pm 10.5	1612.0 \pm 11.0	1637.0 \pm 21.9
Following shocks	1833.0 \pm 8.4	1902.0 \pm 6.7	1935.0 \pm 3.4
(b) Selected energy (J)	Initial current (A)		
<i>Medtronic Physio-Control LIFEPAK 12</i>			
100	35.1 \pm 0.0	19.6 \pm 0.0	10.9 \pm 0.0
150	39.3 \pm 0.0	22.8 \pm 0.1	12.9 \pm 0.0
200	49.8 \pm 0.3	27.7 \pm 0.0	15.4 \pm 0.0
<i>Zoll M-Series Biphasic</i>			
100	19.3 \pm 0.1	15.2 \pm 0.0	12.9 \pm 0.0
150	23.6 \pm 0.0	18.6 \pm 0.0	15.7 \pm 0.0
200	28.3 \pm 0.3	26.6 \pm 0.2	21.4 \pm 0.1
Shock	Initial current (A)		
<i>Laerdal Heartstart ForeRunner</i>			
–	61.4 \pm 0.4	33.1 \pm 0.2	17.1 \pm 0.1
<i>Survivalink FirstSave STAR</i>			
First shock	62.8 \pm 1.4	31.9 \pm 0.2	16.2 \pm 0.2
Second shock	62.9 \pm 0.4	32.2 \pm 0.2	16.4 \pm 0.2
Following shocks	73.3 \pm 0.3	38.0 \pm 0.1	19.4 \pm 0.0

Table 3
Mean ratio of positive and negative waveform phase duration together with the absolute values and the total pulse duration^a

Selected energy (J) ^b	Test resistive load					
	25 Ω		50 Ω		100 Ω	
	Positive	Negative	Positive	Negative	Positive	Negative
<i>Medtronic Physio-Control LIFEPAK 12</i>						
100	55 (5.7 ± 0.0) Total: 10.4 ± 0.0	38 (3.9 ± 0.0)	56 (7.5 ± 0.0) Total: 13.3 ± 0.0	38 (5.1 ± 0.0)	57 (9.7 ± 0.0) Total: 17.0 ± 0.0	39 (6.6 ± 0.0)
150	55 (5.9 ± 0.1) Total: 10.7 ± 0.1	38 (4.0 ± 0.0)	57 (7.7 ± 0.1) Total: 13.5 ± 0.0	38 (5.2 ± 0.0)	57 (9.8 ± 0.0) Total: 17.1 ± 0.1	39 (6.6 ± 0.0)
200	56 (5.7 ± 0.1) Total: 10.3 ± 0.0	38 (3.9 ± 0.0)	56 (7.5 ± 0.0) Total: 13.3 ± 0.0	38 (5.1 ± 0.0)	57 (9.6 ± 0.0) Total: 16.9 ± 0.0	39 (6.5 ± 0.0)
<i>Zoll M-Series Biphasic</i>						
100	60 (5.9 ± 0.0) Total: 9.9 ± 0.0	40 (4.0 ± 0.0)	60 (5.9 ± 0.0) Total: 9.9 ± 0.0	40 (4.0 ± 0.0)	60 (5.9 ± 0.0) Total: 9.9 ± 0.0	40 (4.0 ± 0.0)
150	60 (5.9 ± 0.0) Total: 9.9 ± 0.0	40 (4.0 ± 0.0)	60 (5.9 ± 0.0) Total: 9.9 ± 0.0	40 (4.0 ± 0.0)	60 (5.9 ± 0.0) Total: 9.9 ± 0.0	40 (4.0 ± 0.0)
200	60 (5.9 ± 0.0) Total: 9.9 ± 0.0	40 (4.0 ± 0.0)	60 (5.9 ± 0.0) Total: 9.9 ± 0.0	40 (4.0 ± 0.0)	60 (5.9 ± 0.0) Total: 9.9 ± 0.0	40 (4.0 ± 0.0)
Shock ^b						
<i>Laerdal Heartstart ForeRunner</i>						
–	48 (3.0 ± 0.0) Total: 6.2 ± 0.0	47 (2.9 ± 0.0)	49 (4.3 ± 0.0) Total: 8.7 ± 0.0	49 (4.3 ± 0.2)	59 (9.2 ± 0.0) Total: 15.5 ± 0.0	39 (6.0 ± 0.0)
<i>Survivalink FirstSave STAR</i>						
First shock	49 (3.6 ± 0.0) Total: 7.3 ± 0.1	45 (3.3 ± 0.1)	57 (4.8 ± 0.1) Total: 8.6 ± 0.1	39 (3.3 ± 0.1)	69 (8.1 ± 0.3) Total: 11.7 ± 0.3	28 (3.3 ± 0.0)
Second shock	48 (3.4 ± 0.1) Total: 7.1 ± 0.1	46 (3.3 ± 0.0)	56 (4.6 ± 0.0) Total: 8.3 ± 0.1	39 (3.3 ± 0.0)	66 (7.1 ± 0.1) Total: 10.8 ± 0.1	31 (3.3 ± 0.0)
Following	48 (3.4 ± 0.0) Total: 7.1 ± 0.1	46 (3.3 ± 0.0)	56 (4.7 ± 0.1) Total: 8.4 ± 0.1	39 (3.3 ± 0.0)	66 (7.2 ± 0.1) Total: 10.8 ± 0.0	31 (3.3 ± 0.0)

^a The remaining percentage of waveform duration separates positive and negative waveform phases. The absolute values are given as mean ± S.D.

^b Mean ratio of positive and negative waveform phase duration, absolute values and total pulse duration [% (ms), ms]

Table 4
Mean ratio of the charge flows of the positive and negative waveform phase together with the absolute values and the total charge flow^a

Selected energy (J) ^b	Test resistive load					
	25 Ω		50 Ω		100 Ω	
	Positive	Negative	Positive	Negative	Positive	Negative
<i>Medtronic Physio-Control LIFEPAK 12</i>						
100	76 (132.9 ± 0.0) Total: 91.0 ± 0.0	24 (−41.7 ± 0.1)	72 (106.9 ± 0.2) Total: 65.4 ± 0.1	28 (−41.5 ± 0.0)	69 (84.3 ± 0.1) Total: 45.3 ± 0.0	31 (−38.8 ± 0.0)
150	76 (154.9 ± 1.2) total: 104.5 ± 0.6	24 (−50.2 ± 0.4)	72 (127.8 ± 0.3) Total: 77.1 ± 0.3	28 (−50.4 ± 0.2)	68 (101.1 ± 0.1) Total: 53.8 ± 0.1	32 (−47.1 ± 0.2)
200	76 (188.9 ± 0.5) Total: 129.0 ± 0.4	24 (−59.4 ± 0.3)	72 (151.9 ± 0.3) Total: 92.9 ± 0.1	28 (−58.8 ± 0.2)	68 (118.6 ± 0.1) Total: 63.9 ± 0.1	32 (−54.7 ± 0.0)
<i>Zoll M-Series Biphasic</i>						
100	67 (108.5 ± 0.2) Total: 54.6 ± 0.3	33 (−54.1 ± 0.3)	64 (85.8 ± 0.2) Total: 37.9 ± 0.2	36 (−48.1 ± 0.2)	66 (69.8 ± 0.1) Total: 33.4 ± 0.1	34 (−36.5 ± 0.1)
150	67 (132.6 ± 0.2) Total: 67.0 ± 0.2	33 (−66.1 ± 0.4)	64 (105.0 ± 0.2) Total: 46.0 ± 0.1	36 (−59.1 ± 0.1)	66 (85.1 ± 0.2) Total: 40.8 ± 0.1	34 (−44.3 ± 0.2)
200	69 (155.9 ±) Total: 85.4 ± 0.3	31 (−71.0 ± 0.4)	71 (137.6 ± 0.2) Total: 80.6 ± 0.2	29 (−57.2 ± 0.2)	69 (98.2 ± 0.2) Total: 54.2 ± 0.1	31 (−44.0 ± 0.2)
Shock ^b						
<i>Laerdal Heartstart ForeRunner</i>						
–	73 (115.9 ± 0.3) Total: 74.0 ± 1.1	27 (−42.5 ± 0.0)	68 (97.4 ± 0.3) Total: 52.3 ± 0.8	32 (−45.4 ± 0.0)	76 (105.3 ± 0.1) Total: 71.4 ± 0.1	24 (−33.8 ± 0.2)
<i>Survivalink FirstSave STAR</i>						
First shock	70 (157.1 ± 3.5) Total: 88.8 ± 3.4	30 (−67.9 ± 0.2)	70 (120.4 ± 1.7) Total: 69.5 ± 1.7	30 (−50.9 ± 0.5)	76 (105.2 ± 3.4) Total: 72.4 ± 3.6	24 (−32.5 ± 0.2)
Second shock	70 (153.0 ± 2.3) Total: 89.0 ± 1.4	30 (−64.6 ± 0.5)	70 (116.4 ± 0.6) Total: 66.0 ± 0.5	30 (−50.2 ± 0.6)	75 (95.2 ± 0.3) Total: 62.9 ± 0.6	25 (−32.2 ± 0.3)
Following	70 (182.2 ± 1.6) Total: 104.2 ± 1.9	30 (−77.7 ± 0.2)	70 (140.2 ± 1.8) Total: 79.6 ± 1.8	30 (−60.4 ± 0.5)	75 (114.1 ± 0.9) Total: 75.7 ± 1.1	25 (−38.2 ± 0.3)

^a The absolute values are given as mean ± S.D.

^b Mean ratio of the charge flows of the positive and negative waveform phase, absolute values and total charge flow [% (mC), mC]

Table 5
Tilt given as mean \pm S.D.

	Test resistive load		
	25 Ω	50 Ω	100 Ω
Selected energy (J)	Tilt (%)		
<i>Medtronic Physio-Control LIFEPAK 12</i>			
100	59.0 \pm 0.1	47.9 \pm 0.0	36.1 \pm 0.0
150	57.2 \pm 0.1	46.5 \pm 0.1	35.0 \pm 0.1
200	58.6 \pm 0.1	47.6 \pm 0.1	35.7 \pm 0.0
<i>Zoll M-Series Biphasic</i>			
100	-9.4 \pm 1.2	-3.9 \pm 0.2	15.3 \pm 0.5
150	-8.5 \pm 0.0	-4.3 \pm 0.0	15.0 \pm 0.1
200	-13.1 \pm 1.8	25.6 \pm 0.2	38.1 \pm 0.3
Shock	Tilt (%)		
<i>Laerdal Heartstart ForeRunner</i>			
-	61.4 \pm 0.4	52.1 \pm 0.2	55.5 \pm 0.3
<i>Survivalink FirstSave STAR</i>			
First shock	42.2 \pm 1.2	33.2 \pm 0.4	26.3 \pm 0.9
Second shock	45.2 \pm 0.2	34.7 \pm 0.5	27.9 \pm 0.2
Following shocks	43.6 \pm 1.1	33.8 \pm 0.3	27.8 \pm 0.2

Capacitance and internal resistance (Table 6)

The LIFEPAK 12 showed a capacitance of approximately 200 μ F, which demonstrates the slow exponential decay of the waveform pulse (Fig. 1). The two SAED showed a capacitance of approximately 100 μ F, resulting in a faster exponential decay of the waveform pulse (Fig. 1). For all three defibrillators the computed internal resistances were not negligible in comparison with the resistive loads.

Discussion

The waveforms of four different biphasic defibrillators were analysed. It was found that there are significant differences in the delivered discharge waveforms. The tested defibrillators use different capacitors and different internal resistors, resulting in a varying time constant of exponential decay. The LIFEPAK 12, the ForeRunner and the FirstSave use a biphasic truncated exponential waveform with a time gap between the first and the second phases, whereas the M-Series defibrillator achieves a serrated positive waveform by adjusting the internal resistor in time and does not show any time gap between the first and the second phase.

In the case of the two defibrillators with manually selectable energy (LIFEPAK 12 and M-Series), the delivered energy deviated substantially from the selected energy. The LIFEPAK 12 always delivered less energy than selected, the M-Series less or more depending on the resistive load. One of the two semi-automated defibrillators (ForeRunner) always delivered approximately the same amount of energy, the other one (FirstSave) discharged different energies depending on the number of shocks discharged after turning on the defibrillator. The energy delivered by both MCED increased with increasing resistive load,

Table 6
Capacitance and internal resistance given as mean \pm S.D.

Selected energy (J)	Capacitance (μ F)	Internal resistance [Ω]
<i>Medtronic Physio-Control LIFEPAK 12</i>		
100	201.0 \pm 0.6	5.7 \pm 0.2
150	199.3 \pm 0.7	7.6 \pm 0.2
200	202.1 \pm 1.1	5.6 \pm 0.3
Shock	Capacitance (μ F)	Internal resistance (Ω)
<i>Laerdal Heartstart ForeRunner</i>		
–	100.2 \pm 0.6	3.1 \pm 0.3
<i>Survivalink FirstSave STAR</i>		
First shock	101.3 \pm 1.3	2.1 \pm 0.7
Second shock	101.3 \pm 1.6	2.0 \pm 0.7
Following shocks	102.3 \pm 1.8	2.1 \pm 0.9

whereas the energy delivered by the FirstSave decreased with increasing resistive load.

Impedance-normalised delivered energy of the two SAED varied from 1.5 to 12.5 J/ Ω . In comparison, patent US 5111813 proposed a defibrillation protocol with recommended impedance-normalised delivered energy values between 3 and 4.5 J/ Ω based on a study of human defibrillation using damped sinusoidal waveform shocks [84].

Generally, the initial voltage increased and the initial current decreased with the resistive load. Apart from the anomaly of the M-Series defibrillator at an energy/impedance configuration of 200 J and 100 Ω , the serrated positive waveform pulse of this defibrillator produced the lowest values for initial voltage and the second lowest value for initial current.

The LIFEPAK 12, the M-Series and the FirstSave adjust the amount of energy stored in the capacitor. The capacitor of the ForeRunner defibrillator always charged to approximately the same value, (Table 2b) taking the internal resistance into account. The tilt differed considerably among the tested defibrillators varying from - 13.1 to 61.4% and depended differently on the resistive load. Negative tilt occurs when the initial voltage of the positive phase is smaller than the absolute value of the initial voltage of the negative phase. All negative values were achieved with the M-Series defibrillator.

Concerning total phase duration, all but the M-Series defibrillator showed impedance-adjusted values.

Generally, biphasic defibrillators split their shock into a positive and a negative phase. All tested defibrillators showed greater values for the characteristic parameters of the first phase. Again, some defibrillators used a constant splitting ratio for certain characteristic parameters. None of the tested defibrillators showed a balanced charge flow.

The defibrillators tested in this study do not comprise all biphasic defibrillators in clinical use. This study was a theoretical lab study, thus the different waveforms or the defibrillators for possible efficacy were not assessed.

The various parameters chosen to describe the defibrillator waveforms are not independent in general. Initial voltage U and initial current I are related by Ohm's law $U = I \cdot R$ to the patient's transthoracic impedance R . On the other hand, charge flow Q and energy E are not proportional because $Q = \int I(t)dt$ and $E = \int I(t)^2 R dt$ are integral quantities over a

chosen time interval.

Usually, defibrillation is achieved by successful selection of energy, either manually or automatically. The energy chosen and the patient's individual transthoracic impedance determine the current through the heart. The average adult human impedance is approximately $70\text{--}80\ \Omega$ [83]. According to the AHA guidelines 'ventricular fibrillation and other cardiac arrhythmias can be terminated by electric shock when sufficient current passes through the myocardium' [18]. A promising alternative approach to defibrillation is therefore the use of electric current and charge flow instead of energy. Current-based therapy would prevent attempts to deliver inappropriately low energies to a patient with high impedance, and would prevent high-energy shocks to patients with low impedance, which result in excessive current flow, myocardial damage and failure to defibrillate [18, 83, 84].

Furthermore, possible new technical developments must also be considered. Triphasic waveforms and the use of two separate capacitors for biphasic waveforms are interesting approaches in this connection [77, 164, 165].

This study illustrates the differences in the waveform design and the varying dependence of the waveform characteristic parameters on the patient's transthoracic impedance. Optimal waveform and optimal impedance compensation for biphasic defibrillation have not yet been determined [18, 61].

Acknowledgements

We wish to thank Professor Hermann Gilly of the Department of Anaesthesia, University of Vienna, Austria, for his critical review of the manuscript. This study was supported in part by grant Nos. 4129 and 7276 of the Austrian National Bank, grant No. 98/05 of the Austrian Heart Foundation, a research grant from Bruker (Ettlingen, Germany) and the Department of Anaesthesia and Intensive Care Medicine, University of Innsbruck, Austria.

11.3 Paper 5

The following unpublished manuscript is a follow-up study of [6].

Waveform analysis of biphasic external defibrillators (II)

Klaus Rheinberger[†], Thomas Niederklapfer[‡], Karl Unterkofler[†], Michael Baubin[‡], Anton Amann^{‡1}

[†] *Fachhochschule Vorarlberg, University of Applied Sciences, Hochschulstrasse 1, 6850 Dornbirn, Austria*

[‡] *Department of Anesthesiology and Critical Care Medicine, Leopold-Franzens-University Innsbruck, Innsbruck, Austria*

Abstract

Background and Objective: Modern defibrillators use biphasic waveforms. The aim of the present laboratory study was to determine the discharge waveforms and their characteristic parameters of three manually controllable biphasic external defibrillators. *Methods and Results:* The defibrillators were charged to energies of between 100 and 200 J and discharged into resistances of between 25 and 100 Ω , simulating transthoracic impedance. While two of the tested defibrillators showed traditional biphasic truncated exponentially decaying waveforms generated by a single capacitor and of varying duration, one defibrillator applied a chopped waveform at 5 kHz of constant duration using a single capacitor for each phase. Delivered energy, current, pulse duration, and charge flow were examined with respect to the total pulse and its splitting into positive and negative phases. Two defibrillators showed constant energy splitting and constant charge flow splitting. *Conclusions:* At comparable settings for selected energy and resistance the waveforms of the tested defibrillators showed remarkable differences.

Keywords: Cardiac arrest; Defibrillation; Emergency medical services; Manual defibrillator; Transthoracic impedance

Introduction

Almost half of the patients with out-of-hospital cardiac arrest suffer from ventricular fibrillation [56]. The most effective treatment for ventricular fibrillation is electrical defibrillation [17]. In recent years the body of evidence supporting the efficacy and safety of defibrillators using biphasic waveforms has increased dramatically, and more and more manufacturers offer defibrillators, some of which have very different biphasic waveforms. Monophasic shocks are recommended to be administered at increasing energy levels of 200 J, 200 J (ERC) or 300 J (AHA), and 360 J [17]. A review of evidence concluded that nonescalating low-energy biphasic shocks achieved clinical outcomes equivalent to those of monophasic shocks [43]. State-of-the-art implantable defibrillators use biphasic waveforms [126], which have proved superior to monophasic waveforms [43, 57].

The current study is a follow-up analysis of a previous work done by our group [6], where we determined the discharge waveforms and their characteristic parameters of four

¹Corresponding author. Tel.: + 43-512-504 24636; fax: +43-512-504 24683.
E-mail addresses: anton.amann@uibk.ac.at

manually controllable biphasic external defibrillators (MCED). In the meantime two more MCEDs have become available to us and we improved our measurement setup. This study therefore completes and updates [6] with measurements of two new MCEDs and by correcting previously published data of the Medtronic Physio-Control Lifepak 12 defibrillator. In this connection we would like to clarify that, in contrast to [6], the Survivalink FirstSave STAR defibrillator utilises two separate capacitors with capacitances of 205 and 110 μF for the positive and negative phase, respectively.

Materials and Methods

The methods, especially the selected impedance values, of this study were deliberately taken over from [6] in order to assure the comparability of the results with the earlier tested defibrillators.

Three manually controllable biphasic external defibrillators were tested: the Medtronic Physio-Control Lifepak 12 (LP12), the MRL PIC (MRL), and the Schiller FRED biphasic (FRED). These defibrillators provide a variety of pulse energies, from which 100, 150, and 200 J were selected for the LP12 and MRL, and 110, 150, and 180 J for the FRED, since 100 and 200 J were not selectable for this defibrillator.

Pulse generation

The LP12 and MRL defibrillators use biphasic truncated exponentially decaying waveforms, which are generated by capacitors with nominal capacitances of 200.9 μF and 500 μF , respectively. The FRED defibrillator uses a biphasic truncated exponentially decaying waveform, which is chopped at 5 kHz. For each waveform phase a separate capacitor with a nominal capacitance of 30 μF is used (Figs. 11.3 and 11.4).

Waveform measurement

The LP12 and the MRL defibrillator were discharged into resistive loads of 25, 50, and 100 Ω , simulating patients' various transthoracic impedances. The FRED defibrillator was not dischargeable into resistive loads smaller than 31 Ω , and therefore resistive loads of 31, 50, and 100 Ω were chosen for this defibrillator. For the LP12 defibrillator, the wires of the pads were cut and connected directly to the resistive loads. The paddles of the MRL defibrillator and the pads of the FRED defibrillator were attached to two metal plates, which were connected to the resistive loads.³ The discharge voltage curve was recorded with a PC-based data acquisition system (National Instruments AT-MIO-16XE-50; and Datalogger, custom made software) using two high resistances (1 M Ω , 2.27 k Ω) in a parallel configuration (Fig. 11.5). The resistive loads and the voltage measurement had a maximum error of $\pm 1 \Omega$ and $\pm 1\%$, respectively. The discharge waveforms were digitised and stored at a sampling rate of 200 kHz and 16-bit amplitude resolution. Regular calibration guaranteed reliability and accuracy of the measurement setup. Each test was performed at least three times.

Data analysis

The recorded discharge waveforms were analysed using mathematical software (MatLab 6.5, The Mathworks Inc, Natick, MA).

³The above-described measurement setup for the LP12 defibrillator was chosen, because the delivered energies matched the selected energies slightly better as compared to using paddles or pads.

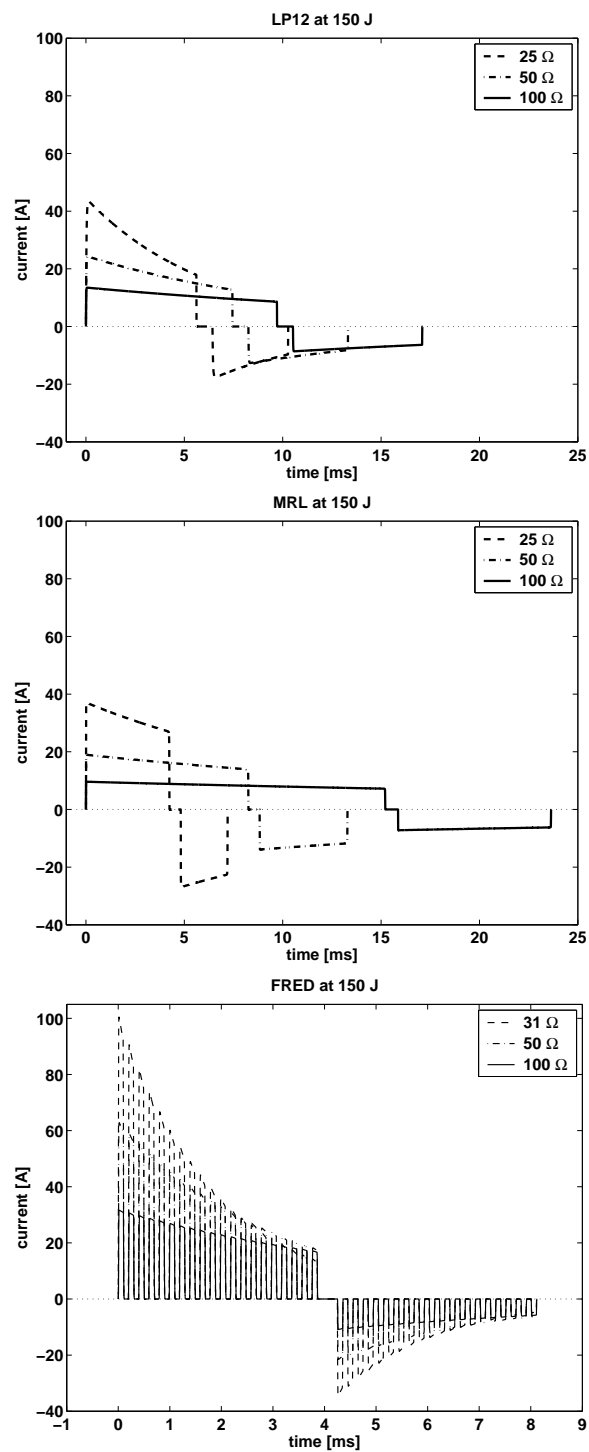


Figure 11.3: Discharge waveforms for each tested defibrillator at 150 J and 25(31), 50, and 100 Ω . Please note that the time axis for the FRED defibrillator was chosen differently in order to display the chopped pulse properly.

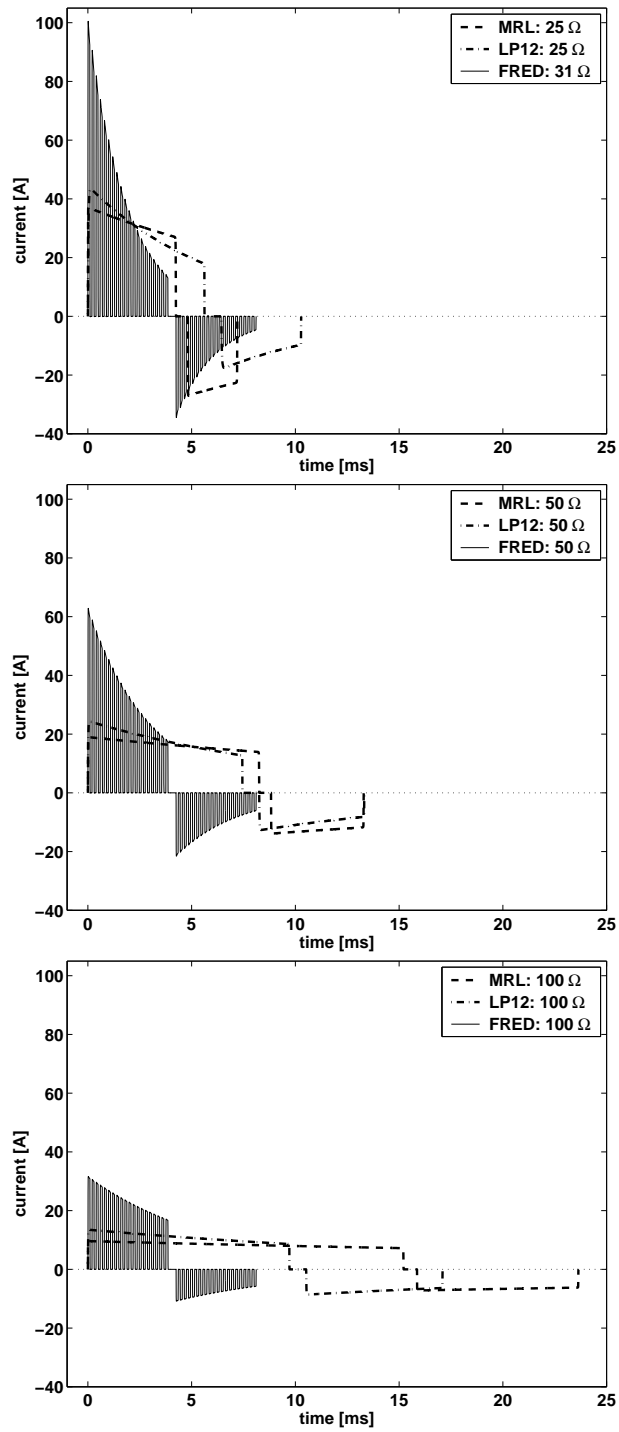


Figure 11.4: Discharge waveforms at 150 J and 25(31), 50, and 100 Ω for all tested defibrillators.

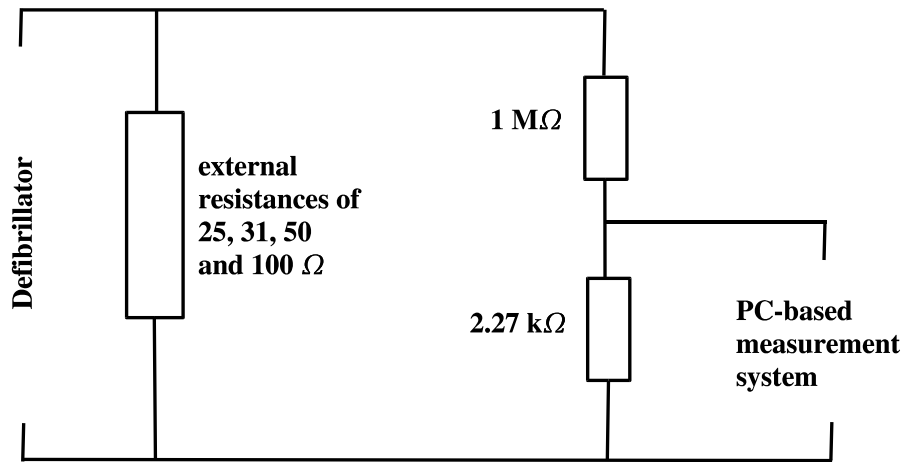


Figure 11.5: Measurement setup: The resistance of the parallel connection (1 MΩ and 2.27 kΩ) does not significantly affect the overall resistance of the circuit

The energy content of the positive and the negative waveform phase, their ratio, the total delivered energy and its percentage deviance from the selected energy were calculated using the energy formula

$$E = \frac{1}{R} \int U(t)^2 dt, \quad (11.3)$$

where $U(t)$ is the discharge voltage as a function of time, R is the chosen resistance, and the integral is to be taken over the time interval of interest. The mean and edge currents of the positive and negative waveform phase were calculated by dividing the respective voltage values by the resistances. The duration of the positive and the negative waveform phases, their ratio, and the total pulse duration were calculated. Finally, the charge flow of the positive and the negative waveform phases (Q_1 and Q_2), their ratio, the total charge flow, and the Q_1/Q_2 ratio were calculated using the charge flow formula

$$Q = \frac{1}{R} \int U(t) dt. \quad (11.4)$$

The absolute values are given as mean \pm S.D., and the ratios are given as mean values of at least three tests. Figure 11.6 depicts some of the parameters calculated for the LP12 waveform at 150 J and 50 Ω as an example.

Results

The typical current discharge waveforms for 150 J and various resistances are represented graphically in Figs. 11.3 and 11.4. The values of the characteristic parameters describing the discharge waveforms at the various energies and resistances are shown in Tables 1 - 4.

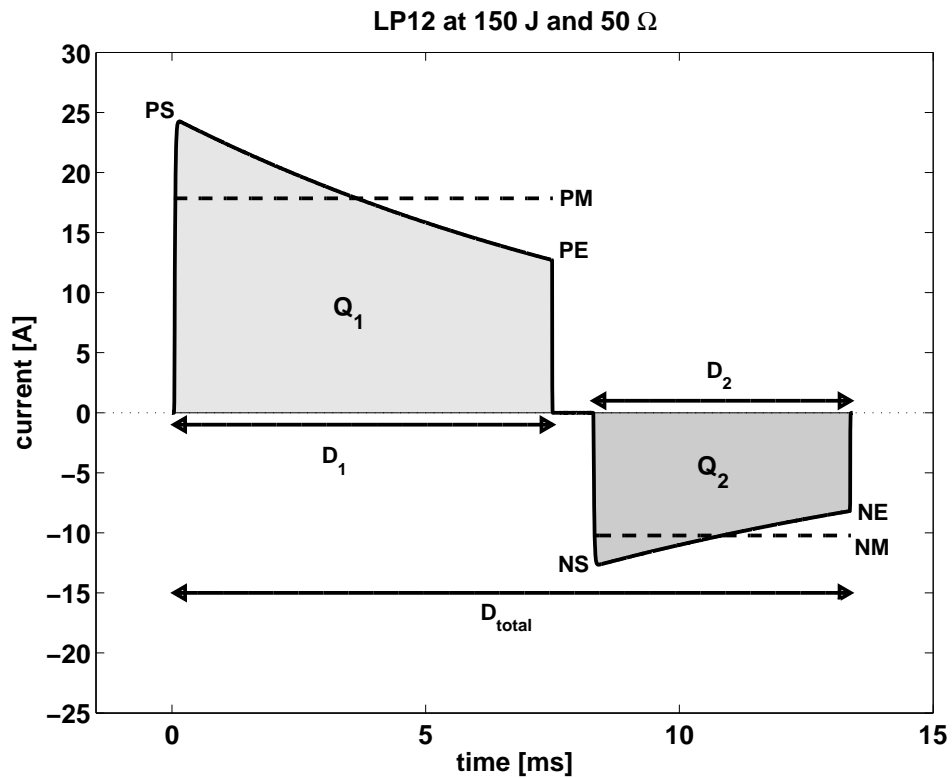


Figure 11.6: Some of the calculated parameters for the LP12 waveform at 150 J and 50 Ω : mean current of the positive (PM) and negative phase (NM), start (PS) and end (PE) edge current of the positive phase, start (NS) and end (NE) edge current of the negative phase, duration of the positive (D_1) and negative phase (D_2), duration of the total pulse (D_{total}), and the charge flow of the positive (Q_1) and negative phase (Q_2), i.e. the area under the current waveform of the positive and negative phase, respectively, cf. charge flow formula (11.4). Note that the energy content of the waveform can not be illustrated, cf. energy formula (11.3).

Discharge waveform (Figs. 11.3 and 11.4)

The LP12 and MRL defibrillators show typical biphasic truncated exponentially decaying waveforms with impedance-dependent durations. The FRED defibrillator applies a chopped biphasic truncated exponentially decaying waveform of an impedance-independent, i.e. constant, duration. In contrast to the LP12 and MRL defibrillators, the start current of the negative phase does not equal the end current of the positive phase, which reflects the fact that the FRED uses a separate capacitor for each phase. The different decaying characteristics of the three defibrillators reflect the capacitance of their different capacitors. The FRED defibrillator applies an apparently higher peak current as compared to LP12 and MRL.

Energy (Table 1)

The maximum error for the resistive loads ($\pm 1 \Omega$) and the voltage measurement ($\pm 1\%$) gives a maximum error for the calculated energy of approximately ± 6 , ± 5 , ± 4 , and $\pm 3\%$ for 25, 31, 50, and 100 Ω , respectively. Assuming no further measurement errors, the LP12 defibrillator always delivered the selected energy within this measurement accuracy, the MRL defibrillator exceeded the measurement tolerance slightly for 100 Ω , and the FRED defibrillator delivered the selected energy for 50 Ω , but delivered approximately 9% too much for 31 Ω and approx. 20% too little for 100 Ω . The LP12 defibrillator showed a variable energy splitting dependent on the resistive load. The MRL and FRED defibrillators showed a constant energy splitting of 75% - 25% and 89% - 11%, respectively.

Table 1

Mean ratio of the energies of the positive and negative waveform phase together with the absolute values, the total delivered energy (TDE) and the percentage deviance of the selected energy (DEV)¹.

Selected energy (J) ²	Test resistive load					
	25 (31) Ω		50 Ω		100 Ω	
	Positive	Negative	Positive	Negative	Positive	Negative
<i>Physio-Control-Lifepak12</i>						
100	88(84.2 \pm 0.0)	12(11.5 \pm 0.0)	82(82.4 \pm 0.0)	18(18.1 \pm 0.0)	76(77.4 \pm 0.4)	24(24.4 \pm 0.0)
	TDE: 95.7 \pm 0.0	DEV: -4.3 \pm 0.0	TDE: 100.5 \pm 0.0	DEV: 0.5 \pm 0.0	TDE: 101.8 \pm 0.4	DEV: 1.8 \pm 0.4
150	88(126.3 \pm 0.2)	12(17.5 \pm 0.1)	82(123.8 \pm 0.0)	18(27.1 \pm 0.0)	76(116.5 \pm 0.0)	24(36.5 \pm 0.0)
	TDE: 143.8 \pm 0.1	DEV: -4.1 \pm 0.1	TDE: 150.9 \pm 0.0	DEV: 0.6 \pm 0.0	TDE: 153.0 \pm 0.0	DEV: 2.0 \pm 0.0
200	88(169.0 \pm 0.1)	12(23.2 \pm 0.0)	82(165.7 \pm 0.1)	18(36.1 \pm 0.0)	76(154.9 \pm 0.0)	24(48.8 \pm 0.0)
	TDE: 192.2 \pm 0.1	DEV: -3.9 \pm 0.1	TDE: 201.7 \pm 0.1	DEV: 0.9 \pm 0.0	TDE: 203.7 \pm 0.0	DEV: 1.8 \pm 0.0
<i>MRL-PIC</i>						
100	75(71.1 \pm 0.5)	25(24.1 \pm 0.2)	75(73.4 \pm 0.1)	25(24.3 \pm 0.1)	75(71.1 \pm 0.2)	25(23.3 \pm 0.1)
	TDE: 95.2 \pm 0.4	DEV: -4.8 \pm 0.4	TDE: 97.7 \pm 0.2	DEV: -2.3 \pm 0.2	TDE: 94.4 \pm 0.3	DEV: -5.6 \pm 0.3
150	75(107.5 \pm 0.2)	25(36.3 \pm 0.1)	75(109.8 \pm 0.8)	25(36.8 \pm 0.2)	75(106.6 \pm 0.2)	25(35.1 \pm 0.1)
	TDE: 143.8 \pm 0.3	DEV: -4.1 \pm 0.2	TDE: 146.6 \pm 0.6	DEV: -2.3 \pm 0.4	TDE: 141.7 \pm 0.2	DEV: -5.5 \pm 0.2
200	75(142.2 \pm 0.4)	25(48.1 \pm 0.0)	75(146.6 \pm 0.8)	25(48.8 \pm 0.1)	75(142.2 \pm 0.6)	25(46.8 \pm 0.2)
	TDE: 190.4 \pm 0.3	DEV: -4.8 \pm 0.2	TDE: 195.5 \pm 0.9	DEV: -2.3 \pm 0.4	TDE: 189.1 \pm 0.6	DEV: -5.5 \pm 0.3
<i>Schiller-FRED</i>						
110	89(106.7 \pm 0.1)	11(13.1 \pm 0.0)	89(99.4 \pm 0.1)	11(12.2 \pm 0.0)	89(79.0 \pm 0.1)	11(9.6 \pm 0.0)
	TDE: 119.7 \pm 0.1	DEV: 8.8 \pm 0.1	TDE: 111.5 \pm 0.1	DEV: 1.4 \pm 0.1	TDE: 88.6 \pm 0.1	DEV: -19.4 \pm 0.1
150	89(145.7 \pm 0.2)	11(17.4 \pm 0.1)	89(135.8 \pm 0.0)	11(16.2 \pm 0.0)	89(108.4 \pm 0.6)	11(12.9 \pm 0.1)
	TDE: 163.1 \pm 0.2	DEV: 8.7 \pm 0.1	TDE: 152.0 \pm 0.0	DEV: 1.4 \pm 0.0	TDE: 121.3 \pm 0.7	DEV: -19.1 \pm 0.5
180	89(174.4 \pm 0.1)	11(20.5 \pm 0.1)	89(162.2 \pm 0.3)	11(19.0 \pm 0.1)	90(128.5 \pm 0.4)	10(15.1 \pm 0.0)
	TDE: 194.9 \pm 0.2	DEV: 8.3 \pm 0.1	TDE: 181.2 \pm 0.4	DEV: 0.7 \pm 0.2	TDE: 143.5 \pm 0.5	DEV: -20.3 \pm 0.3

¹ The absolute values and the percentage deviance are given as mean \pm S.D.

² Mean ratio of the energies of the positive and negative waveform phase, absolute values, TDE and DEV [% (J), J, %]

Current (Table 2)

The FRED defibrillator showed apparently higher peak current values but similar mean current values as compared to the LP12 and MRL defibrillators. For the LP12 and MRL defibrillators the start current of the negative phase equaled the end current of the positive phase. For the FRED defibrillator the start current of the negative phase equaled approximately one-third of the start current of the positive phase. All tested defibrillators showed current values that increased with increasing selected energy and decreasing resistive load.

Table 2

Peak edge currents and mean currents of the positive and negative waveform phase given as mean \pm S.D. [A]

Selected energy (J)	Test resistive load					
	25 (31) Ω		50 Ω		100 Ω	
	Positive	Negative	Positive	Negative	Positive	Negative
<i>Physio-Control-Lifepak12</i>						
100	start: 35.3 \pm 0.0 end: 14.6 \pm 0.0 mean: 23.6 \pm 0.0	start: -14.3 \pm 0.0 end: -8.0 \pm 0.0 mean: -10.9 \pm 0.0	start: 19.8 \pm 0.0 end: 10.4 \pm 0.0 mean: 14.6 \pm 0.0	start: -10.3 \pm 0.0 end: -6.7 \pm 0.0 mean: -8.4 \pm 0.0	start: 11.0 \pm 0.0 end: 7.0 \pm 0.0 mean: 8.9 \pm 0.0	start: -7.0 \pm 0.0 end: -5.2 \pm 0.0 mean: -6.1 \pm 0.0
150	start: 43.3 \pm 0.0 end: 17.9 \pm 0.1 mean: 28.9 \pm 0.0	start: -17.5 \pm 0.1 end: -9.7 \pm 0.1 mean: -13.3 \pm 0.1	start: 24.2 \pm 0.0 end: 12.7 \pm 0.0 mean: 17.9 \pm 0.0	start: -12.7 \pm 0.0 end: -8.2 \pm 0.0 mean: -10.3 \pm 0.0	start: 13.5 \pm 0.0 end: 8.6 \pm 0.0 mean: 10.8 \pm 0.0	start: -8.6 \pm 0.0 end: -6.3 \pm 0.1 mean: -7.4 \pm 0.0
200	start: 50.1 \pm 0.0 end: 20.6 \pm 0.0 mean: 33.4 \pm 0.0	start: -20.2 \pm 0.0 end: -11.1 \pm 0.0 mean: -15.2 \pm 0.0	start: 28.0 \pm 0.0 end: 14.7 \pm 0.0 mean: 20.6 \pm 0.0	start: -14.6 \pm 0.0 end: -9.4 \pm 0.0 mean: -11.8 \pm 0.0	start: 15.6 \pm 0.0 end: 10.0 \pm 0.0 mean: 12.6 \pm 0.0	start: -10.0 \pm 0.0 end: -7.4 \pm 0.0 mean: -8.6 \pm 0.0
<i>MRL-PIC</i>						
100	start: 30.3 \pm 0.0 end: 21.5 \pm 0.1 mean: 25.8 \pm 0.0	start: -22.0 \pm 0.1 end: -16.2 \pm 0.8 mean: -20.0 \pm 0.1	start: 15.5 \pm 0.0 end: 11.1 \pm 0.0 mean: 13.3 \pm 0.0	start: -11.4 \pm 0.0 end: -9.1 \pm 0.1 mean: -10.4 \pm 0.0	start: 7.9 \pm 0.0 end: 5.8 \pm 0.0 mean: 6.8 \pm 0.0	start: -5.9 \pm 0.0 end: -4.7 \pm 0.1 mean: -5.4 \pm 0.0
150	start: 37.1 \pm 0.0 end: 26.1 \pm 0.2 mean: 31.6 \pm 0.0	start: -27.0 \pm 0.0 end: -19.6 \pm 1.2 mean: -24.5 \pm 0.0	start: 19.0 \pm 0.0 end: 13.7 \pm 0.1 mean: 16.3 \pm 0.0	start: -13.9 \pm 0.0 end: -11.0 \pm 0.3 mean: -12.8 \pm 0.0	start: 9.6 \pm 0.0 end: 7.1 \pm 0.0 mean: 8.3 \pm 0.0	start: -7.2 \pm 0.0 end: -5.3 \pm 0.3 mean: -6.7 \pm 0.0
200	start: 42.7 \pm 0.0 end: 30.0 \pm 0.2 mean: 36.4 \pm 0.0	start: -31.1 \pm 0.0 end: -20.2 \pm 1.4 mean: -28.2 \pm 0.0	start: 21.9 \pm 0.0 end: 15.7 \pm 0.0 mean: 18.7 \pm 0.0	start: -16.1 \pm 0.0 end: -11.5 \pm 0.5 mean: -14.7 \pm 0.0	start: 11.1 \pm 0.0 end: 8.2 \pm 0.0 mean: 9.6 \pm 0.0	start: -8.3 \pm 0.0 end: -6.4 \pm 0.4 mean: -7.7 \pm 0.0
<i>Schiller-FRED</i>						
110	start: 86.0 \pm 0.0 end: 11.3 \pm 0.0 mean: 18.5 \pm 0.0	start: -29.9 \pm 0.0 end: -4.0 \pm 0.0 mean: -6.5 \pm 0.0	start: 53.8 \pm 0.0 end: 14.8 \pm 0.0 mean: 15.2 \pm 0.0	start: -18.7 \pm 0.0 end: -5.2 \pm 0.0 mean: -5.4 \pm 0.0	start: 27.1 \pm 0.0 end: 14.3 \pm 0.0 mean: 10.1 \pm 0.0	start: -9.4 \pm 0.0 end: -5.0 \pm 0.0 mean: -3.5 \pm 0.0
150	start: 100.5 \pm 0.1 end: 13.2 \pm 0.0 mean: 21.7 \pm 0.0	start: -34.5 \pm 0.1 end: -4.6 \pm 0.0 mean: -7.5 \pm 0.0	start: 62.8 \pm 0.0 end: 17.4 \pm 0.0 mean: 17.8 \pm 0.0	start: -21.6 \pm 0.0 end: -6.0 \pm 0.0 mean: -6.2 \pm 0.0	start: 31.7 \pm 0.1 end: 16.7 \pm 0.0 mean: 11.8 \pm 0.0	start: -10.9 \pm 0.1 end: -5.8 \pm 0.0 mean: -4.1 \pm 0.0
180	start: 109.8 \pm 0.1 end: 14.5 \pm 0.0 mean: 23.7 \pm 0.0	start: -37.5 \pm 0.0 end: -5.0 \pm 0.0 mean: -8.2 \pm 0.0	start: 68.6 \pm 0.1 end: 19.0 \pm 0.0 mean: 19.5 \pm 0.0	start: -23.4 \pm 0.0 end: -6.5 \pm 0.0 mean: -6.7 \pm 0.0	start: 34.5 \pm 0.1 end: 18.2 \pm 0.0 mean: 12.9 \pm 0.0	start: -11.8 \pm 0.0 end: -6.2 \pm 0.0 mean: -4.4 \pm 0.0

Duration (Table 3)

Generally, total pulse duration was independent of the selected energy. For both the LP12 and MRL defibrillator total pulse duration increased with the resistive load. The FRED pulse always required 8.1 ms. The LP12 and MRL defibrillators applied a longer positive phase, whereas the FRED pulse showed balanced duration splitting.

Charge flow (Table 4)

The absolute charge flow values generally increased with increasing selected energy. At fixed energy selection, the absolute charge flow of the positive phase was approximately

Table 3

Mean ratio of positive and negative waveform phase duration together with the absolute values and the total pulse duration.¹

Selected energy (J) ²	Test resistive load					
	25 (31) Ω		50 Ω		100 Ω	
	Positive	Negative	Positive	Negative	Positive	Negative
<i>Physio-Control-Lifepak12</i>						
100	55(5.7±0.0)	37(3.7±0.0)	56(7.5±0.0)	38(5.1±0.0)	57(9.7±0.1)	38(6.5±0.1)
	Total: 10.2±0.0		Total: 13.3±0.0		Total: 17.0±0.1	
150	55(5.6±0.0)	37(3.8±0.0)	56(7.5±0.0)	38(5.1±0.0)	57(9.7±0.0)	38(6.6±0.0)
	Total: 10.3±0.0		Total: 13.3±0.0		Total: 17.1±0.0	
200	55(5.7±0.0)	37(3.9±0.0)	56(7.5±0.0)	38(5.1±0.0)	57(9.6±0.0)	38(6.5±0.0)
	Total: 10.3±0.0		Total: 13.4±0.0		Total: 17.0±0.0	
<i>MRL-PIC</i>						
100	59(4.2±0.0)	33(2.4±0.0)	62(8.3±0.0)	34(4.5±0.0)	64(15.3±0.1)	33(7.9±0.1)
	Total: 7.2±0.0		Total: 13.3±0.0		Total: 23.7±0.3	
150	59(4.2±0.0)	33(2.4±0.0)	62(8.2±0.1)	34(4.5±0.0)	64(15.2±0.1)	33(7.8±0.0)
	Total: 7.2±0.0		Total: 13.3±0.1		Total: 23.6±0.1	
200	59(4.2±0.0)	33(2.4±0.0)	62(8.3±0.0)	34(4.5±0.0)	65(15.3±0.1)	33(7.8±0.1)
	Total: 7.2±0.0		Total: 13.3±0.0		Total: 23.7±0.2	
<i>Schiller-FRED</i>						
110	48(3.9±0.0)	48(3.9±0.0)	48(3.9±0.0)	48(3.9±0.0)	48(3.9±0.0)	48(3.9±0.0)
	Total: 8.1±0.0		Total: 8.1±0.0		Total: 8.1±0.0	
150	48(3.9±0.0)	48(3.9±0.0)	48(3.9±0.0)	48(3.9±0.0)	48(3.9±0.0)	48(3.9±0.0)
	Total: 8.1±0.0		Total: 8.1±0.0		Total: 8.1±0.0	
180	48(3.9±0.0)	48(3.9±0.0)	48(3.9±0.0)	48(3.9±0.0)	48(3.9±0.0)	48(3.9±0.0)
	Total: 8.1±0.0		Total: 8.1±0.0		Total: 8.1±0.0	

¹ The remaining percentage of waveform duration separates positive and negative waveform phases.

The absolute values are given as mean ± S.D.

² Mean ratio of the positive and negative waveform phase duration, absolute values and total pulse duration [% (ms), ms]

constant for the MRL defibrillator. Overall, the total charge flow was positive, i.e. the positive phase carried more charge than the negative phase. The LP12 defibrillator showed variable Q_2/Q_1 ratios dependent on the resistive load, whereas the MRL and FRED defibrillators always applied an approximately constant Q_2/Q_1 ratio.

Discussion

A previous study investigated traditional and rectilinear biphasic truncated exponentially decaying waveforms [6]. The present study completes and updates that work showing the different biphasic waveform designs of three defibrillator manufacturers by comprising the parameters energy, current, duration and charge flow.

In contrast to the LP12 and MRL defibrillators, which apply traditional biphasic truncated exponentially decaying waveforms of similar characteristic parameters, the waveform design of the FRED defibrillator has several different features. The FRED defibrillator applies a chopped waveform and uses a single capacitor for each phase. It has a fixed pulse duration just as the Zoll M-Series Biphasic [6]. One possible way of comparing the chopped FRED waveform with the continuously decaying waveforms of LP12 and MRL would be to use the local mean amplitude of the FRED discharge waveform, which has approximately half amplitude. In contrast to the LP12 defibrillator, the MRL and FRED defibrillators showed both constant energy splitting and constant charge flow splitting.

Table 4

Mean ratio of the charge flows of the positive and negative waveform phase together with the absolute values, the total charge flow and the Q_2/Q_1 -ratio.¹

Selected energy (J) ²	Test resistive load					
	25 (31) Ω		50 Ω		100 Ω	
	Positive	Negative	Positive	Negative	Positive	Negative
<i>Physio-Control-Lifepak12</i>						
100	77(133.6±0.0)	23(-40.9±0.0)	72(108.9±0.0)	28(-42.5±0.0)	68(85.8±0.6)	32(-39.8±0.1)
	Total: 92.7±0.0	Q_2/Q_1 : 30.6±0.0	Total: 66.4±0.0	Q_2/Q_1 : 39.0±0.0	Total: 46.0±0.4	Q_2/Q_1 : 46.4±0.2
150	76(163.3±0.4)	24(-51.1±0.0)	72(133.4±0.0)	28(-52.0±0.0)	68(105.5±0.0)	32(-48.8±0.0)
	Total: 112.1±0.4	Q_2/Q_1 : 31.3±0.1	Total: 81.5±0.0	Q_2/Q_1 : 39.0±0.0	Total: 56.7±0.0	Q_2/Q_1 : 46.2±0.0
200	76(189.2±0.1)	24(-59.0±0.0)	72(154.7±0.0)	28(-60.0±0.0)	68(121.2±0.0)	32(-56.2±0.0)
	Total: 130.2±0.0	Q_2/Q_1 : 31.2±0.0	Total: 94.7±0.0	Q_2/Q_1 : 38.8±0.0	Total: 65.0±0.0	Q_2/Q_1 : 46.4±0.0
<i>MRL-PIC</i>						
100	69(108.9±0.9)	31(-47.8±0.2)	70(109.5±0.1)	30(-46.6±0.2)	71(103.9±0.6)	29(-42.8±0.4)
	Total: 61.1±1.1	Q_2/Q_1 : 43.9±0.5	Total: 62.9±0.2	Q_2/Q_1 : 42.5±0.2	Total: 61.1±0.2	Q_2/Q_1 : 41.2±0.2
150	70(134.4±0.1)	30(-58.6±0.1)	70(133.7±1.1)	30(-57.3±0.2)	71(126.9±0.4)	29(-52.3±0.2)
	Total: 75.7±0.0	Q_2/Q_1 : 43.6±0.0	Total: 76.4±1.3	Q_2/Q_1 : 42.8±0.5	Total: 74.6±0.4	Q_2/Q_1 : 41.2±0.1
200	70(154.5±0.3)	30(-67.6±0.1)	70(155.0±0.6)	30(-66.0±0.1)	71(147.0±0.4)	29(-60.5±0.5)
	Total: 87.0±0.4	Q_2/Q_1 : 43.7±0.1	Total: 89.0±0.5	Q_2/Q_1 : 42.6±0.1	Total: 86.5±0.4	Q_2/Q_1 : 41.2±0.3
<i>Schiller-FRED</i>						
110	74(71.7±0.0)	26(-25.2±0.0)	74(59.1±0.0)	26(-20.7±0.0)	74(39.1±0.0)	26(-13.7±0.0)
	Total: 46.5±0.0	Q_2/Q_1 : 35.2±0.0	Total: 38.3±0.0	Q_2/Q_1 : 35.1±0.0	Total: 25.4±0.0	Q_2/Q_1 : 35.0±0.0
150	74(83.9±0.0)	26(-29.2±0.0)	74(69.1±0.0)	26(-24.0±0.0)	74(45.8±0.1)	26(-15.9±0.1)
	Total: 54.7±0.0	Q_2/Q_1 : 34.7±0.0	Total: 45.1±0.0	Q_2/Q_1 : 34.7±0.0	Total: 30.0±0.0	Q_2/Q_1 : 34.6±0.1
180	74(91.8±0.0)	26(-31.6±0.0)	74(75.5±0.1)	26(-26.0±0.0)	74(49.9±0.1)	26(-17.1±0.0)
	Total: 60.2±0.0	Q_2/Q_1 : 34.4±0.0	Total: 49.5±0.0	Q_2/Q_1 : 34.4±0.0	Total: 32.8±0.1	Q_2/Q_1 : 34.3±0.0

¹ The absolute values and the Q_2/Q_1 ratio are given as mean ± S.D.

² Mean ratio of the charge flows of the positive and negative waveform phase duration, absolute values, total charge flow and the Q_2/Q_1 ratio [% (mC), mC, %]

Theory

Discussions about exponentially decaying discharge waveforms, no matter whether they are monophasic, biphasic, or additionally chopped, use and sometimes even confuse quite a number of terms, such as energy, current and charge flow. We aim to clarify the mathematical relationship between these parameters, taking as archetypical example a capacitor with capacitance C , which is discharged with initial current I_0 into resistance R for duration T . The discharge current and discharge voltage are $I(t) = I_0 e^{-\frac{t}{RC}}$ and $U(t) = U_0 e^{-\frac{t}{RC}}$, respectively, where $U_0 = I_0 R$ according to Ohm's Law. The energy E delivered during time T can be calculated as

$$E = \int_0^T U(t)I(t)dt = \frac{CU_0^2}{2}(1 - e^{-\frac{2T}{RC}}) = \frac{CR^2I_0^2}{2}(1 - e^{-\frac{2T}{RC}}), \quad (11.5)$$

and the charge flow Q during time T can be calculated as

$$Q = \int_0^T I(t)dt = CU_0(1 - e^{-\frac{T}{RC}}) = CRI_0(1 - e^{-\frac{T}{RC}}).$$

Combining these two results gives

$$E = U_0Q - \frac{Q^2}{2C} = \frac{Q^2}{C(1 - e^{-\frac{T}{RC}})} - \frac{Q^2}{2C} = \frac{Q^2}{2C} \coth\left(\frac{T}{2RC}\right) \quad (11.6)$$

These formulas reflect the generally non-linear relationships among various types of quantities, namely the integral quantities energy and charge flow, the time-dependent quantities

discharge current and discharge voltage, the pulse design parameters C , T , and U_0 , and the patient's impedance R . Specifically, formula (11.6) shows that the same charge flow Q can be achieved with different energies E depending on the duration T of the pulse. This archetypical example considers only the first phase of a biphasic truncated exponentially decaying waveform, but the respective formulas for (chopped) biphasic truncated exponentially decaying waveforms follow easily.

Energy vs. Current

Based on the law of electrostimulation [81], the AHA/ERC guidelines state that 'defibrillation is accomplished by passage of sufficient electric current (amperes) through the heart' [17]. Concurrently, the operation of MCEs, the recommended defibrillation algorithms and most of the studies are energy-based. However, this study and the above considerations show that the electric current depends on more parameters than energy alone and can therefore be very different for the same energy. This obvious discrepancy between the theory and practice of defibrillation most likely has technical and historical reasons, and the AHA/ERC guidelines further state that 'a promising alternative approach to defibrillation is the use of electric current (amperes) instead of energy (joules)'.

Energy and (peak-) current are independent parameters of a defibrillation waveform, i.e. the same energy can be delivered with different currents (cf. formula (11.5)). Our measurements illustrate this fact, e.g. Fig. 11.4 shows the current curves of the different defibrillators at 150 J. Thus, even high energy biphasic defibrillation is associated in some waveforms with moderate peak current (a factor of interest for damage).

Optimal waveform

Unfortunately, there is no generally valid model of defibrillation, from which a patient's optimal biphasic defibrillation waveform can be derived. The diversity in the waveform design of the various manufacturers reflects this fact. The two crucial questions are: which waveform parameters in which combination are relevant for the efficacy of a defibrillation waveform, and which waveform parameters reflect the extent of functional and morphological damage to the heart? Most publications about the design of a waveform refer to the Weiss-Lapicque strength-duration relationship and the charge-burping theory [81, 60, 93, 164, 142, 146, 162], while e.g. Geddes et al. [61] use the Q_2/Q_1 ratio. Niebauer et al. [111] showed that at least part of the myocardial depression following a single monophasic pulse defibrillation was caused by the release of K^+ from the myocardial cells, which was linearly proportional to the charge delivered to the heart. Xie et al. [161] showed that the magnitude of myocardial dysfunction was related in part to the energy delivered during electrical defibrillation. On the other hand, Lumb et al. [101] showed that at equivalent energy levels a truncated exponential waveform caused significantly less myocardial damage than did a damped sine waveform with a higher peak current. It thus appears that research has not yet determined the optimal defibrillation waveform.

Limitations

The defibrillators tested in this study do not comprise all biphasic external defibrillators in clinical use, nor were the efficacy and safety of the tested defibrillators assessed. In this theoretical lab study the patient's transthoracic impedance was simulated with resistances of 25, 31, 50, and 100 Ω .

Acknowledgements

We wish to thank Kenneth F. Olson, Cardiac Science Inc., and Joe Sullivan, Medtronic Physio-Control, for their helpful correspondence in order to revise some results of our previous publication.

List of Some Important Abbreviations

ACF	autocorrelation function
ACLS	advanced cardiac life support
AED	automated external defibrillator
AHA	American heart association
ALR	adaptive lagged regression
ATS	adaptive time-dependent seasonal
BLS	basic life support
CPP	coronary perfusion pressure
CPR	cardiopulmonary resuscitation
ECG	electrocardiogram
EMD	electromechanical dissociation
FS	sampling frequency
IID	independent identically distributed
LAMP	Linux Apache MySQL PHP (or Perl, or Python)
MLE	maximum likelihood estimation
MMSE	minimum mean squared error
MSE	mean squared error
NSR	normal sinus rhythm
OLS	ordinary least squares
PEA	pulseless electrical activity
ROC	receiver operating characteristic
rSNR	restored signal-to-noise ratio
ROSC	return of spontaneous circulation
SCA	sudden cardiac arrest
SI	survival index
SNR	signal-to-noise ratio
TS	time series
VF	ventricular fibrillation
VT	ventricular tachycardia
WN	white noise
XML	extendible markup language

Acknowledgements

I would like to thank the following people for their cordial, patient and competent help!

In alphabetical order:

Ulrich Achleitner
Anton Amann
Michael Baubin
Thomas Breuer
Peter Hamm
Anette Krismer
Wolfgang Lederer
Hannes Lienhart
Viktoria Mayr
Bernhard Meusburger
Andreas Neuraüter
Thomas Niederklapfer
Guy Poupart
Claus Rädler
Alex Schmid
Christian Schmittinger
Karl-Heinz Stadlbauer
Thomas Steinberger
Ulrich Strohmenger
Robert Tratnig
Karl Unterkofler
Horst Wagner-Berger
Volker Wenzel

Curriculum Vitae

Name: Klaus Rheinberger
 Date of Birth: 28.11.1972
 Address: University of Applied Sciences
 Fachhochschule Vorarlberg,
 Hochschulstrasse 1, A-6850 Dornbirn
 Austria, Europe
 Phone: +43 (0)5572 792 7111
 Fax: +43 (0)5572 792 9510
 E-mail: klaus.rheinberger@fhv.at
 Web: <http://www2.staff.fh-vorarlberg.ac.at/~kr>

28.11.1972	born in Feldkirch, Austria; Austrian citizen
1979 - 1983	elementary school in Feldkirch-Altenstadt
1983 - 1991	secondary school at the Bundesgymnasium in Feldkirch
october 1991	starting studies of physics at the Universität Innsbruck
3.2.1994	first diploma examination with distinction
summer term 1994	Erasmus in Padua, Italy
october 1996	starting studies of high school teacher in physics and mathematics
spring 1998	starting M.Sc. thesis in physics with Prof. Gebhard Grübl at the Institute of Theoretical Physics. thesis title: “Die Differentialgeometrie der Schrödingergleichung.”
feb. 1999 - jan. 2000	civil service at the hospital of Innsbruck
13.4.2000	final diploma examination with distinction
june 2000 - now	doctoral thesis (Ph.D.) with Prof. Anton Amann at the Department of Anesthesiology and Critical Care Medicine.
2002 - feb. 2004	coorganisation of the study <i>Defibrillation in out-of-hospital cardiac arrest patients: a comparison of the mono- and biphasic defibrillation pulses of MRL</i>
feb. 2004 - now	research assistant and assistant lecturer at the Research Center for Process and Product Engineering, University of Applied Sciences Vorarlberg.

List of Publications

Theoretical Physics

1. Grübl G., Moser R., Rheinberger K. *Bohmian Trajectories and Klein's Paradox*. J Phys A: Math Gen 34(13):2753-64, 2001.
2. Grübl G., Rheinberger K. *Time of Arrival from Bohmian Flow*. J Phys A: Math Gen 35(12):2907-24, 2002.

Life Sciences - Biomathematics

1. Achleitner U., Rheinberger K., Furtner B., Amann A., Baubin M. *Waveform Analysis of Biphasic External Defibrillators*. Resuscitation 50(1): 61-70, 2001.
2. Amann A., Rheinberger K., Achleitner U. *Algorithms to analyze ventricular fibrillation signals*. Curr Opin Crit Care 7(3):152-6, 2001.
3. Amann A., Rheinberger K., Achleitner U., Krismer A.C., Lingnau W., Lindner K.H., Wenzel V. *Prediction of defibrillation outcome employing a new combination of mean frequency and amplitude in porcine models of cardiac arrest*. Anesth Analg 95(3):716-22, 2002.
4. Voelckel W.G., Raedler C., Wenzel V., Lindner K.H., Krismer A.C., Schmittinger C.A., Herff H., Rheinberger K., Königsrainer A. *Arginine vasopressin, but not epinephrine, improves survival in uncontrolled hemorrhagic shock after liver trauma in pigs*. Crit Care Med 31(4):1160-5, 2003.
5. Stadlbauer K.H., Rheinberger K., Wenzel V., Raedler C., Krismer A.C., Strohmenger H.U., Augenstein S., Wagner-Berger H.G., Voelckel W.G., Lindner K.H., Amann A. *The effects of nifedipine on ventricular fibrillation mean frequency in a porcine model of prolonged cardiopulmonary resuscitation*. Anesth Analg 97(1):226-30, 2003.
6. Stadlbauer K.H., Wagner-Berger H.G., Raedler C., Voelckel W.G., Wenzel V., Krismer A.C., Rheinberger K., Nussbaumer W., Pressmar D., Lindner K.H., Königsrainer A. *Vasopressin, but not fluid resuscitation, enhances survival in a liver trauma model with uncontrolled and otherwise lethal hemorrhagic shock in pigs*. Anesthesiology 98(3):699-704, 2003.
7. Stadlbauer K.H., Wagner-Berger H.G., Wenzel V., Voelckel W.G., Krismer A.C., Klima G., Rheinberger K., Pechlaner S., Mayr V.D., Lindner K.H. *Survival with full neurologic recovery after prolonged cardiopulmonary resuscitation with a combination of vasopressin and epinephrine in pigs*. Anesth Analg 96(6):1743-9, 2003.

8. Wagner-Berger H.G., Wenzel V., Stallinger A., Voelckel W.G., Rheinberger K., Stadlbauer K.H., Augenstein S., Dörge V., Lindner K.H., Hörmann C. *Decreasing peak flow rate with a new bag-valve-mask device: effects on respiratory mechanics, and gas distribution in a bench model of an unprotected airway.* Resuscitation 57(2):193-9, 2003.
9. Wagner-Berger H.G., Wenzel V., Stallinger A., Voelckel W.G., Rheinberger K., Augenstein S., Herff H., Idris A.H., Dörge V., Lindner K.H., Hörmann C. *Optimizing bag-valve-mask ventilation with a new mouth-to-bag resuscitator.* Resuscitation 56(2):191-8, 2003.
10. Lederer W., Rheinberger K., Lischke V., Amann A. *Analyse von Flimmersignalen zur Abschätzung der Defibrillierbarkeit beim Kammerflimmern.* Anaesthesiol Intensivmed Notfallmed Schmerzther 38(12):787-94, 2003.
11. Wagner-Berger H.G., Wenzel V., Voelckel W.G., Rheinberger K., Stadlbauer K.H., Müller T., Augenstein S., von Goedecke A., Lindner K.H., Keller C. *A pilot study to evaluate the SMART BAG: a new pressure-responsive, gas-flow limiting bag-valve-mask device.* Anesth Analg 97(6): 1686-9, 2003.
12. Mayr V.D., Wenzel V., Müller T., Antretter H., Rheinberger K., Lindner K.H., Strohmenger H.U., *Effects of vasopressin on left anterior descending coronary artery blood flow during extremely low cardiac output.* Resuscitation 62(2):229-35, 2004.
13. Rheinberger K., Unterkofler K., Baubin M., Amann A., *Defibrillatortechnik - Arrhythmiedetektion und EKG Analyse.* Promed, Nr.9, 2004.

Abstracts, Proceedings

1. Rheinberger K., Achleitner U., Amann A., Baubin M. *Waveform analysis of biphasic external defibrillators* (Abstract presented at the 30th International Educational & Scientific Symposium "Critical Care: Blending Science and Compassion" February 10-14, 2001, The Moscone Center, San Francisco, CA, USA) Crit Care Med 28, No 12 (Suppl.), A69, 2000.
2. Achleitner U., Rheinberger K., Furtner B., Amann A., Baubin M. *Waveform analysis of biphasic external defibrillators* European J Anesth 18, Supplement 21: A-409, 2001.
3. Amann A., Rheinberger K., Achleitner U., Krismer A.C., Lingnau W., Lindner K.H., Wenzel V. *Prediction of defibrillation outcome combining frequency and amplitude in porcine models of cardiac arrest* British J Anaesth. 87, Supplement 1, AO02, 2001.
4. Amann A., Rheinberger K., Krismer A.C., Lingnau W., Lindner K.H., Wenzel V. *Prediction of defibrillation outcome combining amplitude and frequency in porcine models of cardiac arrest* Anesth Analg 94 (S-1-S-350), S30, 2002.
5. Amann A., Rheinberger K., Achleitner U., Krismer A.C., Lingnau W., Lindner K.H., Wenzel V. *A comparison of different ventricular fibrillation analysing strategies to predict successful countershock* Eur. J. Anesth. 19, Supplement 24, A-665, 2002.

6. Stadlbauer K.H., Wagner-Berger H.G., Raedler C., Voelckel W.G., Wenzel V., Krismer A.C., Rheinberger K., Pressmar D., Lindner K.H., Koenigsrainer A. *Survival with full vital organ function recovery after uncontrolled hemorrhagic shock in a penetrating liver trauma model with vasopressin in pigs*, Scientific Congress of the European Resuscitation Council, Florence, October 3-5, 2002 Fortezza da Basso, und AHA Chicago 2002.
7. Stadlbauer K.H., Wagner-Berger H.G., Wenzel V., Voelckel W.G., Krismer A.C., Klima G., Rheinberger K., Pressmar D., Lindner K.H. *Survival with full neurologic recovery after prolonged cardiopulmonary resuscitation with a combination of vasopressin and epinephrine in pigs*, 6th Scientific Congress of the European Resuscitation Council, Florence, October 3-5, 2002 Fortezza da Basso, und AHA Chicago 2002.
8. Wagner-Berger H.G., Wenzel V., Stallinger A., Voelckel W.G., Rheinberger K., Stadlbauer K.H., Augenstein S., Döriges V., Lindner K.H., Hörmann C. *Decreasing peak flow rate with a new bag valve mask device: effects on respiratory mechanics, and gas distribution in a bench model of an unprotected airway*, 6th Scientific Congress of the European Resuscitation Council, Florence, October 3-5, 2002 Fortezza da Basso, und AHA Chicago 2002.
9. Wagner-Berger H.G., Wenzel V., Stallinger A., Voelckel W.G., Rheinberger K., Augenstein S., Herff H., Idris A.H., Döriges V., Lindner K.H., Hörmann C. *Optimizing bag-valve-mask ventilation with a new mouth-to-bag resuscitator*, 6th Scientific Congress of the European Resuscitation Council, Florence, October 3-5, 2002 Fortezza da Basso, und AHA Chicago 2002.
10. Rheinberger K., Krismer A.C., Lingnau W., Wenzel V., Amann A. *A comparison of different ventricular fibrillation parameters to predict successful countershock*, 6th Scientific Congress of the European Resuscitation Council, Florence, October 3-5, 2002 Fortezza da Basso.
11. Rheinberger K., Amann A., Baubin M. *Waveform analysis of two novel biphasic defibrillators*, 6th Scientific Congress of the European Resuscitation Council, Florence, October 3-5, 2002 Fortezza da Basso.
12. Rheinberger K., *Moderne Methoden für Flimmerdetektion und EKG-Analyse*, Journal für Anästhesie und Intensivbehandlung Nr. 1-2004 S.209, 2004.
13. Rheinberger K., Baubin M., Unterkofler K., Amann A., *Removal of Resuscitation Artefacts from Ventricular Fibrillation ECG Signals Using Kalman Methods*. Proceedings of the 32nd annual international conference on Computers in Cardiology, Lyon, 2005;32:555-558.

Conferences

1. 23rd Annual Meeting of the EAA in Graz, Austria, August 2001.
2. 6th Scientific Congress of the European Resuscitation Council, Florence, October 3-5, 2002 Fortezza da Basso.
3. 32nd Annual International Conference on Computers in Cardiology, Lyon, France, September 25-28, 2005

Invited Lectures

1. 6. Deutscher Interdisziplinärer Kongress für Intensivmedizin und Notfallmedizin (divi2002), 13.-16. November 2002, Hamburg, Deutschland: *Neue Trends in der Arrhythmiedetektion.*
2. 10. Kongress der Österreichischen Gesellschaft für Notfall- und Katastrophenmedizin, 4.-5. September 2003, Wien, Österreich: *Defibrillatortechnik und EKG-Analyse.*
3. 14. Symposium Intensivmedizin/Intensivpflege, 18.-20 Februar 2004, Bremen, Deutschland: *Moderne Technologien für Flimmerdetektion und EKG-Analyse.*
4. 13. Innsbrucker Notfallsymposium, 5.-6. November 2004, Innsbruck, Österreich: *Auswertungsmodelle von Kammerflimmern*

Bibliography

- [1] S.O. Aase, T. Eftestol, J.H. Husoy, K. Sunde, and P.A. Steen. CPR artifact removal from human ECG using optimal multichannel filtering. *IEEE Trans Biomed Eng*, 47(11):1440–9, 2000.
- [2] S.O. Aase and H. Myklebust. Compression depth estimation for CPR quality assessment using DSP on accelerometer signals. *IEEE Trans Biomed Eng*, 49(3):263–8, 2002.
- [3] U. Achleitner. *Analysis of the Ventricular Fibrillation Electrocardiogram. A Comparison of Parameters*. PhD thesis, University of Innsbruck, Austria, December 2002.
- [4] U. Achleitner, A. Amann, M. Stoffaneller, and M. Baubin. Waveforms of external defibrillators: analysis and energy contribution. *Resuscitation*, 41(2):193–200, 1999.
- [5] U. Achleitner, A. Amann, M. Stoffaneller, and M. Baubin. Corrigendum to "Waveforms of external defibrillators: analysis and energy contribution". *Resuscitation*, 44(2):139, 2000.
- [6] U. Achleitner, K. Rheinberger, B. Furtner, A. Amann, and M. Baubin. Waveform analysis of biphasic external defibrillators. *Resuscitation*, 50(1):61–70, 2001.
- [7] U. Achleitner, V. Wenzel, H.U. Strohmenger, A.C. Krismer, K.G. Lurie, K.H. Lindner, and A. Amann. The effects of repeated doses of vasopressin or epinephrine on ventricular fibrillation in a porcine model of prolonged cardiopulmonary resuscitation. *Anesth Analg*, 90(5):1067–75, 2000.
- [8] U. Achleitner, V. Wenzel, H.U. Strohmenger, K.H. Lindner, M.A. Baubin, A.C. Krismer, V.D. Mayr, and A. Amann. The beneficial effect of basic life support on ventricular fibrillation mean frequency and coronary perfusion pressure. *Resuscitation*, 51(2):151–8, 2001.
- [9] A. Amann, U. Achleitner, H. Antretter, J.O. Bonatti, A.C. Krismer, K.H. Lindner, J. Rieder, V. Wenzel, W.G. Voelckel, and H.U. Strohmenger. Analysing ventricular fibrillation ECG-signals and predicting defibrillation success during cardiopulmonary resuscitation employing N(alpha)-histograms. *Resuscitation*, 50(1):77–85, 2001.
- [10] A. Amann, G. Mayr, and H.U. Strohmenger. N(alpha)-histogram analysis of the ventricular fibrillation ECG-signal as predictor of countershock success. *Chaos, Solitons and Fractals*, 11(8):1205–12, 2000.

- [11] A. Amann, K. Rheinberger, and U. Achleitner. Algorithms to analyze ventricular fibrillation signals. *Curr Opin Crit Care*, 7(3):152–6, 2001.
- [12] A. Amann, K. Rheinberger, U. Achleitner, A.C. Krismer, W. Lingnau, K.H. Lindner, and V. Wenzel. The prediction of defibrillation outcome using a new combination of mean frequency and amplitude in porcine models of cardiac arrest. *Anesth Analg*, 95(3):716–22, 2002.
- [13] A. Amann, R. Tratnig, and K. Unterkofler. A new ventricular fibrillation detection algorithm for automated external defibrillators. In *Computers in Cardiology (conference proceedings)*, Lyon, 2005.
- [14] A. Amann, R. Tratnig, and K. Unterkofler. Reliability of old and new ventricular fibrillation detection algorithms for automated external defibrillators (AEDs). *Biomedical Engineering Online*, 2005. Accepted for publication.
- [15] B.D.O. Anderson and J.B. Moore. *Optimal Filtering*. Dover Publications, Inc., Mineola, New York, 2005.
- [16] Anonymous. Guidelines for Cardiopulmonary Resuscitation and Emergency Cardiac Care. Emergency Cardiac Care Committee and Subcommittees, American Heart Association. Part III. Adult advanced cardiac life support. *JAMA*, 268(16):2199–241, 1992.
- [17] Anonymous. Guidelines 2000 for Cardiopulmonary Resuscitation and Emergency Cardiovascular Care. The American Heart Association in collaboration with the International Liaison Committee on Resuscitation. *Resuscitation*, 46(1-3):1–447, 2000.
- [18] Anonymous. Guidelines 2000 for Cardiopulmonary Resuscitation and Emergency Cardiovascular Care. The American Heart Association in collaboration with the International Liaison Committee on Resuscitation. *Circulation*, 102(8 Suppl), 2000.
- [19] Anonymous. 2005 American Heart Association Guidelines for Cardiopulmonary Resuscitation and Emergency Cardiovascular Care. *Circulation*, 112(24 Suppl):IV1–203, 2005.
- [20] Anonymous. 2005 International Consensus on Cardiopulmonary Resuscitation (CPR) and Emergency Cardiovascular Care (ECC) Science With Treatment Recommendations. *Circulation*, 112(22 Suppl):III1–136, 2005.
- [21] M. Arnold, W.H.R. Miltner, H. Witte, R. Bauer, and C. Braun. Adaptive AR Modelling of Nonstationary Time Series by Means of Kalman Filtering. *IEEE Transactions on Biomedical Engineering*, 45(5):553–562, May 1998.
- [22] G.H. Bardy, B.E. Gliner, P.J. Kudenchuk, J.E. Poole, G.L. Dolack, G.K. Jones, J. Anderson, C. Troutman, and G. Johnson. Truncated biphasic pulses for transthoracic defibrillation. *Circulation*, 91(6):1768–74, 1995.
- [23] G.H. Bardy, F.E. Marchlinski, A.D. Sharma, S.J. Worley, R.M. Luceri, R. Yee, B.D. Halperin, C.L. Fellows, T.S. Ahern, D.A. Chilson, D.L. Packer, D.J. Wilber, T.A. Mattioni, R. Reddy, R.A. Kronmal, and R. Lazzara. Multicenter comparison of truncated biphasic shocks and standard damped sine wave monophasic shocks

- for transthoracic ventricular defibrillation. Transthoracic Investigators. *Circulation*, 94(10):2507–14, 1996.
- [24] Heinz Bauer. *Wahrscheinlichkeitstheorie*. Walter de Gruyter, 4th edition, 1991.
- [25] Heinz Bauer. *Maß- und Integrationstheorie*. Walter de Gruyter, 2nd edition, 1992.
- [26] L.B. Becker. Epidemiology: Etiology, Incidence, and Survival Rates. In M.H. Weil, W. Tang, and A. Ross, editors, *CPR: Resuscitation of the arrested heart.*, pages 13–27. W.B. Saunders Company, Philadelphia, 1999.
- [27] L.B. Becker, M.P. Ostrander, J. Barrett, and G.T. Kondos. Outcome of CPR in a large metropolitan area—where are the survivors? *Ann Emerg Med*, 20(4):355–61, 1991.
- [28] L.B. Becker, D.W. Smith, and K.V. Rhodes. Incidence of cardiac arrest: a neglected factor in evaluating survival rates. *Ann Emerg Med*, 22(1):86–91, 1993.
- [29] Brain Resuscitation Clinical Trial II Study Group. A randomized clinical study of a calcium-entry blocker (lidoflazine) in the treatment of comatose survivors of cardiac arrest. *N Engl J Med*, 324(18):1225–31, 1991.
- [30] Peter J. Brockwell and Richard A. Davis. *Time Series: Theory and Methods*. Springer Series in Statistics. Springer, 2nd edition, 1991.
- [31] Peter J. Brockwell and Richard A. Davis. *Introduction to Time Series and Forecasting*. Springer, 2nd edition, 2002.
- [32] C.G. Brown and R. Dzwonczyk. Signal analysis of the human electrocardiogram during ventricular fibrillation: frequency and amplitude parameters as predictors of successful countershock. *Ann Emerg Med*, 27(2):184–8, 1996.
- [33] C.G. Brown, R. Dzwonczyk, H.A. Werman, and R.L. Hamlin. Estimating the duration of ventricular fibrillation. *Ann Emerg Med*, 18(11):1181–5, 1989.
- [34] C.G. Brown, R.F. Griffith, P. Van Ligten, J. Hoekstra, G. Nejman, L. Mitchell, and R. Dzwonczyk. Median frequency—a new parameter for predicting defibrillation success rate. *Ann Emerg Med*, 20(7):787–9, 1991.
- [35] M. Callaham, O. Braun, W. Valentine, D.M. Clark, and C. Zegans. Prehospital cardiac arrest treated by urban first-responders: profile of patient response and prediction of outcome by ventricular fibrillation waveform. *Ann Emerg Med*, 22(11):1664–77, 1993.
- [36] C.W. Callaway, L.D. Sherman, M.D. Scheatzle, and J.J. Menegazzi. Scaling structure of electrocardiographic waveform during prolonged ventricular fibrillation in swine. *Pacing Clin Electrophysiol*, 23(2):180–91, 2000.
- [37] S.L. Campbell and C.D. Meyer. *Generalized Inverses of Linear Transformations*. Dover Publications, 1991.
- [38] E.J. Carlisle, J.D. Allen, W.G. Kernohan, J. Anderson, and A.A. Adgey. Fourier analysis of ventricular fibrillation of varied aetiology. *Eur Heart J*, 11(2):173–81, 1990.

- [39] E.J. Carlisle, J.D. Allen, W.G. Kernohan, W. Leahey, and A.A. Adgey. Pharmacological analysis of established ventricular fibrillation. *Br J Pharmacol*, 100(3):530–4, 1990.
- [40] P.B. Chase, K.B. Kern, A.B. Sanders, C.W. Otto, and G.A. Ewy. Effects of graded doses of epinephrine on both noninvasive and invasive measures of myocardial perfusion and blood flow during cardiopulmonary resuscitation. *Crit Care Med*, 21(3):413–9, 1993.
- [41] L.A. Cobb, C.E. Fahrenbruch, T.R. Walsh, M.K. Copass, M. Olsufka, M. Breskin, and A.P. Hallstrom. Influence of cardiopulmonary resuscitation prior to defibrillation in patients with out-of-hospital ventricular fibrillation. *JAMA*, 281(13):1182–8, 1999.
- [42] B. Cruz and J.T. Niemann. Experimental studies on precordial compression or defibrillation as initial interventions for ventricular fibrillation. *Crit Care Med*, 28(11 Suppl):N225–7, 2000.
- [43] R.O. Cummins, M.F. Hazinski, R.E. Kerber, P. Kudenchuk, L. Becker, G. Nichol, B. Malanga, T.P. Aufderheide, E.M. Stapleton, K. Kern, J.P. Ornato, A. Sanders, T. Valenzuela, and M. Eisenberg. Low-energy biphasic waveform defibrillation: evidence-based review applied to emergency cardiovascular care guidelines: a statement for healthcare professionals from the American Heart Association Committee on Emergency Cardiovascular Care and the Subcommittees on Basic Life Support, Advanced Cardiac Life Support, and Pediatric Resuscitation. *Circulation*, 97(16):1654–67, 1998.
- [44] G.W. Dalzell and A.A. Adgey. Determinants of successful transthoracic defibrillation and outcome in ventricular fibrillation. *Br Heart J*, 65(6):311–6, 1991.
- [45] O.C. Deale and B.B. Lerman. Intrathoracic current flow during transthoracic defibrillation in dogs. Transcardiac current fraction. *Circ Res*, 67(6):1405–19, 1990.
- [46] H.G. Deshmukh, M.H. Weil, C.V. Gudipati, R.P. Trevino, J. Bisera, and E.C. Rackow. Mechanism of blood flow generated by precordial compression during CPR. I. Studies on closed chest precordial compression. *Chest*, 95(5):1092–9, 1989.
- [47] A. Di Massa, M. Scardigli, L. Bruni, and L. Valentino. Biphasic waveforms for automatic external defibrillation in human: a review. *Minerva Anesthesiol*, 66(1-2):45–53, 2000.
- [48] T.G. Dietz and M.P. Schubert. *EKG-Knacker. Das Notfall-EKG-Buch*. Walter de Gruyter, 1998.
- [49] W.A.N. Dorland. *Dorland's Illustrated Medical Dictionary*. W.B. Saunders Company, Philadelphia, USA, 1994.
- [50] R. Dzwonczyk, C.G. Brown, and H.A. Werman. The median frequency of the ECG during ventricular fibrillation: its use in an algorithm for estimating the duration of cardiac arrest. *IEEE Trans Biomed Eng*, 37(6):640–6, 1990.
- [51] T. Eftestol. *Signal analysis of out-of-hospital cardiac arrest electrocardiograms for decision support during cardiopulmonary resuscitation*. PhD thesis, Stavanger University College, September 2000.

- [52] T. Eftestol, K. Sunde, S. Ole Aase, J.H. Husoy, and P.A. Steen. Predicting outcome of defibrillation by spectral characterization and nonparametric classification of ventricular fibrillation in patients with out-of-hospital cardiac arrest. *Circulation*, 102(13):1523–9, 2000.
- [53] T. Eftestol, K. Sunde, and P.A. Steen. Effects of interrupting precordial compressions on the calculated probability of defibrillation success during out-of-hospital cardiac arrest. *Circulation*, 105(19):2270–3, 2002.
- [54] T. Eftestol, L. Wik, K. Sunde, and P.A. Steen. Effects of cardiopulmonary resuscitation on predictors of ventricular fibrillation defibrillation success during out-of-hospital cardiac arrest. *Circulation*, 110(1):10–5, 2004.
- [55] J. Eilevstjonn, T. Eftestol, S.O. Aase, H. Myklebust, J.H. Husoy, and P.A. Steen. Feasibility of shock advice analysis during CPR through removal of CPR artefacts from the human ECG. *Resuscitation*, 61(2):131–41, 2004.
- [56] M.S. Eisenberg and T.J. Mengert. Cardiac resuscitation. *N Engl J Med*, 344(17):1304–13, 2001.
- [57] E.S. Fain, M.B. Sweeney, and M.R. Franz. Improved internal defibrillation efficacy with a biphasic waveform. *Am Heart J*, 117(2):358–64, 1989.
- [58] M.P. Feneley, G.W. Maier, K.B. Kern, J.W. Gaynor, S.A. Gall, Jr, A.B. Sanders, K. Raessler, L.H. Muhlbaier, J.S. Rankin, and G.A. Ewy. Influence of compression rate on initial success of resuscitation and 24 hour survival after prolonged manual cardiopulmonary resuscitation in dogs. *Circulation*, 77(1):240–50, 1988.
- [59] R.J. Gazmuri, M.H. Weil, J. Bisera, and E.C. Rackow. End-tidal carbon dioxide tension as a monitor of native blood flow during resuscitation by extracorporeal circulation. *J Thorac Cardiovasc Surg*, 101(6):984–8, 1991.
- [60] L. A. Geddes, W. A. Tacker, C. F. Babbs, and J. D. Bourland. Ventricular defibrillating threshold: strength-duration and percent-success curves. *Med Biol Eng Comput*, 35(4):301–5, 1997.
- [61] L.A. Geddes and W. Havel. Evolution of the optimum bidirectional (+/- biphasic) wave for defibrillation. *Biomed Instrum Technol*, 34(1):39–54, 2000.
- [62] R.H. Geuze and J. de Vente. Effects of duration of ventricular fibrillation and heart massage on haemodynamic responses after defibrillation in dogs. *Cardiovasc Res*, 17(5):282–9, 1983.
- [63] B.E. Gliner, T.E. Lyster, S.M. Dillion, and G.H. Bardy. Transthoracic defibrillation of swine with monophasic and biphasic waveforms. *Circulation*, 92(6):1634–43, 1995.
- [64] H.L. Greene, J.P. DiMarco, P.J. Kudenchuk, M.M. Scheinman, A.S. Tang, M.J. Reiter, D.S. Echt, P.D. Chapman, M.R. Jazayeri, F.W. Chapman, and et al. Comparison of monophasic and biphasic defibrillating pulse waveforms for transthoracic cardioversion. Biphasic Waveform Defibrillation Investigators. *Am J Cardiol*, 75(16):1135–9, 1995.

- [65] Mohinder S. Grewal and Agnus P. Andrews. *Kalman Filtering: Theory and Practice Using Matlab*. Wiley, 2nd edition, 2001.
- [66] C.V. Gudipati, M.H. Weil, J. Bisera, H.G. Deshmukh, and E.C. Rackow. Expired carbon dioxide: a noninvasive monitor of cardiopulmonary resuscitation. *Circulation*, 77(1):234–9, 1988.
- [67] P.R. Halmos. *Introduction to Hilbert Space: And the Theory of Spectral Multiplicity*. Chelsea Pub Co, 2nd edition, 1998.
- [68] James D. Hamilton. *Time Series Analysis*. Princeton University Press, 1994.
- [69] J.A. Hanley and B.J. McNeil. The meaning and use of the area under a receiver operating characteristic (ROC) curve. *Radiology*, 143(1):29–36, 1982.
- [70] J.A. Hanley and B.J. McNeil. A method of comparing the areas under receiver operating characteristic curves derived from the same cases. *Radiology*, 148(3):839–43, 1983.
- [71] Andrew C. Harvey. *Forecasting, Structural Time Series Models and the Kalman Filter*. Cambridge University Press, 1989.
- [72] M. F. Hazinski, V. M. Nadkarni, R. W. Hickey, R. O'Connor, L. B. Becker, and A. Zaritsky. Major changes in the 2005 AHA Guidelines for CPR and ECC: reaching the tipping point for change. *Circulation*, 112(24 Suppl):IV206–11, 2005.
- [73] J. Herlitz, J. Bahr, M. Fischer, M. Kuisma, K. Lexow, and G. Thorgeirsson. Resuscitation in Europe: a tale of five European regions. *Resuscitation*, 41(2):121–31, 1999.
- [74] J.W. Hoekstra, J.R. Banks, D.R. Martin, R.O. Cummins, P.E. Pepe, H.A. Stueven, M. Jastremski, E. Gonzalez, and C.G. Brown. Effect of first-responder automated defibrillation on time to therapeutic interventions during out-of-hospital cardiac arrest. The Multicenter High Dose Epinephrine Study Group. *Ann Emerg Med*, 22(8):1247–53, 1993.
- [75] J.A. Hoerter, M.V. Miceli, D.G. Renlund, W.E. Jacobus, G. Gerstenblith, and E.G. Lakatta. A phosphorus-31 nuclear magnetic resonance study of the metabolic, contractile, and ionic consequences of induced calcium alterations in the isovolumic rat heart. *Circ Res*, 58(4):539–51, 1986.
- [76] D.W.J. Hosmer and S. Lemeshow. *Applied Logistic Regression*. Wiley Series in Probability and Statistics - Applied Probability and Statistics Section. John Wiley, New York, 1989.
- [77] J. Huang, B.H. KenKnight, D.L. Rollins, W.M. Smith, and R.E. Ideker. Ventricular defibrillation with triphasic waveforms. *Circulation*, 101(11):1324–8, 2000.
- [78] J.H. Husoy, J. Eilevstjonn, T. Eftestol, S.O. Aase, H. Myklebust, and P.A. Steen. Removal of cardiopulmonary resuscitation artifacts from human ECG using an efficient matching pursuit-like algorithm. *IEEE Trans Biomed Eng*, 49(11):1287–98, 2002.

- [79] A.H. Idris, L.B. Becker, J.P. Ornato, J.R. Hedges, N.G. Bircher, N.C. Chandra, R.O. Cummins, W. Dick, U. Ebmeyer, H.R. Halperin, M.F. Hazinski, R.E. Kerber, K.B. Kern, P. Safar, P.A. Steen, M.M. Swindle, J.E. Tsitlik, I. von Planta, M. von Planta, R.L. Wears, and M.H. Weil. Utstein-style guidelines for uniform reporting of laboratory CPR research. A statement for healthcare professionals from a task force of the American Heart Association, the American College of Emergency Physicians, the American College of Cardiology, the European Resuscitation Council, the Heart and Stroke Foundation of Canada, the Institute of Critical Care Medicine, the Safar Center for Resuscitation Research, and the Society for Academic Emergency Medicine. Writing Group. *Circulation*, 94(9):2324–36, 1996.
- [80] A.H. Idris, E.D. Staples, D.J. O’Brien, R.J. Melker, W.J. Rush, K.D. Del Duca, and J.L. Falk. Effect of ventilation on acid-base balance and oxygenation in low blood-flow states. *Crit Care Med*, 22(11):1827–34, 1994.
- [81] W. Irnich. The fundamental law of electrostimulation and its application to defibrillation. *Pacing Clin Electrophysiol*, 13(11 Pt 1):1433–47, 1990.
- [82] X. Jin, A. Pernat, and J. Bisera. Electrical Causes of Cardiac Arrest and Their Management. In M.H. Weil, W. Tang, and A. Ross, editors, *CPR: Resuscitation of the arrested heart.*, pages 37–51. W.B. Saunders Company, Philadelphia, 1999.
- [83] R.E. Kerber, C. Kouba, J. Martins, K. Kelly, R. Low, R. Hoyt, D. Ferguson, L. Bailey, P. Bennett, and F. Charbonnier. Advance prediction of transthoracic impedance in human defibrillation and cardioversion: importance of impedance in determining the success of low-energy shocks. *Circulation*, 70(2):303–8, 1984.
- [84] R.E. Kerber, J.B. Martins, M.G. Kienzle, L. Constantin, B. Olshansky, R. Hopson, and F. Charbonnier. Energy, current, and success in defibrillation and cardioversion: clinical studies using an automated impedance-based method of energy adjustment. *Circulation*, 77(5):1038–46, 1988.
- [85] K.B. Kern, G.A. Ewy, W.D. Voorhees, C.F. Babbs, and W.A. Tacker. Myocardial perfusion pressure: a predictor of 24-hour survival during prolonged cardiac arrest in dogs. *Resuscitation*, 16(4):241–50, 1988.
- [86] K.B. Kern and J.T. Niemann. Coronary perfusion pressure during cardiopulmonary resuscitation. In N.A. Paradis, H.R. Halperin, and R.M. Nowak, editors, *Cardiac arrest: The science and practice of resuscitation medicine.*, chapter 14 A, pages 270–285. Williams & Wilkins, Baltimore, 1996.
- [87] K.B. Kern, A.B. Sanders, W.D. Voorhees, C.F. Babbs, W.A. Tacker, and G.A. Ewy. Changes in expired end-tidal carbon dioxide during cardiopulmonary resuscitation in dogs: a prognostic guide for resuscitation efforts. *J Am Coll Cardiol*, 13(5):1184–9, 1989.
- [88] A. Klotz, A. Amann, and H.G. Feichtinger. Removal of CPR artifacts in ventricular fibrillation ECG by local coherent line removal. In *EUSIPCO (12th European Signal Processing Conference Proceedings)*, 2004.
- [89] A. Klotz, H.G. Feichtinger, and A. Amann. Elimination of CPR-artefacts in VF-ECGs by time frequency methods. *Biomedizinische Technik*, 48(Ergänzungsband 1):218–219, 2003.

- [90] Y. Koretsune and E. Marban. Cell calcium in the pathophysiology of ventricular fibrillation and in the pathogenesis of postarrhythmic contractile dysfunction. *Circulation*, 80(2):369–79, 1989.
- [91] A.C. Krismer, Q.H. Hogan, V. Wenzel, K.H. Lindner, U. Achleitner, S. Oroszy, B. Rainer, A. Wihaidi, V.D. Mayr, P. Spencker, and A. Amann. The efficacy of epinephrine or vasopressin for resuscitation during epidural anesthesia. *Anesth Analg*, 93(3):734–42, 2001.
- [92] A.C. Krismer, K.H. Lindner, V. Wenzel, B. Rainer, G. Mueller, and W. Lingnau. Inhibition of nitric oxide improves coronary perfusion pressure and return of spontaneous circulation in a porcine cardiopulmonary resuscitation model. *Crit Care Med*, 29(3):482–6, 2001.
- [93] M. W. Kroll. A minimal model of the single capacitor biphasic defibrillation waveform. *Pacing Clin Electrophysiol*, 17(11 Pt 1):1782–92, 1994.
- [94] A. Langhelle, T. Eftestol, H. Myklebust, M. Eriksen, B.T. Holten, and P.A. Steen. Reducing CPR artefacts in ventricular fibrillation in vitro. *Resuscitation*, 48(3):279–91, 2001.
- [95] M.P. Larsen, M.S. Eisenberg, R.O. Cummins, and A.P. Hallstrom. Predicting survival from out-of-hospital cardiac arrest: a graphic model. *Ann Emerg Med*, 22(11):1652–8, 1993.
- [96] C.T. Leng, N.A. Paradis, H. Calkins, R.D. Berger, A.C. Lardo, K.C. Rent, and H.R. Halperin. Resuscitation after prolonged ventricular fibrillation with use of monophasic and biphasic waveform pulses for external defibrillation. *Circulation*, 101(25):2968–74, 2000.
- [97] H.G. Lienhart, W. John, and V. Wenzel. Cardiopulmonary resuscitation of a near-drowned child with a combination of epinephrine and vasopressin. *Pediatr Crit Care Med*, 6(4):486–8, 2005.
- [98] Lennart Ljung. *System identification - theory for the user*. PTR Prentice Hall, Upper Saddle River, N.J., 2nd edition, 1999.
- [99] G. Lombardi, J. Gallagher, and P. Gennis. Outcome of out-of-hospital cardiac arrest in New York City. The Pre-Hospital Arrest Survival Evaluation (PHASE) Study. *JAMA*, 271(9):678–83, 1994.
- [100] David G. Luenberger. *Optimization by Vector Space Methods*. John Wiley & Sons, Inc., 1969.
- [101] G. Lumb, G. J. Anderson, M. L. Kase, and D. V. Woo. Damage in canine hearts following defibrillator shocks. *Ann Clin Lab Sci*, 16(3):171–9, 1986.
- [102] J.E. Manning and P.M. Zoll. Therapy of bradyasystolic arrest. In N.A. Paradis, H.R. Halperin, and R.M. Nowak, editors, *Cardiac arrest: The science and practice of resuscitation medicine.*, chapter 33, pages 621–640. Williams & Wilkins, Baltimore, 1996.

- [103] D.R. Martin, C.G. Brown, and R. Dzwonczyk. Frequency analysis of the human and swine electrocardiogram during ventricular fibrillation. *Resuscitation*, 22(1):85–91, 1991.
- [104] G. Martin, J. Cosin, M. Such, A. Hernandez, and P. Llamas. Relation between power spectrum time course during ventricular fibrillation and electromechanical dissociation. Effects of coronary perfusion and nifedipine. *Eur Heart J*, 7(7):560–9, 1986.
- [105] V.D. Mayr, V. Wenzel, W.G. Voelckel, A.C. Krismer, T. Mueller, K.G. Lurie, and K.H. Lindner. Developing a vasopressor combination in a pig model of adult asphyxial cardiac arrest. *Circulation*, 104(14):1651–6, 2001.
- [106] S. Mittal, S. Ayati, K.M. Stein, B.P. Knight, F. Morady, D. Schwartzman, D. Cavlovich, E.V. Platia, H. Calkins, P.J. Tchou, J.M. Miller, J.M. Wharton, R.J. Sung, D.J. Slotwiner, S.M. Markowitz, and B.B. Lerman. Comparison of a novel rectilinear biphasic waveform with a damped sine wave monophasic waveform for transthoracic ventricular defibrillation. ZOLL Investigators. *J Am Coll Cardiol*, 34(5):1595–601, 1999.
- [107] S. Mittal, S. Ayati, K.M. Stein, D. Schwartzman, D. Cavlovich, P.J. Tchou, S.M. Markowitz, D.J. Slotwiner, M.A. Scheiner, and B.B. Lerman. Transthoracic cardioversion of atrial fibrillation: comparison of rectilinear biphasic versus damped sine wave monophasic shocks. *Circulation*, 101(11):1282–7, 2000.
- [108] K.G. Monsieurs, H. De Cauwer, F.L. Wuyts, and L.L. Bossaert. A rule for early outcome classification of out-of-hospital cardiac arrest patients presenting with ventricular fibrillation. *Resuscitation*, 36(1):37–44, 1998.
- [109] E. Murphy, J.F. Aiton, C.R. Horres, and M. Lieberman. Calcium elevation in cultured heart cells: its role in cell injury. *Am J Physiol*, 245(5 Pt 1):C316–21, 1983.
- [110] Y. Nakagawa, M.H. Weil, and W. Tang. The History of CPR. In M.H. Weil, W. Tang, and A. Ross, editors, *CPR: Resuscitation of the arrested heart.*, pages 1–12. W.B. Saunders Company, Philadelphia, 1999.
- [111] M. J. Niebauer, L. A. Geddes, and C. F. Babbs. Potassium efflux from myocardial cells induced by defibrillator shock. *Med Instrum*, 20(3):135–7, 1986.
- [112] J.T. Niemann, C.B. Cairns, J. Sharma, and R.J. Lewis. Treatment of prolonged ventricular fibrillation. Immediate countershock versus high-dose epinephrine and CPR preceding countershock. *Circulation*, 85(1):281–7, 1992.
- [113] J.T. Niemann, B. Cruz, D. Garner, and R.J. Lewis. Immediate countershock versus cardiopulmonary resuscitation before countershock in a 5-minute swine model of ventricular fibrillation arrest. *Ann Emerg Med*, 36(6):543–6, 2000.
- [114] M. Noc, M.H. Weil, R.J. Gazmuri, S. Sun, J. Biscera, and W. Tang. Ventricular fibrillation voltage as a monitor of the effectiveness of cardiopulmonary resuscitation. *J Lab Clin Med*, 124(3):421–6, 1994.
- [115] M. Noc, M.H. Weil, W. Tang, S. Sun, A. Pernet, and J. Bisera. Electrocardiographic prediction of the success of cardiac resuscitation. *Crit Care Med*, 27(4):708–14, 1999.

- [116] N.A. Paradis, G.B. Martin, E.P. Rivers, M.G. Goetting, T.J. Appleton, M. Feingold, and R.M. Nowak. Coronary perfusion pressure and the return of spontaneous circulation in human cardiopulmonary resuscitation. *JAMA*, 263(8):1106–13, 1990.
- [117] A. Patwardhan, S. Moghe, K. Wang, H. Cruise, and F. Leonelli. Relation between ventricular fibrillation voltage and probability of defibrillation shocks. Analysis using Hilbert transforms. *J Electrocardiol*, 31(4):317–25, 1998.
- [118] A. Patwardhan, S. Moghe, K. Wang, and F. Leonelli. Frequency modulation within electrocardiograms during ventricular fibrillation. *Am J Physiol Heart Circ Physiol*, 279(2):H825–35, 2000.
- [119] A. Patwardhan, K. Wang, S. Moghe, and F. Leonelli. Bispectral energies within electrocardiograms during ventricular fibrillation are correlated with defibrillation shock outcome. *Ann Biomed Eng*, 27(2):171–9, 1999.
- [120] J.E. Poole, R.D. White, K.G. Kanza, F. Hengstenberg, G.T. Jarrard, J.C. Robinson, V. Santana, D.K. McKenas, N. Rich, S. Rosas, S. Merritt, L. Magnotto, J.V. Gallagher, 3rd, B.E. Gliner, D.B. Jorgenson, C.B. Morgan, S.M. Dillon, R.A. Kronmal, and G.H. Bardy. Low-energy impedance-compensating biphasic waveforms terminate ventricular fibrillation at high rates in victims of out-of-hospital cardiac arrest. LIFE Investigators. *J Cardiovasc Electrophysiol*, 8(12):1373–85, 1997.
- [121] H.P. Povoas and J. Bisera. Electrocardiographic waveform analysis for predicting the success of defibrillation. *Crit Care Med*, 28(11 Suppl):N210–1, 2000.
- [122] T.H. Rainer and C.E. Robertson. Adrenaline, cardiac arrest, and evidence based medicine. *J Accid Emerg Med*, 13(4):234–7, 1996.
- [123] D.G. Renlund, E.G. Lakatta, E.D. Mellits, and G. Gerstenblith. Calcium-dependent enhancement of myocardial diastolic tone and energy utilization dissociates systolic work and oxygen consumption during low sodium perfusion. *Circ Res*, 57(6):876–88, 1985.
- [124] J. Ruiz, E. Aramendi, S. Ruiz de Gauna, A. Lazkano, L.A. Leturiendo, and J.J. Gutierrez. Ventricular fibrillation detection in ventricular fibrillation signals corrupted by cardiopulmonary resuscitation artifacts. *Computers in Cardiology*, pages 221–4, 2004.
- [125] Y. Sato, M.H. Weil, S. Sun, W. Tang, J. Xie, M. Noc, and J. Bisera. Adverse effects of interrupting precordial compression during cardiopulmonary resuscitation. *Crit Care Med*, 25(5):733–6, 1997.
- [126] T. Schneider, B. Wolcke, A. Liebrich, K.G. Kanza, and W. Dick. [New aspects of electric defibrillation]. *Anaesthesist*, 47(4):320–9, 1998.
- [127] H.P. Schuster and H.J. Trappe. *EKG-Kurs für Isabel*. Thieme, Stuttgart, 2005.
- [128] L.D. Sherman, C.W. Callaway, and J.J. Menegazzi. Ventricular fibrillation exhibits dynamical properties and self-similarity. *Resuscitation*, 47(2):163–73, 2000.
- [129] M. Small, D. Yu, R.G. Harrison, C. Robertson, G. Clegg, M. Holzer, and F. Sterz. Characterizing Nonlinearity in Ventricular Fibrillation. *Computers in Cardiology*, 26, 1999.

- [130] M. Small, D. Yu, R.G. Harrison, C. Robertson, G. Clegg, M. Holzer, and F. Sterz. Deterministic nonlinearity in ventricular fibrillation. *Chaos*, 10(1):268–277, 2000.
- [131] C.S. So. *Praktische EKG-Deutung*. Thieme, Stuttgart, 2004.
- [132] K.H. Stadlbauer, K. Rheinberger, V. Wenzel, C. Raedler, A.C. Krismer, H.U. Strohmenger, S. Augenstein, H.G. Wagner-Berger, W.G. Voelckel, K.H. Lindner, and A. Amann. The effects of nifedipine on ventricular fibrillation mean frequency in a porcine model of prolonged cardiopulmonary resuscitation. *Anesth Analg*, 97(1):226–30, 2003.
- [133] K.H. Stadlbauer, H.G. Wagner-Berger, V. Wenzel, W.G. Voelckel, A.C. Krismer, G. Klima, K. Rheinberger, S. Pechlaner, V.D. Mayr, and K.H. Lindner. Survival with full neurologic recovery after prolonged cardiopulmonary resuscitation with a combination of vasopressin and epinephrine in pigs. *Anesth Analg*, 96(6):1743–9, table of contents, 2003.
- [134] A.J. Stewart, J.D. Allen, and A.A. Adgey. Frequency analysis of ventricular fibrillation and resuscitation success. *Q J Med*, 85(306):761–9, 1992.
- [135] H.U. Strohmenger, T. Eftestol, K. Sunde, V. Wenzel, M. Mair, H. Ulmer, K.H. Lindner, and P.A. Steen. The predictive value of ventricular fibrillation electrocardiogram signal frequency and amplitude variables in patients with out-of-hospital cardiac arrest. *Anesth Analg*, 93(6):1428–33, table of contents, 2001.
- [136] H.U. Strohmenger, K.H. Lindner, and C.G. Brown. Analysis of the ventricular fibrillation ECG signal amplitude and frequency parameters as predictors of countershock success in humans. *Chest*, 111(3):584–9, 1997.
- [137] H.U. Strohmenger, K.H. Lindner, A. Keller, I.M. Lindner, E. Pfenninger, and U. Bothner. Effects of graded doses of vasopressin on median fibrillation frequency in a porcine model of cardiopulmonary resuscitation: results of a prospective, randomized, controlled trial. *Crit Care Med*, 24(8):1360–5, 1996.
- [138] H.U. Strohmenger, K.H. Lindner, A. Keller, I.M. Lindner, and E.G. Pfenninger. Spectral analysis of ventricular fibrillation and closed-chest cardiopulmonary resuscitation. *Resuscitation*, 33(2):155–61, 1996.
- [139] H.U. Strohmenger, K.H. Lindner, K.G. Lurie, A. Welz, and M. Georgieff. Frequency of ventricular fibrillation as a predictor of defibrillation success during cardiac surgery. *Anesth Analg*, 79(3):434–8, 1994.
- [140] H.U. Strohmenger, K.H. Lindner, A.W. Prengel, E.G. Pfenninger, U. Bothner, and K.G. Lurie. Effects of epinephrine and vasopressin on median fibrillation frequency and defibrillation success in a porcine model of cardiopulmonary resuscitation. *Resuscitation*, 31(1):65–73, 1996.
- [141] H.U. Strohmenger and V. Wenzel. Electrocardiographic prediction of cardiopulmonary resuscitation success. *Curr Opin Crit Care*, 6(3):192–5, 2000. Enter text here.

- [142] C. D. Swerdlow, W. Fan, and J. E. Brewer. Charge-burping theory correctly predicts optimal ratios of phase duration for biphasic defibrillation waveforms. *Circulation*, 94(9):2278–84, 1996.
- [143] W. Tang, M.H. Weil, S. Sun, H. Yamaguchi, H.P. Povoas, A.M. Pernat, and J. Bisera. The effects of biphasic and conventional monophasic defibrillation on postresuscitation myocardial function. *J Am Coll Cardiol*, 34(3):815–22, 1999.
- [144] R. Tratnig. *Reliability of new detection algorithms for automated external defibrillators (AEDs)*. PhD thesis, Technische Universität Graz, 2005.
- [145] J.M. Van Nueten and P.M. Vanhoutte. Improvement of tissue perfusion with inhibitors of calcium ion influx. *Biochem Pharmacol*, 29(4):479–81, 1980.
- [146] G. P. Walcott, R. G. Walker, A. W. Cates, W. Krassowska, W. M. Smith, and R. E. Ideker. Choosing the optimal monophasic and biphasic waveforms for ventricular defibrillation. *J Cardiovasc Electrophysiol*, 6(9):737–50, 1995.
- [147] G.P. Walcott, S.B. Melnick, F.W. Chapman, J.L. Jones, W.M. Smith, and R.E. Ideker. Relative efficacy of monophasic and biphasic waveforms for transthoracic defibrillation after short and long durations of ventricular fibrillation. *Circulation*, 98(20):2210–5, 1998.
- [148] J.N. Watson, P.S. Addison, G.R. Clegg, M. Holzer, F. Sterz, and C.E. Robertson. A novel wavelet transform based analysis reveals hidden structure in ventricular fibrillation. *Resuscitation*, 43(2):121–7, 2000.
- [149] W.D. Weaver, L.A. Cobb, D. Dennis, R. Ray, A.P. Hallstrom, and M.K. Copass. Amplitude of ventricular fibrillation waveform and outcome after cardiac arrest. *Ann Intern Med*, 102(1):53–5, 1985.
- [150] M.H. Weil, J. Bisera, R.P. Trevino, and E.C. Rackow. Cardiac output and end-tidal carbon dioxide. *Crit Care Med*, 13(11):907–9, 1985.
- [151] M.H. Weil, W. Tang, and A. Ross, editors. *CPR: Resuscitation of the Arrested Heart*. W.B. Saunders Company, Philadelphia, 1999.
- [152] V. Wenzel, A.C. Krismer, H.R. Arntz, H. Sitter, K.H. Stadlbauer, and K.H. Lindner. A comparison of vasopressin and epinephrine for out-of-hospital cardiopulmonary resuscitation. *N Engl J Med*, 350(2):105–13, 2004.
- [153] V. Wenzel, K.H. Lindner, A.C. Krismer, E.A. Miller, W.G. Voelckel, and W. Lingnau. Repeated administration of vasopressin but not epinephrine maintains coronary perfusion pressure after early and late administration during prolonged cardiopulmonary resuscitation in pigs. *Circulation*, 99(10):1379–84, 1999.
- [154] V. Wenzel, K.H. Lindner, A.C. Krismer, W.G. Voelckel, M.F. Schocke, W. Hund, M. Witkiewicz, E.A. Miller, G. Klima, J. Wissel, W. Lingnau, and F.T. Aichner. Survival with full neurologic recovery and no cerebral pathology after prolonged cardiopulmonary resuscitation with vasopressin in pigs. *J Am Coll Cardiol*, 35(2):527–33, 2000.

- [155] V. Wenzel, S.A. Padosch, W.G. Voelckel, A.H. Idris, A.C. Krismer, R. Bettschart-Wolfensberger, and K.H. Lindner. Survey of effects of anesthesia protocols on hemodynamic variables in porcine cardiopulmonary resuscitation laboratory models before induction of cardiac arrest. *Comp Med*, 50(6):644–8, 2000.
- [156] R.D. White and D.M. Blanton. Biphasic truncated exponential waveform defibrillation. *Prehosp Emerg Care*, 3(4):283–9, 1999.
- [157] L. Wik, T.B. Hansen, F. Fylling, T. Steen, P. Vaagenes, B.H. Auestad, and P.A. Steen. Delaying defibrillation to give basic cardiopulmonary resuscitation to patients with out-of-hospital ventricular fibrillation: a randomized trial. *JAMA*, 289(11):1389–95, 2003.
- [158] B. Wolcke, J. Brachlow, and W. Dick. Biphasische Defibrillation - Ein Fallbericht zur Ultima Ratio bei supraventrikulärer Tachykardie. *Notfall und Rettungsmedizin*, Heft 2:104–6, 2000.
- [159] World Wide Web Consortium (W3C). Extensible Markup Language (XML). Technical report, <http://www.w3.org/XML/>, 2004.
- [160] World Wide Web Consortium (W3C). Extensible Markup Language (XML) 1.0 (third edition). Technical report, <http://www.w3.org/TR/2004/REC-xml-20040204/>, 2004.
- [161] J. Xie, M.H. Weil, S. Sun, W. Tang, Y. Sato, X. Jin, and J. Bisera. High-energy defibrillation increases the severity of postresuscitation myocardial dysfunction. *Circulation*, 96(2):683–8, 1997.
- [162] Y. Yamanouchi, J. E. Brewer, K. A. Mowrey, M. W. Kroll, A. M. Donohoo, B. L. Wilkoff, and P. J. Tchou. Sawtooth first phase biphasic defibrillation waveform: a comparison with standard waveform in clinical devices. *J Cardiovasc Electrophysiol*, 8(5):517–28, 1997.
- [163] Y. Yamanouchi, J.E. Brewer, A.M. Donohoo, K.A. Mowrey, B.L. Wilkoff, and P.J. Tchou. External exponential biphasic versus monophasic shock waveform: efficacy in ventricular fibrillation of longer duration. *Pacing Clin Electrophysiol*, 22(10):1481–7, 1999.
- [164] Y. Yamanouchi, J.E. Brewer, K.A. Mowrey, A.M. Donohoo, B.L. Wilkoff, and P.J. Tchou. Optimal small-capacitor biphasic waveform for external defibrillation: influence of phase-1 tilt and phase-2 voltage. *Circulation*, 98(22):2487–93, 1998.
- [165] Y. Yamanouchi, J.E. Brewer, K.F. Olson, K.A. Mowrey, T.N. Mazgalev, B.L. Wilkoff, and P.J. Tchou. Fully discharging phases. A new approach to biphasic waveforms for external defibrillation. *Circulation*, 100(8):826–31, 1999.
- [166] D. Yu, M. Small, R.G. Harrison, C. Robertson, G. Clegg, M. Holzer, and F. Sterz. Complexity Measurements for Analysis and Diagnosis of Early Ventricular Fibrillation. *Computers in Cardiology*, 26, 1999.
- [167] D. Yu, M. Small, R.G. Harrison, C. Robertson, G. Clegg, M. Holzer, and F. Sterz. Measuring temporal complexity of ventricular fibrillation. *Physics Letters A*, 265:68–75, 2000.

Index

- $L^2(\Omega, \mathbb{F}, P)$, 56
- $N(\mu, \sigma^2)$, 61
- \mathbb{N} , *see* natural numbers
- $\{\Omega, \mathbb{F}, P\}$, 48
- *.bda, 36

- a posteriori estimate, 72
- a priori estimate, 72
- accuracy, 134
- ACF, *see* autocorrelation function
- ACLS, *see* advanced cardiac life support
- advanced cardiac life support, 3
- AED, *see* automated external defibrillator
- ALR, 103
- annotation files, 23, 24
- asystole, 3, 8
- ATS, 98
- autocorrelation function, 99
 - windowed sample ACF, 100
- automated external defibrillator, 3, 8
 - fully-automatic AED, 8
 - semi-automatic AED, 8

- backward shift operator, 48
- basic life support, 3
- Bayes' theorem, 50
- best constant MSE forecast, 54
- best linear MSE forecast, 55
- best MSE forecast, 54
- BLS, *see* basic life support

- cardiopulmonary resuscitation, 2, 3
- cardiopulmonary system, 2
- Cauchy-Schwarz inequality, 56
- conditional density function, 50
- conditional expectation, 50
- conjugate complex, 56
- control theory, 66
- coronary perfusion pressure, 7
- correlation, 53
- covariance, 52
- covariance matrix, 53
- CPP, *see* coronary perfusion pressure
- CPR, *see* cardiopulmonary resuscitation
- CPR artefact removal, 14, 89
 - data, 107
 - evaluation, 114
 - evaluation methods, 93
 - optimisation, 108
 - previous work, 95
 - results, 114
 - sampling and mixing, 108

- database, 24, 25
- defibrillation, 6
 - waveform, 6, 151, 157, 170
 - biphasic, 152, 164
 - charge flow, 158, 171
 - current, 171
 - energy, 157, 170
 - initial current, 157
 - initial voltage, 157
 - optimal, 174
 - pulse duration, 157, 171
 - theory, 173
 - tilt, 158
- defibrillator
 - capacitance, 161
 - capacitor, 153
 - external, 152, 164
 - internal resistance, 156, 161
 - pulse generation, 153, 165
- detrended random variables, 57

- ECG, 8
- ECG rhythms, 38
- electromechanical dissociation, 8
- EMD, *see* electromechanical dissociation
- epinephrine, 10, 12
- example
 - IID, 52
 - kalman prediction, 70

- random walk, 52
 - WN, 53
- expectation, 49
- forecast, 54
- Gaussian random variables, 61
- generalised inverse of a matrix, 60
- hands-off interval, 8, 89
- Hilbert space, 56
 - of random variables, 56
- identity matrix, 104
- IID, *see* independent identically distributed
- incident, 37
- independent, 51
- independent identically distributed, 52
- inner product, 56
- inner product space, 56
- innovation, 60, 68
- international guidelines
 - 2000, 3
 - 2005, 9
- joint distribution function, 50
- jointly Gaussian, 61
- Kalman
 - filtering problem, 68
 - filtering theorem, 72
 - gain, 68
 - prediction problem, 68
 - prediction theorem, 68
 - properties of recursions, 76
 - recursions, 66
 - smoothing problem, 68
 - smoothing theorem, 75
- LAMP, 35
- law of iterated expectations, 51
- law of iterated projections, 60
- law of updating a projection, 60
- likelihood, 79
- linear regression, 59
- logistic distribution, 134
- loss function, 54
- marginal density function, 50
- Markov property, 66
- maximum likelihood estimation, 79, 80
 - structural state-space models, 80
- mean, 49
- mean squared error, 54, 84
- minimum mean squared error, 79, 84
- MLE, *see* maximum likelihood estimation
- MMSE, *see* minimum mean squared error
- MRL, 33
- mrl2bda, 36
- MSE, *see* mean squared error
- multivariate Gaussian, 61
- myocardial metabolism, 6
- MySQL, 25
- natural numbers, 52
- negative predictive value, 134
- nifedipine, 141
- norm, 56
- normal sinus rhythm, 2, 8
- normalised state-space model, 76
- NSR, *see* normal sinus rhythm, *see* normal sinus rhythm
- observation equation, 65
- OLS, *see* ordinary least squares
- ordinary least squares, 58
- overdetermined system of linear equations, 58
- overlapping of frequencies, 90
- parallelogram law, 56
- PEA, *see* pulseless electrical activity
- positive predictive value, 134
- prediction equations, 58
- prediction error, 58
- probability density function, 49
- probability distribution function, 49
- probability for ROSC, 7
- probability space, 48
- projection theorem, 57
- pulseless electrical activity, 3, 8
- Pythagoras, 57
- random walk, 52
 - symmetric, 52
- receiver operating characteristic, 133
- reduced likelihood, 81, 83
- reference signal, 100
 - lagging, 101

- residual, 102
- restored signal-to-noise ratio, 93
- resuscitation, *see* cardiopulmonary resuscitation
- return of spontaneous circulation, 3
- rhythm detection algorithms, 8, 10
- ROC, *see* receiver operating characteristic
- ROSC, *see* return of spontaneous circulation
- rSNR, *see* restored signal-to-noise ratio

- sample ACF, 99
- sample ACVF, 99
- sample autocovariance function, 99
- SCA, *see* sudden cardiac arrest
- seasonal state-space model, 97
- sensitivity, 131
- sesqui-linear, 56
- SI, *see* survival index
- signal-to-noise ratio, 93
- SNR, *see* signal-to-noise ratio
- specificity, 131
- state equation, 66
- state-space model, 65
- stochastic process, 48
- structural state-space model, 80
- sudden cardiac arrest, 2
- survival index, 130, 134
- survival rate, 2

- tachycardia, 3
- threshold, 139
- time series, 47
- TOP-data, 21
- transpose of a matrix or vector, 53
- transthoracic impedance, 153
- triangle inequality, 56
- TS, *see* time series

- uncorrelated, 53
- Utstein-style guidelines, 131

- variance, 50
- vasopressin, 10, 12
- vectors of random variables, 53, 55, 59
- ventricular fibrillation, 2
- ventricular tachycardia, 8
- VF, *see* ventricular fibrillation
- VF analysis
 - amplitude, 12, 131
 - amplitude spectrum area, 13
 - bispectral, 13
 - combination of parameters, 14, 130
 - frequency, 12, 131, 141
 - $N(\alpha)$ -histograms, 14
 - nonlinear dynamics, 13
 - wavelets, 13
- VT, *see* ventricular tachycardia

- white noise, 53
- WN, *see* white noise

- XML, 24

- zero-mean, 52